(2)

A COLLABORATIVE US/UK RESEARCH PROGRAM IN ADVANCED SILICA MACROMOLECULAR MICRO-OPTICS

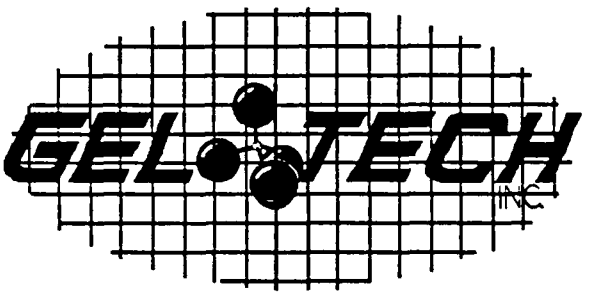

FINAL TECHNICAL REPORT PREPARED FOR
AIR FORCE OFFICE OF SCIENTIFIC RESEARCH
BOLLING AFB DC 20332

CONTRACT # F49620-88-C-0010

The views and conclusions contained in this document are those of the authors and should not be interpreted as necessarily representing the official policies or endorsements, either expressed or implied, of the Air Force Office of Scientific Research or the U. S. Government.

SECURITY CLASSIFICATION OF THIS PAGE

REPORT DOCUMENTATION PAGE

1a. REPORT SECURITY CLASSIFICATION Unclassified	1b. RESTRICTIVE MARKINGS
2a. SECURITY CLASSIFICATION AUTHORITY	3. DISTRIBUTION / AVAILABILITY OF REPORT Approved for public release Distribution unlimited
2b. DECLASSIFICATION / DOWNGRADING SCHEDULE	
4. PERFORMING ORGANIZATION REPORT NUMBER(S) Final Technical Report	5. MONITORING ORGANIZATION REPORT NUMBER(S) AFOSR-TR- 90-0523
6a. NAME OF PERFORMING ORGANIZATION GELTECH Inc.	6b. OFFICE SYMBOL (If applicable)
7a NAME OF MONITORING ORGANIZATION AFSOR/NC	
6c. ADDRESS (City, State, and ZIP Code) One Progress Blvd., Box 18 Alachua, FL 32615	7b ADDRESS (City, State, and ZIP Code) Building 410 Bolling Air Force Base Washington, DC 20332-6448
8a. NAME OF FUNDING / SPONSORING ORGANIZATION A.F.S.O.R.	8b OFFICE SYMBOL (If applicable) NC
9 PROCUREMENT INSTRUMENT IDENTIFICATION NUMBER F49620-88-C-0010	
8c. ADDRESS (City, State, and ZIP Code) Building 410 Bolling Air Force Base Washington, DC 20332-6448	10 SOURCE OF FUNDING NUMBERS PROGRAM ELEMENT NO. 61102-F PROJECT NO. 1693 TASK NO. 06 WORK UNIT ACCESSION NO.

11. TITLE (Include Security Classification)

A Collaborative US-UK Research Program in Advanced Silica Macromolecular Micro-Optics (U)

12. PERSONAL AUTHOR(S)

Nogues, Jean-Luc Robert (Principal Investigator)

13a. TYPE OF REPORT	13b. TIME COVERED	14. DATE OF REPORT (Year, Month, Day)	15. PAGE COUNT
Final Technical Report	FROM 87-10-15 TO 90-2-14	900430	161

16. SUPPLEMENTARY NOTATION

17. COSATI CODES			18. SUBJECT TERMS (Continue on reverse if necessary and identify by block number)
FIELD	GROUP	SUB-GROUP	Sol-Gel, optics, silica, porous silica, mixing, casting, aging, drying, stabilization, densification, organic/inorganic composite, liquid crystals, laser, arrays, and titania. (TAS)

19. ABSTRACT (Continue on reverse if necessary and identify by block number)

See Reverse

20 DISTRIBUTION / AVAILABILITY OF ABSTRACT	21 ABSTRACT SECURITY CLASSIFICATION
☒ UNCLASSIFIED/UNLIMITED ☐ SAME AS RPT. ☐ DTIC USERS	Unclassified
22a NAME OF RESPONSIBLE INDIVIDUAL Donald R. Ulrich	22b. TELEPHONE (Include Area Code) 202-767-4960
	22c. OFFICE SYMBOL NC

DD FORM 1473, 84 MAR 83 APR edition may be used until exhausted. All other editions are obsolete.

SECURITY CLASSIFICATION OF THIS PAGE

Unclassified

19. ABSTRACT:

The major challenge facing sol-gel processing of advanced optical materials, and in fact the entire field of chemically derived ceramics, is to relate processing variables to final properties. Fundamental studies of sol-gel processing science pursued at GELTECH during the last few years have led to two major accomplishments:

1) Development of a generic sol-gel process for producing fully dense silica monoliths (Type V Silica)
2) Development of a generic sol-gel process for producing porous silica monoliths (Type VI Silica)

These two new materials present many unique properties and offer enormous potential for the development of new optical components and advanced optic systems with unique capabilities. In order to take full advantage of the unique capabilities of the GELSIL® process, considerable efforts have been devoted to develop international collaboration in the field of advanced optical systems. This effort lead to the establishment of several research programs in some of the world leader laboratories in the field of advanced optics. These research programs and a summary of results to date are given below.

1) Preparation of Silica Optical Prototypes

GELTECH's objectives are to conduct sol-gel basic research for the preparation of porous and dense optical prototypes which are used in the other research programs. The University of Florida - AMRC is pursuing research for the production of monolithic titania-silica gels with 0-15% TiO_2 using organometallic sol-gel processing.

2) Sol-Gel Basic Science Programs

The major results of these programs are: 1) The understanding of the structure of water absorbed into the pores of gel silica monoliths using Dielectric Relaxation Spectroscopy (DRS) and Differential Scanning Calorimetry (DSC). 2) The determination of the structural energies of gel-silica by quantum calculations for rings and chains of silica tetrahedra using Huckel and Intermediate Neglect of Differential Overlap Molecular Orbital models.

3) Porous Gel-Silica Optics Research Programs

The research program at the University College London involves the development of micro-optical arrays. Stacked planar optics is an attractive technology for digital optic applications, in particular optical computing. The basic component for digital optics has been identified as modulator and detector arrays which in many cases rely on microlens arrays for imaging. The results presented in this report briefly consider the basic modulator array and discuss in detail the fabrication conditions for microlens arrays.

The aims of one project at the University of Manchester are to use GELSIL® porous matrices as carriers for liquid crystal systems, thereby overcoming many of the problems associated with current liquid crystal devices.

A program for the development of densification techniques for sol-gel matrices using lasers is under development at the University of Manchester. Work has concentrated on the use of a carbon dioxide laser to effect full densification of thin surface layers on partially densified discs.

4) Dense Gel-Silica Optics Research Programs

Another project at the University of Manchester involves the development of tunable doped gel-silica glass lasers. Initial measurements of laser relevant properties of neodymium doped GELSIL® are presented in this report.

Ultraviolet laser development was initiated at the Loughborough University of Technology. The results presented in this report discuss some possibilities associated with the emergent technology of sol-gel glass, for the generation of novel optical elements for intra-cavity use in ion lasers.

EXECUTIVE SUMMARY

The major challenge facing sol-gel processing of advanced optical materials, and in fact the entire field of chemically derived ceramics, is to relate processing variables to final properties. Fundamental studies of sol-gel processing science pursued at GELTECH during the last few years have led to two major accomplishments:

1) Development of a generic sol-gel process for producing fully dense silica monoliths (Type V Silica), and
2) Development of a generic sol-gel process for producing porous silica monoliths (Type VI Silica).

These two new materials present many unique properties and offer enormous potential for the development of new optical components and advanced optic systems with unique capabilities. Exploratory research at GELTECH and at Advanced Materials Research Center (AMRC) has shown that these materials, named GELSIL®, can serve as a host matrix for rare earth elements such as Ce, Er and Nd, thus establishing the possibility for a high intensity solar powered Q-switched glass laser. Successful doping of the GELSIL® matrix with metallic oxides including all of the transition elements has also been achieved. This generic doping process, combined with a unique manipulation of index of refraction by density gradients, opens up the possibility for new designs of graded refractive index lenses, micro-optical arrays, planar silica waveguides, optical couplers, radiation hard optical storage devices, fast holographic storage, matrices for non-linear optics, and eventually a low power optical computer and solar powered high intensity laser.

In order to take full advantage of the unique capabilities of the GELSIL® process, considerable efforts have been devoted to develop international collaboration in the field of advanced optical systems. This effort lead to the establishment of several research programs in some of the world leader laboratories in the field of advanced optics. These research programs and a summary of results collected during this contract are given below.

1. Preparation of Silica Optical Prototypes

GELTECH's laboratory's objectives are to conduct sol-gel basic research for the preparation of porous and dense optical prototypes which are used in the other research programs. The University of Florida - AMRC is pursuing research for the production of monolithic titania-

silica gels with 0-15% TiO_2 using organometallic sol-gel processing.

2. Sol-Gel Basic Science Programs

The AMRC research focus is on three objectives: 1) Sol-gel optical science, necessary to produce controlled gradients of ultrastructure and dopants in sol-gel derived glass matrices; 2) Ultrastructure characterization, necessary to interpret and predict performance of unique optical designs using sol-gel derived matrices; 3) Processing-property relationships, particular to the components defined by the joint US-UK investigative teams.

The major results of this research program are:

1) The understanding of the structure of water absorbed into the pores of alkoxide derived gel silica monoliths using Dielectric Relaxation Spectroscopy (DRS) and Differential Scanning Calorimetry (DSC).

2) The determination of the structural energies of gel-silica by quantum calculations for rings and chains of silica tetrahedra using Huckel and Intermediate Neglect of Differential Overlap Molecular Orbital models.

3. Porous Gel-Silica Optics Research Programs

The research program at the University College London involves the development of micro-optical arrays. Stacked planar optics is an attractive technology for digital optic applications, in particular optical computing.

The basic components for digital optics have been identified as modulator and detector arrays which in many cases rely on microlens arrays for imaging. The results presented in this report briefly consider the basic modulator array and discusses in detail the fabrication conditions for microlens arrays.

The aims of one project at the University of Manchester are to use GELSIL® porous matrices as carriers for liquid crystal systems, thereby overcoming many of the problems associated with current liquid crystal devices. These difficulties include the construction of large area arrays, maintenance of a constant and accurate sample thickness of typically 5 mm, electrical addressing of the liquid crystals, and where possible, increasing the switching speed of the medium. The use of porous GELSIL® matrices can, in principle, contribute to the solution of all of these problems. They have potential for easy processing in large areas with a well-defined pore size, and the possibility of ion impregnation together with the matrices high optical integrity makes them ideal candidates for new liquid crystal display (and non-display) applications.

The program during this contract has essentially progressed in two complementary directions: 1) The optimization of new liquid crystal systems for use in displays, and; 2) the incorporation of these and other more conventional materials into the GELSIL® matrices.

A program for the development of densification techniques for sol-gel matrices, using lasers was developed at the University of Manchester. Work has concentrated on the use of a

carbon dioxide laser to effect full densification of thin surface layers on partially densified discs. Using microhardness as a characterization method the upper (damage) threshold and lower energy thresholds to effect densification were measured as 6.32 ±0.25 and 4.26 ±0.25 Joules per square centimeter of surface irradiated, as opposed to calculated values of 11.31 and 7.42 J/cm^2 respectively.

4. Dense Gel-Silica Optics Research Programs

Another project at the University of Manchester involves the development of tunable doped gel-silica glass lasers. Initial measurements of laser relevant properties of neodymium doped GELSIL® are presented in this report. Samples doped with Nd only reveal anomalously short fluorescence lifetimes characteristic of concentration quenching, TEM measurements revealing clumping of the neodymium. Co-doping with aluminum allows better dispersion of the neodymium throughout the GELSIL® matrix, but fluorescence lifetimes are still shorter than expected. Photon quenching by residual OH ions is suspected, absorption, FTIR and Raman spectroscopy being used to support this theory.

Ultraviolet laser development was initiated at the Loughborough University of Technology. The results presented in this report discuss some possibilities, associated with the emergent technology of sol-gel glass, for the generation of novel optical elements for intra-cavity use in ion lasers. The special low absorbance of densified sol-gel glass leads to unusual absorption spectra with full transmittance extending out to the theoretical band edge in the ultra violet. We report an unusual find associated with the performance of a sol-gel etalon in an Argon-Ion laser. It has been observed that a plane parallel etalon made of sol-gel prepared and densified silica has shown single mode power from the cavity of an ion laser approaching that of the single line power before the etalon is fitted. Some theoretical sketches are outlined to explain the phenomenon.

LIST OF PROFESSIONAL PERSONNEL ASSOCIATED WITH THE RESEARCH EFFORT

Jean-Luc R. Noguès - Vice President of R&D and Present Principal Investigator
Tony J. LaPaglia - President & CEO
Joseph L. Lombardi - Controller
Canan Balaban - Manager of Manufacturing and Engineering
Rong-Shenq Sheu - Research Scientist
William V. Moreshead - Research Scientist
Fred Chapman - Group Support Engineer
Larry L. Hench - University of Florida (AMRC) - Subcontract Manager and Former Principal Investigator
Jon K. West - University of Florida (AMRC) - Subcontract Manager
Robert W. Gould - University of Florida (AMRC) - Former Subcontract Manager
John E. Midwinter - University College London - Subcontract Manager
Michael T. Flanagan - University College London
Margaret M. Stallard - University College London
Harry J. Cole - University of Manchester - Subcontract Manager
Helen F. Gleeson - University of Manchester
Terry A. King - University of Manchester - Subcontract Manager
Andrew J. Berry - University of Manchester
Daniel J. Shaw - University of Manchester
C. Whitehurst - University of Manchester
Nicholas J. Phillips - Loughborough Univ. of Technology - Subcontract Manager

LIST OF PUBLICATIONS AND PRESENTATIONS

1. **Sol-Gel Processing of Large Silica Optics** - L.L. Hench, M.J.R. Wilson, C. Balaban, J.L. Noguès - Presented and Published in the Proceedings of the Fourth International Ultrastructure Symposium on Processing of Ceramics, Glasses and Composites, Tucson (1989)

2. **Sol-Gel Derived Titania-Silica Gel-Glasses** - Y.C. Cheng, L.L. Hench - Presented and Published in the Proceedings of the Fourth International Ultrastructure Symposium on Processing of Ceramics, Glasses and Composites, Tucson (1989)

3. **Structural Analysis of Water Adsorbed in the Pores of Alkoxide Derived Silica Gel Monoliths** - S. Wallace, L.L. Hench - Presented and Published in the Proceedings of the Fourth International Ultrastructure Symposium on Processing of Ceramics, Glasses and Composites, Tucson (1989)

4. **Quantum Calculations on Sol-Gel Silica Clusters** - J.K. West, S. Wallace, L.L. Hench, C.R. Lishawa - Presented and Published in the Proceedings of the Fourth International Ultrastructure Symposium on Processing of Ceramics, Glasses and Composites, Tucson (1989)

5. **Micro-Optical Arrays for Stacked Planar Optics** - M.M. Stallard - Presented at the US-UK Optical Glass and Macromolecular Materials Symposium #1, Pitlochry (1988)

6. **Optimisation of New Liquid Crystal Systems and their Incorporation into Gelsil® Matrices** - H.F. Gleeson, H.J. Cole - Presented at the US-UK Optical Glass and Macromolecular Materials Symposium #1, Pitlochry (1988)

7. **Gelsil® Matrices for Liquid Crystals** - H.J. Coles, H.F. Gleeson - Presented at the US/UK Optical Glass and Macromolecular Materials Symposium #1, Pitlochry (1988)

8. **Development of Tunable Doped Gel-Silica Glass Lasers** - A.J. Berry, T.A. King - Presented at the US-UK Optical Glass and Macromolecular Materials Symposium #1, Pitlochry (1988)

9. **Laser Densification of Sol-Gel Matrices** - D.J. Shaw, A.J. Berry, T.A. King - Presented at the US-UK Optical Glass and Macromolecular Materials Symposium #1, Pitlochry (1988)

10. **Novel Intra-Cavity Elements for Use in Ion Lasers Using Sol-Gel Glass Technology** - N.J. Phillips - Presented at the US-UK Optical Glass and Macromolecular Materials Symposium #1, Pitlochry (1988)

11. **Intra-Cavity Optical Elements for Lasers Using Sol-Gel Glass** - N.J. Phillips - Presented at the US-UK Optical Glass and Macromolecular Materials Symposium #1, Pitlochry (1988)

12. **Porous Gel-Silica, a Matrix for Optically Active Components** - J.L. Noguès and W. V. Moreshead - Published in the Proceedings of the Fifth International Workshop on Glasses and Ceramics from Gels, Rio de Janeiro (1989)

13. **Processing, Properties and Applications of Sol-Gel Silica Optics** - J.L. Noguès and A.J. LaPaglia - Presented and Published in the Proceedings of The International Society for Optical Engineering, San Diego (August, 1989)

14. **Preparation, Processing, and Fluorescence Characteristics of Neodymium-Doped Silica Glass Prepared by the Sol-Gel Process** - W.V. Moreshead, J.L. Noguès, and R.H. Krabill - Presented and Published in the Proceedings of the Fifth International Workshop on Glasses and Ceramics from Gels, Rio de Janeiro (1989)

15. **Processing of Gel-Silica Monoliths for Optics, Drying Behavior of Small Pore Gels** - L.L. Hench and M.J.R. Wilson - To be Published.

16. **Structural Evolution During Sintering of Optical Sol-Gel Silica** - W.L. Vasconcelos, R.T. DeHoff, and L.L. Hench - Presented and Published in the Proceedings of the Fifth International Workshop on Glasses and Ceramics from Gels, Rio de Janeiro (1989)

17. **Physical Evolution of Gel-Silica Monoliths** - W.L.Vasconcelos, R.T. DeHoff, and L.L. Hench -Presented and Published in the Proceedings of the First Florida-Brazil Seminar on Materials, Rio de Janeiro (1989)

18. **Molecular Orbital Modeling of Water Adsorption on a Tetrasiloxane Ring** - J.K.

West and S. Wallace - Presented and Published in the Proceedings of the Better Ceramics Through Chemistry IV Symposium of the Materials Research Society, San Francisco (1990)

19. **Quantum Chemistry of Sol-Gel Silica Clusters** - J.K.West, B.F. Zhu, Y.C. Cheng, and L.L. Hench - Presented and Published in the Proceedings of the Fifth International Workshop on Glasses and Ceramics from Gels, Rio de Janeiro (1989

20. **Liquid Crystals in Gel-Silica Matrices** - H.J. Coles and H.F. Gleeson - Presented at the US/UK Optical Glass and Macromolecular Materials Symposium #2, Ilkley (1989)

21. **Organic Dyes in Silica Glass** - C. Whitehurst, D. Shaw, and T. A. King - Presented at the US/UK Optical Glass and Macromolecular Materials Symposium #2, Ilkley (1989)

22. **Laser Densification of Sol-Gel Silica Glass** - D.J. Shaw, A.J. Berry, and T.A. King - Presented at the International Conference for Non-linear and Electro-optics, Cambridge (1989). Published in Inst. Phys. Conf. Ser. No 103: Part 1, p85

23. **Laser Densification Modeling** - T. Chia, L.L. Hench, C. Qin, and C.K. Hsieh - Presented and Published in the Proceedings of the Better Ceramics Through Chemistry IV Symposium of the Materials Research Society, San Francisco (1990)

24. **Multifunctional Silica Optics** - L.L. Hench and A. Fosmoe - Presented and Published in the Proceedings of the Materials Research Society Fall Meeting, Boston (1989)

25. **Characterisation of Doped Sol-Gel Derived Silica Hosts for Use in Tunable Glass Lasers** - A.J. Berry, T.A. King - Published in J. Phys. D: Appl. Phys. **22** (1989) 1419-1422

26. **Progress in the Study of Gel-Silica Optics for Intra-Cavity Laser Use** - N.J. Phillips - Presented at the US/UK Optical Glass and Macromolecular Materials Symposium #2, Ilkley (1989)

CONTENTS

1. INTRODUCTION

Many SDIO/AFOSR programs involve precision optical components, often requiring unique combinations of low weight, good strength, and special optical, thermal and radiation resistant characteristics. GELTECH's low temperature sol-gel technology offers the potential for rapid production of large, near net shape optical components with a wide range of optical and physical properties not possible with classical glass melting methods that require very high temperatures. In addition, GELTECH's technology may lead to the development of new optically active components.

The GELTECH sol-gel optics technology uses proprietary drying control chemical additives (DCCA's), developed in the beginning at the University of Florida with support by the Air Force Office of Scientific Research. The DCCA's and special low temperature thermal schedule, developed later in GELTECH's laboratories, make it possible to control the hydrolysis and condensation chemical reactions that produce both pure silica and multicomponent silica solid structures from liquid chemical precursors such as tetramethoxysilane (TMOS) and tetraethoxysilane (TEOS). The low temperatures involved make total computer control of the continuous mixing, casting, gelation, aging, drying and densification stages of sol-gel derived near net shape optics a goal with a very high pay off if successful. In contrast, traditional optical glass manufacture involves very high temperature, long annealing schedules, extensive grinding and polishing, considerable labor, and energy.

Low temperature sol-gel processing of ultrahigh purity, ultrahomogeneous silica (GELSIL®) offers enormous potential for the development of new optical components and systems with unique capabilities. GELTECH's sol-gel silica optics facility, supported by AFOSR, has successfully produced GELSIL® optical blanks with uniquely low absorption in the UV visible, and near IR.

With SDI-ISTO/AFOSR support, GELTECH Inc. is putting into operation a sol-gel optics research laboratory capable of making prototype advanced optical components of sufficient quantity to establish statistically based optical design parameters and lifetime predictions. This is a unique optical materials laboratory because it uses full computer control of a continuous batch process for making and studying chemically derived optical components. Consequently, ultrahigh purity can be achieved and maintained for the preparation of optical prototypes required for the research programs. It has never before been possible to achieve such high levels of purity in sol-gel derived optical components, and maintain the purity from sample to sample and batch to batch. This capability offers many totally new possibilities for achieving advanced optical systems.

Because of ultrapure processing, sol-gel derived silica has a uniquely low coefficient of

thermal expansion (CTE) over the temperature range of 40℃ to 700℃. Research at GELTECH and Advanced Materials Research Center (AMRC) has also shown that GELSIL® can serve as host matrix for rare earth elements such as Ce, Er, and Nd, thus establishing the possibility for a high intensity solar powered Q-switched glass laser. Successful doping of the GELSIL® matrix with metallic oxides including all of the transition elements has also been achieved. This generic doping process, combined with a unique manipulation of index of refraction by density gradients, opens up the possibility for new designs of graded refractive index lenses, micro-optical arrays, planar silica waveguides, optical couplers, radiation hard optical storage devices, fast holographic storage, matrices for non-linear optics, and eventually a low power optical computer and solar powered high intensity laser.

In order to take full advantage of the unique capabilities of the GELSIL® process, considerable effort has been devoted during the last two years to developing international collaboration in the field of advanced optical systems. This Final Technical Report summarizes the research accomplished in both laboratories in the United States and the United Kingdom. The goal is to produce a new generation of advanced optical systems based upon sol-gel technology. This report emphasizes interaction with optics programs in the United kingdom which have world leadership capabilities. Special sections of this report are included in the fields of: 1) sol-gel basic science; 2) micro-optical arrays; 3) liquid crystal NLO matrices; 4) laser densified optics; 5) tunable laser; and 6) UV laser optics.

The overall management and program coordination of this contract is performed by GELTECH Inc. The company administers subcontracts with the University of Florida and several Universities in the United Kingdom, and compiles regular project evaluation reports. The program plan for the US/UK sol-gel science optics collaboration is presented in Figure 1.

In addition, GELTECH conducts sol-gel basic research for the preparation of porous and dense optical prototypes which are characterized and/or used in the subcontractor's research programs.

A brief summary of each subcontractor's research programs are given below, and the results of the research accomplished during this contract are given in the following sections of this Final Technical Report.

Note: Some of the results presented in this Final Technical Report are from research programs partially funded, in addition to the US-UK contract, by AFOSR contracts #F49620-85-C-0079, F49620-86-C-0120 and F49620-89-C-0006.

The University of Florida - Advanced Materials Research Center (AMRC)
Professor Larry Hench, Dr. Jon West and Dr. Robert Gould

The University of Florida Advanced Materials Research Center is coordinating a subcontract which involves studies in sol-gel science to support the research being conducted in GELTECH and the Universities in the UK.

The AMRC research focuses on three objectives: 1) Sol-gel optical science, necessary to produce controlled gradients of ultrastructure and dopants in sol-gel derived glass matrices; 2) Ultrastructure characterization, necessary to interpret and predict performance of unique optical designs using sol-gel derived matrices; 3) Processing-property relationships, particular to the components defined by the joint UK-US investigative teams. This research is conducted under the direction of Dr. L.L. Hench and J.K. West.

The sol-gel chemical science studies extend the exploratory work already initiated in the AFOSR-MIRP program. The work includes measurements of diffusion coefficients of dopant elements that can produce localized index of refraction gradients and specific index profiles. The measurements are performed as a function of ultrastructural density gradients.

Drs. R.W. Gould and J.K. West performed measurements of ultrastructural densities which will be correlated and interpreted using precision X-ray diffraction analyses of pair function distribution functions. Previous studies on fast neutron radiation damaged fused silica, directed by Profs. Gould and Hench, showed localized regions of order in the amorphous matrix. Precise true density measurements of GELSIL® optical samples also indicate such ultrastructural characteristics. These results of high localized densities must be confirmed by precise X-ray analyses in order to know the appropriate localized densities and indices of refraction to use in calculations of graded index optics and solar powered laser studies.

Likewise, processing-property relationships, including mechanical and thermal properties as well as optical must be established for specific ultrastructural densities in order for predictive equations to be written. The AMRC also includes quantum chemistry calculations for molecular orbital modeling of water absorption on tetrasiloxane rings.

It is very important that the research efforts include a strong understanding of the structure and behavior of sol-gel glasses at the molecular level.

University College London
Professor John Midwinter, Dr. Mike Flanagan and Dr. Margaret Stallard

This is a very large, well-staffed program in electro-optics, waveguides, optical information processing, laser enhanced processing, and micro-optics. Extensive discussions between Professor Midwinter and his research team, GELTECH and AMRC have identified the field of micro-optical arrays as one which should benefit greatly from a collaboration. It should be possible to control the diffusion profiles of index modifiers in the ultraporous pure silica gel matrix to a high level of precision, thereby producing the cross sectional index profiles required for various types of micro-optical arrays. Upon densification, the microdiffusion arrays will become

incorporated within the silica glass network.

Because the array is established by diffusion into the ultraporous matrix at ambient temperature instead of high temperature diffusion into bulk glass, it should be possible to apply electrical fields to modify the index profiles with considerable precision. Thus, this effort interfaces with the sol-gel silica waveguide program being launched at the University of Florida by Professor Ramaswamy under AFOSR support.

GELTECH, Inc. was providing the well characterized silica matrices to Prof. Midwinter's team for development of the micro-optical arrays, Prof. Ramaswamy for development of field assisted planar waveguides and Prof. Hench and AMRC for establishing fundamental relationships between the diffusion kinetics, ultraporosity, and indices of refraction of GELSIL®.

University of Manchester - Liquid Matrices
Dr. H. Cole and Dr. H. Gleeson

The first collaborative research project with the Department of Physics at the University of Manchester is with Dr. Harry Cole's research groups on non-linear optical polymers. The emphasis in this project is the use of ultraporous GELSIL® matrices as hosts for liquid crystals and polymer doped liquid crystal mixtures. Special emphasis is given to systems with potentially high multiplexing capability.

University of Manchester - Laser Densified Sol-Gel Matrices
Dr. T. King, Dr. A. Berry, and Dr. Shaw

The second collaborative research program with the Department of Physics at the University of Manchester is with Dr. Terry King's research group. A first research project with Dr. King's Laser Research Laboratory is laser enhanced densification of sol-gel derived silica matrices. The goals are: 1) to understand the nature of the laser radiation interaction with the porous gel-glass matrix; 2) to investigate the glass structure produced during laser densification; 3) compare the efficiency and structures resulting from both 10.6 μm CO_2 lasers and lasers in the 2.5-3.0 μm and 200-300 nm region with deeper penetration; and 4) establish the feasibility of using lasers for surface densification of large lightweight mirrors, micro-optical arrays, planar waveguides, etc.

University of Manchester - Tunable Solid State Glass Lasers
Dr. T. King and Dr. A Berry

A second project to collaborate on the optical physics of tunable solid state glass lasers is also in progress with Dr. T. King's Laser Research Laboratory. Two types of tunable gas and

liquid lasers are now in production in Manchester Science Park at a spinoff corporation from the University, VUMAN lasers, resulting from Dr. Terry King's research. The goal of this UK-US collaboration is based upon use of specific doping of GELSIL® optical components to achieve a high power tunable glass laser using GELSIL® laser hosts.

Loughborough University of Technology
Dr. N. Phillips

The Physics Department a the University of Loughborough have had a world class laser R&D program for many years. Several visits by Prof. Hench indicate that collaboration in high precision UV lasers should be very promising. The advanced laser technology is already in place at the University of Loughborough but performance is limited by the UV absorption of traditional silica optics. The ultralow UV absorption of GELTECH's GELSIL® should result in a major advancement in UV laser design.

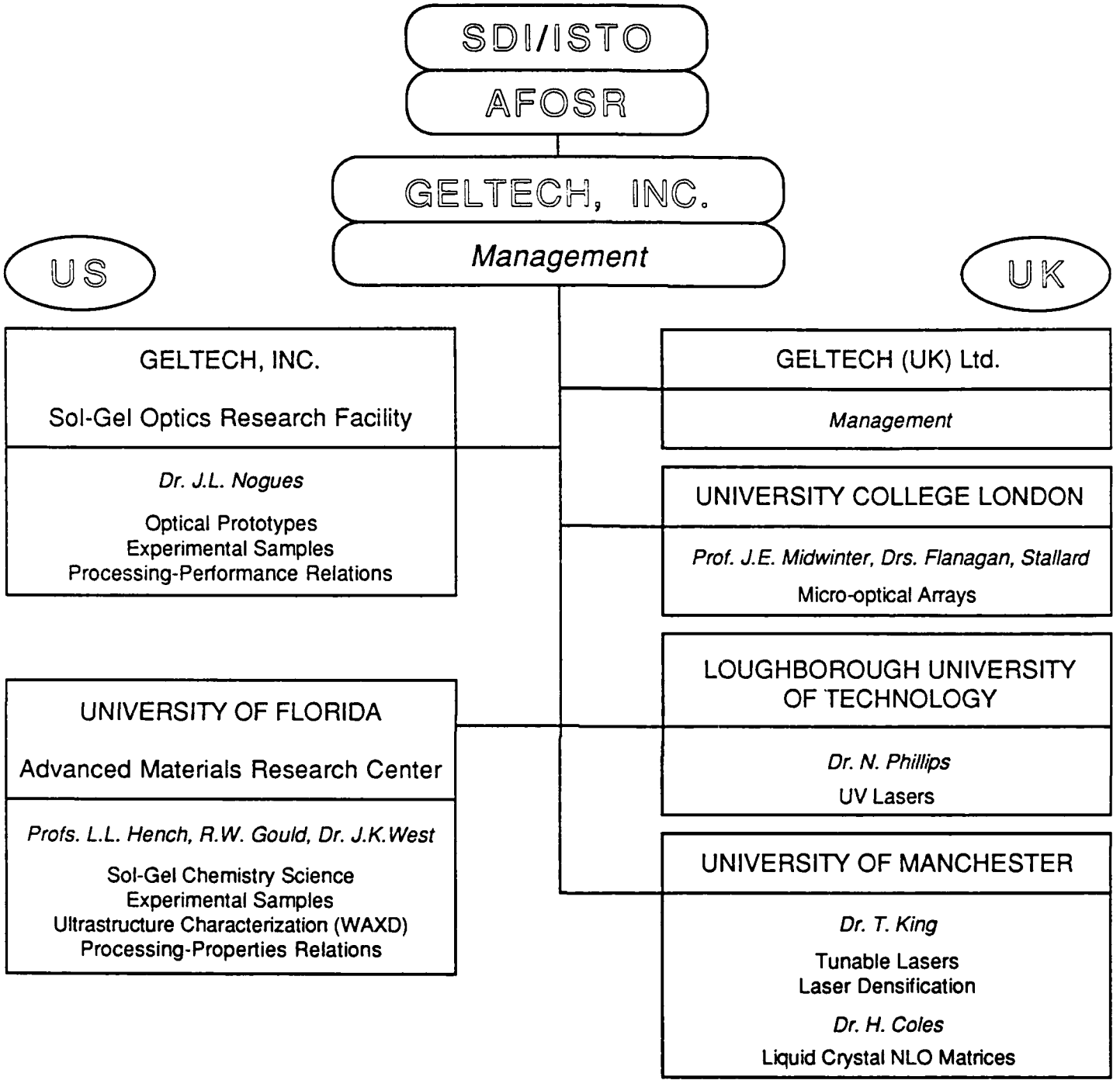

Figure 1

Program Plan for

US-UK SOL-GEL SCIENCE OPTICS COLLABORATION

2. PREPARATION OF SILICA OPTICAL PROTOTYPES

2.1 Preparation of Porous Gel-Silica Optical Prototypes

•Appendix 2: **Porous Gel-Silica, a Matrix for Optically Active Components** - J.L. Noguès and W. V. Moreshead - Published in the Proceedings of the Fifth International Workshop on Glasses and Ceramics from Gels, Rio de Janeiro (1989)

2.2 Preparation of Dense Gel-Silica Optical Prototypes

•Appendix 1: **Sol-Gel Processing of Large Silica Optics** - L.L. Hench, M.J.R. Wilson, C. Balaban, J. L. Noguès - Presented and Published in the Proceedings of the Fourth International Ultrastructure Symposium on Processing of Ceramics, Glasses and Composites, Tucson (1989). The full paper is printed in the Annual Technical Report (March, 1989). Abstract and Conclusions are given in Appendix 1.

•Appendix 3: **Processing, Properties and Applications of Sol-Gel Silica Optics** - J.L. Noguès and A.J. LaPaglia - Presented and Published in the Proceedings of The International Society for Optical Engineering, San Diego (August, 1989)

2.3 Preparation of Multicomponent Gel-Silica Optical Prototypes

•Appendix 1: **Sol-Gel Derived Titania-Silica Gel-Glasses** - Y.C. Cheng, L.L. Hench - Presented and Published in the Proceedings of the Fourth International Ultrastructure Symposium on Processing of Ceramics, Glasses and Composites, Tucson (1989). The full paper is printed in the Annual Technical Report (March, 1989). Abstract and Conclusions are given in Appendix 1.

•Appendix 4: **Preparation, Processing, and Fluorescence Characteristics of Neodymium-Doped Silica Glass Prepared by the Sol-Gel Process** - W.V. Moreshead, J.L. Noguès, and R.H. Krabill - Presented and Published in the Proceedings of the Fifth International Workshop on Glasses and Ceramics from Gels, Rio de Janeiro (1989)

3. SOL-GEL BASIC SCIENCE PROGRAMS

3.1 Structural Analysis of Porous Gel-Silica Monoliths

•Appendix 1: **Structural Analysis of Water Adsorbed in the Pores of Alkoxide Derived Silica Gel Monoliths** - S. Wallace, L.L.Hench - Presented and Published in the Proceedings of the Fourth International Ultrastructure Symposium on Processing of Ceramics, Glasses and Composites, Tucson (1989). The full paper is printed in the Annual Technical Report (March, 1989). Abstract and Conclusions are given in Appendix 1.

•Appendix 5: **Processing of Gel-Silica Monoliths for Optics, Drying Behavior of Small Pore Gels** - L.L. Hench and M.J.R. Wilson - To be Published.

•Appendix 6: **Structural Evolution During Sintering of Optical Sol-Gel Silica** - W.L. Vasconcelos, R.T. DeHoff, and L.L. Hench - Presented and Published in the Proceedings of the Fifth International Workshop on Glasses and Ceramics from Gels, Rio de Janeiro (1989)

•Appendix 7: **Theory of Thermal Expansion** -Y.C. Cheng - Interim Research Report (1989)

•Appendix 8: **Physical Evolution of Gel-Silica Monoliths** - W.L.Vasconcelos, R.T. DeHoff, and L.L. Hench -Presented and Published in the Proceedings of the First Florida-Brazil Seminar on Materials, Rio de Janeiro (1989)

3.2 Quantum Calculations on Gel-Silica

•Appendix 1: **Quantum Calculations on Sol-Gel Silica Clusters** - J.K. West, S. Wallace, L.L. Hench, C.R. Lishawa - Presented and Published in the Proceedings of the Fourth International Ultrastructure Symposium on Processing of Ceramics, Glasses and Composites, Tucson (1989). The full paper is printed in the Annual Technical Report (March, 1989). Abstract and Conclusions are given in Appendix 1.

•Appendix 9: **Molecular Orbital Modeling of Water Adsorption on a Tetrasiloxane Ring** - J.K. West and S. Wallace - Presented and Published in the Proceedings of the Better Ceramics Through Chemistry IV Symposium of the Materials Research Society, San Francisco (1990)

•Appendix 10: **Quantum Chemistry of Sol-Gel Silica Clusters** - J.K.West, B.F. Zhu, Y.C. Cheng, and L.L. Hench - Presented and Published in the Proceedings of the Fifth International Workshop on Glasses and Ceramics from Gels, Rio de Janeiro (1989)

4. POROUS GEL-SILICA OPTICAL RESEARCH PROGRAMS

4.1 Micro-optical Components Fabricated in Gel-Silica Glass

•Appendix 1: **Micro-Optical Arrays for Stacked Planar Optics** - M.M. Stallard - Presented at the US/UK Optical Glass and Macromolecular Materials Symposium #1, Pitlochry (1988). The full paper is printed in the Annual Technical Report (March, 1989). Abstract and Conclusions are given in Appendix 1.

4.2 Gelsil® Matrices for Liquid Crystal and Laser Dyes

•Appendix 1: **Optimisation of New Liquid Crystal Systems and their Incorporation into Gelsil® Matrices** - H.F. Gleeson and H.J. Coles - Presented at the US/UK Optical Glass and Macromolecular Materials Symposium #1, Pitlochry (1988). The full paper is printed in the Annual Technical Report (March, 1989). Abstract and Conclusions are given in Appendix 1.

•Appendix 1: **Gelsil® Matrices for Liquid Crystals** - H.J. Coles and H.F. Gleeson - Presented at the US/UK Optical Glass and Macromolecular Materials Symposium #1, Pitlochry (1988). The full paper is printed in the Annual Technical Report (March, 1989). Abstract and Conclusions are given in Appendix 1.

•Appendix 11: **Liquid Crystals in Gel-Silica Matrices** - H.J. Coles and H.F. Gleeson - Presented at the US/UK Optical Glass and Macromolecular Materials Symposium #2, Ilkley (1989)

•Appendix 12: **Organic Dyes in Silica Glass** - C. Whitehurst, D. Shaw, and T. A. King - Presented at the US/UK Optical Glass and Macromolecular Materials Symposium #2, Ilkley (1989)

4.3 Laser Densification of Sol-Gel Matrices

•Appendix 1: **Laser Densification of Sol-Gel Matrices** - D.J. Shaw, A.J. Berry, T.A. King - Presented at the US/UK Optical Glass and Macromolecular Materials Symposium #1, Pitlochry (1988). The full paper is printed in the Annual Technical Report (March, 1989). Abstract and Conclusions are given in Appendix 1.

•Appendix 13: **Laser Densification of Sol-Gel Silica Glass** - D.J. Shaw, A.J. Berry, and T.A. King - Presented at the International Conference for Non-linear and Electro-optics, Cambridge (1989). Published in Inst. Phys. Conf. Ser. No 103: Part 1, p85

•Appendix 14: **Laser Densification Modeling** - T. Chia, L.L. Hench, C. Qin, and C.K. Hsieh - Presented and Published in the Proceedings of the Better Ceramics Through Chemistry IV Symposium of the Materials Research Society, San Francisco (1990)

4.4 Gelsil® Matrices for Transpiration Cooled Windows

•Appendix 15: **Multifunctional Silica Optics** - L.L. Hench and A. Fosmoe - Presented and Published in the Proceedings of the Materials Research Society Fall Meeting, Boston (1989)

5. DENSE GEL-SILICA OPTICAL RESEARCH PROGRAMS

5.1 Tunable Solid State Glass Laser

•Appendix 1: **Development of Tunable Doped Gel-Silica Glass Lasers** - A.J. Berry, T.A. King - Presented at the US/UK Optical Glass and Macromolecular Materials Symposium #1, Pitlochry (1988). The full paper is printed in the Annual Technical Report (March, 1989). Abstract and Conclusions are given in Appendix 1.

•Appendix 16: **Characterisation of Doped Sol-Gel Derived Silica Hosts for Use in Tunable Glass Lasers** - A.J. Berry, T.A. King - Published in J. Phys. D: Appl. Phys. **22** (1989) 1419-1422

5.2 Ultraviolet Laser Development

•Appendix 1: **Novel Intra-Cavity Elements for Use in Ion Lasers Using Sol-Gel Glass Technology** - N.J. Phillips - Presented at the US/UK Optical Glass and Macromolecular Materials Symposium #1, Pitlochry (1988). The full paper is printed in the Annual Technical Report (March, 1989). Abstract and Conclusions are given in Appendix 1.

•Appendix 1: **Intra-Cavity Optical Elements for Lasers Using Sol-Gel Glass** - N.J. Phillips - Presented at the US/UK Optical Glass and Macromolecular Materials Symposium #1, Pitlochry (1988). The full paper is printed in the Annual Technical Report (March, 1989). Abstract and Conclusions are given in Appendix 1.

•Appendix 17: **Progress in the Study of Gel-Silica Optics for Intra-Cavity Laser Use** - N.J. Phillips - Presented at the US/UK Optical Glass and Macromolecular Materials Symposium #2, Ilkley (1989)

APPENDIX 1

Sol-Gel Processing of Large Silica Optics

L.L. Hench, M.J.R. Wilson, C. Balaban, J.L. Noguès

Presented and Published in the Proceedings of the Fourth International Ultrastructural Symposium on Processing of Ceramics, Glasses and Composites, Tucson (1989)

Abstract

Since the first Ultrastructure Processing Conference the progress made in sol-gel science allowed the development of two new types of optical silica. A fully dense sol-gel derived silica, termed Type V Gel-Silica, can be made either with a colloidal or an organometallic process. An optically transparent porous silica, termed Type VI Gel-Silica can be made by the organometallic route and can be used for applications such as an optical element with a second phase impregnated within the pores or as a substrate for laser written waveguides.

The major progress was made in size scale-up by: 1) developing an understanding of the chemical mechanisms involved in sol-gel glass processing, and 2) establishing careful process controls for each processing step. This progress allowed the production of optics of 75 and 100 mm in diameter or larger for both Type V and Type VI silicas respectively.

The physical properties of the organometallic derived Type V Gel-Silica are equal or superior to Types I-IV optical silicas and include: short UV cutoff, low optical absorption throughout the spectrum, high homogeneity, very few defects, low strain birefringence, and low coefficient of thermal expansion.

Both the colloidal and the organometallic methods can be used to produce complex net shapes by direct casting at ambient temperature. This unique property of the sol-gel process can be used to make optics with special shapes and surface features such as lightweight mirrors, Fresnel lenses and aspheric optical components.

Conclusions

Since the first Ultrastructure Processing Conference the progress made in sol-gel science allowed the development of two new types of optical silica. A fully dense sol-gel derived silica, termed Type V Gel-Silica, can be made either with a colloidal process or an organometallic process. The colloidal method results in optically opaque gels due to large pores of >200 nm in diameter with ≥80% porosity requiring 1500-1720°C densification temperatures. The organometallic process results in optically transparent gels with 45% pores of only 2.5 nm in diameter and require a densification temperature of only 1150°C. An optically transparent sol-gel derived porous silica, termed Type VI Gel-Silica can be made by the organometallic route. This new type of silica can be used for applications such as an optical element with a second phase

impregnated within the pores or as a substrate for laser written waveguides.

The major progress was made in size scale-up. This was achieved by: 1) developing an understanding of the chemical mechanisms involved in each of the seven sol-gel-glass processing steps, and 2) establishing careful process controls for each processing step. It is the precise control over the chemical mechanisms and rates of reactions that allows the production of optics of 75 and 100 mm in diameter or larger for both Type V and Type VI silicas respectively.

The physical properties of the organometallic derived Type V Gel-Silica are equal or superior to Types I-IV optical silicas and include: short UV cutoff, low optical absorption throughout the spectrum, high homogeneity, very few defects, low strain birefringence, and low coefficient of thermal expansion.

Both the colloidal and the organometallic methods of optical gel-silica manufacture can be used to produce complex net shapes by direct casting at ambient temperature. This unique property of the sol-gel process can be used to make optics with special shapes and surface features such as lightweight mirrors, Fresnel lenses and aspheric optical components.

Sol-Gel Derived Titania-Silica Gel-Glasses

Y.C. Cheng, L.L. Hench

Presented and Published in the Proceedings of the Fourth International Ultrastructure Symposium on Processing of Ceramics, Glasses and Composites, Tucson (1989)

Abstract

Monolithic titania-silica gels with 0-15% TiO_2 were prepared using organometallic sol-gel processing. During densification, bloating occurred in ambient static air but not in a controlled dried air atmosphere at a temperature of 800℃. This was attributed to the difference of the water content in the sample, since the controlled atmosphere is more effective in dehydrating the gels. The densification of gel-glass is enhanced as titania content increases. This is attributed to the introduction of more easily deformed Ti-O-Si bonds.

Conclusions

Large, monolithic TiO_2-SiO_2 gel-glasses were produced using organometallic sol-gel technology. The physical properties of the gel-glasses do not change significantly below 600℃ in either ambient static or controlled dried air atmosphere. Above 600℃, the properties change rapidly with densification temperature. Bloating of the samples was observed when sintering was carried out in ambient static but not in controlled dried air atmosphere. This was attributed to the difference in the water content of the samples which resulted in the difference in densification rates. The network structure is strengthened as densification temperature increases, as indicated by the increase in the wavenumbers of IR vibration peak. The vibrational band associated with TiO_4 tetrahedra is obtained at 945 cm^{-1}. The increase in densification with increasing titania concentration is explained in terms of the weaker nature of the Ti-O-Si bond, increasing the ease of structural rearrangement as titania content increases.

Structural Analysis of Water Adsorbed in the Pores of Alkoxide Derived Silica Gel Monoliths

S. Wallace, L.L. Hench

Presented and Published in the Proceedings of the Fourth International Ultrastructure Symposium on Processing of Ceramics, Glasses and Composites, Tucson (1989)

Abstract

The structure of water adsorbed into the pores of alkoxide derived silica gel monoliths is analyzed using Dielectric Relaxation Spectroscopy (DRS) and Differential Scanning Calorimetry (DSC). Assumptions about the pore geometry allow calculation of the thickness of the bound non-melting portion and the free portion of the adsorbed water. The thickness of the bound, non-freezing layer of adsorbed water is independent of the surface silanol concentration but increases with increasing temperature and/or average pore radius.

Conclusions

The structure of water adsorbed in the pores of alkoxide derived silica gels, and specifically the bound layer adjacent to the surface, is governed by the temperature and the geometry of the pores in these fractal materials rather than by the adsorbent-adsorbate physisorption interactions. Analysis by both DSC and DRS using flat and cylindrical models show that the thickness of the bound, non-freezing layer of adsorbed water is independent of silanol concentration, but increases with increasing temperature and/or average pore radius.

Quantum Calculations on Sol-Gel Silica Clusters

J.K. West, S. Wallace, L.L. Hench, C.R. Lishawa

Presented and Published in the Proceedings of the Fourth International Ultrastructure Symposium on Processing of Ceramics, Glasses and Composites, Tucson (1989)

Abstract

Quantum calculations for rings and chains of silica tetrahedra have been made using Huckel and Intermediate Neglect of Differential Overlap molecular orbital models. The structural energies indicate a limiting dimension for chain growth. Non-doped and doped clusters were used to determine the UV cutoff wavelength and the relative molecular energies for each structure. The theoretical UV cutoff wavelength and the relative molecular energies for each structure. The theoretical UV cutoff wavelength increases with increasing concentrations of Na^{+}, Al^{3+}, and OH^{-} ions.

Conclusions

The HMO molecular orbital model is relatively simple and can be run on personal computers. The INDO model is more sophisticated and consequently more accurate; it also requires larger computational power e.g. Sun Microsystem. The differences in the INDO structural energies between rings and chains indicate that chain structures are the most stable up to about 10-12 silica tetrahedra. The calculated UV cutoffs in the pure silica is lower than the experimental values, however the ring structures with 5 tetrahedra are close to experimental values of pure gel-silica optics. Small concentrations of hydroxyl , sodium, or water increase the UV cutoff wavelength, as expected.

Micro-Optical Arrays for Stacked Planar Optics

M.M. Stallard

Presented at the US-UK Optical Glass and Macromolecular Materials Symposium, Pitlochry (1988)

Abstract

Key components for stacked planar optical circuits are considered. In particular, the fabrication conditions favoring aberationless microlens arrays are discussed.

Conclusions

Microlens array is a key component in stacked planar optics. Standard fabrication techniques suffer from problems. An alternative approach is to use GELSIL™, which is compatible with fiber, makes the diffusions process more flexible, makes high index changes feasible, and has a high quality finished product.

Optimization of New Liquid Crystal Systems and their Incorporation into Gelsil™ Matrices

H.F. Gleeson and H.J. Coles

Presented at the US-UK Optical Glass and Macromolecular Materials Symposium, Pitlochry (1988)

Abstract

The aims of this project were to use GELSIL™ porous matrices as carriers for liquid crystal systems, thereby overcoming many of the problems associated with current liquid crystal devices. These difficulties include the construction of large area arrays, maintenance of a constant and accurate sample thickness of typically 5μm, electrical addressing of the liquid crystals, and where possible, increasing the switching speed of the medium. The use of porous GELSIL™ matrices can , in principle, contribute to the solution of all of these problems. They have potential for easy processing in large areas with a well-defined pore size, and the possibility of ion impregnation together with the matrices' high optical integrity makes them ideal candidates for new liquid crystal display (and non-display) applications. We can summarize our displays objectives as follows:

(a) low cost
(b) large area
(c) lightweight
(d) low power and voltage drivers
(e) high brightness and contrast

Our approach is to use the fast bistable switching of fluorescent and dichroic dyed ferroelectric liquid crystals in rigid porous sol-gel matrices.

The program to date has essentially progressed in two complementary directions:

i) the optimization of new liquid crystal systems for use in displays, and,
ii) the incorporation of these and other more conventional materials into the GELSIL™ matrices.

In the first sections of this report we will consider each of these areas separately. In the final section we describe preliminary results showing magnetic-optic effects in liquid crystal filled

GELSIL™ matrices, and consider some new directions forward.

Conclusions

The program to date has allowed us to:

a) Solve many of the current display difficulties by modifying the liquid crystal materials. Our work will allow us to use much thicker samples ~ 10-20μm without significantly degrading the optical effects, thereby reducing some of the constraints previously placed on our requirement for thin (< 2μm) GELSIL™ matrices,

b) Develop an apparatus and technique for filling the GELSIL™ matrices with a variety of liquid crystal materials, and

c) Observe a magnetic field induced reduction in the intensity of light transmitted by a GELSIL™/l.c. matrix.

GELSIL™ Matrices for Liquid Crystals

H.J. Coles and H.F. Gleeson

Presented at the US-UK Optical Glass and Macromolecular Materials Symposium, Pitlochry (1988)

Abstract

The work carried out in this research program may be effectively divided into three separate but complimentary areas which are detailed below.

a) Ferroelectric Liquid Crystal Devices
The study of the guest-host effect in ferroelectric liquid crystal systems has been expanded and large area high contrast fluorescent ferroelectric displays have been demonstrated. In addition, fast, zero polarizer double devices have been made.

b) Magneto-Optics
Preliminary studies of magneto-optic effects in guest-host liquid crystal/GELSIL™ systems, presented in a previous report have been expanded. Some anomalous effects, not yet fully explained are reported here in detail.

c) Phase Behavior
There has been evidence that the liquid crystalline materials may be affected by contact with the GELSIL™ matrices. This possibility has been examined via differential scanning calorimetry (DSC). Pre-treatment of the GELSIL™ matrices to remove excess water has also been considered.

Some new effects have been considered which may be important for future work. A description of these possible new directions is given in the concluding section of the report.

Conclusions

Initial measurements of the fluorescence lifetime of the lasing level of Nd doped into GELSIL™ found it to be too short, indicative of concentration quenching. TEM measurements revealed the expected clumping of the Nd_2O_3 and we have shown that co-doping with a glass modifier such as Al prevents this effect provided the Al/Nd dopant ratio is high enough. We show, however, that the samples are still too "wet", residual OH^- probably being responsible for the still

rather short lifetimes and the low fluorescence efficiencies we are observing. OH^- can be removed in undoped samples, however, and we are confident, therefore, that a "dry" co-doped rod shaped sample will soon exhibit laser action.

Laser Densification of Sol-Gel Matrices

D.J. Shaw, A.J. Berry, T.A. King

Presented at the US-UK Optical Glass and Macromolecular Materials Symposium, Pitlochry (1988)

Abstract

A program for the development of densification techniques for sol-gel matrices, using lasers is presented. Work has concentrated on the use of a carbon dioxide laser to effect full densification of thin surface layers on partially densified discs. Using microhardness as a characterization method the upper (damage) threshold and lower energy thresholds to effect densification were measured as 6.32 ±0.25 and 4.26 ±0.25 Joules per square centimeter of surface irradiated, as opposed to calculated values of 11.31 and 7.42 J/cm^2 respectively.

Conclusions

The damage and densification energy thresholds have been measured as 6.32 ±0.25J/cm^2 and 4.26 ±0.25J/cm^2 respectively. These results, however, only hold for a laser power output of 17 Watts. With the laser giving our 8 Watts and the gel-silica disc moving at lower speeds through the beam, energies well above the previously measured damage threshold failed to densify a surface layer of gel-silica, i.e. there exists a time limit during which energy must be inputted into a given volume of gel in order to effect densification, otherwise thermal conduction stops the temperature of that volume rising high enough to effect densification.

Development of Tunable Doped Gel-Silica Glass Lasers

A.J. Berry, T.A. King

Presented at the US-UK Optical Glass and Macromolecular Materials Symposium, Pitlochry (1988)

Abstract

Initial measurements of laser relevant properties of neodymium doped GELSIL™ are described. Samples doped with ND only reveal anomalously short fluorescence lifetimes characteristic of concentration quenching, TEM measurements revealing clumping of the neodymium. Co-doping with aluminum allows better dispersion of the neodymium throughout the GELSIL™ matrix, but fluorescence lifetimes are still shorter than expected. Phonon quenching by residual OH^- ions is suspected, absorption. FTIR and Raman spectroscopy being used to support this theory.

Conclusions

Initial measurements of the fluorescence lifetime of the lasing level of Nd doped into GELSIL™ found it to be too short, indicative of concentration quenching. TEM measurements revealed the expected clumping of the Nd_2O_3 and we have shown that co-doping with a glass modifier such as Al prevents this effect provided the Al/Nd dopant ratio is high enough. We show, however, that samples are still too "wet", residual OH^- ions probably being responsible for the still rather short lifetimes and the low fluorescence efficiencies we are observing. OH^- can be removed in undoped samples, however, we are confident therefore that a "dry" co-doped rod shaped sample will soon exhibit laser action.

Novel Intra-Cavity Elements for Use in Ion Lasers Using Sol-Gel Glass Technology

N.J. Phillips

Presented at the US-UK Optical Glass and Macromolecular Materials Symposium, Pitlochry (1988)

Abstract

This paper discusses some possibilities associated with the emergent technology of sol-gel glass for the generation of novel optical elements for intra-cavity use in ion lasers. The special low absorptance of densified sol-gel glass leads to unusual absorption spectra with full transmittance extending out to the theoretical band edge in the ultra violet. We report an unusual find associated with the performance of a sol-gel etalon in an Argon-Ion laser. It has been observed that a plane parallel etalon made of sol-gel prepared and densified silica has shown single mode power from the cavity of an ion laser approaching that of the single line power before the etalon is fitted. Some theoretical sketches are outlined to explain the phenomenon.

Conclusions

Discussions have been presented of possible variations in intra-cavity optics for ion laser development. The materials of interest exhibit extremely low levels of UV absorption out to about 150nm and thus the work is seen to be of relevance particularly to the generation of coherent UV at 363.8 nm in an Argon ion laser.

It is evident from preliminary experiments that sol-gel silica samples have shown an immediate improvement over conventional fused silica etalons in the generation of single mode light with low loss.

Some possible configurations of etalons have been discussed and it is evident that the curvature proposed by Hariharan is a good idea in terms of alignment and stability. However, it must be concluded that if we do exploit the concentric etalon idea then the cavity instability proposed for the front part of the system i.e. between M_1 and M_2 is not necessary if the properties of the sol-gel element are carried over from the planar model. It is evidently a good idea to create concentric etalons in which all cavities are stable as well as models in which the destabilizing of the front part of the cavity is achieved.

In a general sense, the use of cast optical elements (cast against diffractive relief elements) opens the door to a new range of intra-cavity optical devices for wavelength selection. The problems of optical symmetry that this introduces need careful consideration however if losses are

to be avoided.

A this stage of the program, a modest level of work with replacement of the Brewster prism and windows is being attempted. the production of void-free silica is of course essential to this strategy.

The most interesting fact to emerge so far is the freak performance of the planar GELSIL™ etalon. Further theoretical work is well advanced to demonstrate the possibility that this success might be due to a variable index effect which is a natural consequence of the production method for sol-gel derived layers. Alternatively, the result may just be a natural consequence of reduced absorptance. Further work is necessary to confirm the mechanism.

Intra-Cavity Optical Elements for Lasers Using Sol-Gel Glass

N.J. Phillips

Presented?

Abstract

We examine some of the technical routes toward the understanding of the anomalous performance of sol-gel etalons used in the cavity of an Argon-ion laser to achieve single mode operation. The observance of unusual levels of conversion efficiency (the ratio of the single mode power output to the single line power output) may possibly be explained by the presence of refractive index gradients withing the etalon due to natural effects of densification in sol-gel glass. We present some of the theoretical ideas and report on progress in establishment of the laboratory program.

Conclusions

The first phase of work on the intracavity optics program has concentrated on the observations of the low insertion loss of sol-gel etalons. It is abundantly clear that graded index effects offer at least a preliminary avenue of investigation and that such territory is essentially new.

From the laser industry, we are still getting reports of difficulties with Brewster windows, i.e., the generation of very thin (2mm) but very flat optical windows. Thus although the etalon section is of great immediate interest the window problem is of significance to the manufacturing industry.

APPENDIX 2

POROUS GEL SILICA, A MATRIX FOR OPTICALLY ACTIVE COMPONENTS

Jean-Luc R. Noguès and William V. Moreshead

GELTECH, Inc., One Progress Blvd, Box 18, Alachua, Florida 32615 (USA)

Abstract

The sol-gel process has been used to prepare optically active components in a silica matrix. In most cases this involves introducing an optically active material such as an organic dye into the initial sol prior to gelation. An alternative sol-gel route involves first the preparation of porous, pure silica monoliths which can then be impregnated with the desired organic or inorganic material. Critical to the usefulness of this material is a knowledge of the properties, such as thermal stability, UV/vis/nIR spectra and pore size. In this paper the structural evolution of these porous silica monoliths prepared by the sol-gel process is presented as a function of process temperature. Sample preparation and thermal treatments are briefly described, and results of sample characterizations are given in detail. Results of this study and their implications for the usefulness of the materials will be discussed.

Subject index codes: a2, d10, o7, s5, s9.

1. Introduction

Over the past several years there has been an increasing interest in sol-gel techniques for the manufacture of glasses, glass-ceramics and ceramics. This new route has been utilized for a variety of products ranging from optical fibers and lenses to special coatings and to production of ultra-pure powders. As early as 1984 organic molecules were added to monoliths prior to gelation[1,2], porous thin films[3], and more recently partially densified monoliths[4].

The purpose of this paper is to focus in a first part on the processing and the properties of porous gel-silica glass monoliths to be used as matrix for the preparation of optically active components and new kinds of optical devices. This new material presents many properties of the dense pure silica glass but presents in addition many unique characteristics which could lead to very special and novel developments in optics. Several applications such as microoptical arrays, scintillation detectors and optical waveguides are briefly described in the second part of this paper.

2. Porous gel-silica matrix preparation, processing, and properties

2.1. Experimental

Porous gel-silica samples used in this study were manufactured by hydrolyzing a silica precursor, tetramethylorthosilicate (TMOS, Petrarch, Inc.) with deionized water. After complete homogenization this sol was cast into 60 mm polystyrene petri dishes to gel and age. The wet gel was then dried to give a transparent gel-silica monolith.

Further heat treatment was done in static air to study the evolution in gel properties with temperature. The rate of heating was selected low enough to maintain the monolithic aspect of the gels and to avoid a temperature gradient inside the sample which can cause heterogeneity in gel properties. Isotherms at 620°C and 800°C were observed to evacuate solvent and by-products from the gel structure, and to observe the evolution in sample properties during a soak. Samples were removed from the furnace at a given temperature and quenched in air at room temperature.

Shrinkage during densification was measured in static air using a Dupont 943 Thermomechanical analyzer (TMA). The heating rate was 0.5°C/min.

The textural characteristics were measured using an Autosorb-6 from Quantachrome Corporation. The results were analyzed according to the BET theory and a cylindrical pore model was used for the calculations of the pore radius distribution.

The density measurements were done on oven-dried samples using a specific gravity bottle with mercury as the fluid.

The microhardness was measured using a LECO Model-700 Microhardness Tester with a diamond Vickers indenter.

UV-vis-nIR spectra were recorded on a Lambda-9 Spectrophotometer from Perkin-Elmer.

2.2. Results and Discussion

Figure 1 presents the TMA thermogram of a dry gel monolith between room temperature and 685°C, the maximum temperature of the equipment. The heat treatment cycle was repeated three times without removing the sample from the cell, and with recalibration of the zero position before each cycle.

After the first cycle to 685°C the sample underwent a net shrinkage of 8.4% after returning to room temperature. After the second cycle the shrinkage was not negligible but was greatly reduced

(0.5%). A third cycle resulted in a total shrinkage of 0.2%.

These results lead to an important conclusion regarding the usefulness of these materials as porous matrixes: further heating to a temperature close to, equal to, or higher than the maximum temperature to which the gel has been previously heated will induce new variations in the structure of the gel-silica. However, a sample can be considered to be thermally stable at temperatures well below this maximum temperature.

Changes in other gel characteristics and properties measured for this study during densification are in good agreement. The results are summarized in table 1. These changes are smooth and regular as the treatment temperature is increased to 950℃. At this temperature the behavior of the gel changes drastically and the material loses its characteristics for porous matrix applications. Although the magnitude of the changes are greater for the soak at 620℃ than for the soak at 800℃, the trends were similar.

The transmission spectra of samples stabilized at 620, 900 and 950℃ show the well-known absorption bands due to the silanol groups (Si-OH) and the molecular water (figure 2).[5-7] With the stabilization temperature increasing, two phenomena occur: 1) the absorption bands decrease in intensity corresponding to the release of "water" by the sample, and 2) the transmission cutoff in the ultraviolet range shifts to lower wavelengths. For the sample stabilized at 950℃ the spectrum presents only the major absorption bands of the Si-OH.

Figure 3 shows the variation of the OH radical concentration in the gel as a function of temperature. The calculation of this OH radical content was done using a formula derived from the one used for OH content determination in silica glasses [8] and applied to the absorption band at 1.36 μm of the first overtone of the fundamental absorption peak of Si-OH groups (2.73 μm). Since the extinction coefficient is not presently available to quantify the water content using this band, the results are plotted in arbitrary units. However, this figure shows that the OH radical content in the gel decreases rapidly with increasing temperature

The data collected in this study allow the definition of three different sequences during the sintering treatment.

1) Between room temperature and 900℃ there is a continuous evolution of the gel properties. This evolution is faster for the higher temperatures, especially between 800℃ and 900℃. This evolution occurs mainly by loss of water. The specific surface area and the total pore volume decrease as a result of condensation reactions which cause the network to become more

and more interconnected without causing any change in the calculated average pore radius (figure 4). As interconnectivity increases the bulk density and microhardness increase by the same trend, as expected (Table 1). The trend in microhardness is illustrated in figure 3.

2) Between 900℃ and 950℃ the densification takes place more rapidly since the viscosity of the material is low enough to allow viscous sintering. Measured changes are much more dramatic.

3) Above 950℃, pores remaining in the sample begin to close resulting in bloating of the sample. At this stage the sample loses its transparency, its homogeneity and its ability to be used as porous matrix for optical components.

The ultrastructure data also shows that the sintering of this particular type of gel silica occurs without variation of the average pore size, maintaining or enhancing the optical transmission of the porous sample.

3. Potential applications of porous gel-silica matrices

The properties and characteristics of porous gel-silica, in particular porosity and transmission, make this material adequate for the development of new types of optical elements.[9] The porous phase of this gel-silica matrix can be filled with a second phase with very special properties to produce a composite material. The completely open porosity and the very small size of the pores allow the production of a nano-scale composite with good macro homogeneity. The doping phase can be either an inorganic material such as metallic cations or an organic compound which leads to the preparation of organic/inorganic composites. Examples of these two types of applications is briefly described below, as well as a possible direct application of the porous gel-silica matrix.

3.1. Microoptical arrays [10]

The basic components for digital optics have been identified as modulator and detector arrays, which in many cases require microlens arrays for imaging. Stacked planar optics is an attractive technology for digital optics, and can be used for many possible applications, such as optical computing, camera auto focus modules, or imaging bar lenses in photocopiers.

The basic unit of the array is the individual microlens which is a region with an index gradient embedded in a glass substrate as a result of selective doping. The actual manufacture of this type of lens is difficult and often leads to optical aberrations, limiting the number of components which

may be stacked together.

Sol-gel technology offers the possibility to minimize spatial aberration by doping a porous gel-silica matrix or preform. The porous gel-silica is doped selectively with polarisable ions, e.g. Ba^{2+}, or glass structure modifiers, e.g. Pb^{2+}, and the dopant elements are trapped in the glass by subsequent densification to form a microlens array.

3.2. Scintillations detectors [4]

Organic plastic scintillators have been used for particle detection for about thirty years. They have two advantages: 1) Fluorescence decay times as short as 1 nanosecond, and 2) Light output proportional to energy deposition in the detector. It is well known, however, that plastic scintillators are rather sensitive to ambient radiation which results in strong absorption of light for doses as small as 10^5 rd.

Scintillating glasses have been developed slowly over the last twenty five years but never came into general use as particle detectors. Because of the high temperature used in the production of glass, organic fluors were excluded as dopants and only inorganic dopants such as cerium and terbium oxides could be used. The advantages of scintillating glasses are that they are heavier and less sensitive to radiation than plastic scintillators. On the other hand, their fluorescence decay times have been found to be rather long.

To meet the present day rate and radiation dose requirements it would be desirable to have a scintillator with the high radiation resistance of pure silica glass and the short fluorescence decay time of organic fluors. Because of the high radiation resistance of silica, sol-gel technology opens the exciting possibility of doping glass with fast organic fluors which would provide an important advancement in particle detection. Although the sol-gel scintillators produced to date are far from being optimized, the first results prove the feasibility of producing a fast, radiation hard scintillator using the sol-gel process. Reference four explains in detail the optical characteristics of prototypes of fast, radiation hard scintillation detectors.

3.3. Optical waveguides

Optical waveguides on a glass substrate represent the basis for passive components such as multiplexers, couplers, or wavelength filters used in integrated optical applications for optical communication and sensors .

Various techniques for fabricating glass waveguides have been reported in the literature and include: techniques such as sputtering, ion implantation, ion-exchange, and chemical vapor deposition. Today, these last two techniques are the most successful. The ideal would be waveguides made in silica substrates, preferably without any dopant for tailoring the index profile, and maintaining the monolithic nature of the devices.

The sol-gel technology leading to the manufacture of porous gel-silica matrix offers a possible substrate for waveguides. Two approaches can be pursued. First, the selective doping of the substrate using controlled diffusion in the porous silica in order to change the refractive index of the material. Second, the local heating of some selected portion of the substrate to increase the density and index of refraction of the glass.[11] By CO_2 laser densification, optical waveguides have been made using laser writing of higher density tracks on porous gel-silica substrate.[12]

It was demonstrated that both of these techniques can induce the index of refractive changes of the right magnitude to fabricate single mode waveguides. The second technique presents the possibility to produce ideal pure silica waveguide. The major advantage of this type of waveguide is that it matches the index of refraction of silica fiber optics, which is not the case for ion-exchanged or diffusion based waveguides.

The technique of doping a pure gel-silica matrix with inorganic or organic compounds is not restricted to the applications described in this paper, but can be used for the preparation of a wide variety of optically active materials, such as optical filters [13], dye lasers, non linear optic components, optical data storage media, and many others.

4. Conclusion

This study showed that it is possible to produce stabilized sol-gel monoliths with a range of properties, and free of organic residues. The sintering of this type of gel silica occurs in roughly three stages, with the last resulting in pore closure and ultimate destruction of the sample above about 950℃. If heating is stopped prior to this a semi-stable, porous, gel-silica matrix can be produced. Demonstration of possible applications of such a matrix, such as microlens arrays, scintillating detectors, and waveguides have been reported.

Acknowledgments

The authors gratefully acknowledge financial support of Air Force Office of Scientific Research

Contracts #F49620-86-C-0120 and F49620-88-C-0010 and the encouragement of D. R. Ulrich throughout this research. Also the technical assistance of Robert H. Krabill is greatly appreciated.

References

1. D. Avnir, D. Levy, R. Reisfeld, J. Phys. Chem., 88 (1984) 5956.
2. A. Makishima, T. Tani, Com. Amer. Ceram. Soc., 69 (4) (1986) C72.
3. D. Avnir, V. R. Kaufman, R. Reisfeld, J. Non-Cryst. Solids 74 (1985) 395.
4. J. L. Noguès, S. Majewski, J. K. Walker, M. Bowen, R. Wojcik, W. V. Moreshead, J. Amer. Ceram. Soc., 71 (12) (1988) pp. 1159-63.
5. M. Grayson, Ed., Encyclopedia of Glass, Ceramics, and Cement, (John Wiley & Sons, NY, 1985).
6. R. F. Bartholomew, B. L. Butler, H. L. Hoover, C. K. Wu, J. Amer. Ceram. Soc., 63 (9-10) (1980).
7. D. L. Wood, E. M. Rabinovich, D. W. Johnson, JR., J. B. MacChesney, E. M. Vogel, J. Amer. Ceram. Soc., 66 (10) (1983).
8. J. E. Shelby, J. Vitco Jr., R. E. Benner, Com. Amer. Ceram. Soc., 65 (4) (1982).
9. L. L. Hench, S. H. Wang, J. L. Noguès, SPIE Vol. 878 Multifunctional Materials, (1988) pp 81-85
10. M.M. Stallard, "Microoptical arrays", Presented at the US-UK Optical Glass and Macromolecular *Materials Symposium, Pitlochry*, Scotland (1988).
11. R. V. Ramaswamy, T. Chia, R. Srivastava, A. Miliou, & J. West, SPIE Vol. 878 Multifunctional Materials, (1988) pp. 86-93.
12. D.J. Shaw, A.J. Berry, T.A. King, "Laser Densification of Sol-Gel Matrices", Same as Ref. 6.
13. S. H. Wang and L. L. Hench, in Science of Ceramic Chemical Processing, Edited by L. L. Hench and D. R. Ulrich., John Wiley & Sons, NY (1986) pp. 201-207

Table Caption

1. Properties and characteristics of porous gel-silica monoliths vs densification temperature

Figure Captions

1. Thermomechanical analysis of a porous gel-silica monolith
2. Optical transmission of gel-silica monolith vs densification temperature
3. OH Radical Content ([OH]) and Sample Microhardness (SMH) vs Densification Temperature
4. Specific Surface Area (SSA) and Total Pore Volume (TPV) vs Densification Temperature

Temperature °C	SSA sq.m/g	TPV cc/g	APR Å	SBD g/cc	SMH Kg/sq.mm	[OH] a.u.
200	768	0.47	12.2	1.172	41	193
400	707	0.42	11.8	1.224	65	189
550	672	0.39	11.7	1.299	88	172
620	620	0.37	11.8	1.308	101	161
620	537	0.31	11.6	1.391	97	157
700	522	0.30	11.6	1.393	115	143
750	449	0.26	11.7	1.424	160	132
800	438	0.26	11.8	1.438	183	122
800	393	0.23	11.7	1.460	--	122
850	--	--	--	1.502	233	94
900	290	0.17	11.8	1.510	285	66
950	9	0.01	13.9	2.113	447	9
1000	4	0.00	15.6	2.109	--	--
1050	3	0.00	16.8	1.651	--	--

SSA: specific surface area; TPV: total pore volume; APR: average pore radius;
SBD: sample bulk density; SMH: sample microhardness; [OH]: OH radical content

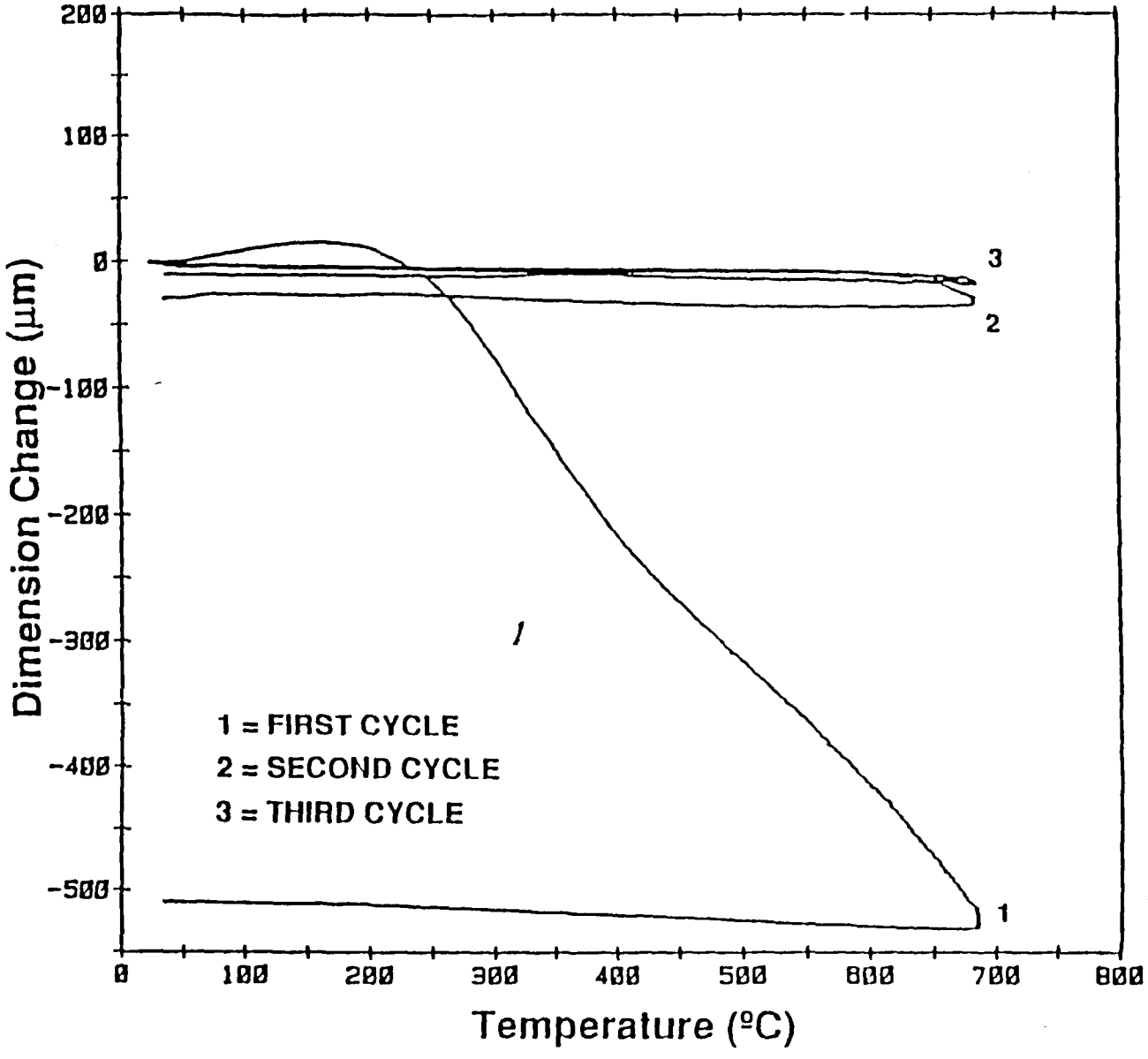
200
100
0
-100
-200
-300
-400
-500
Dimension Change (µm)
0
100
200
300
400
500
600
700
800
Temperature (°C)
1 = FIRST CYCLE
2 = SECOND CYCLE
3 = THIRD CYCLE
1
2
3

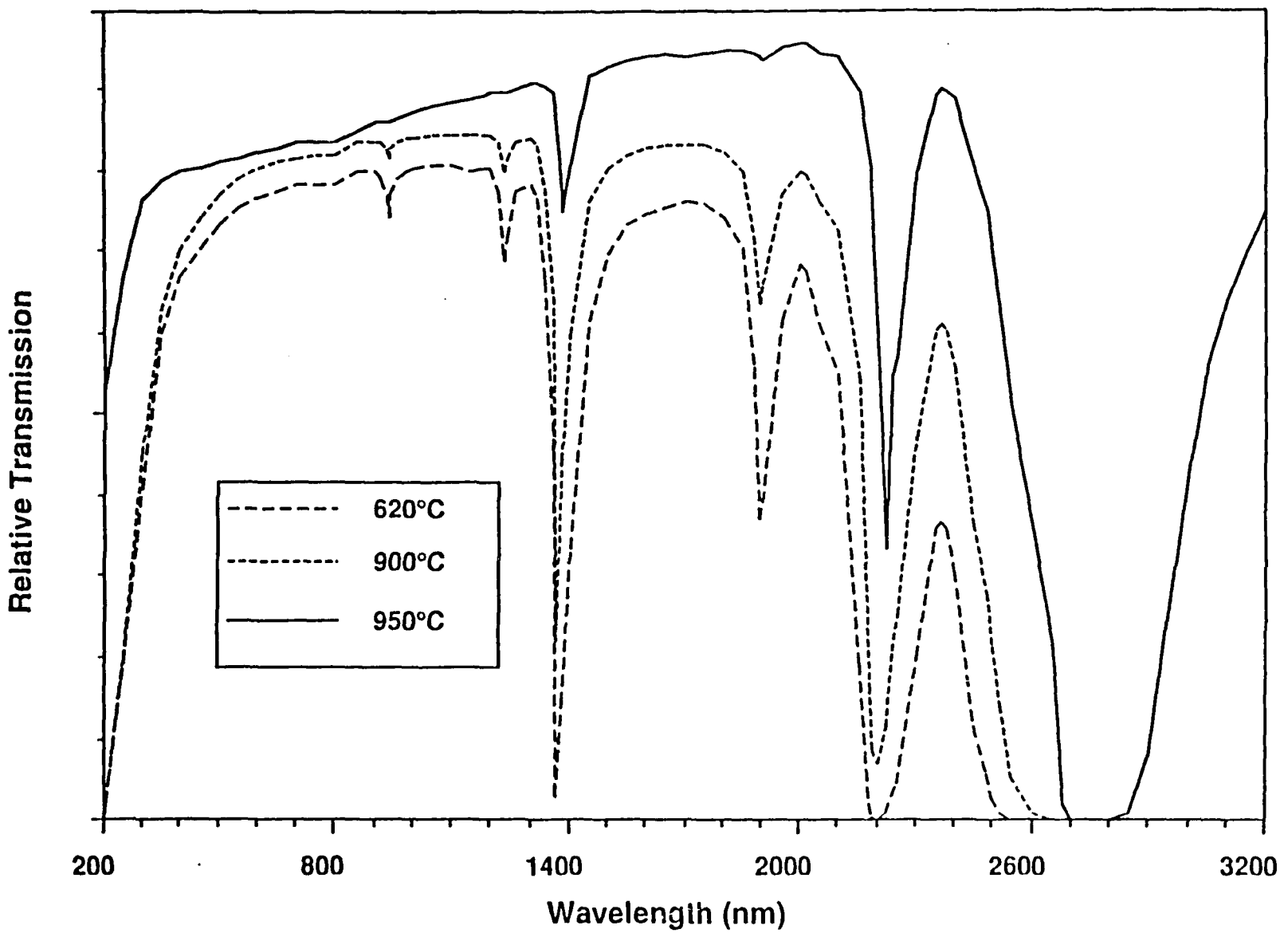
Relative Transmission
620°C
900°C
950°C
200
800
1400
2000
2600
3200
Wavelength (nm)

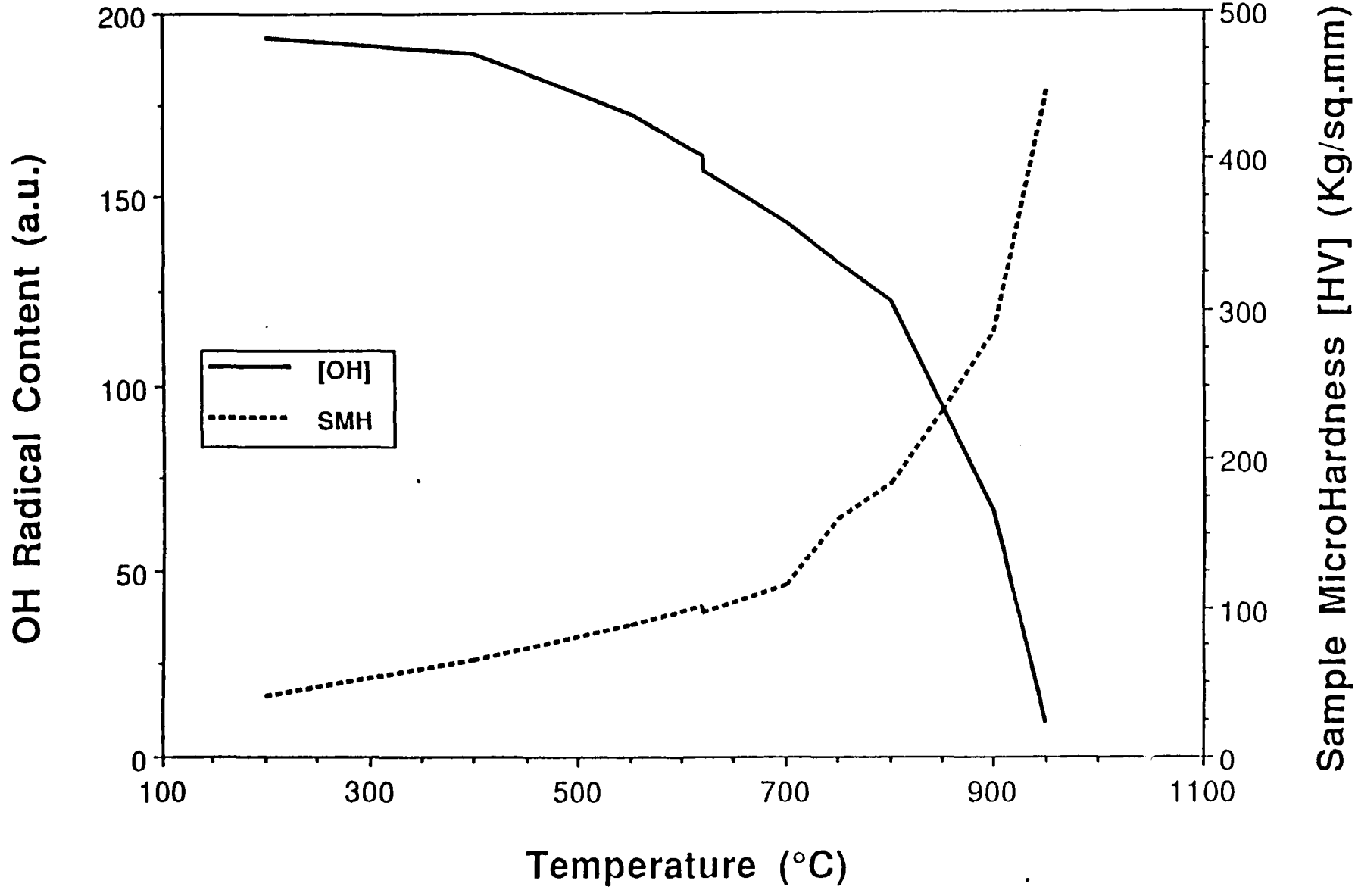
OH Radical Content (a.u.)
Sample MicroHardness [HV] (Kg/sq.mm)
Temperature (°C)
[OH]
SMH
200
150
100
50
0
500
400
300
200
100
0
100
300
500
700
900
1100

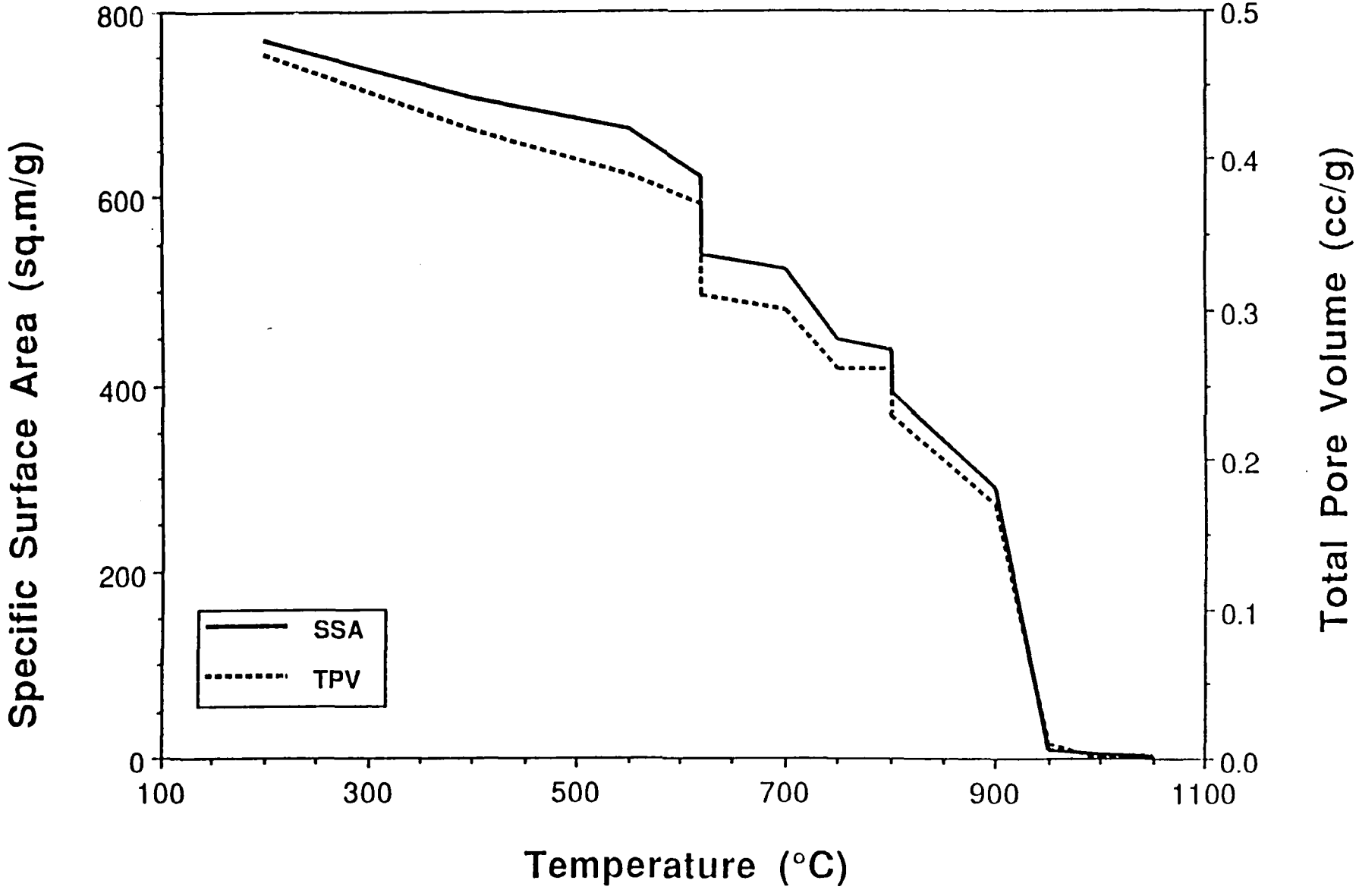
800
600
400
200
0
0.5
0.4
0.3
0.2
0.1
0.0
100
300
500
700
900
1100
Specific Surface Area (sq.m/g)
Total Pore Volume (cc/g)
Temperature (°C)
SSA
TPV

APPENDIX 3

Processing, properties and applications of sol-gel silica optics

Jean-Luc R. Noguès and Anthony J. LaPaglia

GELTECH, Inc., One Progress Blvd., Box 18, Alachua, Florida 32615, (904)462-2358

ABSTRACT

For many years the market share maintained by U.S. optics manufacturers has been declining continuously caused in part by intense competition principally from countries in the Far East, and in part by the lack of a highly trained cadre of opticians to replace the current generation.
This fact could place in jeopardy the defense system of the United States in case of international war. For example, in 1987, optical glass component imports accounted for approximately 50 percent of the Department of Defense (DOD) consumption.
GELTECH's sol-gel technology is a new process for making a high quality optical glass and components for commercial and military uses. This technology offers in addition to being a local source of optics, the possibility to create new materials for high-tech optical applications, and the elimination of the major part of grinding and polishing for which the skill moved off-shore.
This paper presents a summary of the sol-gel technology for the manufacture of high quality optical glass and components. Properties of pure silica glass made by sol-gel process (Type V and Type VI silicas) are given and include: ultraviolet, visible and near infrared spectrophotometry, optical homogeneity and thermal expansion. Many applications such as near net shape casting or Fresnel lens surface replication are discussed. Several potential new applications offered by the sol-gel technology such as organic-inorganic composites for non linear optics or scintillation detection are also reported in this paper.

1. SOME TRENDS OF THE U.S. OPTICAL INDUSTRY

In 1985, the optics production capacity for defense applications was estimated to be able to supply 87 percent of the optical component military needs but the production capacity was dropping regularly by over 20 percent per year. The possibility to reverse this trend and to increase the production capacity of U.S. manufacturers looked difficult and long, due to shortages of skilled opticians and long lead times for raw materials.

In 1987, the Department of Defense's Joint Logistics Commanders anticipated in peacetime a requirement of approximately 100,000 optical components per month of the types used for direct applications in military systems.[1] In case of mobilization, the requirement for military optical components were found to be much greater.

The same year, optical glass component imports already accounted for more than 50 percent of the Department of Defense (DOD) consumption. The potential of converting commercial production capacity to military production appeared inadequate to support the rapid increase in optical elements needed to meet emergency defense requirements and would ruin the development of the commercial optical industry.

During the last few years the increasing need of optical elements was boosting the imports from all over the world with a large predominance from the small countries of the Pacific Rim (Korea, Taiwan, Malaysia, Hong-Kong) where labor rates are perhaps one-tenth those of the U.S..

Figure 1 presents the trends of imports and exports of all optical elements over a time period from 1978 to 1986. This figure shows that the imports increased by more than a factor 2 over a few years while the exports were decreasing slightly. This means that the U.S. manufacturer share of the market of optical components was decreasing drastically over the years. This trend applies for all optical market segments such as for example laser applications and figure 2 presents the estimated sources of laser optics by world regions. It was estimated in 1984 that 62 percent of the laser optics used in the U.S. were from domestic source, the projection for 1990 predicts a U.S. market share of about only 37 percent.[2] Because the need for this type of optical component is expected to increase by over 40 percent, the decrease in market share becomes even more dramatic.

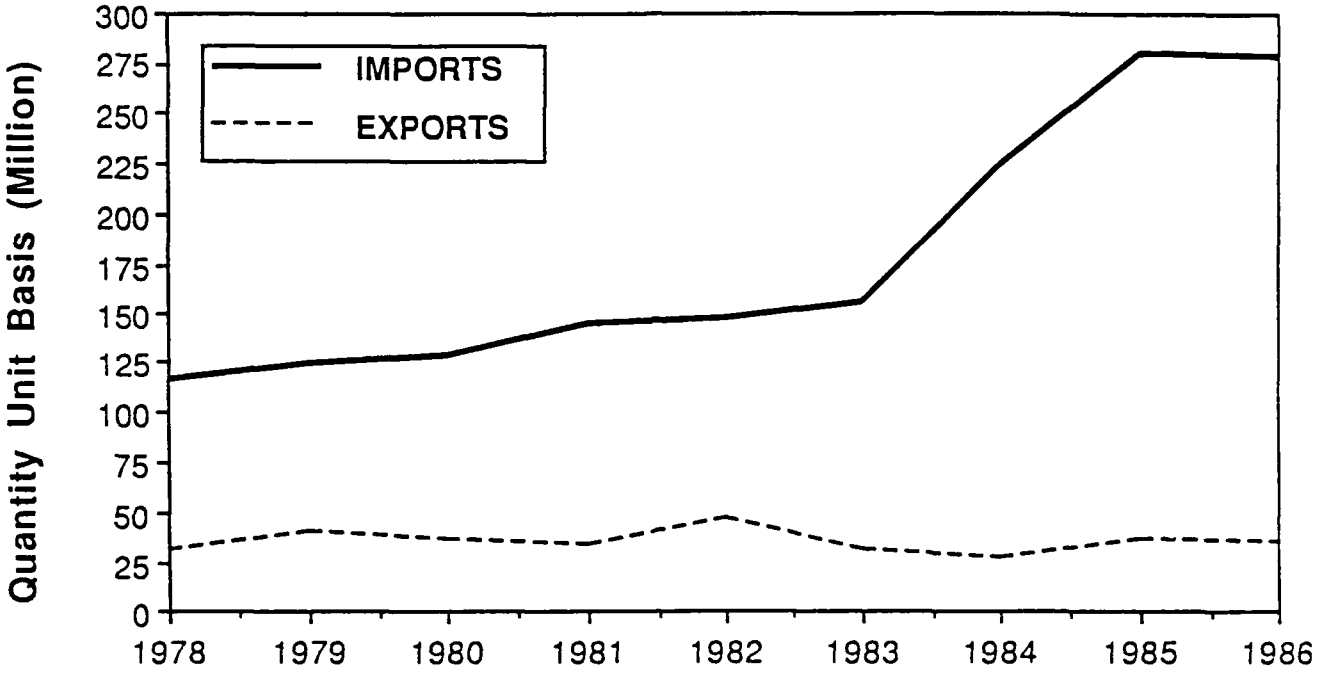

Fig. 1. U.S. Trade balance (All optical elements)

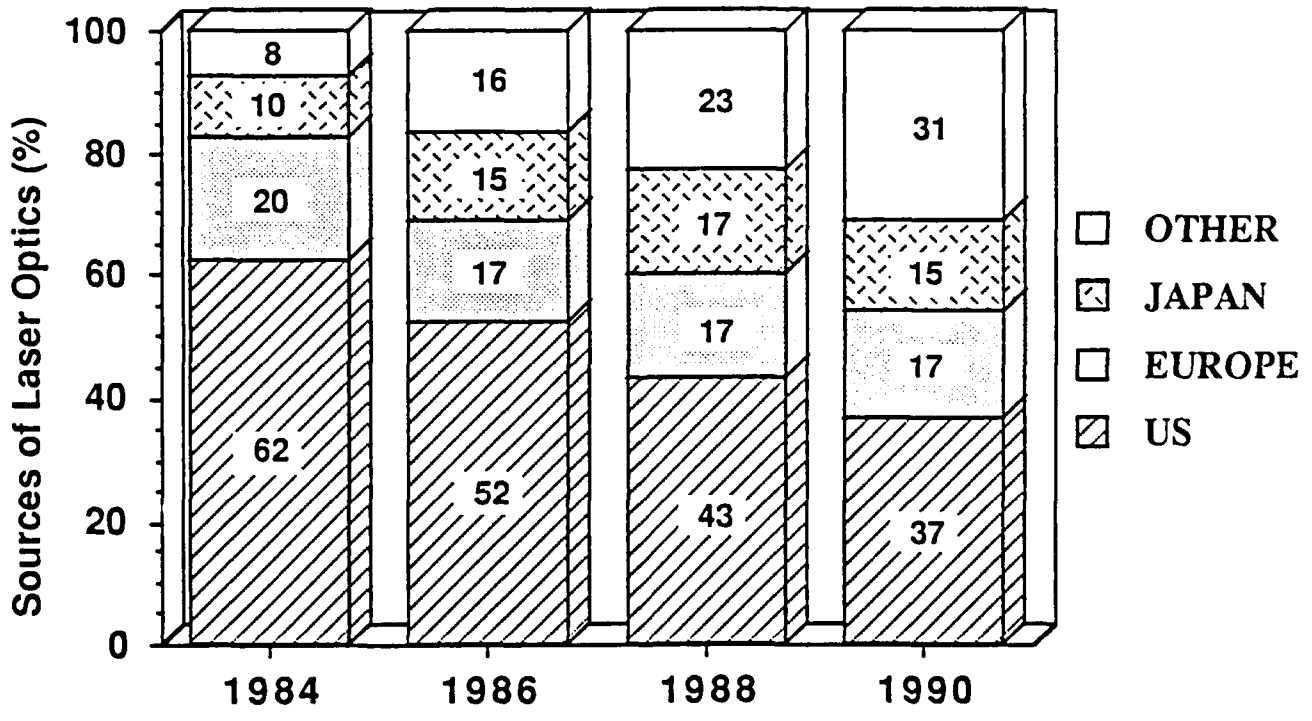

Fig. 2. Estimated sources of laser optics by world region

Today, most optical companies are reliant to some degree, between 36 and 70 percent function of the type of components, on imports of materials, parts and production equipment. In general, imports are used because of three main reasons: availability of materials or equipment, lower prices, and sole sources due to the extinction of U.S. suppliers or the set up of subsidiaries in the Far East in an attempt to reduce production costs and increase competitiveness.

Every phase of the business from raw materials to finished optical products has been impacted. For the past few years more than 70 percent of the glass used by U.S. optical component producers were imported and this percentage is expected to increase in the near future. The percentage of optical components from overseas rises up to 98 percent for some specific optical applications. Another consequence of these circumstances is that the overall employment in the optical industry has declined by over 40 percent in only five years.

In summary, the need of optical components in the United States is growing very rapidly but the market share maintained by U.S. optical manufacturers has been declining continuously for many years caused in part by intense competition principally from countries in the Far East and in part by the lack of a highly trained cadre of opticians to replace the current generation. The requirement of large imports of military optical components represents a real threat which could place in jeopardy the defense system of the United State.

Today the U.S. optical manufacturers have to try to reverse these trends and have to define new strategies for the future if they want to keep or increase their market share, and at the same time decrease the dependency of the U.S. on foreign suppliers. An identification of the key elements in the optical industry is at this point necessary to understand better the factors leading to the decline of the U.S. optical industry.

The manufacture of optical components involves three broadly defined stages of production. The first stage is the raw glass production mainly by melting various raw materials in high temperature furnaces. The second stage begins with the annealing of the blocks, slabs or gobs manufactured in stage 1 and continues with the cutting, slicing and even pressing of the raw glass to produce blanks or preforms. Both stages are capital intense operations and require large volume production to achieve cost economies. The third stage of optical element production is the finishing stage. It is a very labor intense stage which requires special skilled personnel and represents up to 80-90 percent of the component cost. At this stage the blanks are ground to near net shape and further polished to the adequate standard for each specific optical application. The process to manufacture optical elements is in fact high capital and high labor intense operations. Today the U.S. equipment park is old and the skilled personnel is not replaced after retirement. To be competitive on the market place very large investments (equipment and personnel) are an indispensable necessity but with the purchasing of large quantities of optical components offshore, domestic manufacturers could not generate enough profits to modernize their capital equipment and simultaneously form an apprenticeship program to develop a new generation of opticians. This route, to be very successful in the optical industry, looks very difficult and many companies are investigating other alternatives.

Some companies are doing very well in the optical business because they developed a specialty in a high-tech segment of the market and they are trying to stay in front of the progress. Examples of high-tech segments include laser development, infrared materials and optoelectronic applications. Other small companies are devoting their effort to develop niche marketing applications but they are always vulnerable to smaller and more aggressive niche marketers.

Another way to be successful in the optical application business is to look for new technologies such as sol-gel processes, diamond turning, gradient index optics, replication, molding, and other novel solutions. In this paper we will focus on Sol-Gel Technology as a new manufacturing process which can offer smart solutions to the crucial problem of the U.S. optical component manufacture industry. This work addresses in particular the manufacture of pure silica for commercial and military optical applications.

2. SOL-GEL TECHNOLOGY BACKGROUND

The sol-gel technology for forming glasses and glass-ceramics received a great deal of attention during the last two or three decades because of the recognized advantages inherent in the method.[3-5] The three main advantages of the sol-gel process are:

1. The possibility of obtaining glasses difficult to prepare with a high degree of homogeneity by conventional methods of fusion. The good homogeneity is obtained at the beginning of the process by mixing the different liquid precursors together at relatively low temperature. This mixing allows an homogeneity of the various elements at a molecular level and this homogeneity can be kept in many cases through the complete processing.

2. The possibility of obtaining high purity due to the chemical aspects of the raw materials which can be supplied in an electronic grade for the majority of them.

3. The potential of molding to near net shape by casting at low temperatures the sol into molds of predetermined shapes.

The first two advantages allows for the preparation of excellent materials for high-tech applications such as advanced optics, optoelectronic devices and tailored ceramics. The third advantage allows for the preparation of parts at lower manufacturing costs and opens the possibility of the manufacture of elements with special surface features. Table 1 shows a list of potential advantages offered by the sol-gel technology toward the preparation of glasses and glass ceramics.

Table 1. Some advantages of the sol-gel processing

Better homogeneity
Better purity
Lower temperature of preparation
New noncrystalline solids
New crystalline solids
Special products such as films
Near net shape casting
Surface feature optics

The sol-gel process can be divided in three main steps:

1. Gel formation.
2. Drying.
3. Consolidation (densification, sintering).

In the first step, the necessary ingredients are mixed to produce a sol. By destabilization or hydrolysis and polycondensation of the sol, the three dimensional network of the future glass is formed and the solution sets into a stiff gel called wet gel. After an aging step necessary to develop the formation of the initial texture of the material, the aged wet gel is dried. This crucial step consists of eliminating the interstitial liquid from the gel body. This induces a drastic modification of the texture of the gel which leads often to the destruction of the monolith aspect of the material. The dry gel is then heat-treated to convert the porous solid into an homogeneous glass free of porosity.

The sol-gel technology is very complex and many processes have been developed for very specific applications. The following parts of this paper address the production of pure gel-silica monolithic glass for optics applications.

3. GEL-SILICA PROCESS

A large amount of the optics used in the world are made in pure silica glass because of its very good optical transmission, refractive index homogeneity, low coefficient of thermal expansion, very good thermal and chemical stability, and its ability to be polished to high standards.

There are presently four major methods of manufacturing silica optics. The first two methods involve melting at high temperatures natural quartz crystals. These processes produce Type I and Type II *Fused Quartz* which provides for average optical properties due to substantial amounts of cation and hydroxyl impurities, defects, seeds, bubbles, inclusions, and microcrystallites.

The other two processes produce Type III and Type IV *Fused Silicas*. They are made by vapor-phase hydrolysis and oxidation of pure silicon tetrachloride respectively. The higher purity of the raw materials allows cation impurity contents substantially lower than in fused quartz. These two processes lead to a higher quality of glass than Types I and II but do not permit the direct manufacture of neat net shape optics.[6]

The sol-gel processing of pure silica glass has the potential of producing a high quality optical glass due to the high purity of raw materials and at the same time the production of near net shape parts which require a minimum of finishing.

The pure silica sol-gel process described in this paper includes several steps: mixing, casting, gelation, aging, drying, densification, and requires total control of each process variable to be successful. Figure 3 gives a synoptic of the entire gel-silica process.

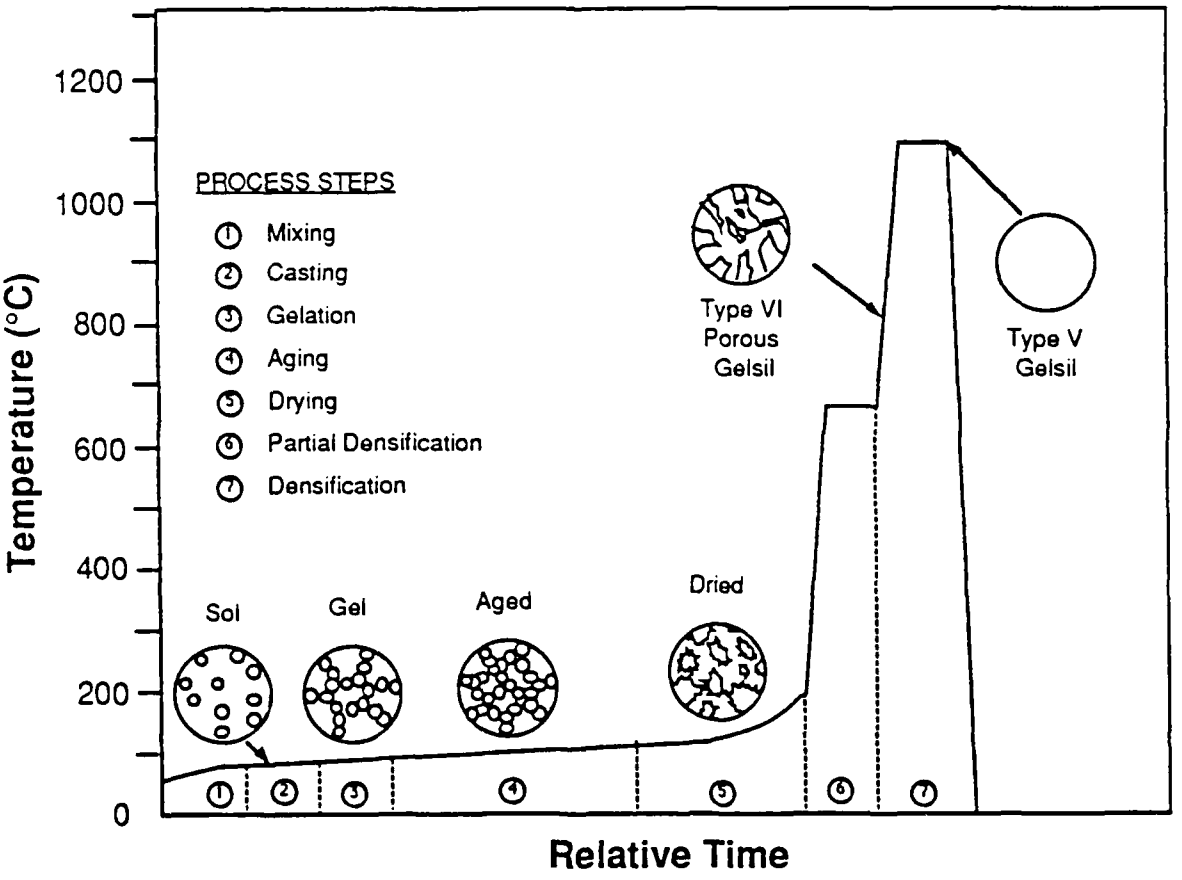

Fig. 3. Gel-silica process sequence

Alkoxide silicon precursors are choosing over colloidal suspension raw materials because of their higher level of purity. Typical silica precursors are tetraethylorthosilicate (TEOS) and tetramethylorthosilicate (TMOS) which can be produced in the USA in various levels of purity. The silica sol is prepared by adding the silica precursor to deionized water. Hydrolysis of the silica precursor and condensation reactions occur during this mixing step:

Hydrolysis: $Si(OR)_4 + 4\,H_2O \longrightarrow Si(OH)_4 + 4\,ROH$ (1)

Condensation: $Si(OH)_4 \longrightarrow SiO_2\,(gel) + 2\,H_2O$ (2)

After complete homogeneity of the sol is reached, the solution is cast into molds of specific shapes. The polycondensation reaction continues and the silica particles randomly link together and form a three-dimensional network. This mechanism increases the viscosity, the sol loses its freedom of movement and becomes a rigid, wet gel having the shape and surface quality of the mold. This phenomena is called gelation.

During the aging step, the polycondensation reaction continues to build the glass network giving at the same time enough strength to the gel to resist and support without cracking the tremendous stresses developed during the drying step. During this drying step, the by-products of the hydrolysis and condensation reactions are eliminated and the final product is an ultraporous monolithic body with the shape and surface details of the original mold.

The last step of this process corresponds to the densification of the dried gel via elimination of the porosity by heat treatment. During the first part of this densification treatment (up to 600°C) the organic impurities present in the pore of the gel are eliminated in order to leave a pure silica material which can be heated up for full densification after an additional dehydration period. This dehydration treatment is necessary to drop the residual hydroxyl group content lower than 5 ppm in the fully dense pure gel-silica glass (Type V). When the process of densification is stopped before reaching complete densification, a partially dense pure gel-silica glass (Type VI) is produced and can be used for some very novel applications as described below.

The glasses manufactured by this specific process developed in GELTECH, Inc. are identified as Dense Gelsil™ (Type V silica) and Porous Gelsil™ (Type VI silica) for the fully dense and partially dense glass respectively. Details of the production processes of these two gel-silicas were published elsewhere.

4. PROPERTIES AND APPLICATIONS OF GEL-SILICAS

4.1 Properties of dense gel-silica (Type V Silica)[7]

One of the primary reasons for use of alkoxide derived silica glass is an improvement of purity and homogeneity. The high purity of the raw materials in addition to a lower temperature process have permitted the manufacture of gel-silica glass with a very high optical transmission throughout the optical spectrum and in particular an outstanding ultraviolet transmission cut-off. Figure 4(a) presents a comparison of the optical transmission in the ultraviolet wavelength range for Type V silica and a Type III silica available on the market. Figure 4(b) shows the elimination of the absorption bands in the near infrared for Type V silica in comparison with Type III silica which exhibits peaks at 1400 nm and 2200 nm, and a very broad absorption band at 2730 nm.

The quality of the raw material in addition to a very well controlled process allows for the manufacture of glass with an index of refraction homogeneity of about $1\text{-}6 \times 10^{-6}$, no evidence of bubbles, no striae, very low strain birefringence of 4-6 nm/cm, and very low residual hydroxyl group concentration.

A very low coefficient of thermal expansion and very good thermal stability are also important physical properties for pure silica optical glass. The alkoxide derived process leads to the manufacture of Type V silica having a lower expansion than the National Institute of Standards and Technology (NIST) silica standard and Types III and IV commercial silicas over the temperature range of 25°C to 700°C as shown in figure 5. Figure 6 shows the good thermal stability of Type V silica over the same range of temperature.

The overall properties measured on alkoxide derived Type V silica are generally equivalent to or superior to the best grades of Types I to IV commercial optical silicas. This Type V silica represents a potential alternative to all the different types of pure silica commercially available today and used for civilian or military applications. The Type V silica production is not an equipment or labor intensive operation, does not require any special equipment available only from overseas, and decreases part of the dependency of the United States on foreign suppliers.

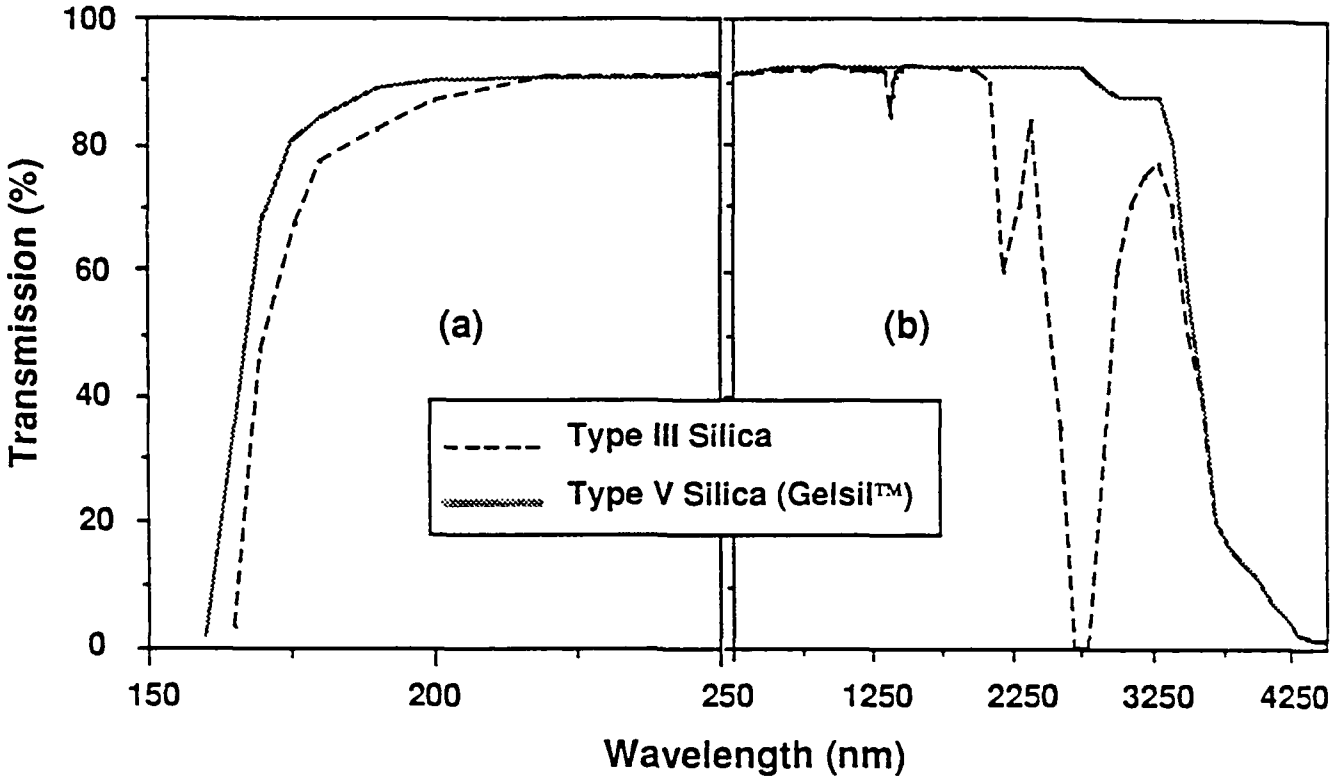

Fig. 4. Optical transmission of various silicas

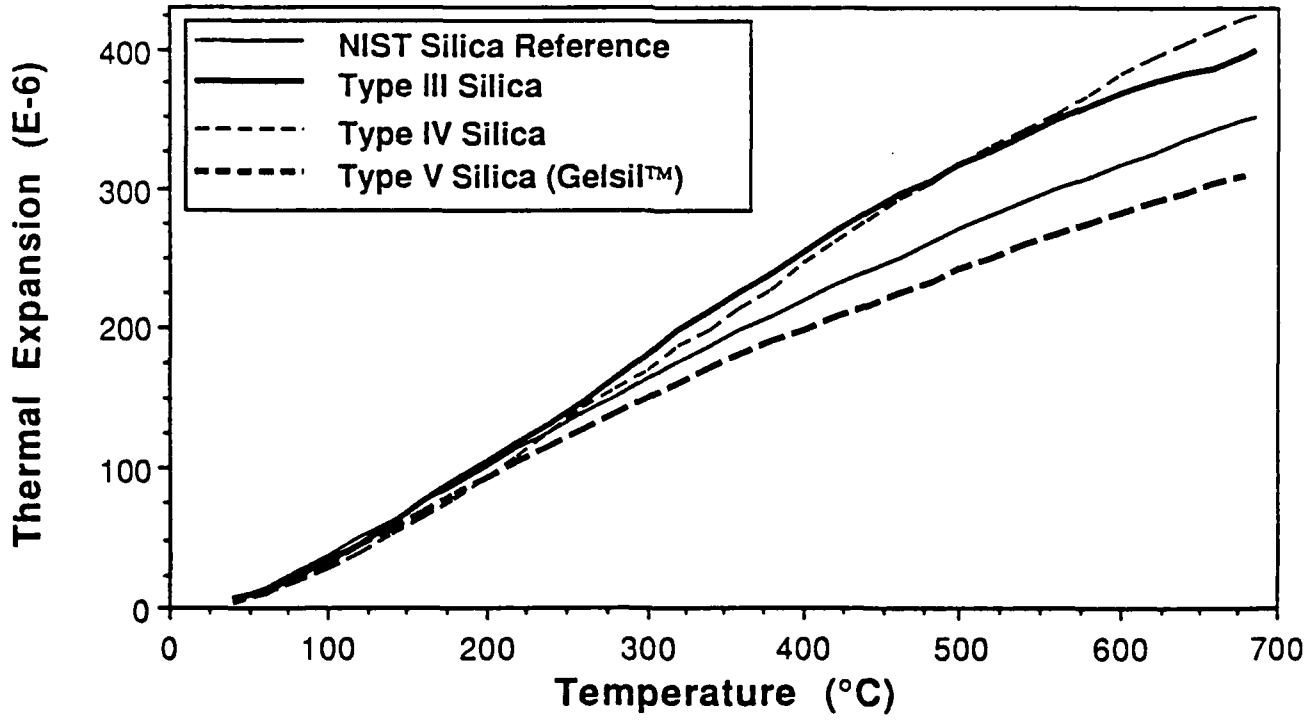

Fig. 5.Thermal expansion of various silicas

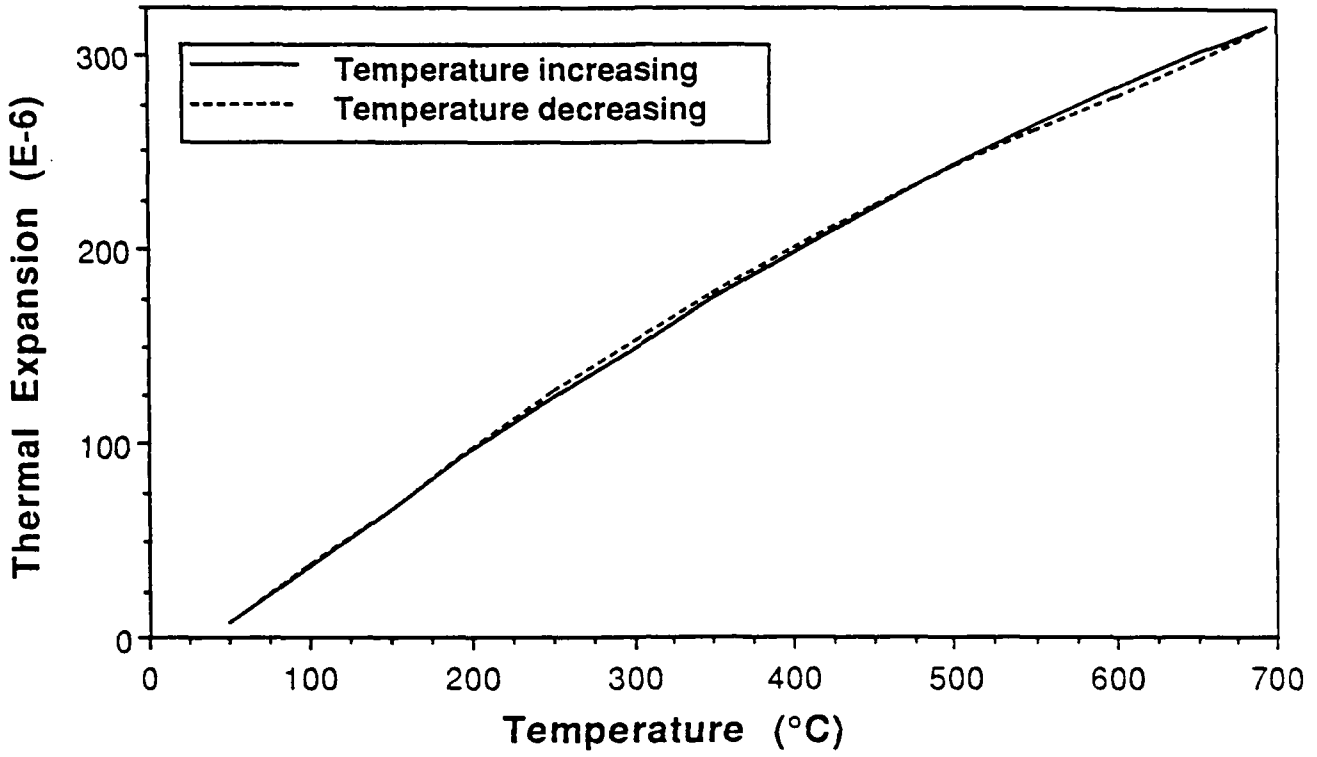

Fig. 6. Thermal stability of dense gel-silica (Type V)

4.2 Properties of porous gel-silica (Type VI Silica)[8]

An important feature of the alkoxide derived silica process is that with sufficient control of the kinetics and ultrastructure, it is possible to produce an optically transparent pure silica which has a substantial residual porous volume (Type VI silica). This Type VI silica is transparent because the pores have a very small average diameter of about 2.5 nm and do not induce too much light scattering. The transmission spectra of a porous gel-silica is shown in figure 7. This spectrum shows that the samples still transmits 50 percent of light at wavelength as low as 290-300 nm, and displays the typical absorption bands principally due to the residual hydroxyl groups and their overtones.

The properties of this material are a function of the final maximum temperature of densification. This feature in addition to the possibility to be able to change the pore diameter during the process allows for the manufacture of tailored porous gel-silica for specific applications.

There is very little change in the average diameter of the interconnected pores during the densification but their number decreases rapidly as the temperature increases. Consequently the ultrastructure and physical properties of the gel change dramatically during the consolidation treatment. Figure 8 shows the decrease in total porous volume and specific surface area, determined by quantitative nitrogen absorption-desorption measurements, of gel-silica samples over a temperature range of 200°C and 900°C. Figure 9 presents the increase in bulk density and microhardness over the same range of temperature.

For a practical range of densification temperature from 600°C to 900°C, the porous gel-silica presents the following ranges of characteristics:

Total pore volume:	0.4 to 0.2 cc/g
Specific surface area:	620 to 290 sq. m/g
Bulk density:	1.3 to 1.5 g/cub. cm
Microhardness:	100 to 285 Kg/sq. mm

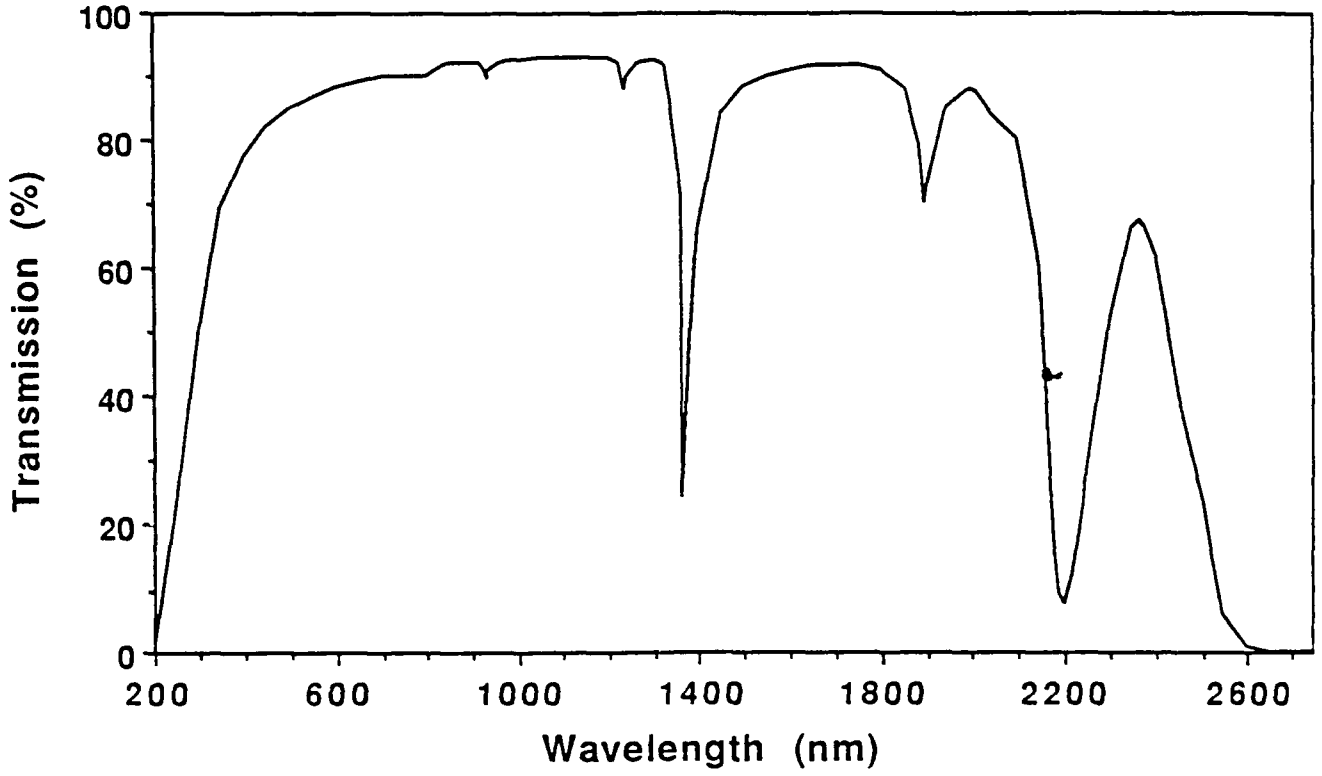

Fig. 7. Optical transmission of porous gel-silica (Type VI)

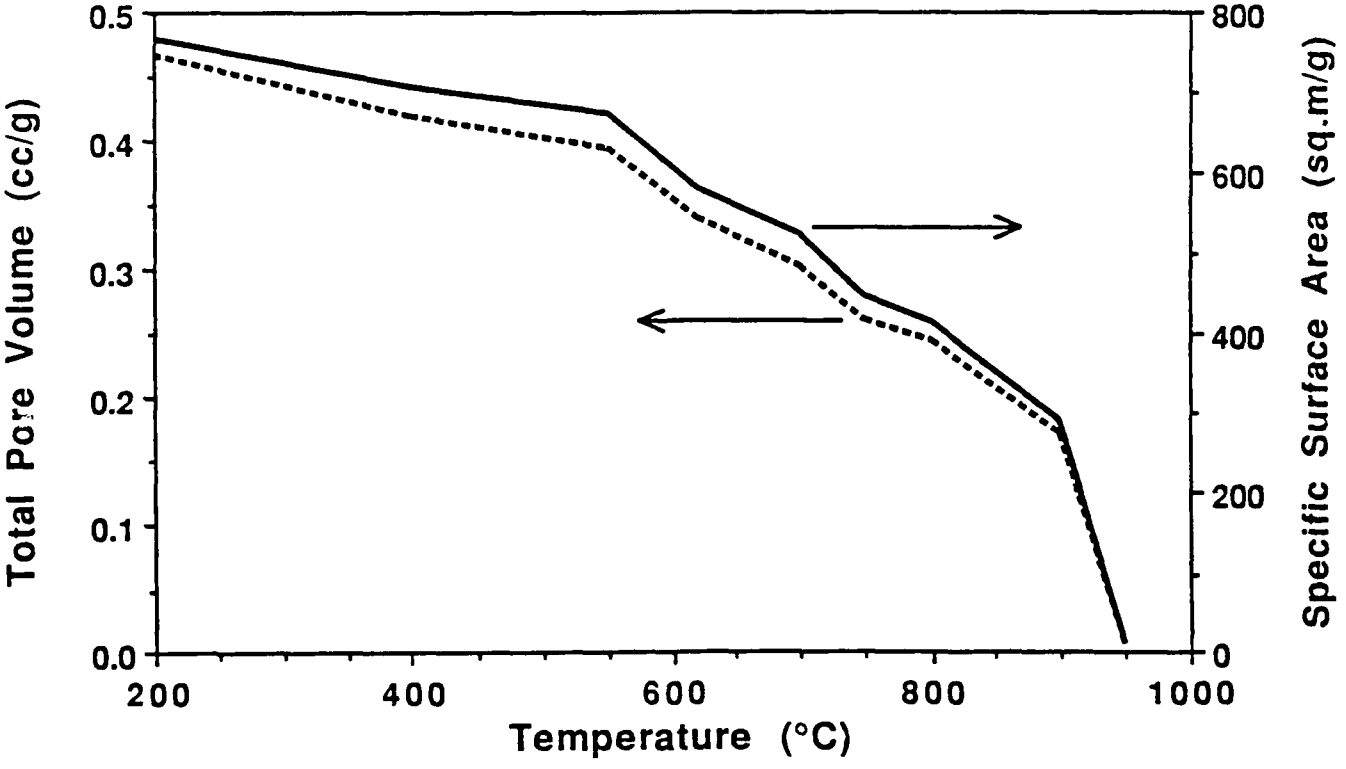

Fig. 8. Ultrastructure characteristics of porous gel-silica (Type VI)

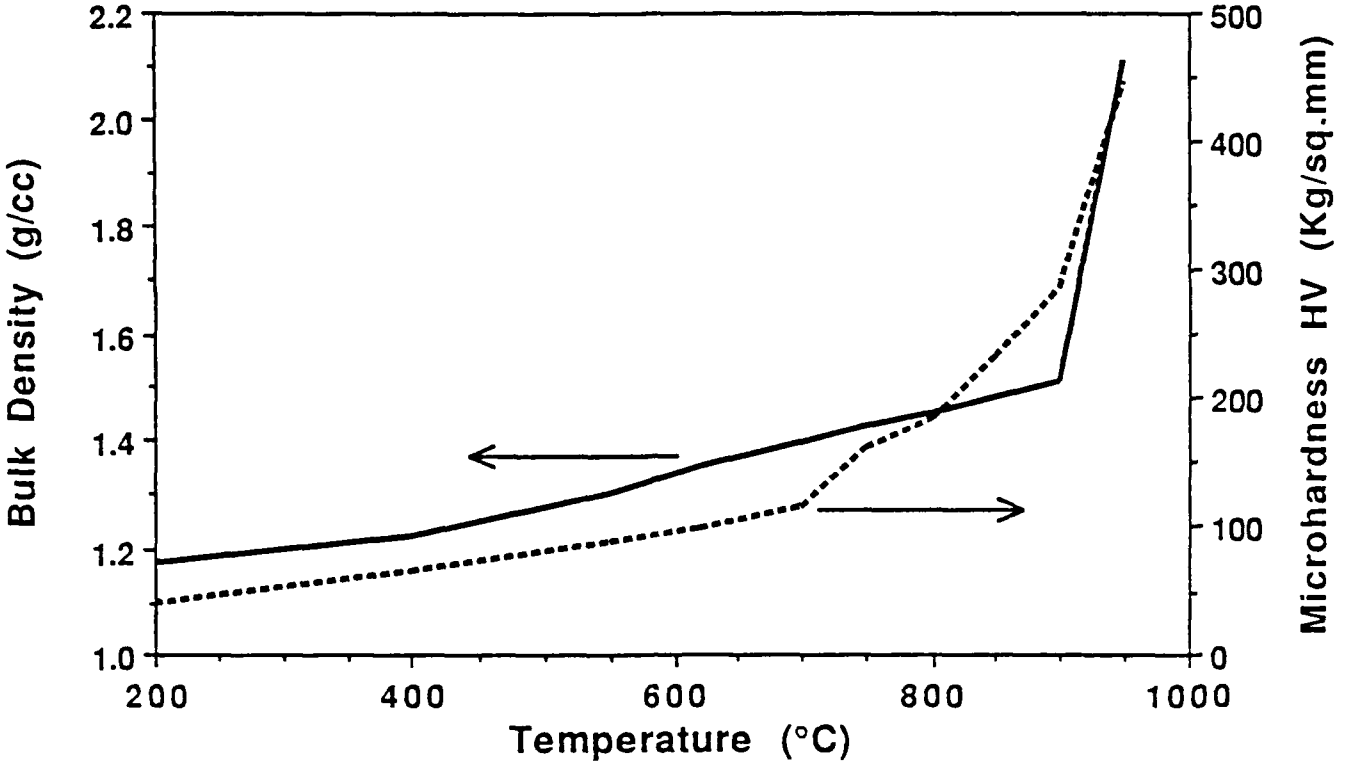

Fig. 9. Physical characteristics of porous gel-silica (Type VI)

The physical properties of porous gel-silica (Type VI) described above are attractive for many potential applications. The low density can be interesting for lightweight optical component applications. The interconnected residual porosity of the components makes them desirable for thermally cooled optics or for molecular filtration devices. This type of porous glass can be used as substrates for diffusion to produce graded refractive index optics (GRIN) or as substrates for silica waveguides. The type of applications where the most investigations were accomplished is for the production of composites by doping or impregnation of a second phase into the interconnected pore network. This technique allows the production of nano-scale composites because of the size of the pore of about 2 to 10 nanometers in diameter. Many composites had already been prepared and successfully tested at laboratory scale. These composites include the impregnation of the porous gel-silica matrices with organic fluors, wavelength shifters[9], non-linear optical polymers or compounds, laser dyes, liquid crystals, etc. Details of properties and specific potential applications of porous gel-silica are published elsewhere.[10]

Another unique application of Type VI silica is for pure silica optical waveguide substrates.[11] By laser densification, optical waveguides have been made using laser writing of higher density tracks on the porous gel-silica substrate. The higher density tracks have a greater index of refraction than the porous matrix and therefore can serve as a planar waveguide. The major advantage of this type of waveguide is that it matches the index of refraction of silica fiber optics, which is not the case for ion-exchanged or diffusion based waveguides.

This Type VI porous silica represents a new material with tremendous potential possibilities of developments for optical and optoelectronic applications.

5. AS-CAST SHAPES AND SURFACE FEATURES

Another area of potential advantage of sol-gel optics processing is that of obtaining net shapes and surfaces, or at least near-net shapes and surfaces, directly through casting sols at low temperature into molds of predetermined configurations.

As explained in the first part of this paper, the grinding and polishing of a lens from the raw glass represents up to 80-90

percent of its cost. If this third stage of the optics manufacture could be eliminated the production cost of optical components would be dramatically reduced. The concept of grinding and polishing elimination is already used for manufacture by the pressing of lenses, but this technique can be used only for low temperature glasses and low quality optics, and definitely not for pure silica and high quality components. However, it is for the pure silica glass and high quality components that the cost of grinding and polishing is the most expensive.

The concept of casting to shape is an old concept used all around us for the manufacture of many products but its application to the sol-gel process is a challenge due to the high level of shrinkage, the fragility of the gel during the first steps of the process, and the relatively high temperature of the densification. The complexity of this process requires control and a high understanding of each process variable. The synoptic of the casting to shape concept is presented in figure 10.

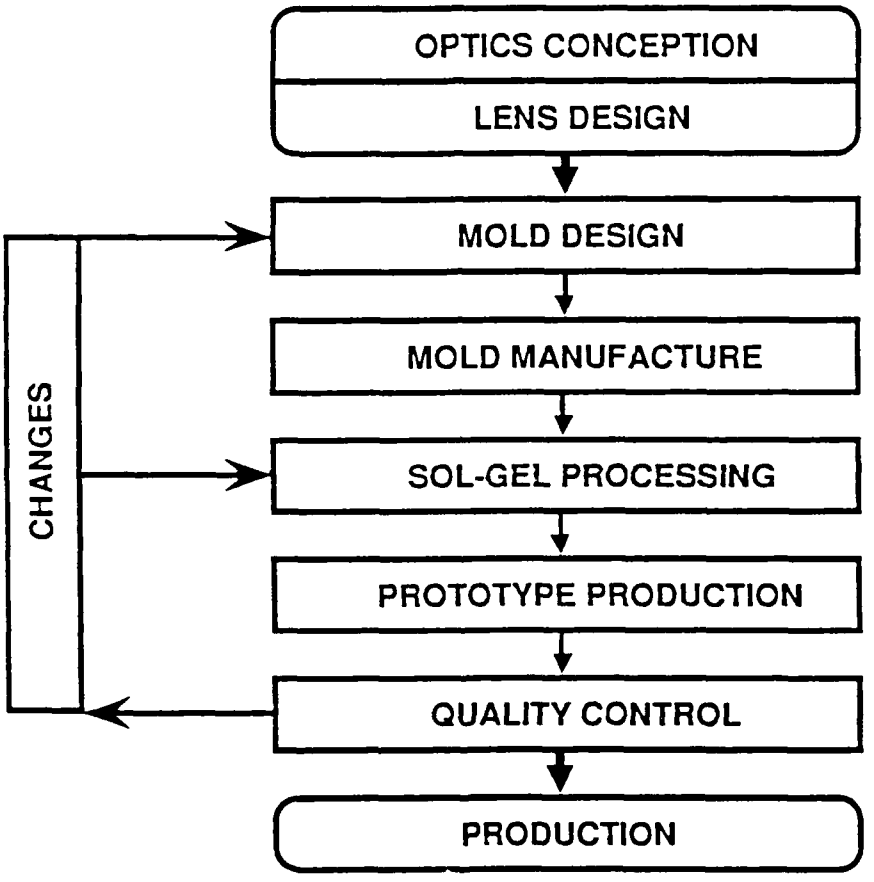

Fig. 10. The different steps of the casting to shape concept

The first step of the casting to shape processing is the design of a mold from the design of the lens to produce. This design is done based on a multitude of data on the shrinkage of the gel during the process as a function of its shape and its dimensions (diameter, thickness, radius of curvature, etc.). All this data on shrinkage is necessary to build a computer model and reduce the number of iterations to achieve the production of parts with the initial dimensional tolerances.

The second step consists of modifying the sol-gel process to be able to age, dry and densify the gel without cracking after casting the sol into the manufactured mold.

Each different optical component requires the design of a specific mold and an adaption of the sol-gel process. But these operations have to be done only once and their cost amortized over a large number of parts, whereas the cost of grinding and polishing is directly proportional to the number produced.

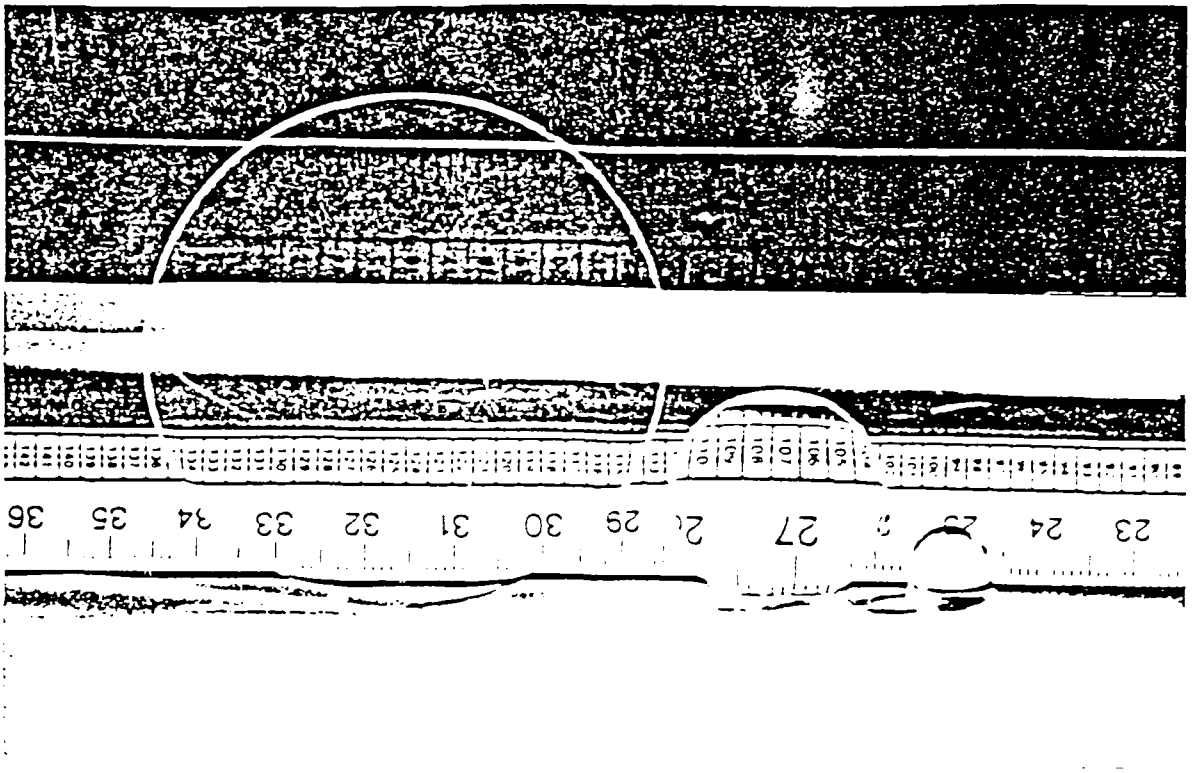

Fig. 11. Plano/convex gel-silica lenses (Dried and dense)

Figure 11 shows the photograph of plano-convex lenses produced by casting to shape without any additional processing. Their dimensions are in good agreement with the dimensional limits of commercial lenses.

This concept of casting to shape is even more important and more economic when the optical element presents a complex shape such as aspheric or cylindrical. The advantages of near net shape casting includes the ability to form internal cavities using a modification of the normal sol-gel process.

Another application of net shape casting is the replication of specific surface features. For example, Fresnel lens were manufactured by directly casting the sol into a mold having a surface with the negative indentation of the surface to reproduce. Microscopy and profilometry shown that the replication of the surface details is good and was maintained through full densification. The advantages of the silica Fresnel lens over a polymer lens is the very good chemical and thermal stability in addition to superior optical properties. The surface feature replication is a new possibility for optical components and will offer many new developments for optics and optoelectronic applications.

6. CONCLUSIONS

The trends of the optical industry shows that the market share maintained by U.S. manufacturers has been declining continuously and dramatically over the years. With the increasing need of optical components and the tremendous level of imports to fill this need, the dependency of the U.S. to foreign suppliers, especially for defense applications, represents a real threat.

The sol-gel technology can represent a good alternative by offering the U.S. a source of high quality optical components. This technology in not as capital and labor intensive as the conventional manufacturing process and should allow U.S. sol-gel optics producers to set up easily production facilities and to be competitive enough to reverse todays trends.

The specific sol-gel process described in this paper allows the production of a dense gel-silica (Type V) with excellent optical, physical and structural characteristics, generally equivalent to or superior to the best grades of commercial available Type I to IV optical silicas. In addition this process permits the production of a new material called porous gel-silica (Type VI) which presents good optical and physical properties, and could be used for many novel applications.

Both Types V and VI silica offer the advantage of near net shape casting and surface feature replication which can eliminate to a large extent the need of grinding and polishing, and the production of optics with surface details such as Fresnel lens.

Even though new technologies such as sol-gel process are under investigation in order to try reverse actual optical market trends, it is easy to prognosticate that domestic manufacturers can look forward to at least a few more painful years. The future of the optical business will certainly be challenging.

7. ACKNOWLEDGMENTS

The authors gratefully acknowledge financial support of Air Force Office of Scientific Research Contracts #F49620-86-C-0120 and F49620-88-C-0010 and the encouragement of D. R. Ulrich throughout this research.

8. REFERENCES

1. R. P. O'Shaughnessy, et al., Joint Precision Optics Technical Group's Final Report, Department of Defense's Joint Logistics Commanders, Precision Optics Study, June 1987.
2. R. Cunningham, "Trough the Looking Glass", Lasers & Optonics, 7 [5] 45-51 (1988).
3. L. L. Hench & D. R. Ulrich, eds., Ultrastructure Processing of Ceramics, Glasses, and Composites, John Wiley & Sons, NY, 1984, and Science of Ceramic Chemical Processing, John Wiley & Sons, NY, 1986. J. D. Mackenzie & D. R. Ulrich, eds., Ultrastructure Processing of Advanced Ceramics, John Wiley & Sons, NY, 1988.
4. C. J. Brinker, D. E. Clark, and D. R. Ulrich, eds., Better Ceramics Through Chemistry, Vol. 32, North-Holland, NY, 1984; Better Ceramics Through Chemistry II, Vol. 73, North-Holland, NY, 1986; and Better Ceramics Through Chemistry III, Vol. 121, North-Holland, NY, 1988.
5. V. Gottardi, ed., Proceedings of the International Workshop on Glasses and Glass Ceramics from Gels, J. Non-crystal. Solids, 48 [1], (1982); H. Scholze, ed., Proceedings of the Second International Workshop on Glasses and Glass Ceramics from Gels, J. Non-crystal. Solids, 63 [1&2], (1984); J. Zarzycki, ed., Proceedings of the Third International Workshop on Glasses and Glass Ceramics from Gels, J. Non-crystal. Solids, 82 [1-3], (1986); and S. Sakka, ed., Proceedings of the Fourth International Workshop on Glasses and Glass Ceramics from Gels, J. Non-crystal. Solids, 100 [1-3], (1988).
6. M. Grayson, ed., Encyclopedia of Glass, Ceramics, Clay and Cement, John Wiley & Sons, NY, 1985.
7. L. L. Hench, M. J. R. Wilson, C. Balaban, and J. L. Noguès, "Sol-Gel Processing of Large Silica Optics", Presented at the Fourth International Conference on Ultrastructure Processing of Ceramics, Glasses, and Composites, Tucson, AZ, February 1989.
8. L. L. Hench, S. H. Wang, and J. L. Noguès, "Gel-Silica Optics", SPIE - Multifunctional Materials, R.L. Gunshor, ed., Vol. 878, 76-85 (1988).
9. J. L. Noguès, S. Majewski, J. K. Walker, M. Bowen, R. Wojcik, & W. V. Moreshead, "Fast, Radiation Hard Scintillating Detector, A Potential Application for Sol-Gel Glass", J. Am. Ceram. Soc., 71 [12] 1159-63 (1988).
10. J. L. Noguès and W. V. Moreshead, "Porous Gel Silica, a Matrix for Optically Active Components", Presented at the Fifth International Workshop on Glasses and Glass Ceramics from Gels, Rio de Janeiro, August 1989.
11. R. V. Ramaswamy, T. Chia, R. Srivastava, A. Miliou, & J. West, "Gel-Silica Waveguides", SPIE - Multifunctional Materials, R.L. Gunshor, ed., Vol. 878, 86-93 (1988).

Note: † Gelsil™ is a trademark of GELTECH, Inc.

APPENDIX 4

PREPARATION, PROCESSING, AND FLUORESCENCE CHARACTERISTICS OF NEODYMIUM-DOPED SILICA GLASS PREPARED BY THE SOL-GEL PROCESS

William V. Moreshead, Jean-Luc R. Noguès, and Robert H. Krabill*

GELTECH, Inc., One Progress Blvd. #18, Alachua, FL 32615 (USA)

Abstract

For high-powered laser applications silica glass has favorable thermal and mechanical properties. However, the limited solubility of neodymium oxide in silica has prevented its use without the addition of other components, both to increase the solubility of the neodymium oxide and to reduce processing temperatures, minimizing impurities such as platinum inclusions. The preparation of up to 20 weight percent Nd-doped silica has been reported recently using the sol-gel process, and the fluorescence spectrum of a one weight percent composition was given.[1] In this paper we report the preparation and thermal processing of three to five weight percent compositions, including BET, density, thermal and spectral analyses. The fluorescence spectrum of the material and its fluorescence lifetime are then correlated with TEM/EDS results.

Subject index codes: d10, 11, s5, s6, s9

1. Introduction

Silica glass has many favorable properties for use in high-powered glass lasers, such as: 1) a broad transmission range from ultraviolet to infrared, 2) a low nonlinear index of refraction, and 3) a low coefficient of thermal expansion. However, the high processing temperatures required and the low solubility of neodymium oxide in silica have prevented the preparation of such glasses with reasonable amounts of neodymium oxide without the addition of other elements to the glass. The addition of these other elements greatly diminishes the desirable properties of the glass for use as a laser host. In 1973 Stone and Burrus[2] reported the preparation of silica fibers doped with 0.5 wt.% Nd_2O_3, but only recently, using the sol-gel process Pope and Mackenzie have reported the preparation of Nd-doped silica containing up to 20 wt.% Nd_2O_3[1] The sol-gel process holds some potential advantages for this application because of: 1) lower processing temperatures than

traditional melt glass techniques, 2) better control of purity, and 3) the potential for greater homogeneity on a molecular scale since it involves the mixing of precursors at low temperatures (<100℃).

In this paper the preparation, structural evolution, and visible and fluorescence spectra of three to five weight percent glass prepared by the sol-gel process are reported. In addition the fluorescence lifetimes are given and correlated with TEM results.

2. Experimental

Tetramethylorthosilicate (TMOS, Petrarch, Inc.) was mixed with deionized water in which was dissolved neodymium nitrate (Aldrich, Inc.). After complete homogenization this sol was cast into 60 mm petri dishes where it was allowed to gel and age between room temperature and 80℃ over a period of about two days. The wet gel was then dried to give a transparent gel monolith. Further heat treatment was done to study the evolution in properties with temperature. Samples were removed at desired temperatures and quenched in air.

Differential thermal analysis was done on a Dupont Instruments 910 DTA connected to a 1090 Thermal Analyzer. The sample was heated at a rate of 10℃/min up to a temperature of 1200℃, and alumina was used as the reference.

After each treatment temperature, the textural characteristics of the sol-gel monoliths were measured using an Autosorb-6 from Quantachrome Corporation, and the results were analyzed according to the BET theory.

The density measurements were done on oven-dried samples using a normal specific gravity bottle, with mercury being used as the liquid for displacement. Values given represent at least seven repetitions.

The shrinkage of the samples was determined by measuring the diameter of the disc-shaped monoliths after each of the selected temperatures. A minimum of two measurements of the diameter was done per sample using a digital caliper with an accuracy of ±0.01 mm.

The visible absorption spectra of the sol-gel samples were recorded on a Lambda-9 spectrophotometer from Perkin-Elmer.

Fluorescence spectra and fluorescence lifetimes were measured at Litton Laser Systems, Apopka, FL, by Dr. John Daly and Dr. Bill Williams.

Transmission electron microscopy was done at Microanalytical Laboratories, Gainesville, FL, by

E. J. Jenkins.

3. Results and Discussion

3.1. Visual Characteristics

All the sol-gel samples were clear, reddish purple, and monolithic after processing except the ones heated to 1150℃ and 1175℃, which started to turn white and opaque with the onset of foaming.

3.2. Differential Thermal Analysis

Figure 1 shows the results of the differential thermal analysis on a five weight percent composition. At least three features can be seen: 1) an endotherm between 50 and 150℃ due to loss of absorbed water, 2) an exotherm between approximately 250 and 400℃, due to the burning of organic residues, and 3) an exotherm between 1050 and 1100℃, which gives evidence of crystallization.

3.3. Textural and Physical Characteristics

The textural and physical characteristics of the samples are summarized in table 1. These gels show trends with heat treatment very similar to pure silica.[3] As the gels are heated the specific surface area and total pore volume decrease while the bulk density and the shrinkage of the samples increase. Changes in each of these characteristics follows a similar trend, changing slowly until the temperature reaches 800 to 850℃, and then changing much more quickly as pore closure occurs. Finally, if the heating is continued foaming due to the release of OH trapped in the pores after closure will begin. Figures 2 and 3 show these trends. One noticeable distinction between the Nd-doped gels and the pure silica is the ability to heat the doped samples to higher temperatures before foaming occurs. Also, during the thermal treatments the doped gels appeared to be less susceptible to cracking and/or crazing.

3.4. Visible Spectroscopy

Absorption of the gels was measured after several treatment temperatures to observe the evolution of the environment of the neodymium in the matrix. Pope and Mackenzie indicated that for a five percent composition the peak position representing the $^4I_{9/2}$ to $^4F_{5/2}$ transition shifted from 794 to 806 nm as treatment temperature increased, reaching a maximum at a temperature of 200℃.[1] For

the five percent gels described in this paper this behavior was not observed. Instead, the shift occurred over the entire range of temperatures until the maximum of 1150℃ was reached, although the shift was less significant above about 600℃. This result is understandable, however, considering the fact that several changes are taking place over this temperature range. Not only are the burning of organic residues and dehydration of the gel occurring, but the neodymium nitrate is decomposing and the neodymium oxide is forming clusters or aggregates due to solubility limits, as will be discussed later. Neodymium nitrate reportedly decomposes first to the oxynitrate, but not until it reaches 830℃ is it completely converted to the oxide.[4]

3.5. Fluorescence Spectroscopy and Lifetimes

A representative fluorescence spectrum of a neodymium-doped gel having three or five weight percent neodymia is presented in figure 4. This spectrum shows a maximum emission near 1.06 microns, which is typical for neodymium oxide in silicate glasses (see figure 4). For concentrations near one weight percent neodymium oxide in silica the maximum is reported to occur at 1.08 microns.[2,5]

Measurement of the fluorescence lifetimes gave very low values: on the order of 5 to 7 microseconds, as opposed to values greater than 150 μsec for commercial laser glasses. A lifetime greater than 100 μsec is necessary to make the glass commercially usable. These low values are presumably due in part to concentration quenching of the neodymium, as described by Namikawa, et. al.[6] Because neodymium oxide is immiscible in silica glass in the composition range from around two to 26 weight percent,[7] it forms aggregates or clusters in which cross relaxation can give rise to non-radiative de-excitation of neodymium, resulting in very short lifetimes. Clustering of the neodymium in the glass would also explain why the maximum emission in the fluorescence spectrum is similar to that of a silicate glass. The neodymium oxide-rich regions are apparently behaving more as a silicate glass than a doped silica matrix. These results are in agreement with those of Arai, et. al., who prepared neodymia-silica glasses by plasma torch CVD.[8] Another factor contributing to the short lifetimes is no doubt a high concentration of water in the gel, which has also been shown to shorten the fluorescence decay.[9]

3.6. Transmission Electron Microscopy

In order to further demonstrate the existence of neodymium oxide aggregation in the silica matrix

TEM was done on a sample. It was found that these clusters could be seen by observing the thin edge of a powdered sample. Figure 5 shows TEM micrographs of both pure silica and neodymium-doped samples. More extensive characterization of these neodymium-doped samples has been done at the University of Manchester, UK using both TEM and EDS.[10] Using EDS to measure the Nd concentration in both the clusters and the matrix, the clusters were found to be rich in neodymium, and show some evidence of crystallinity. The concentration of Nd_2O_3 in the matrix was much lower.

Preliminary investigations to solve the immiscibility problem are underway at GELTECH, Inc. in collaboration with the University of Manchester team. Galant, et. al.[11] have demonstrated laser action in quartz glass after the addition of a small amount of a "buffer component", which does not greatly diminish the desirable thermal properties of the silica host. Arai and coworkers[12] have shown using the CVD process that aluminum or phosphorus can be used as this third component to more homogeneously disperse the neodymium oxide and eliminate the concentration quenching. First results at GELTECH, Inc have shown that the addition of a few percent of either of these codopants reduce to a large extent the formation of clusters. Prototype samples with lifetimes between 90 and 110 have been produced, showing some good possibility for the development of this laser material.

4. Conclusion

The use of the sol-gel process to make neodymium-doped laser glasses for high power applications was investigated. Samples of three to five weight percent neodymium oxide were prepared and their structural evolution was followed over a range of temperatures using differential thermal analysis, BET, shrinkage, density, and visible spectroscopy. The fluorescence spectrum and fluorescence lifetimes were given and the results further explained using transmission electron microscopy. The fluorescence spectrum was shown to be typical of a silicate glass matrix, with lifetimes far too short to be useful for laser action. These short lifetimes were attributed to concentration quenching of the neodymium and quenching by the high concentration of water in the matrix. Although the sol-gel process allows the preparation of much higher concentrations than the melt process, the usefulness of these materials for laser applications is limited by the immiscibility of neodymium oxide in silica glass. Research is currently underway to develop potential laser materials having a small percent of a third component to solve the immiscibility

problem and lengthen fluorescence lifetimes without greatly changing the desirable properties of silica as a host glass.

Acknowledgements

The encouragement of Dr. D. R. Ulrich is gratefully acknowledged along with the financial contribution of contracts from SDI and AFOSR. Research sponsored by Air Force Office of Scientific Research (AFSC), under contract #F49620-89-C-0006. The United States Government is authorized to reproduce and distribute reprints for governmental purposes notwithstanding any copyright notation hereon. The authors also wish to thank Drs. John Daly and Bill Williams of Litton Laser Systems, Apopka, FL for measuring the fluorescence spectra and lifetimes.

*Present Address: American Matrix, Inc., 118 Sherlake Dr., Knoxville, TN 37922 (USA)

,1[illegible](1988)236.

)73)388.

Silica, A matrix for Optically Active

..,5[illegible](1987)143.

, and H. Tanaka, Japan J. Appl.

Supplement, (The American Ceramic

naka, and I. Iida; Jpn. J. Appl. Phys.,

and V. F. Surkova, Opt.-Mekh. Prom-

nable Doped Gel-Silica Glass Lasers",

lecular Materials Symposium, Pitlochry,

T[illegible]. Prokhorova, M. N.Tolstoi, and V.

[illegible]hii, and T. Handa, J. Appl. Phys.,

Densification Temperature

l:Gel

l Pore Volume (TPV) vs Densification Temperature

Average Sample Shrinkage (ASS) vs Densification

ight Percent Neodymium Oxide-Silica Glass

a Five Weight Percent Neodymium Oxide-Silica Glass

Temperature ℃	SSA sq.m/g	TPV cc/g	SBD g/cc	ASS %
160	777	0.477	1.50	57.28
400	751	0.499	1.22	57.22
600	607	0.388	1.26	58.20
800	569	0.359	1.28	59.15
975	BDL	BDL		63.68
1025	BDL	BDL	2.12	65.47
1075	BDL	BDL	2.27	66.28
1125	BDL	BDL	2.23	66.13
1150	BDL	BDL	2.20	66.17
1175	BDL	BDL		66.28

SSA: Specific Surface Area; TPV: Total Pore Volume; SBD: Sample Bulk density;
ASS: Average Sample Shrinkage; BDL: Below Detection Limit.

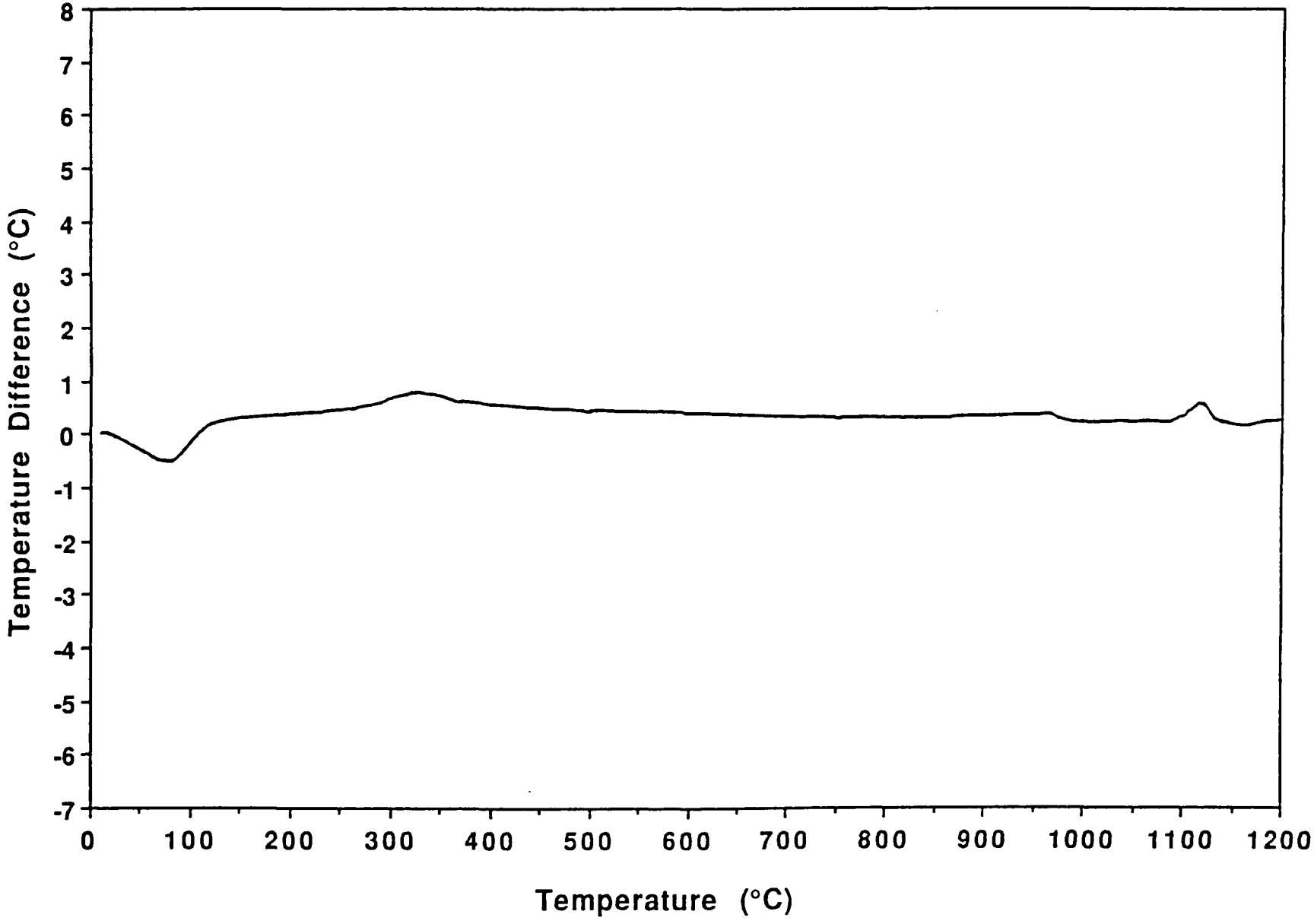
8
7
6
5
4
3
2
1
0
-1
-2
-3
-4
-5
-6
-7
Temperature Difference (°C)
0
100
200
300
400
500
600
700
800
900
1000
1100
1200
Temperature (°C)

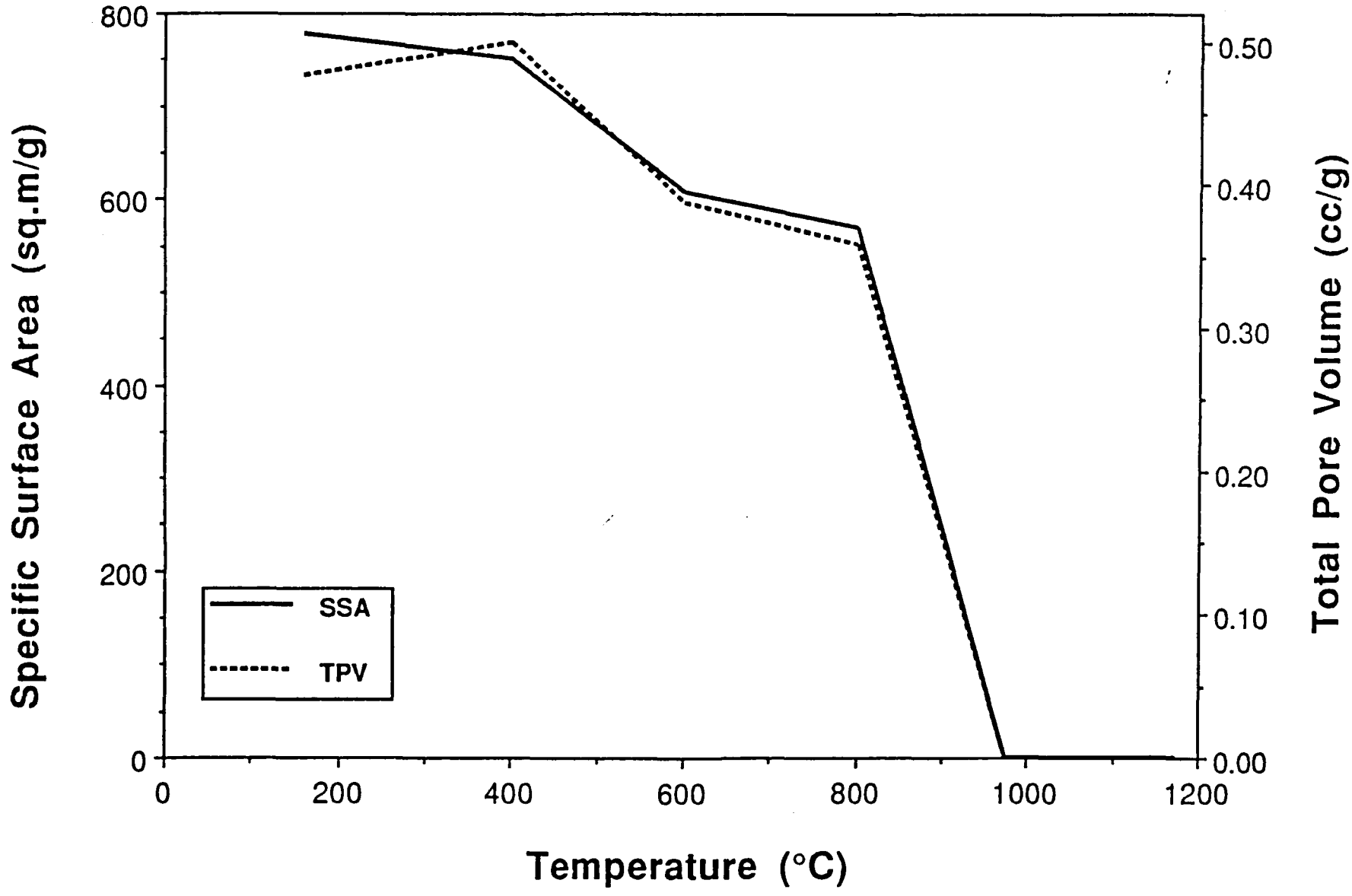
Specific Surface Area (sq.m/g)
800
600
400
200
0
0
200
400
600
800
1000
1200
Temperature (°C)
0.50
0.40
0.30
0.20
0.10
0.00
Total Pore Volume (cc/g)
SSA
TPV

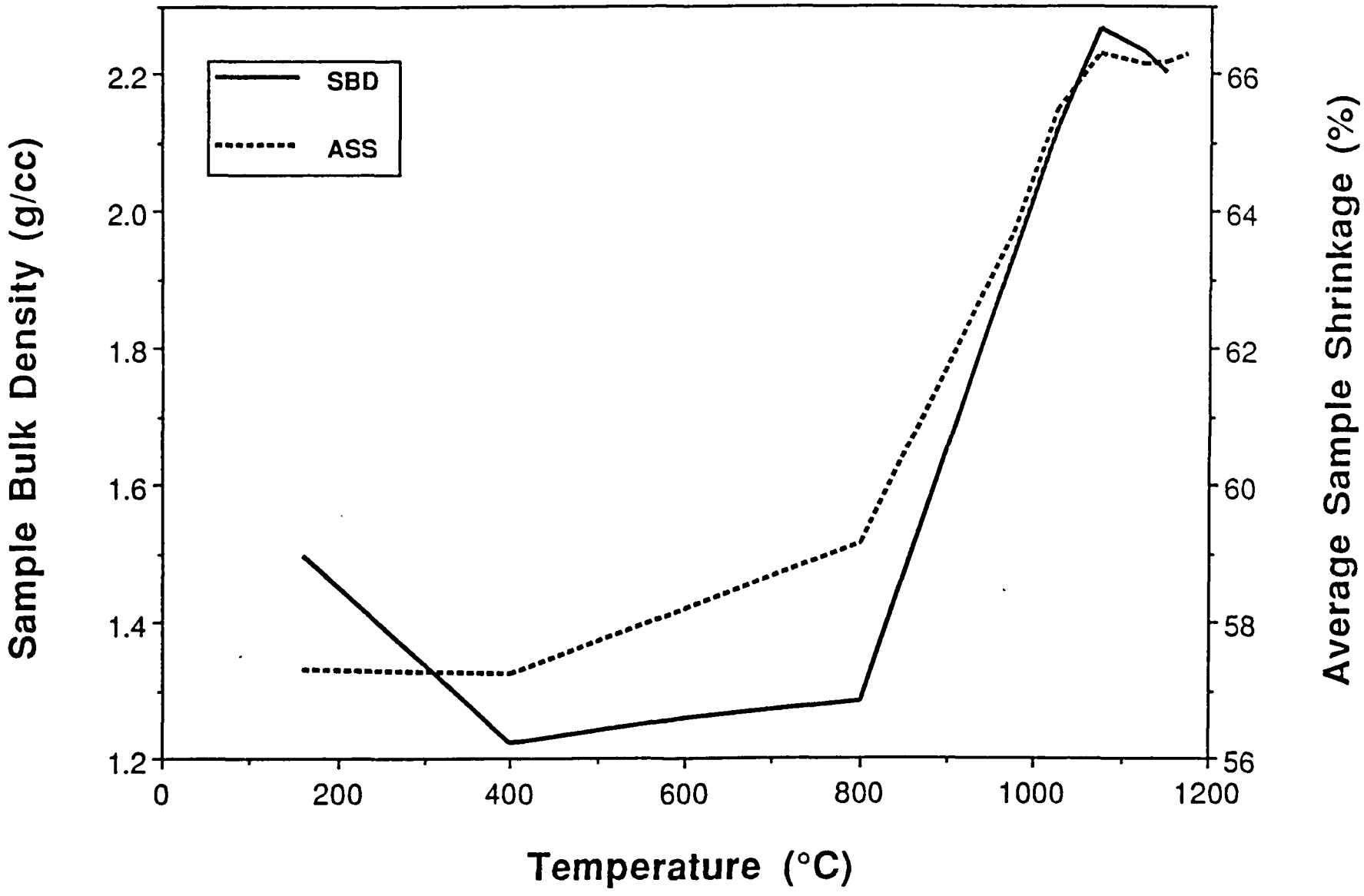
SBD
ASS
Sample Bulk Density (g/cc)
Average Sample Shrinkage (%)
Temperature (°C)
2.2
2.0
1.8
1.6
1.4
1.2
66
64
62
60
58
56
0
200
400
600
800
1000
1200

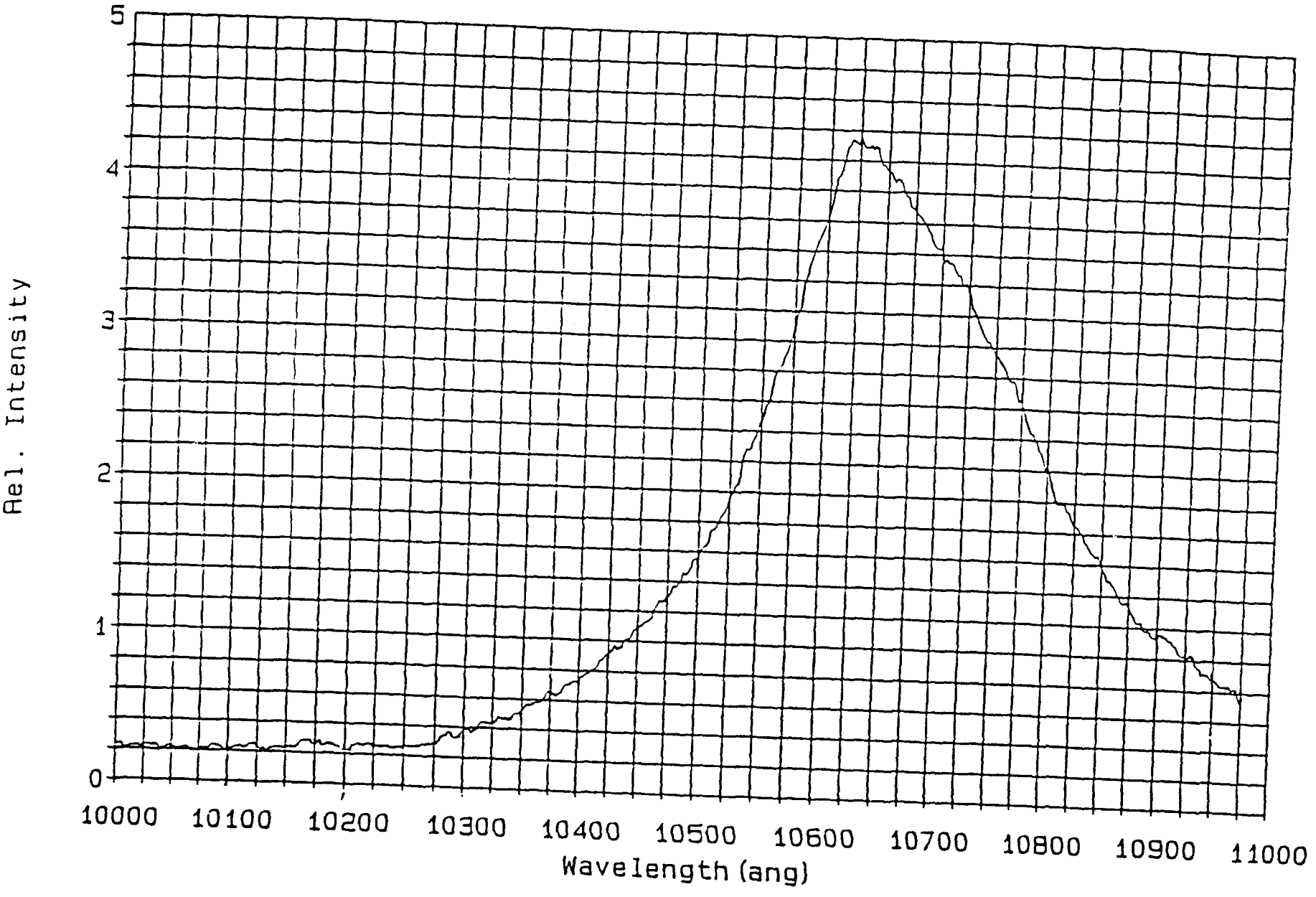
Rel. Intensity
5
4
3
2
1
0
10000
10100
10200
10300
10400
10500
10600
10700
10800
10900
11000
Wavelength (ang)

APPENDIX 5

PROCESSING OF GEL-SILICA MONOLITHS FOR OPTICS

Drying Behavior of Small Pore Gels

L.L.Hench and M.J. R. Wilson

Advanced Materials Research Center, University of Florida,

One Progress Blvd. #14, Alachua Florida 32615.

Abstract

Processing and optical properties of fully dense sol-gel derived silica, termed Type V Gel-Silica, are described. Drying of large optically transparent acid catalyzed alkoxide derived monolithic silica xerogels is emphasized. Changes in the weight, dimensions and optical properties are monitored during drying which allows a quantitative analysis of the drying process to be made. Results show three stages of drying.

Stage 1. Where the greatest changes in volume, weight and structure occur. This stage is controlled by evaporation from the surface of the body and ends when shrinkage ceases. There is no constant rate period of drying but a progressive reduction in loss rate as pores shrink from 3.9 nm to 2.3 nm.

Stage 2. Where changes in weight and volume are small but large changes in optical characteristics occur. This opaque stage is controlled by flow through small pores and liquid layers over the pore surfaces. Most of the pore emptying occurs during this stage.

Stage 3. Where there are no further dimensional changes, but a progressive loss of weight occurs until equilibrium is reached. This stage starts when ~94% of the liquid has been removed. Liquid pathways to the surface become discontinuous, and the remaining liquid can only be removed by evaporation within the pores and diffusion of the vapor to the surface.

After stabilization and densification the silica xerogel monoliths have a degree of homogeneity, purity and optical and thermal properties superior to other commercial optical silicas.

1.Introduction

The sol-gel method of producing pure monolithic silica glasses from alkoxides has generated widespread interest due to inherent advantages of the method including: low temperature processing, high purity, and high homogeneity [1,2]. Two new types of optical silica have been achieved by use of sol-gel processing [3,4].Type V gel-silica is fully dense with a very high level of purity and homogeneity. Type VI gel-silica is optically transparent and chemically and thermally stable but has 15-35% of interconnected porosity . The nature of the sol-gel process allows molding of pieces with complex geometries such as aspheric optics and lightweight ribbed mirrors.Net shape casting and high quality surface finishes are possible requiring little or no grinding and polishing and complex surface structures such as fresnel lenses can be accurately reproduced. The dried gel is both porous and transparent, it can be stabilized to produce type VI silica which can be used as a host matrix for organic polymers or metallic ions. Type VI silica can also be controllably densified to produce laser densified waveguides. When fully densified, the Type V gel-silica possesses superior physical and optical properties including a lower coefficient of thermal expansion (CTE), lower vacuum ultraviolet cutoff, higher homogeneity, fewer defects and lower dispersion than type I-IV commercial silicas.

2. Gel Drying

An important aspect of processing both Types V and VI Gel-Silicas is the production and control of very small pores during hydrolysis, condensation, and gelation [4]. The hydrolysis and polycondensation of tetramethoxysilane at low pH, used in making Types V and VI gel-silica optics [4], results in gels with very small pores (1-2 nm) which, although advantageous in some stages of the process, make the drying of large (>30g, >1cm thick) monolithic xerogels very difficult [5]. Warping and cracking can occur due to differential evaporation caused by inhomogeneous heating, and large internal stress gradients can develop if the drying rate is not carefully controlled.

When describing the drying of xerogels Zarzycki [5] applied an analysis developed by Cooper [6] for the drying of clays. However the conclusions reached were qualitative in nature since there was little experimental data to use in the description. A more detailed analysis was performed by Scherer [7] who related the various drying phenomena experimentally observed by Kawaguchi [8] and

Dwivedi [9] to changes in the physical processes and microstructure that occur during drying.

It is generally agreed that three distinct stages exist in drying: the constant rate period, the first falling rate period and the second falling rate period. During the constant rate period the negative pressure in the liquid filled pores, created by formation of a meniscus, is much greater than the strength of the solid network, which collapses in order to remain within the 'body' of liquid. The rate of evaporation per unit area of the drying surface is assumed to remain constant and is close to that obtained from a dish of freely evaporating liquid [9]. The first falling rate period, stage 2, starts when the critical point is reached. The critical point (or leatherhard point in classical drying theory [10]) occurs when the network becomes strong enough, as a consequence of the increased packing density of the solid phase, to resist further shrinkage. As the resistance to shrinkage increases, the radius of the meniscus reduces until the contact angle approaches zero and the radius of the meniscus equals the radius of the pore. This condition creates the highest capillary pressure and, unable to compress the gel any further, the pores begin to empty. As the volume of remaining liquid decreases the volume of open porosity increases and the remaining liquid becomes isolated within the pores. Flow through surface films and small pores down a pressure gradient transports liquid to the surface where most of the evaporation occurs. As the moisture level drops progressively smaller pores empty and flow to the surface slows. Eventually the liquid can only be removed by evaporation within the gel and diffusion of the vapor through the pores to the surface of the gel body. When this mechanism becomes dominant drying is said to enter stage 3, the second falling rate period.

These characteristics of drying are based on relatively little data. The data presented by Kawaguchi et al [8] concerned SiO_2 gels formed from tetraethylsilane at high pH. These gels possessed a distribution of pore radii from 10-100 nm., linear shrinkage was ~25%, and drying was achieved in ~1hr. Dwivedi [9] studied the drying behavior of thin alumina gels, of very high surface area to volume ratio, prepared using the Yoldas [11] method, again showing short drying times and high evaporation rates.

Consequently, there is considerable need for accurate drying data on various gel systems, specifically the family of acid catalyzed, alkoxide derived monolithic silica gels used to produce Type V and VI silica, with sufficient precision to discriminate between the three stages of drying. This

need has led to the construction of a drying apparatus capable of monitoring the diameter, thickness, weight and optical properties of gel monoliths continuously during their drying and transformation into rigid porous solids. In this paper the drying behavior of a large (60mm diameter, 30g weight dry) silica gel monolith is analyzed.

3.Experimental

The drying apparatus, describe previously [12,13], uses optical means to monitor changes in gel thickness, diameter and weight during drying. The optical technique allows data to be collected without contacting the sample. Gels up to 150mm diameter are suspended below a balance within a drying chamber contained within an oven. The drying chamber and the oven have windows to provide 360° viewing of the sample. An automatic 35 mm camera used in conjunction with mirrors records the gel dimensions and balance readout at any time interval from 1 second to 120 hours. Calibration of the 35mm slides to standards allows the actual gel diameter and thickness to be determined. An automatic data collection system records temperature at several locations within the chamber to confirm temperature homogeneity. Temperature control is provided by a Micristar™ ramp and soak controller with a precision of ±0.5°C up to a maximum of 150°C.

The gel monolith was made by adding 1 mole of TMOS to 16.17 moles of DI water containing 0.089 moles of nitric acid at pH ~1.5. This produced a transparent sol in < 10 minutes, with a temperature rise from 25°C to 55°C. The sol was cooled to 23°C density = 1.036 g/cm^3. The sol was cast into a 110mm diameter mold, with gelation in 55 hours at 23°C followed by aging for 3 mo. at 23°C, (see Ref. 13. for details).

The gels were dried using the apparatus described above. The drying chamber was heated at a rate of 5°C/hr to 110°C and maintained at this temperature until no further changes in weight or dimension occurred. Measurements of weight, diameter, and thickness were made at three hour intervals. After equilibrium was established the chamber was cooled to 25°C in <3 hours. The sample was removed from the chamber, weighed, measured then heated in a box furnace in ambient air at 20°C/hr. to 430°C. This temperature was maintained for 24 hrs. before rapid (< 2 hr.) cooling to ~25°C and recording of any further changes in weight and dimension.

4.Results

The absolute size and weight of the sample at various stages of processing are shown in Table 1. The drying data obtained is expressed in terms of the three drying periods described above (hereafter referred to as stage 1, stage 2, and stage 3). The changes that occur during drying are summarized in Fig 1(a,b,c,d). These are:(a) temperature, weight, (b) loss rate normalized for surface area, (c) linear shrinkage expressed as $\Delta L/L\%$ and (d) total volume. The first stage of drying accounts for ~85% of the total weight loss while taking ~40% of the total time. Cessation of shrinkage characterizes the end of the first stage and the start of the second. This critical point corresponds to the highest observed density of 1.479 g/cm^3. It represents the point at which the meniscus recedes into the bulk and is characterized by the low loss rate. During stage 2 the gel turns opaque, starting at the edges, progressing linearly towards the center. During this opaque transition the gel undergoes a small amount of further shrinkage equivalent to ~1.1% linearly, Fig.1(c), although it expands back to its previous dimensions by the time transparency is regained. Stage 2 accounts for only ~10% of the total weight loss, while taking ~35% of the total drying time. Once transparency is regained, the loss rate drops from ~0.006 g/hr/cm^2 to ~ 0.001 g/hr/cm^2 marking the start of stage 3, which accounts for the remaining drying time and weight loss.

The gel was transparent and completely colorless on removal from the drying chamber. The dried gel was stable to the atmosphere and could be exposed to adsorption and desorption of moisture without cracking. The dimension of the sample after drying was 59mm diameter 13.1mm thick. Heating the dried gels to 430°C resulted in a the loss of a small amount of chemisorbed water (see Table 1). After the 430°C heat treatment the sample was tested for surface area, pore volume, and pore radius by nitrogen adsorption and BET, these data showed a surface area of 549 m^2/g, a pore volume of 0.654 cm^3/g and an average pore radius of 2.3 nm.

5.Discussion

The drying process starts as soon as the gel is removed from the pore liquid in the aging chamber and a liquid/vapor interface is established at the surface. As the heating rate in the drying chamber cannot exceed an experimentally determined rate, a period of time exists during which the

temperature is not constant but increases to 110°C. This is the 'heating' portion of Figs.1(a-d) Once isothermal conditions are attained, the drying behavior follows three successive stages.

Stage 1. During which the greatest changes in volume weight and structure occur.

Stage 2. In which changes in weight and volume are small but large changes in optical characteristics are seen; ie., opacity develops.

Stage 3. In which there are no further dimensional changes, but there is a progressive loss of weight to the minimum attainable value.

During the rise in temperature, the gel expanded by a small amount (~1% linear, Fig 1 (c,d)). The maximum volume was measured when the chamber reached 70°C. This is attributed to the thermal expansion characteristics of the pore liquid, which on heating expands before evaporative losses dominate and shrinkage begins [13].

5.2 Stage 1.

The silica gel monolith studied here did not exhibit a constant rate of loss during stage 1, even when normalized for surface area, Fig 1(b). This result is contradictory to those of Dwivedi [9] who found, when drying thin alumina gels, that evaporation rate per unit area of drying surface was independent of time and similar to the rate obtained from a dish of freely evaporating liquid. However Dwivedi's results, and those of Kawaguchi [8], for a large pore silica gel, involve shorter drying times (at lower temperatures) and much higher loss rates than those presented here for large monoliths. Their gels apparently had a larger scale than those studied here.

In a saturated material the evaporation rate is dictated by the difference between the vapor pressure at the evaporating surface (P_s) and the vapor pressure of the ambient atmosphere within the drying chamber (P_a). Evaporation will continue as long as $P_s > P_a$ with the rate defined by

$$V_e = K_e (P_s - P_a) \qquad (1)$$

where V_e is the rate of evaporation, and K_e is an evaporation constant that depends on air flow conditions. The ambient vapor pressure in the drying chamber, P_a, decreases during drying [13]. This increase the difference $(P_s - P_a)$ and if the evaporation constant K_e does not change then the evaporation rate also increases. This suggests that the vapor pressure at the evaporating surface P_s m ust decrease considerably to explain the drop in evaporation rate measured during stage 1.

The driving force for shrinkage during stage 1 is capillary pressure that develops when menisci of very small radii form in the pores of the gel. The smallest meniscus that can form in a given pore is equal to the radius of the pore. When the radius of the meniscus diminishes to equal the radius of the pore, the pressure maximizes and the meniscus, unable to reduce its radius any further, enters the pore. For drying gels this occurs at the critical point. Consequently, during stage 1 while the meniscus remains at the surface, $r_m > r_p$, where r_m is the meniscus radius, and r_p is the pore radius. However the large pressures required to shrink the gel during stage 1 infer that the meniscus radii, r_m, are probably close to r_p.

An important aspect of the pressure difference that can arise when these menisci form is the reduction in vapor pressure that can occur. The vapor pressure is related to the capillary pressure by the Gibbs-Kelvin equation (15),

$$\ln \frac{P_s}{P_o} = \frac{V_{mol}\,\gamma}{R\,T} \cdot \frac{2}{r_m} \qquad (2)$$

where P_s is the vapor pressure over the meniscus, P_o is the vapor pressure over a flat surface (760 mm Hg), V_{mol} is the molar volume of the pore liquid (m^3/mol), R the gas constant (8.314 J mol^{-1} K^{-1}), T the temperature (°K), r_m the radius of curvature of the meniscus (m^{-1}), and γ the surface tension of the liquid (J/m^{-1}).

The meniscus radius r_m is defined as negative because the center of curvature is in the vapor phase. The molar volume (V_{mol}) and the surface tension (γ) change with both composition and temperature and in order to solve this equation the changes in pore liquid composition during stage 1 must be taken into account. The initial composition (determined from the density and stoichiometric calculation) is 40% methanol and 60% water (by volume). This composition has a molar volume of 2.75E-6 m^3/mol and a surface tension of 0.030 J/m^{-1} at 100°C. As stage 1 drying progresses the methanol preferentially evaporates and the molar volume decreases and surface tension increases to the values exhibited by water at the drying temperature (V_{mol} =1.87E-6 m^3/mol, γ = 0.065 J/m^{-1}). The change in composition measured in ref. 13 can be used to determine these intermediate values.

The average pore radius of gel A when dry was ~2.3 nm and the linear reduction during drying was ~41% therefore the pores in the wet (aged) gel should be 41% larger than that measured in the dry state by BET. For gel A the radius of pores prior to drying is calculated to be 3.9 nm. These dimensions represent the pore radii at the beginning (3.9 nm) and end (2.3 nm) of stage 1. These values represent the average pore radius and thus the minimum meniscus radius (r_m) used in equation (2). During stage 1 the meniscus is at the surface and thus the meniscus radius (r_m) must be greater than the pore radius (r_p) or pore invasion would occur. However in solving equation (2) it is assumed that the meniscus radius is the same as the pore radius as it decreases thus representing the maximum possible vapor pressure suppression that could occur. These data are shown in Fig 2. Similar results were obtained for other silica monoliths [13].

The pore radius is obtained by measuring the pore volume and surface area by N_2 adsorption isotherms and using the classical BET relationship [16]. It is important to recognize that BET pore size analysis is performed after considerable degassing at high temperature (430°C). At low temperatures, such as in the drying gels, the pore radius is effectively changed by the presence of a bound water layer on the pore surfaces. The bound water layers possess properties such as melting and boiling points that are markedly different from those of bulk water. Wallace and Hench [14], using Dielectric Relaxation Spectroscopy (DRS) and Differential Scanning Calorimetry (DSC) analyzed the properties and calculated the thickness of this bound water layer in acid catalyzed gels of similar porosity to gel A. The non-freezing bound water layer was ~0.97 nm thick for pores in the range of 2.5 -> 4.0 nm. If the bound water layer is present at the drying temperatures used here then it must be taken into account in determining the true hydraulic radius of the pores. This bound layer can usually be ignored, however in the case of pores of this dimension its thickness can significantly reduce the overall radius. This effective reduction in pore radius affects the minimum meniscus radius possible, and thereby the value of P_s / P_o predicted by equation (2). These data are shown in Fig 2.

It has often been questioned as whether the Gibbs-Kelvin equation remains valid at the dimensions reported here [15]. The equation has been verified for small droplets but attempts to measure the vapor pressure reduction in small capillaries has produced some odd results. Shereshefsky et al [17] reported that evaporation of water and toluene from capillaries a few microns

in radius resulted in vapor pressures 10-80 times lower than the predicted value. Scherer, in his review of drying [7] concludes that the Gibbs-Kelvin equation is valid for radii as small as ~1nm for organic liquids, but with water deviations exist in the 1.5 nm to 5 nm radius range, ie the pore sizes studied here. Scherer attributes the difference to the long range hydration forces in water that can affect the surface tension in films less than 5 nm thick.

These results indicate that vapor pressure reduction over menisci of nanometer radius occurs, and is primarily responsible for the dramatic reduction of the evaporation rate during stage 1 drying, especially when one includes the effects of a bound water layer on effective evaporation area and the hydraulic radius of the pores. This analysis of effects of pore radius on stage 1 evaporation also explains why this decrease in evaporation rate was not seen by Dwivedi [9] and Kawaguchi [8] who observed a constant rate period during the drying of their gels. The magnitude of vapor pressure reduction required to produce a noticeable decrease in evaporation rate during stage 1 drying does not occur until menisci of $r_m < 15$ nm are formed. Menisci of this radius cannot form in pores of the dimensions reported for their gels, and no significant change in the evaporation rate was seen during stage 1 drying..

5.2 Stage 2. The Opaque stage.

The second stage starts at the critical (or leatherhard) point. At this point the meniscus radius is equal to the pore radius and is able to penetrate the bulk. The loss rate falls to a, low value of ~0.008 g/hr/cm^2. This stage is consistent with the stage Scherer terms the "first falling rate period" [7]. Liquid is driven to the surface by gradients in capillary pressure, where it evaporates due to the ambient vapor pressure being lower than inside the pores.

Shortly after entering the second stage, the gel turns opaque, starting at the edges and progresses in a direction perpendicular to the surface toward the center. Possible causes of this phenomena including phase separation of the pore liquid or exsolution of gas from the liquid. The most plausible explanation is by Shaw [18,19] who suggests that this phenomenon is caused by light scattering from isolated pores (or groups of pores) in the process of emptying, of such a dimension that they are able to scatter light. The data obtained during stage 2 indicate an increase in open porosity from ~0.012 cm^3/g. to ~0.364 cm^3/g. during the opaque transition.

5.3 Stage 3 .

After transparency is regained, the loss rate gradually falls to a value of ~0.001g/hr/cm^2 until no further weight changes occur. The transition to stage 3 is the hardest to identify. Its start is probably best defined as the end of the opaque stage. Scherer [7] describes stage 3 as the "second falling rate period", where the temperature of the body is not as strongly suppressed as when evaporation rates were higher. The remaining liquid evaporates within the pores and is removed by diffusion of its vapor to the surface. By the start of stage 3 the gel is to all essentially dry. It can be removed from the drying chamber and dehydrated under much more severe conditions (180°C at 0.1 Torr) without risk of cracking. Stress birefringence measurements [13] indicate a reduction in residual stress during this period.

5.5 Drying failure.

The drying times reported here fall within an experimentally determined range for gels of this size. Shorter drying times have been recorded but usually involve a greater percentage of failure. However, when samples fail they do so at distinct points within the drying sequence. Cracking during stage 1 is rare but can occur when the gel has had insufficient aging and thus a low strength (see Scherer (7)) and does not possess the dimensional stability to withstand the increasing compressive stress. If the loss rate is increased (by lowering the vapor pressure of the ambient atmosphere or increasing the draft rate) there comes a point where it exceeds the maximum rate of shrinkage. If this occurs, localized pore emptying results and surface cracks develop.

Most failures occur around the critical point at the end of stage 1, and the early part of stage 2. At the start of stage 2 the modulus of the gel is very high and the compressive stress is in the order of ~100 MPa. The possibility of cracking at this point is great due to the high stresses and low strain tolerance of the material. Measurements indicate that the point at which the gel stops shrinking and the point at which the meniscus falls below the surface are not nescesarily simultaneous. This suggests that shrinkage is still occurring within dry (or empty) pores. A distribution of pore sizes exists in these materials, and therefore some pores must empty before others. The pores that empty first (at the larger end of the distribution) stop shrinking at the point of emptying, and if a pore at the larger end of the distribution empties before its neighbors (and is thus surrounded by full pores), it can only

shrink passively under their influence. Extending this concept further (into stage 2), if regions of wet and dry pores are established then the dry regions can only shrink under the influence of the wet. Given that the compressibility of these regions is different, then cracking at the boundaries can occur. Cracking has been observed throughout stage 2, but becomes less likely as dehydration progresses. Cracking during stage 3 does not occur, in our experience. The moisture level and thus the stress is considerably diminished by this point and cracking will not occur even under fairly extreme dehydration conditions (180°C at 0.1 Torr).

6.Conclusions Regarding Drying

Drying of large (>30g, >1cm thick) monolithic silica xerogels has been achieved by careful control of the drying environment, the steps preceding drying, and elimination of defects which can serve as stress risers [4]. The drying behavior of these acid catalyzed, alkoxide derived silica gels can be described in terms of three stages:

Stage 1. Rapid loss of weight and volume to ~20% of aged values. During this stage the rate of loss is not constant. The evaporation rate decreases due to suppression of vapor pressure at the gel surface by pore menisci <4nm. However, measured rates were lower than those predicted by the Gibbs-Kelvin equation.

Stage 2. When shrinkage ceases the rate of weight loss becomes linear and the gel turns opaque. During this second stage the gel undergoes a small but temporary reduction in volume. The likelihood of cracking is greatest during the early part of this stage.

Stage 3. The rate of loss falls to a lower value. The third stage takes considerable time, but results in a gel within ~3% of theoretical dry weight at 110°C.

These stages are consistent with drying behavior reported by other researchers investigating gel based systems. However major differences in behavior are seen during stage 1 which arise as a consequence of the extremely small scale of the silica gel structure.

7. Optical Properties

Due to the very high level of purity and very high homogeneity of the acid catalyzed alkoxide derived silica monoliths they have exceptionally good optical properties. Figs. 3 and 4 summarizes

the optical transmission of a densified gel-silica 75mm plano-plano sample made with a drying process similar to that described herein.These results, based on Ref. 4, show a vacuum UV cutoff of 159 nm which is substantially better than Type III silica optics now on the market for UV applications. A major advantage of the new Type V gel-silica optics, illustrated in Fig. 4 (Refs.3,4), is the absence of OH absorbtion bands. As shown by West et al [20] ,using quantum mechanical calculations, the elimination of OH groups is responsible for the improved vacuum UV transmission of the Type V gel-silica material, termed GELSIL™. As discussed in Refs. 3,4, commercial Type V GELSIL™ also has a level of homogeneity that is better than 1 ppm, based upon optical interferometry, and as shown in Ref. 21 has 0 bubbles and inclusions and <5nm/cm strain birefringence. Of particular interest for severe optical applications, such as intracavity laser optics, the coefficient of thermal expansion (CTE) of Type V GELSIL™ is significantly lower than other commercial Type III or IV optical silicas [4]. The low value of CTE exists over a wide temperature range from 0°C to 650°C. Thus, nearly all of the potential advantages of sol-gel processing to improve the physical properties of dense silica optics have now been realized. The potential advantages of casting and drying silica sols to produce monoliths with net shape and net surface finish for precision optics have also been realized, as discussed by Nogues et al in this proceedings. Likewise, the sol-gel process has been used to produce optically transparent Type VI ultraporous optical components containing polymers impregnated into the structure as an optically active second phase [3,4]. The porous Type VI gel-silica monoliths have also been used successfully as substrates for laser densification of waveguides [22].

Consequently, during the last few years it has been possible to produce a wide range of unique optical materials by use of sol-gel processing. With additional understanding of the drying processes involved in the production of these new materials with nanometer scale structures, such as discussed in this paper, it should be feasible to achieve even further advances in the control of the ultrastructure and properties of silica optics.

Acknowledgments

The authors are grateful to the U.S. Air Force Office of Scientific Research under contract AFOSR#F49620-88-C-0073 for supporting this work.

References

(1) J.D.Mackenzie, D.R.Ulrich. Eds. Ultrastructure Processing of Advanced Ceramics. John Wiley and Sons, New York, 1988.

(2) C. Jeffrey Brinker, D.E.Clark, D.R.Ulrich, Eds. Better Ceramics Through Chemistry Vol 3. Mat. Res. Soc. Symp. Proc. Vol 121, Pittsburgh Pennsylvania, 1988.

(3) L.L. Hench, S.H. Wang and J.L. Nogues, Multifunctional Materials SPIE Vol. 878, 1988, 76.

(4) L.L. Hench, M.J.R. Wilson, C. Balaban, and J.L. Nogues, in: Proceedings of IVth Ultrastructure Processing Conference, Tuscon, Az , Eds. D. Uhlmann, M.Weinberg, and D.R. Ulrich, John Wiley and Sons, New York, 1989.

(5) J. Zarzycki, in Ultrastructure Processing of Ceramics, Glasses, and Composites, L.L.Hench, D.R.Ulrich, Eds. John Wiley and Sons, New York, 1984, p27.

(6) A.R.Cooper, In Ceramics Processing Before Firing, Eds, G.Y.Onoda, L.L.Hench, John Wiley and sons, New York, 1978.

(7) C.J. Brinker and G.W. Scherer, Sol-Gel Science. In press, Academic Press, 1989.

(8) T.Kawaguchi, J.Iura, N.Taneda, H.Hishikura, Y.Kokubu. J. Non-Cryst. Solids 1986, 82, 50-56.

(9) R.K. Dwivedi, J. Mater. Sci. Lett. 1986, 5, 373.

(10) R.W.Ford, Ceramics Drying, Pergamon, New York, 1986.

(11) B.E.Yoldas, J. Mater. Sci. 1975, 10, 1856.

(12) M.J.R. Wilson, L.L.Hench, "Real time monitoring of silica gel drying behavior" Proceedings of the IVth. Ultrastructure Processing Conference. Tuscon, Arizona. Feb 1989.

(13) M.J.R. Wilson, Masters thesis, Drying Kinetics of Pure Silica Xerogels University of Florida, 1989.

(14) S. Wallace, L.L.Hench, Proceedings of the IVth. Ultrastructure Processing Conference. Tuscon, Arizona. Feb 1989.

(15) Authur W. Adamson, Physical Chemistry of Surfaces, 4th edition
John Wiley and Sons, New York, 1982, pp 54-55.

(16) S. Lowell and J.E.Shields, Powder Surface Area and Porosity 2nd. edition, Chapman and Hall, London, 1984, 14-28.

(17) M. Folman, J.L. Shereshefsky, J. Phys Chem 1955, 59, 667.

(18) T.M. Shaw, Mat.Res.Soc.Symp. Proc. Vol 73 1986.

(19) T.M. Shaw, Phys. Rev. Lett. 1987, 59, 15. p1671-1674.

(20) J.K.West, S.Wallace, L.L.Hench and G.R.Lishawa, Proceedings of the IVth Ultrastructure Processing Conference , Tuscon, Arizona., Feb. 1989.

(21) S.H. Wang, C. Campbell and L.L. Hench, in: Ultrastructure Processing of Advanced Ceramics, Eds. J. D. Mackenzie and D.R. Ulrich, John Wiley and Sons, New York, 1988 p.145.

(22) R.V. Ramaswamy, T. Chia, R. Srivastava, A. Milou, and J.K. West, Multifunctional Materials SPIE Vol. 878 1988, p. 86

Table A. Physical Dimensions of gel A

State	Diameter (mm)	Thickness (mm)	Weight (g)	Density (g/cm^3)
As cast	108.9	24.3	234.2	1.036
Aged	99.5	21.2	178.1	1.080
Dry(110°C)	59.0	13.1	34.3	0.961
Dry(430°C)	58.6	13.0	32.4	0.925
Theoretical dry weight	-----	-----	31.1	------

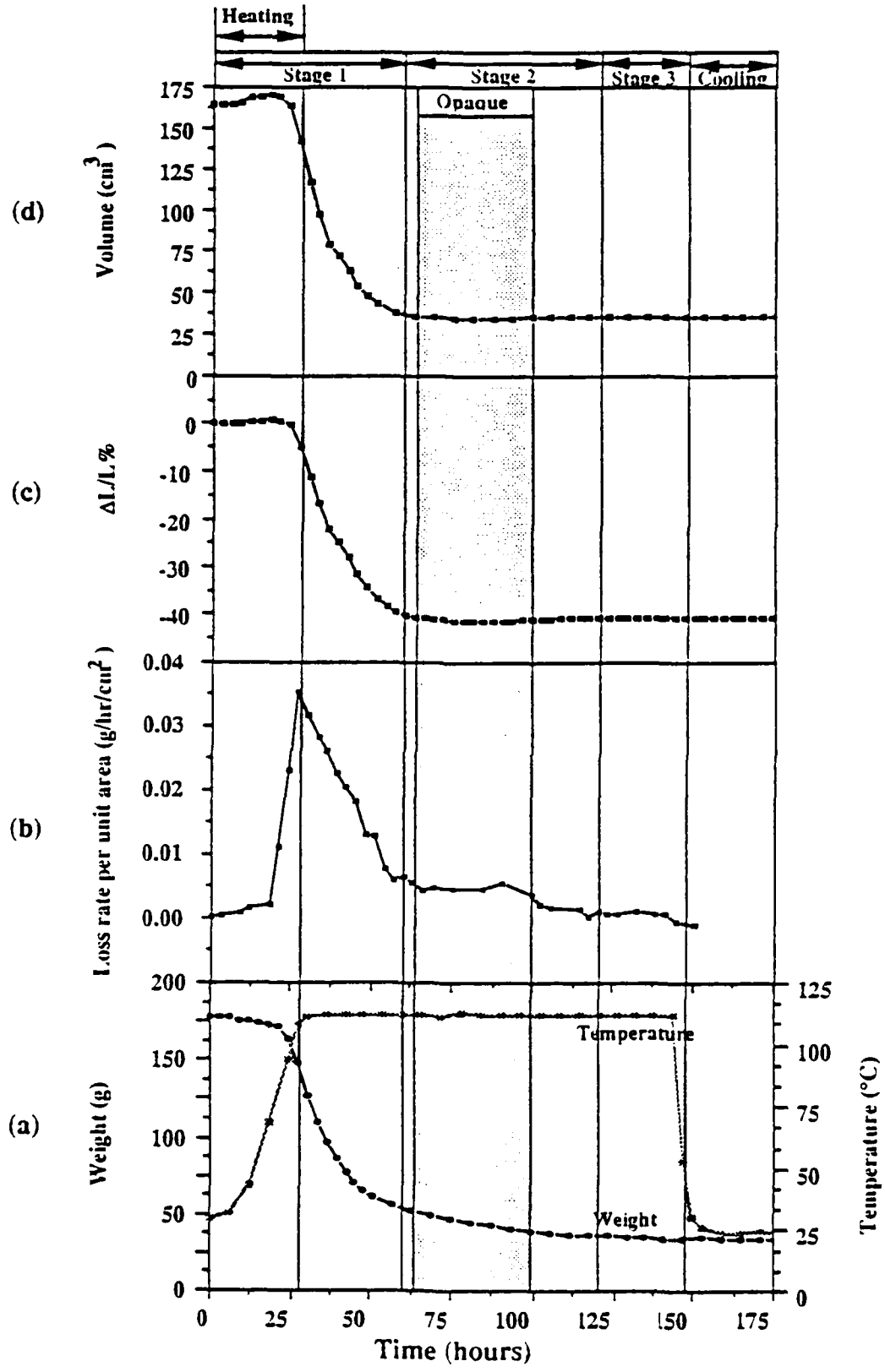

Figure 1. Time dependence of
(a) Temperature and weight
(b) Loss rate per unit area
(c) Linear shrinkage
(d) Volume
for gel A

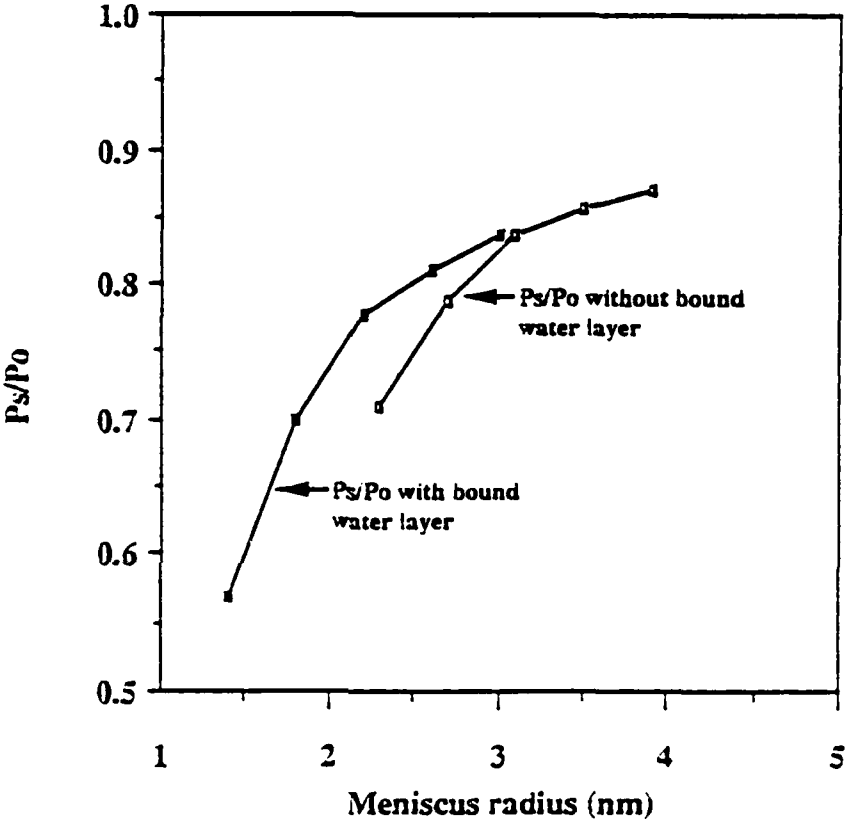

Figure 2. Reduction of vapor pressure with decreasing meniscus radius as predicted by the Gibbs-Kelvin equation for the size of menisci expected in this system.

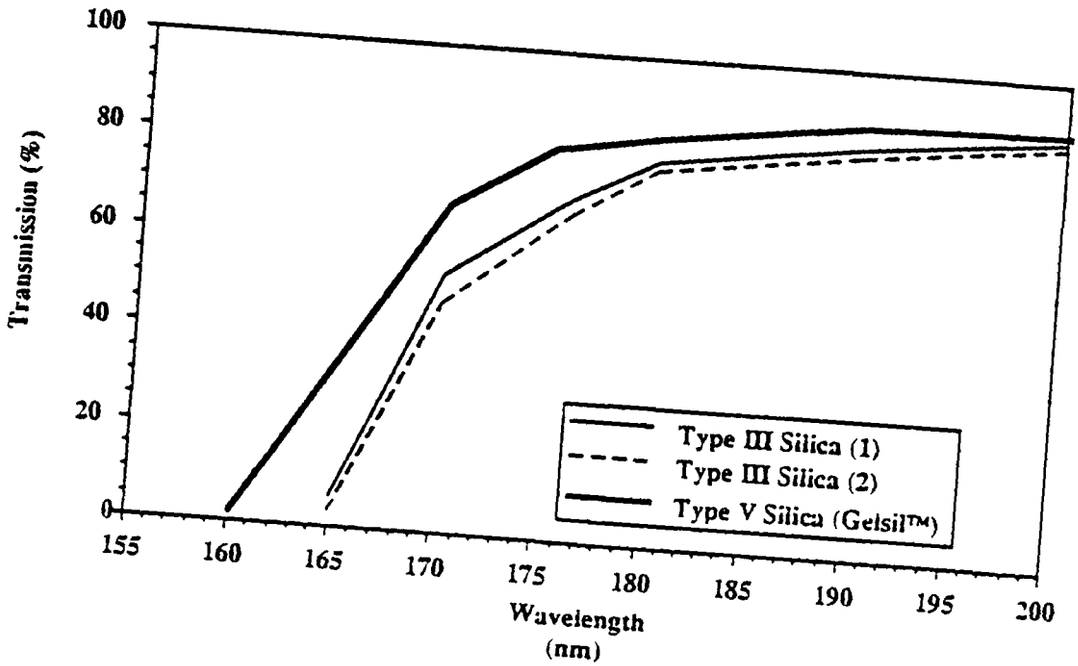

Figure 3. UV transmission of densified type V Gelsil™ and type III silica

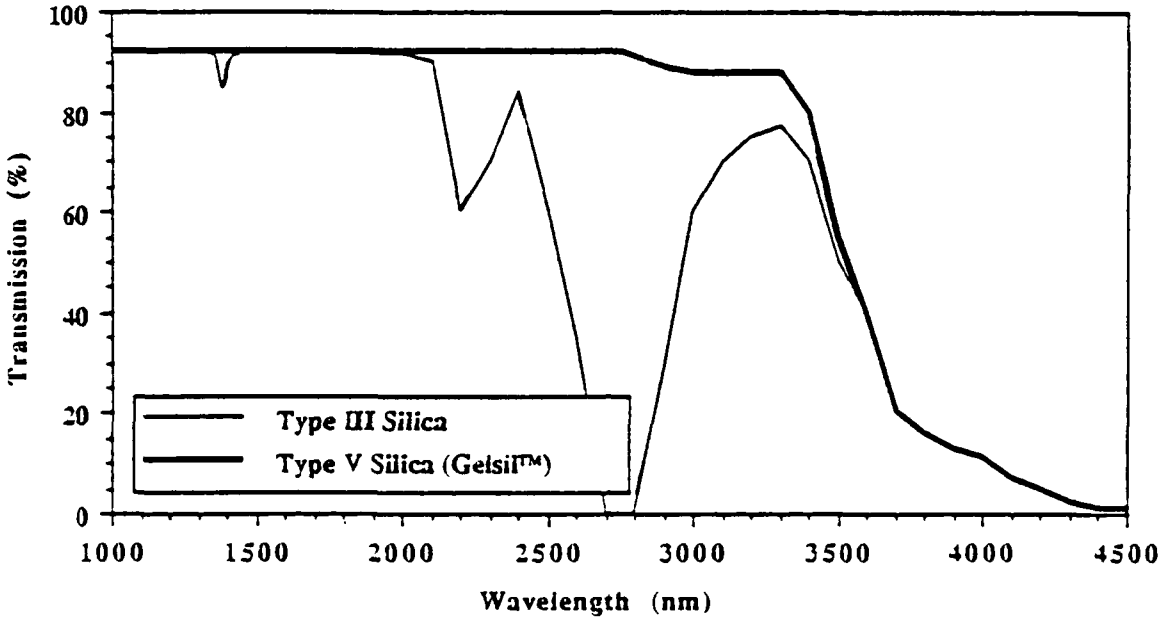

Figure 4. NIR transmission of densified type V Geisil™ and type III silica

APPENDIX 6

STRUCTURAL EVOLUTION DURING SINTERING OF OPTICAL SOL-GEL SILICA

W.L. VASCONCELOS, R.T. DeHOFF and L.L. HENCH
Dept. Materials Science and Eng., University of Florida, Gainesville FL 32610 USA

The evolution of the structure of sol-gel derived optical silica monoliths is described in terms of both metric and topological parameters. The characterization of the structural evolution is based on nitrogen gas adsorption and helium and mercury pycnometry. A topological model is introduced which permits estimation of the number of branches, number of nodes, connectivity and number of separate parts of the pore structure.

Topology, Sintering, Densification, Silica, Sol-Gel Method

1. Introduction

The growth of sol-gel technology research is due to the many unique applications of that class of materials [1-9]. An understanding of the densification of sol-gel materials presents a remarkable opportunity for controlling their final properties.

Usually the sintering process is followed by means of the volume fraction of pores (V_V), which is a metric parameter. The introduction of topological parameters to describe microstructural evolution during sintering was carried out about 30 years ago by Rhines [10]; development of the topological and stereological description of the structure of materials have continued [11-13]. The first application of topological concepts to the study of densification of a sol-gel material was introduced recently by the authors [14,15]. That previous work shows that different geometries assumed for modelling the pore structure yield similar paths for the structural evolution, because of the topological nature of the sintering process. This work is intended to describe the structural evolution of sol-gel silica monoliths using both metric and topological properties.

2. Experimental Procedure

Samples of optical sol-gel silica monoliths were prepared using tetramethylorthosilicate (TMOS) and DI-water, with acid catalysis by HNO_3. A set of samples was dried at 180°C in Teflon® containers, and those samples are termed "type A samples" in this work. A second set of samples was prepared in similar conditions, but the drying procedure was modified to provide for a slower rate of water removal, resulting in the "type B samples." A third set of samples was catalyzed using HF, and those samples are termed "type C samples." After drying at 180°C the samples were densified with controlled heating rates and maximum temperatures in the range of 500°C to 1100°C in a dry-air atmosphere, and in a chlorine atmosphere at 1150°C.

After densification the samples were analyzed in an automatic gas adsorption machine type Autosorb 6 (Quantachrome Corp.) for volume and surface area of pores. True density measurements were performed in a helium micropycnometer (Quantachrome Corp.).

3. Results and Discussion

The gas adsorption analysis, the helium pycnometry and the mercury bulk density measurements lead to the results shown in fig.1. The type A samples present an average BET pore radius of 12Å in the dried stage and this average pore radius remains fairly constant during the entire densification process [16]. The volume fraction of pores in the dried stage is about 0.5 for type A samples, and about 0.6 and 0.7 for type B and C samples respectively.

The average pore radii for dried type B and C samples are 32Å and 81Å respectively. The average pore radius for type B samples decreases slightly as densification proceeds, while for type C samples the pore size decreases slightly up to about 1000°C and then it decreases rapidly for higher densification temperatures [14].

As the densification temperature increases the volume fraction of pores decreases relatively slowly for type A samples as shown in fig.1. After about 800°C the decrease in V_V of pores with increasing densification temperature is more pronounced. For type B samples the greater porosity

levels are kept until temperatures higher than for type A samples. Type C samples present a sharp decrease in porosity around 800°C.

As the porosity decreases with sintering, the bulk density increases, as shown in fig.2. The maximum value of bulk density for the three types of samples is around 2.2 g/cm^3. While the bulk density increases continuously with increasing densification temperature, the skeletal (or true) density varies as depicted in fig.3. The true density increases continuously from the dried stage up to a temperature in the range of 800°C to 1000°C, depending on the pore size, and then it decreases for higher densification temperatures. It is possible that these variations in skeletal density are associated with changes in Si-O atomic structures.

In order to obtain information on the topological state of silica gel samples, the pore structure is modelled as cylinders [14,15]. The general expression correlating the genus (G_V), number of branches (B_V), number of nodes (N_V) and number of separate parts (P_V) is given by [12]

$$G_V = B_V - N_V + P_V. \quad (1)$$

Assuming an initial coordination number of pores (CN) of 4, the variation of the topological parameters B_V, N_V, G_V and P_V with CN is shown in fig.4. A sensitivity analysis [14] of the initial pore coordination number reveals that initial CN's between 4 and 8 yield the most reasonable and consistent results. An initial CN of 4 is used in this work in order to permit comparisons with previous work [15] in which a tetrahedral model was used. Figure 4 shows that as densification proceeds and CN goes from 4 to zero, B_V decreases continuously, while N_V is initially constant and starts decreasing towards zero when CN becomes equal to 2. When CN reaches 2 the genus becomes zero and the number of separate parts (isolated pores) starts increasing. In order to evaluate B_V, N_V, G_V and P_V when the pore coordination number varies between 2 and zero, it is assumed that N_V follows a linear relationship with CN, as shown in fig.4. N_V is estimated by using the following expression [14]:

$$N_V = \frac{\sqrt{2}\, S_V}{9\, D\, L}, \quad (2)$$

where D is the average pore diameter and L the average pore branch length. In the region where CN varies from 2 to zero the pore coordination number is given by

$$CN = \frac{2\,N_V}{N_V^0}, \tag{3}$$

where N_V^0 is the number of nodes present in the dried stage. In the same region, the number of branches per unit volume is given by

$$B_V = \frac{CN\,N_V}{2}, \tag{4}$$

while the number of separate parts is given by

$$P_V = N_V - B_V. \tag{5}$$

When the topological parameters are plotted as a function of densification temperature the results are as shown in fig.5, for type A silica gel samples. The initial situation in fig.5 is at a temperature of 180°C, corresponding to the dried stage. As the densification temperature increases both the number of branches (B_V) and the genus (G_V) decrease, while the number of nodes remains constant at N_V^0, and the number of separate parts remains constant at unity. The position where the pore coordination number (CN) decreases to 2 (fig.4) corresponds in fig.5 to the point where B_V reaches the value of N_V^0, which occurs at a temperature just above 1000°C for that set of samples. At that point the genus goes to zero and the number of separate parts increases from unity and decreases again towards zero at the end of the densification.

The variation of the pore connectivity, as expressed by the genus, as a function of densification temperature is shown in fig.6 for type A samples, B and C. Type A samples present a continuously decreasing pore connectivity as the temperature increases, while type B samples and C show an increase in pore connectivity in the initial stages of the heating treatment. For type B samples the genus decreases towards zero at temperatures above 1000°C, while for type C samples the decrease in genus occurs earlier, at around 900°C.

4. Conclusions

With densification, the structure of optical sol-gel silica monoliths evolve in such a way that the volume fraction of pores decreases relatively slowly in the beginning of the heating treatment and decreases sharply at higher temperatures. The levels of porosity and density, and the temperatures in which the structural evolution changes its pace, all depend on the pore size of the

silica monoliths. Using a topological model it is possible to estimate the number of branches, number of nodes, connectivity and number of separate parts of nanometer scale pore structures.

The authors acknowledge the support of the US-AFOSR (contract n° F49620-88-C-0073). One of the authors (WLV) is indebted to the support of UFMG (Federal University of Minas Gerais) and CAPES (Brazilian Agency of Post-Graduation).

References

[1] L.L Hench and D.R. Ulrich, Eds., Ultrastructure Processing of Ceramics, Glasses and Composites (Wiley, New York, 1984)

[2] L.L. Hench and D.R. Ulrich, Eds., Science of Ceramic Chemical Processing (Wiley, New York, 1986)

[3] J.D. Mackenzie and D.R. Ulrich, Eds., Ultrastructure Processing of Advanced Ceramics (Wiley, New York, 1988).

[4] L.L. Hench and L.K. West, Chem. Reviews, in press.

[5] L.L. Hench, M.J.R. Wilson, C. Balaban and J.L. Nogues, in: Proc. 4th International Conference on Ultrastructure Processing of Ceramics, Glasses and Composites, Tucson, Arizona (February, 1989).

[6] D.R. Ulrich, J.Non-Cryst. Solids 73 (1985) 174.

[7] H. Dislich, J. Non-Cryst. Solids 73 (1985) 599.

[8] G.W. Scherer, J. Non-Cryst. Solids, 73 (1985) 661.

[9] J. Wenzel, J. Non-Cryst. Solids 73 (1985) 693.

[10] F.N. Rhines, Plansee Proc., 3rd seminar, Reutte, Tyrol (1958) 38.

[11] R.T. DeHoff and F.N. Rhines, Eds., Quantitative Microscopy (McGraw-Hill, New York, 1968).

[12] F.N. Rhines, R.T. DeHoff and J. Kronsbein, A Topological Study of the Sintering Process, Final Report to the US-AEC (University of Florida, Gainesville, 1969).

[13] E.E. Underwood, Quantitative Stereology (Addison-Wesley, Reading, MA, 1970).

[14] W.L. Vasconcelos. PhD Dissertation (University of Florida. Gainesville. 1989).

[15] W.L. Vasconcelos. R.T. DeHoff and L.L. Hench. in: Proc. 4th International Conference on Ultrastructure Processing of Ceramics. Glasses and Composites. Tucson. Arizona (February. 1989).

[16] T.W. Zerda. W.L. Vasconcelos and L.L. Hench. in: Proc. 5th International Workshop on Glasses and Ceramics from Gels. Rio de Janeiro. Brazil (August. 1989).

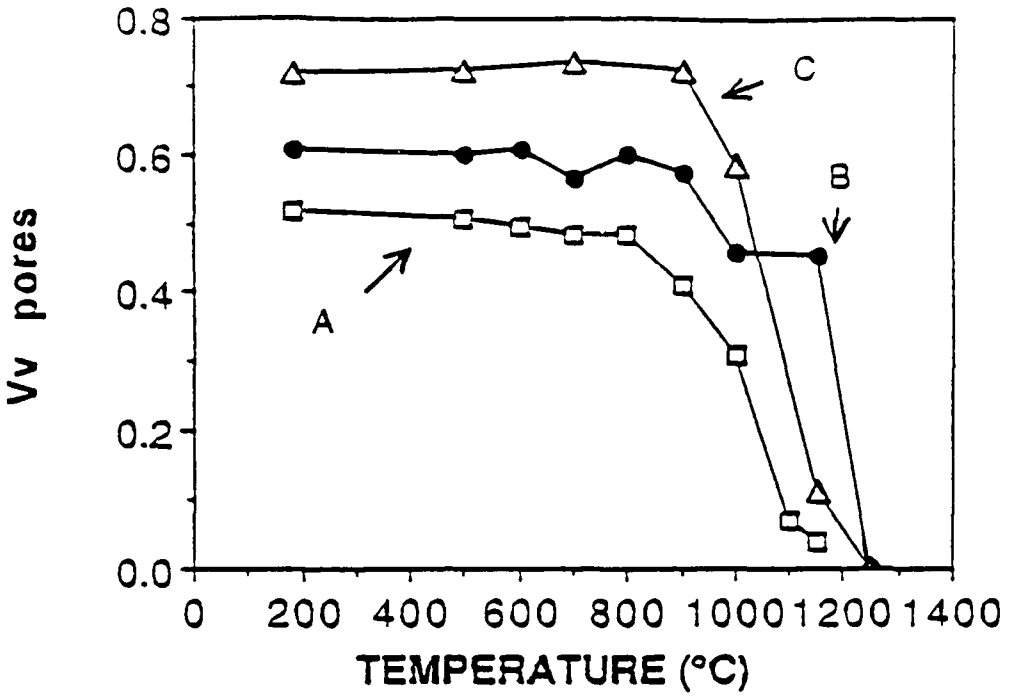

Fig. 1. Variation of the volume fraction of pores (V_V) as a function of densification temperature for silica gels type A, B and C.

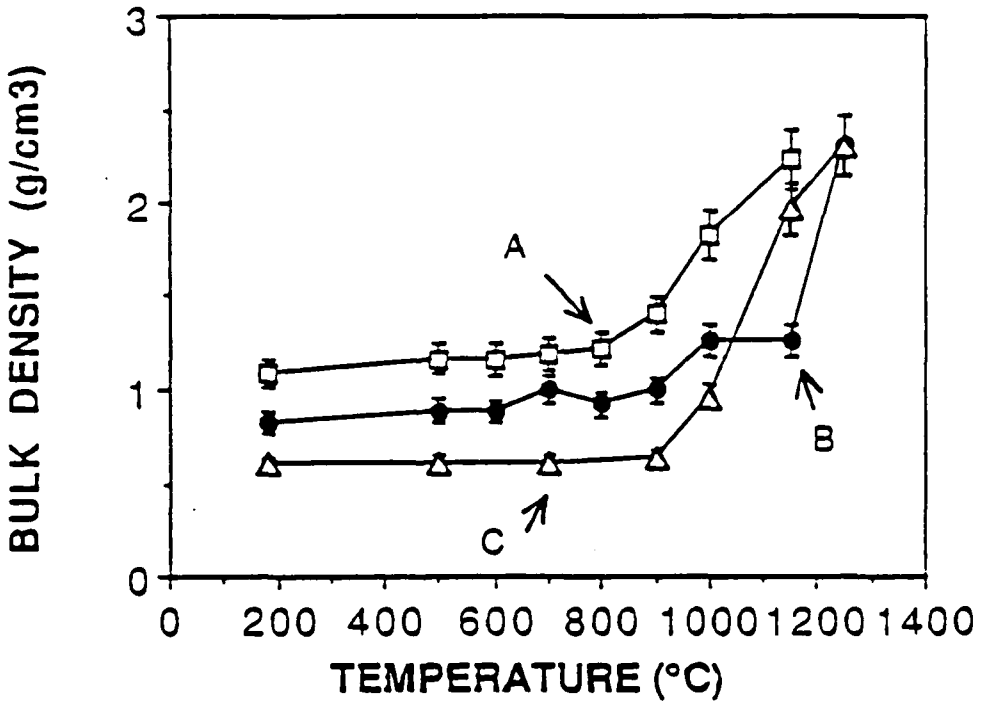

Fig. 2. Bulk density versus densification temperature for silica gels type A, B and C.

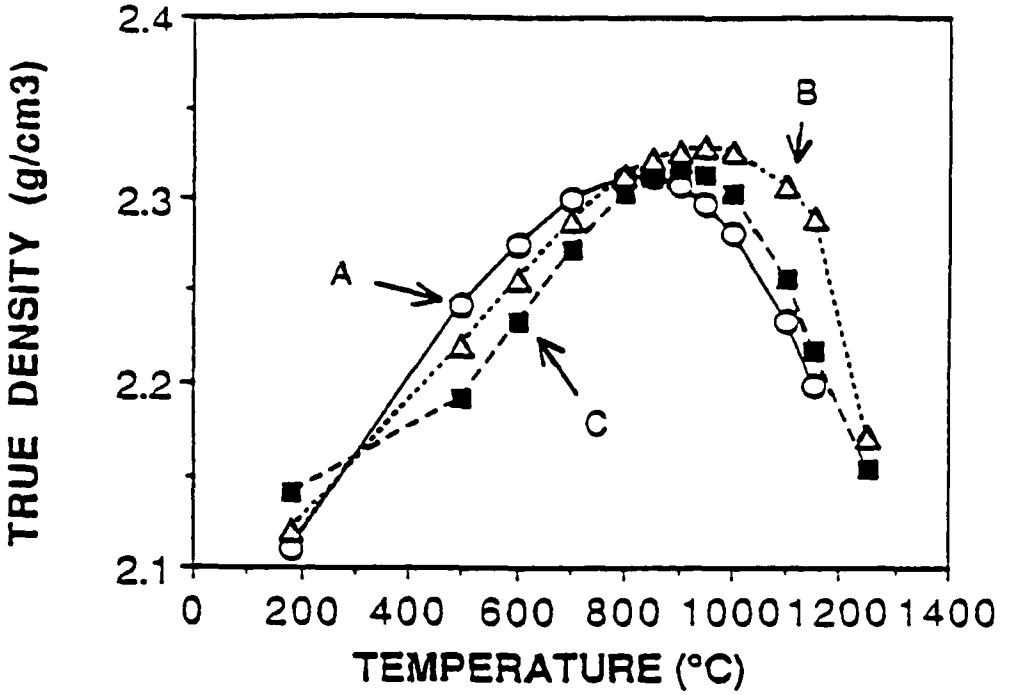

Fig. 3. Variation of true density as a function of densification temperature for silica gels type A, B and C.

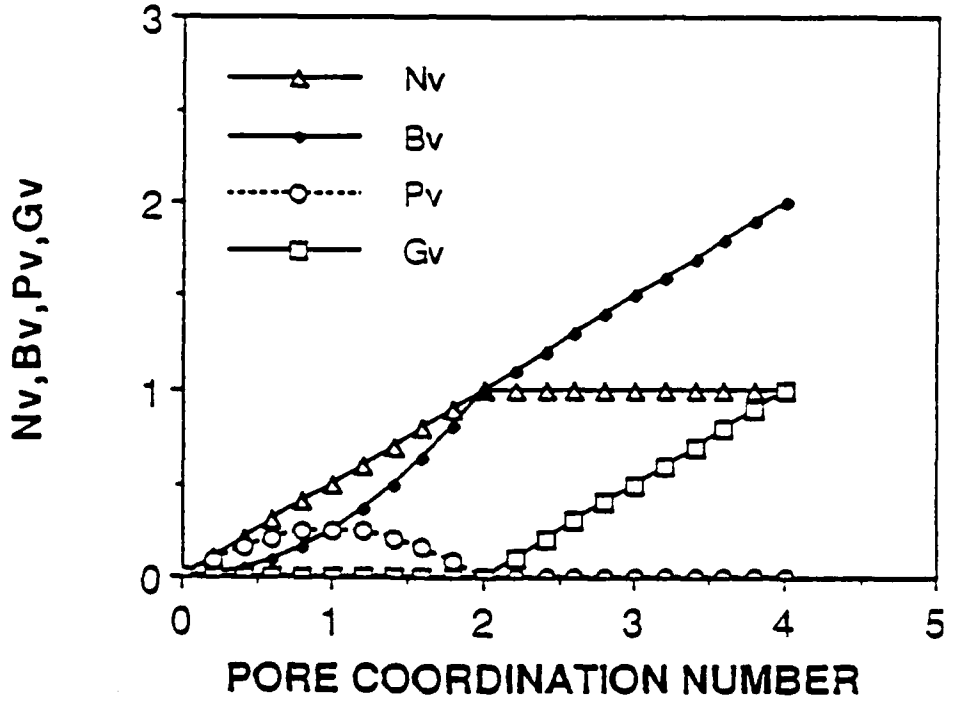

Fig. 4. Variation of the number of nodes (N_v), number of branches (B_v), number of separate parts (P_v) and genus (G_v) versus pore coordination number (CN).

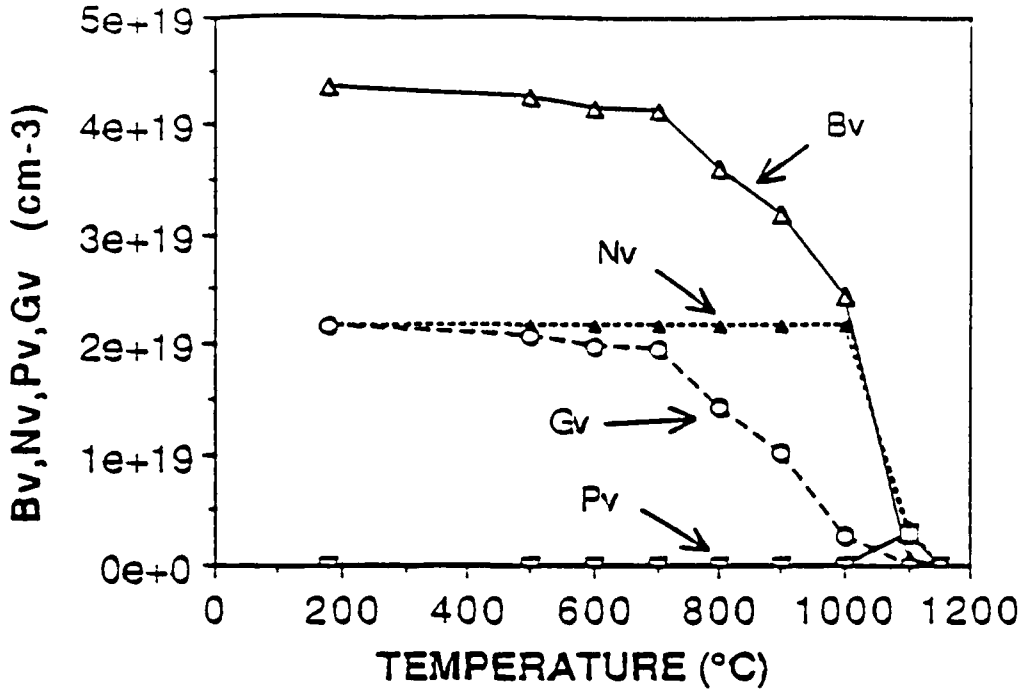

Fig. 5. Variation of the number of nodes (N_V), number of branches (B_V), number of separate parts (P_V) and genus (G_V) versus densification temperature for silica gels type A.

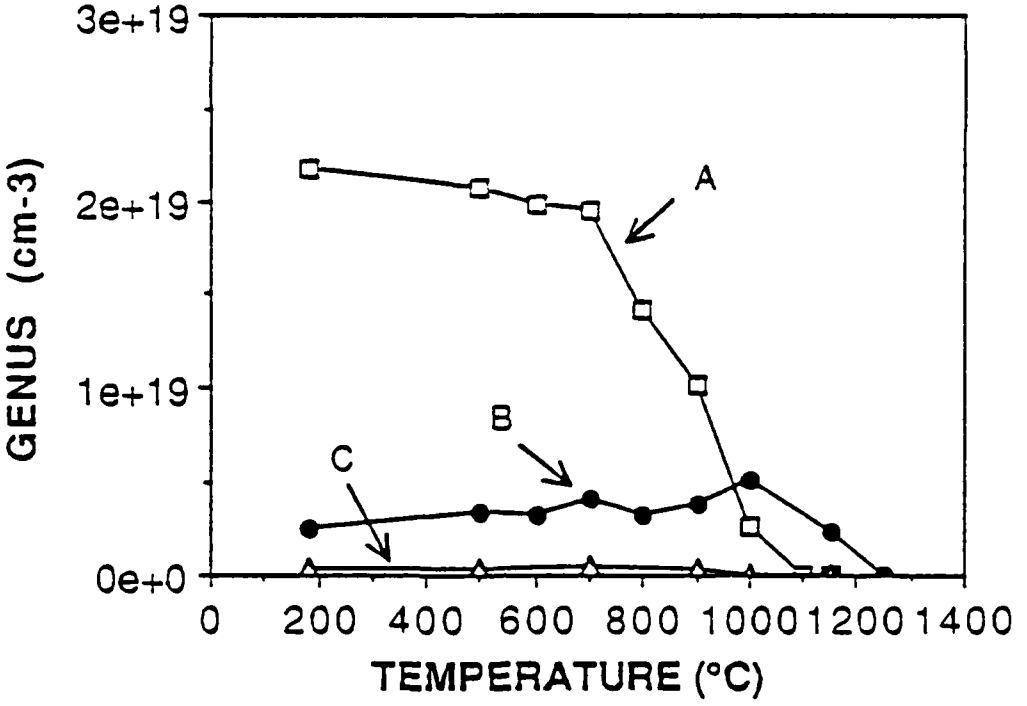

Fig. 6. Variation of the genus (Gv) as a function of densification temperature for silica gels type A, B and C.

APPENDIX 7

THEORY OF THERMAL EXPANSION

YEU-CHYI CHENG
DEC 6, 1989

I. Thermodynamic Definition

The coefficient of volume thermal expansion is defined as:

$$\beta = 1/V(\partial V/\partial T)p$$

The coefficient of linear thermal expansion is defined as

$$\alpha = 1/L(\partial L/\partial T)p$$

For isotropic materials , e.g. single crystal having cubic symmetry, annealed glass or amorphous materials, then

$$\beta = 3\alpha$$

II. Classical Description

Basically, all solids show dimensional changes as they undergo temperature variation. Classically, this behavior can be visualized by considering the vibrations of the atoms constitute the solids. As the temperature increases, the amplitudes of the vibrations of the atoms become greater and greater and the volume of the solid increases.

SIMPLE HARMONIC APPROACH

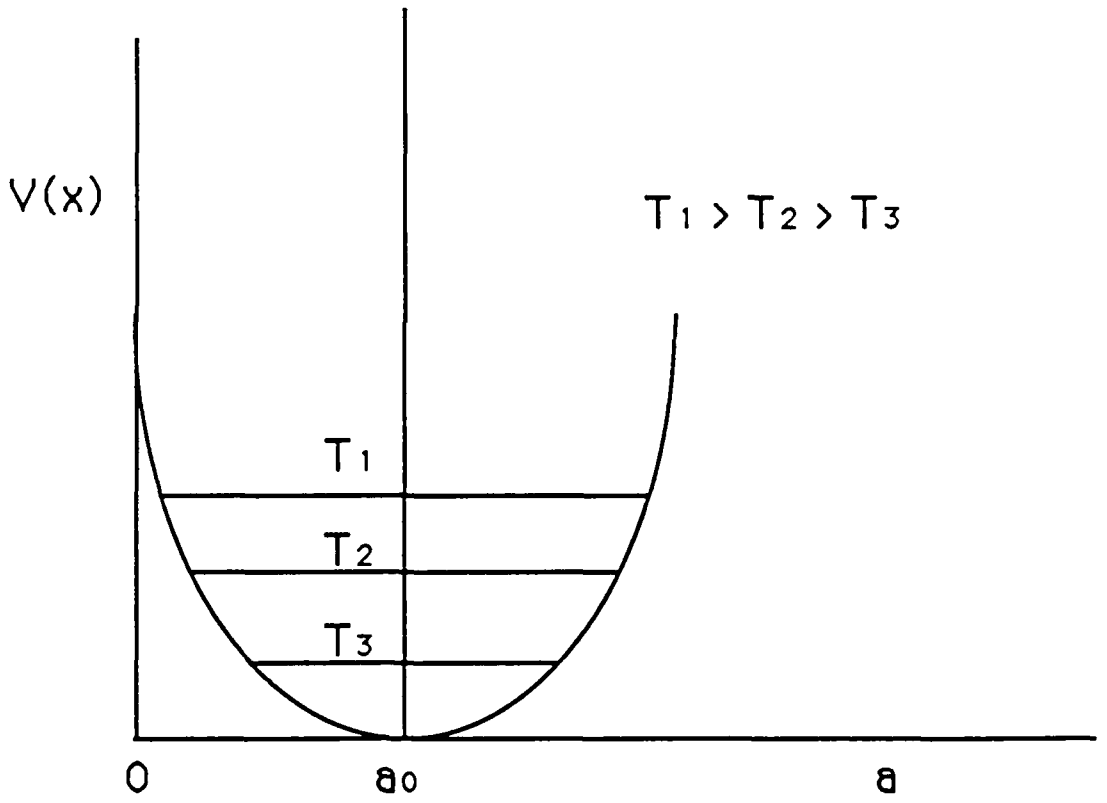

Figure 1. Average vibration amplitude of an atom as a function of temperature.

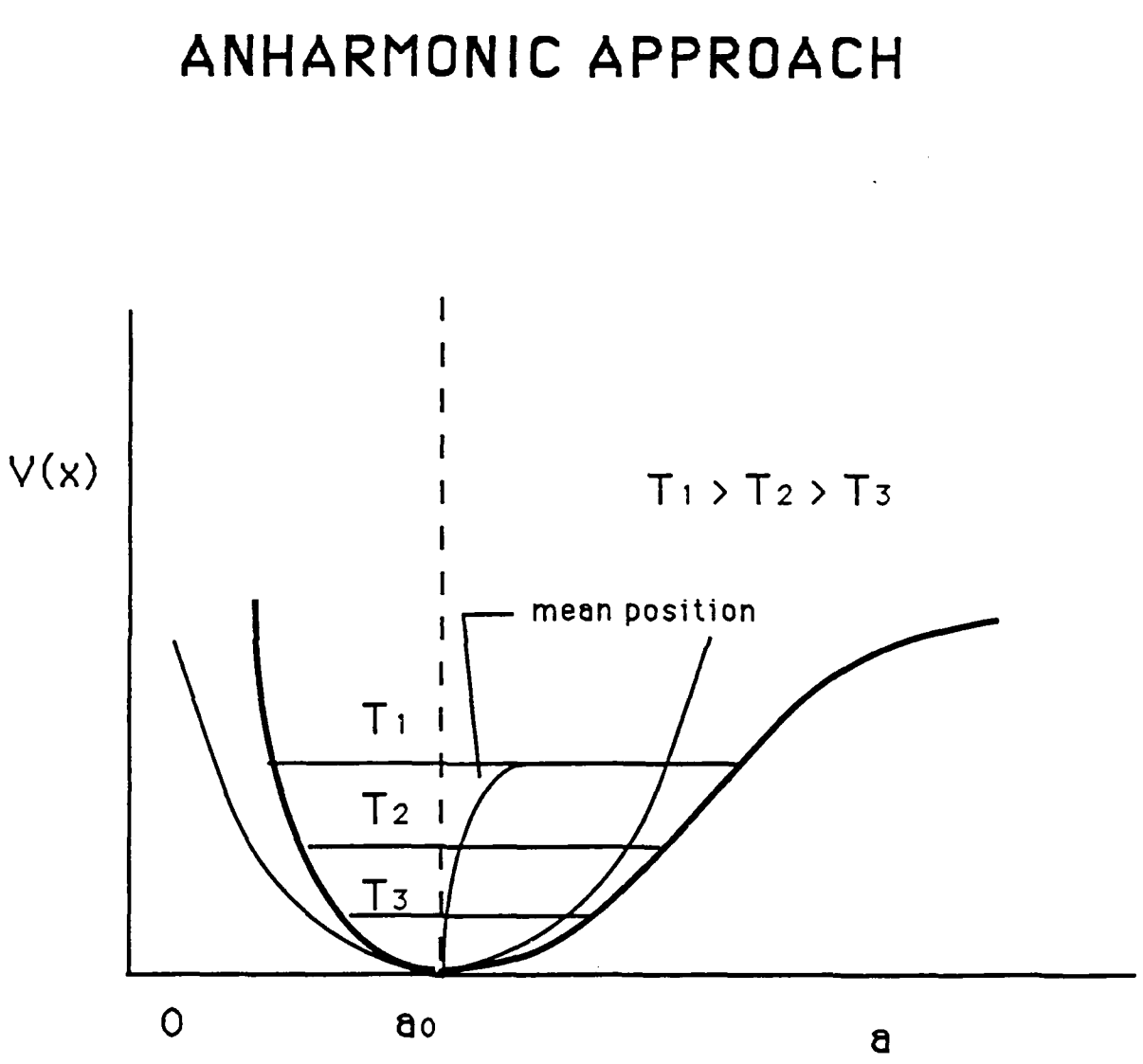

Figure 2. Average amplitude of vibration for an atom as a function of temperature.

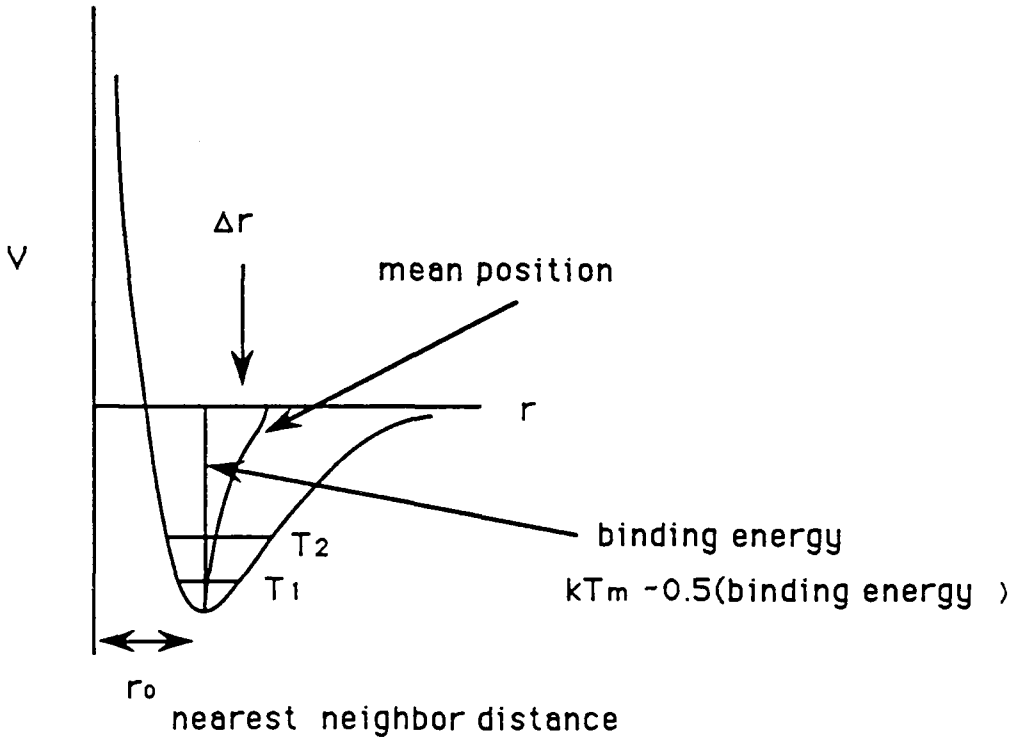

Figure 3. Potential energy well for atoms in a solids.

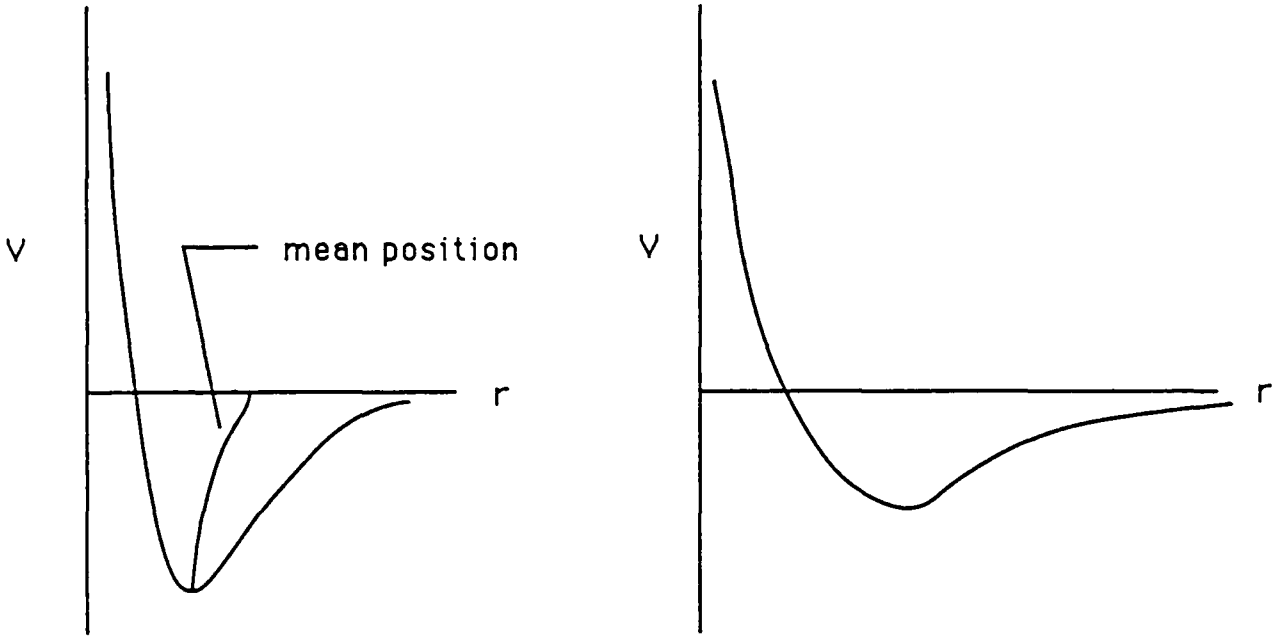

High Melting Point
High Elastic Modulus
Low Thermal Expansion Coefficient

Low Melting Point
Low Elastic Modulus
High Thermal Expansion Coefficient

Figure 4. Illustration of the relationship between physical properties of a material to the potential energy well.

Born-Mayer-Huggin Approach:

potential = attractive potential + repulsive potential

$$V_{ij} = \frac{Z_i Z_j e^2}{r} + \frac{a_{ij}}{r^n}$$

use Born-Mayer-Huggin form of repulsive energy

$$V_{ij} = A_{ij} e^{-r/} + \frac{Z_i Z_j e^2}{r}$$

$$A_{ij} = \left(1 + \frac{Z_i}{n_i} + \frac{Z_j}{n_j} \right) b \exp\left[\frac{r_i + r_j}{} \right]$$

where Z_i = ionic charge
b = constant
n_i = No. of valence electrons

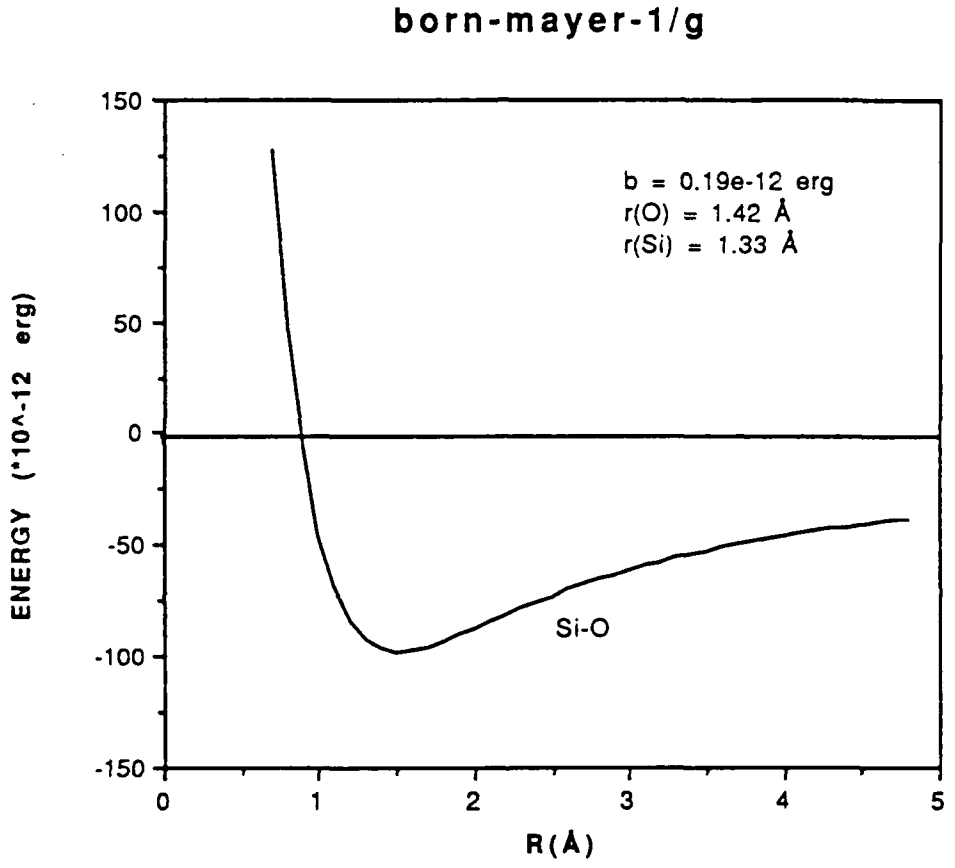

Figure 5. Pair potential between silicon and oxygen as a function of interatomic distance.

Si-O distance 1.58Å (calculated)
Silica (RDF) 1.62Å
Quartz 1.60Å

α(20°C-700°C) = 7.83*E-7 (calculated)
α(20°C-700°C) = 5*E-7 (experimental)

Table 1. Gruneisen Gamma for Several Materials

MATERIAL	FREQUENCY cm-1	CALCULATED gamma
QUARTZ	459	0.07
	698	0.08
	783	0.07
	800	no shift
	1168	no shift
FUSED SILICA	475	-0.05
	815	0.07
	1095	no shift
VYCOR	469	no shift
	814	0.22
	1095	no shift
	1384	0.14
PYREX	471	no shift
	812	0.12
	1095	no shift
	1390	0.06

Summary

Thermodynamic definition gives the way of measure coefficient of thermal expansion experimentally.
This is a macroscopic description.

Gruneisen gamma gives a measure of the anharmonic interaction between atoms which is directly related to the thermal expansion. This is a microscopic view.

The titanium has a higher atomic weight than that of silicon. Yet, as titania is added to the silica skeleton, the density of the glass remains constant for up to 8wt% of titania added. Thus, the structure of the titania-silica glass is more open than that of the silica, i.e. there is more free volume. Therefore, as temperature increases, there is more space to accomodate the increased vibration amplitude of the atoms. Therefore, the titania-silica glass has a lower value of thermal expansion than that of vitreous siica.
The pressure IR experiment will be conducted to determine the Gruneisen gamma for each vibration mode of the silica and silica-titania glass which reflects the amount of expansion contributes from the corresponding mode of vibration.

HMO CALCULATION

Crystalline form of titania: anatase, rutile.
Both have a tetragonal crystalline structure
Band gap of titania = 4.77 eV.
h and k parameter was determined by matching the band gap.

h	k	Band Gap	Ground Energy
0.6	0.3	4.7412	-29.276
0.7	0.73	4.7735	-30.402
0.8	0.98	4.7693	-31.528
0.9	1.18	4.7713	-32.654
1	1.32	4.6677	-33.78

SiO_2-TiO_2 4-member Ring Structure

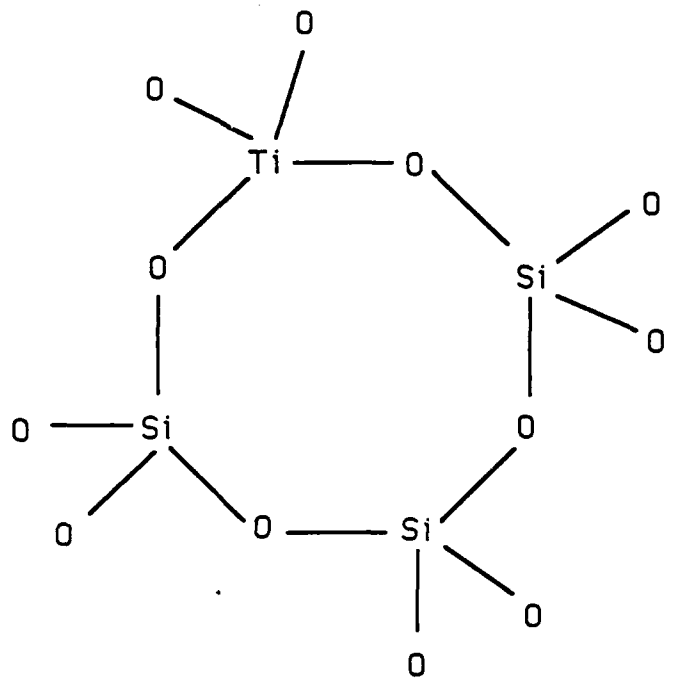

Heteroatom Parameter				Band gap	UV
h		k		eV	nm
Si	0.8	Si-O	1.4		
O	1	Ti-O	0.73	5.4989	204
Ti	0.7				
Si	0.8	Si-O	1.4		
O	1	Ti-O	0.98	5.7871	214
Ti	0.8				

SiO_2-TiO_2 5-member Ring Sturcture

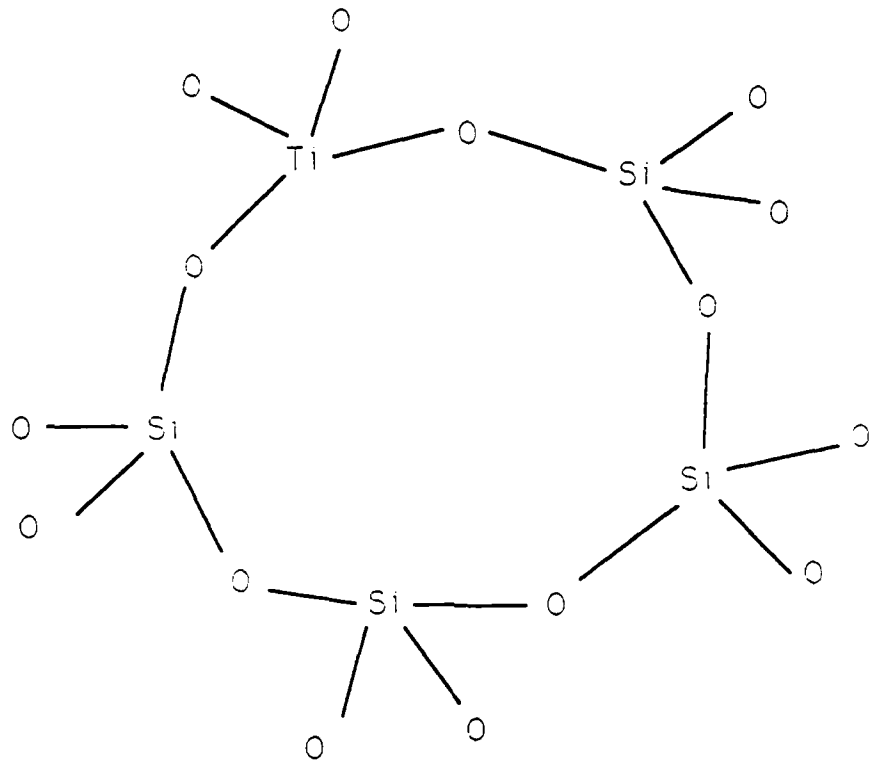

Heteroatom Parameter				Band gap	UV
	h		k	eV	nm
Si	0.8	Si-O	1.4		
O	1	Ti-O	0.73	5.3459	232
Ti	0.7				

APPENDIX 8

Physical Evolution of Gel-Silica Monoliths

W.L. Vasconcelos, R.T. DeHoff, L.L. Hench

Dept. Materials Science and Eng.
University of Florida
Gainesville, Florida 32611, USA

Abstract

During densification of gel-silica monoliths, the ultrastructure evolves in such a way that the strength of the material increases continuously. That increase in strength occurs more rapidly after a certain temperature range which corresponds to sharp changes in porosity and in the extent of interconnection of the pore network. Evaluations of uniaxial compression strength, flexural strength, tensile modulus and Vickers hardness number were performed in silica gel samples densified in the range of 180°C to 1150°C. Gel-silica monoliths with different pore radius present different properties during densification, as shown by hardness analysis. Dimensional change experiments show an increasing thermal stability of gel-silica monoliths as densification proceeds.

Introduction

The expanding research on sol-gel technology is due to the great potential of unique applications for that class of materials [1-5]. Of paramount importance in the study of sol-gel materials is the variation of physical properties that occur during densification.

Based on nitrogen gas adsorption measurements and on evaluations of true density by helium micropycnometry, it is possible to model the pore structure of the silica gels so that topological parameters can be estimated [6,7]. One of the important concepts of topology is the genus (G_V), which is defined by DeHoff [8] as "the maximum number of non-self reentrant closed curves which may be constructed on the surface without dividing it into two separate parts." As densification proceeds, the pore connectivity (as described by the genus, G_V) increases during the first stage of densification, due to neck formation between particles. G_V decreases to zero during the second stage, and it remains constant at zero during the third stage of densification. The temperature ranges for which those three stages occur depend on the average pore size of the silica gel [6,7]. In order to facilitate comparisons between different structural conditions, the concept of relative genus (γ) is introduced as follows [6]:

$$\gamma = \frac{G_V}{G_V^o} \quad , \tag{1}$$

where G_V^o is the genus of the dried sample.

The objective of this work is to evaluate the physical (mechanical and thermal) evolution of silica gel monoliths as densification proceeds.

Experimental Procedure

Silica gel monoliths were prepared using a mixture of TMOS and DI-water and acid catalyzed by HNO_3 (samples type A). After gelation at room temperature and aging at 60°C for two days, the samples were dried at 180°C. The densification experiments were carried out in a tube furnace with a dry-air atmosphere for temperatures up to 1000°C, and under a chlorinated atmosphere for higher temperatures. Fig.1 shows a set of pure gel-silica monoliths type A densified in the range of 180°C to 1150°C. Another set of gel-silica samples was prepared in similar conditions, except that the acid used as catalyst was HF. This set of samples is referred to as "samples type B" in this work.

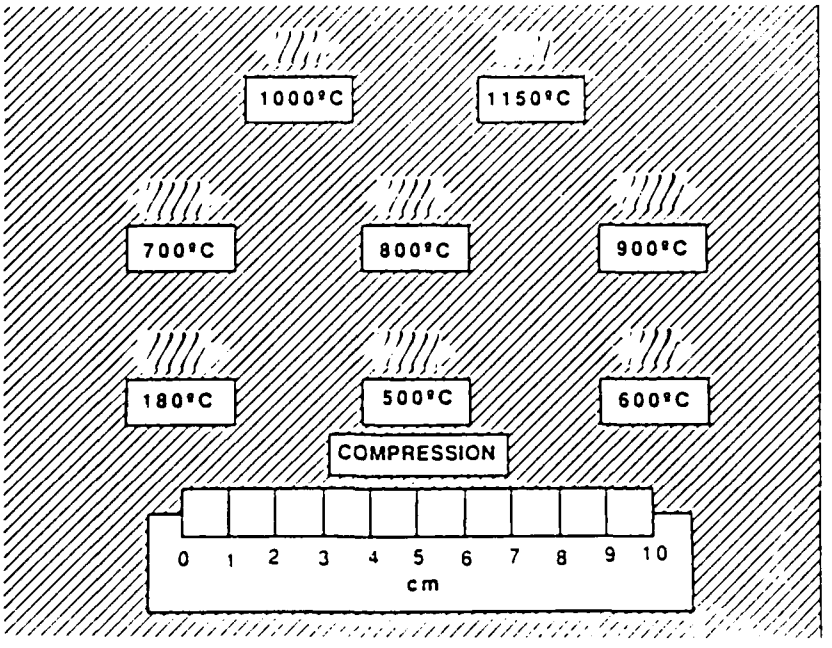

Fig.1 Silica gel monoliths prepared in a dry-air atmosphere (500°C to 1000°C), and in a chlorine atmosphere (1150°C)

Silica gel monoliths densified in the range 180°C to 1150°C were analyzed in an automatic nitrogen gas adsorption machine type Autosorb 6 (Quantachrome Corp.) for volume of pores, surface area of pores and average pore radius.

A mechanical testing machine type MTS 810/458 with a cross head speed of 0.02 mm/min was used to obtain uniaxial compression strength of gel-silica monoliths. The flexural strength data were obtained using a MTS 810/442 and a four point bending fixture. All the flexural tests were performed in ambient air using a cross head speed of 0.016 mm/min. In order to obtain the flexural strength (σ_c), the following expression was used [8]:

$$\sigma_c = \frac{3\,P\,(L - l)}{2\,w\,t^2}\,, \qquad (2)$$

where P is the load at fracture;
L is the distance between the lower supporting points;
l is the distance between the upper loading points;
w is the width of the tested sample;
t is the thickness of the tested sample.

Tensile modulii of gel-silica monoliths densified in the range of 180°C to 1000°C were obtained using a dynamic mechanical tester machine type DMA-982 (Dupont Instr.).

Dimensional change experiments were carried out using an automatic recording differential push-rod dilatometer Dilatronic II-R (Theta Ind.). The heating and cooling rate used was 3°C/min.

Results and Discussion

The variation of compression strength with densification temperature for a set of gel-silica monoliths of 12Å average pore radius is shown in Fig.2. The figure shows an increase in compression strength as the densification temperature increases. As shown in Fig.2, the compression strength for a set of dried silica gels with 81Å average pore radius is lower than the strength of silica gels with 12Å average pore radius. The lower strength of the larger pore size structure is probably associated with the higher volume fraction of pores (V_V) present in those samples (about 0.7) as compared to the smaller pore size silica gels, which have a V_V of about 0.5 in the dried stage.

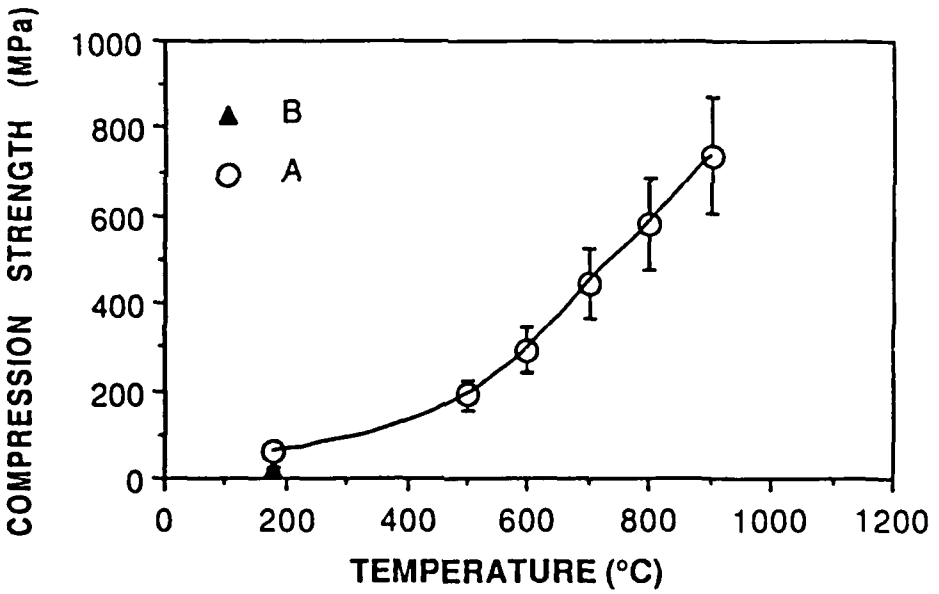

Fig.2 Variation of the compression strength as a function of densification temperature for samples type A and B.

The flexural strength increases continuously as the densification temperature increases, as shown in Fig.3. The variation of flexural strength with densification temperature can be divided into two distinct regions: (1) at lower temperatures (below 700°C) the increase in flexural strength with temperature is relatively slow; (2) as the densification temperature increases above 700°C, the increase in flexural strength is more pronounced.

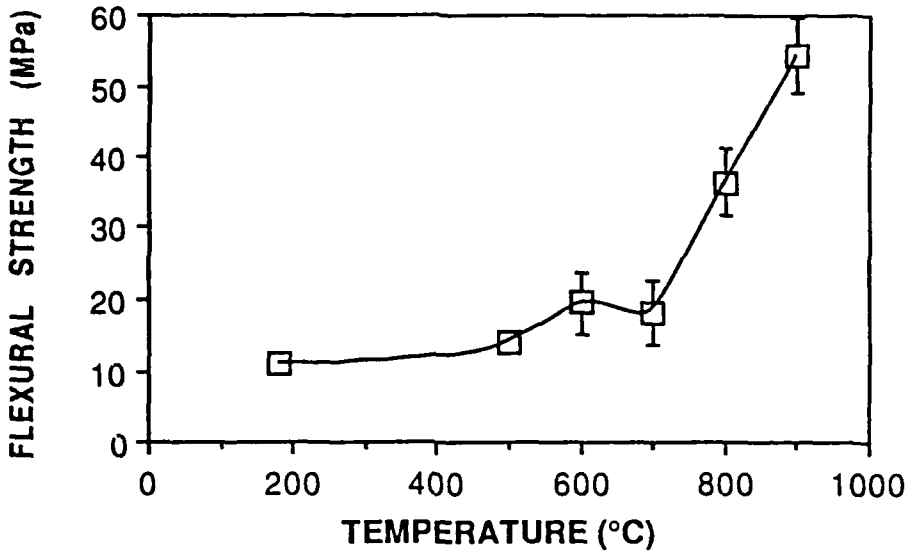

Fig.3 Variation of flexural strength as a function of densification temperature for samples type A.

With the increase in densification temperature the tensile modulus of gel-silica increases continuously, as seen in Fig.4. Similarly to the variation in flexural strength, Fig.4 can be divided into two regions: (1) below 800°C, the increase in tensile modulus is relatively slow with the increase in densification temperature, and (2) above 800°C the increase in tensile modulus is more pronounced.

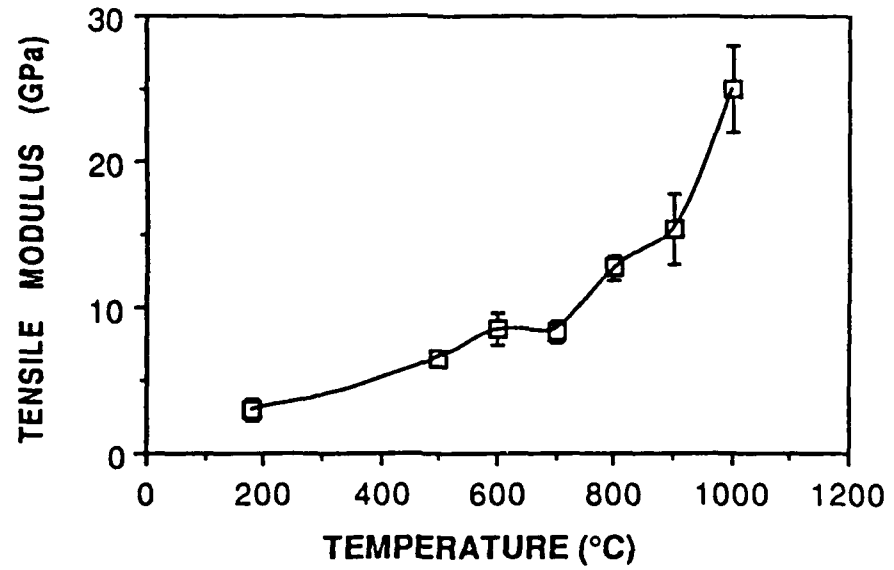

Fig.4 Variation of tensile modulus as a function of densification temperature for samples type A.

The observation of the two regions in terms of variation of physical properties suggest the occurrence of structural transformations that are associated with the physical property changes. The gas adsorption analysis reveals that both the porosity and the surface area of pores decrease more rapidly when the densification temperature is higher than about 800°C. The topological analysis shows corresponding types of structural changes.

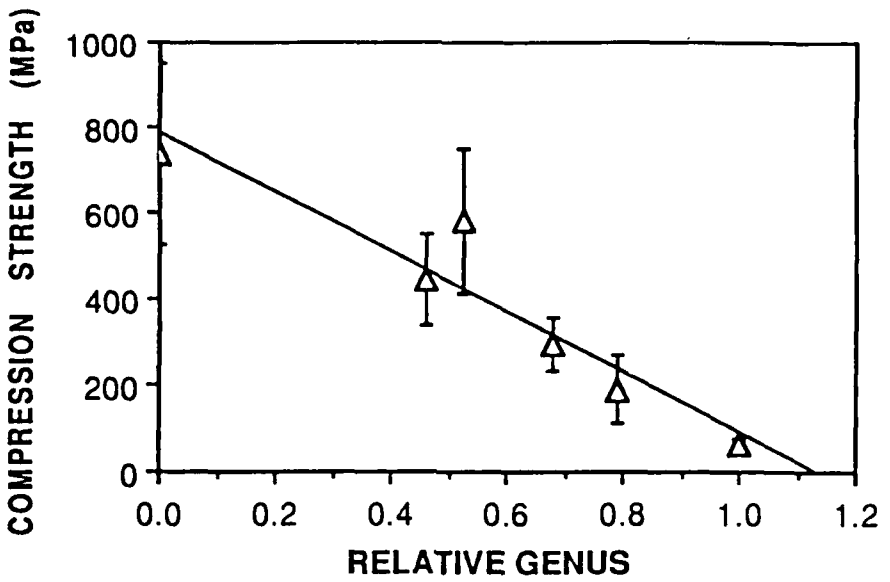

Fig.5 Variation of compression strength as a function of relative genus for samples type A.

The variation of compression strength with relative genus (γ) is shown in Fig.5. The fairly good linear relationship shown in Fig.5 suggests the existence of a close association between compression strength and the pore connectivity. Fig.6

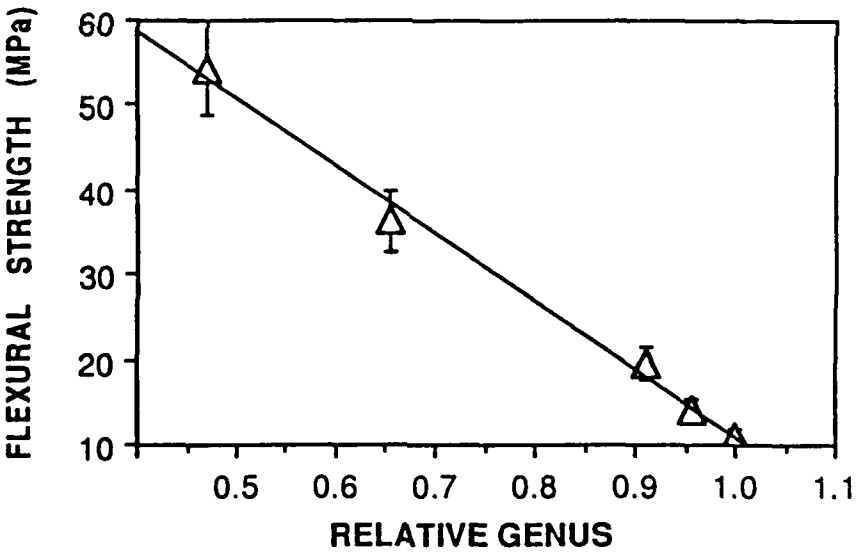

Fig.6 Variation of flexural strength as a function of relative genus for samples type A.

shows the variation of flexural strength with relative genus. In this case the relationship between the mechanical property and the pore connectivity is better than the one shown for compression strength. The linear relationship shown in Fig.7 for the dependence of tensile modulus with relative genus is an additional reinforcement of the association between strength and pore connectivity for the silica gel samples tested.

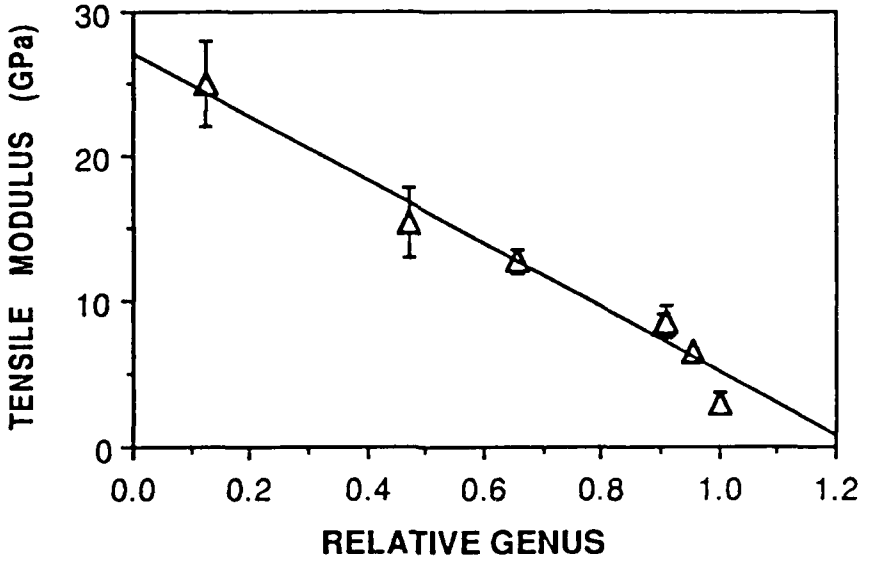

Fig.7 Variation of tensile modulus as a function of relative genus for samples type A.

It is possible that the correlation between strength and pore connectivity is associated with increased stress concentration when the pore coordination is high (meaning high genus). As densification proceeds, the pore coordination decreases, because the number of branches that are part of the pore network decreases, resulting in nodes (intersection of branches) with less branches and less stress concentration, which results in stronger silica gels.

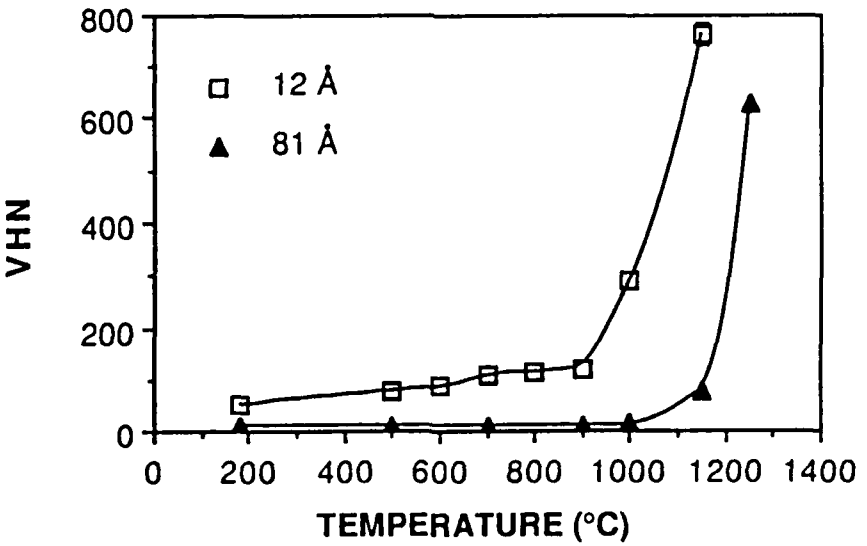

Fig.8 Variation of the Vickers hardness number (VHN) as a function of densification temperature for silica gel samples of 12Å and 81Å average pore radii.

The variation of Vickers hardness number (VHN) with densification temperature for sets of silica gel samples with 12Å and 81Å average pore radii is shown in Fig.8. It can be seen from this figure that for both sets of samples the VHN increases with increasing sintering temperatures and the rate of increase is

sharper after a certain critical temperature which increases for the larger pore size material.

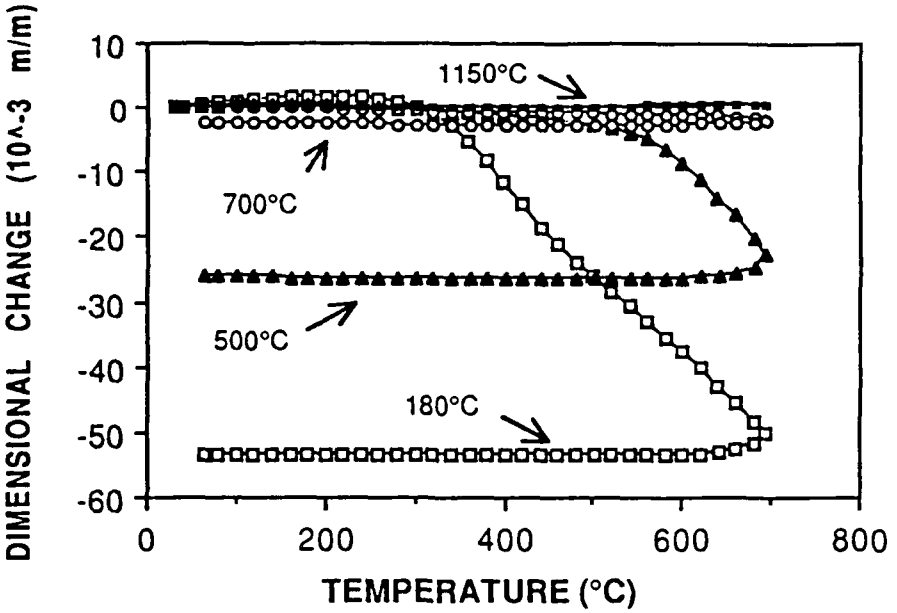

Fig.9 Variation of the dimensional change with testing temperature for samples type A previously densified in the range of 180°C to 1150°C.

When a dried silica gel monolith is heated, initially it experiences an increase in its dimensions, due to the presence of water in the structure [6], as shown in Fig.9. However, after a certain temperature (around 300°C) the sample start shrinking, because of the occurrence of densification. As shown in Fig.9, the maximum testing temperature used in these experiments was 700°C. When the temperature of the samples reach 700°C they are cooled to room temperature. Fig.9 shows the variation of dimensional change as a function of testing temperature for samples previously densified in the range of 180°C to 1150°C. As the densification temperature increases, the dimensional changes become smaller, meaning that the silica gel samples become increasingly more thermally stable as the densification temperature increases. The sample densified at 1150°C shows no shrinkage, but only thermal expansion, with an average coefficient of thermal expansion (CTE) of 0.5×10^{-6} °C^{-1}.

Conclusions

As shown in this work, the compression strength, flexural strength and tensile modulus of gel-silica monoliths increases continuously as densification proceeds. The variation of strength with densification temperature can be divided into two regions: (1) in a lower temperature region the strength increases relatively slowly with the increase in processing temperature; (2) at higher densification temperatures the increase in strength is more pronounced. The observed changes in mechanical properties seem to be associated with variations in the pore connectivity of the silica gel samples. For the first region (at lower temperatures) the pore network is essentially interconnected. When the pore closure associated with the third stage of densification occurs, the material becomes stronger.

Silica gel monoliths with different pore sizes present different mechanical and structural properties. Larger pore size structures are essentially weaker than the small pore size silica gels. The VHN variations show that the second region (of sharper increase in strength) occurs at higher temperatures for silica gels with 81Å average pore radius than for samples of 12Å average pore radius. Dimensional change experiments show that the silica gel monoliths become increasingly more thermally stable as the densification temperature increases.

Acknowledgments

The authors acknowledge the support of the US-AFOSR (Contract n° F49620-88-C-0073). One of the authors (WLV) is indebted to the support of UFMG (Federal University of Minas Gerais) and CAPES (Brazilian Agency of Post-Graduation).

References

[1] L.L. Hench, Ed., *Ultrastructure Processing of Advanced Structural and Electronic Materials* (Noyles, Park Ridge, New Jersey, 1984).

[2] L.L. Hench and D.R. Ulrich, Eds., *Ultrastructure Processing of Ceramics, Glasses and Composites* (Wiley, New York, 1984).

[3] J. Wenzel, *J.Non-Cryst.Solids*, 73 (1985) 693.

[4] L.L. Hench and D.R. Ulrich, Eds., *Science of Ceramic Chemical Processing* (Wiley, New York, 1986).

[5] J.D. Mackenzie and D.R. Ulrich, Eds., *Ultrastructure Processing of Advanced Ceramics* (Wiley, New York, 1988).

[6] W.L. Vasconcelos, *Topological Evolution and Properties of Sol-Gel Silica Monoliths*, Ph.D. Dissertation (University of Florida, 1989).

[7] W.L. Vasconcelos, R.T. DeHoff and L.L. Hench, in: *Proc. 4th International Conference on Ultrastructure Processing of Ceramics, Glasses and Composites*, Tucson, Arizona (February, 1989).

[8] Testing Method for Flexural Strength, *Japanese Industrial Standard JIS R 1601-1981* (Japanese Standards Association, 1981).

[9] R.T. DeHoff, in: *Quantitative Microscopy*, R.T. DeHoff and F.N. Rhines, Eds. (McGraw-Hill, New York, 1968) p.291.

APPENDIX 9

MOLECULAR ORBITAL MODELING OF WATER ADSORPTION ON A TETRASILOXANE RING

J. K. WEST AND S. WALLACE
Advanced Materials Research Center, University of Florida, One Progress Blvd. #14, Alachua, Fl 32615.

ABSTRACT

A water molecule hydrogen bonded to a surface SiOH group produces an IR vibrational transmission peak (ν_3) at 2.82 μm. Water was adsorbed into the pores of a metal alkoxide derived silica gel monolith, and the increase in the wavelength of the first vibrational overtone ($2\nu_3$) of this peak was measured as a function of the adsorbed water content W (g H_2O/g SiO_2). The peak shifted from 1.390 to 1.420 μm as W increased by 0.14 g/g. Intermediate Neglect of Differential Overlap (INDO) Molecular Orbital (MO) theory was used to model this process. The effect of a H_2O molecule, hydrogen bonded to a hydroxylated tetrasiloxane ring, on the structure of the ring and the water molecule was investigated. The bond length of the O-H group H-bonded to the water molecule increased, as expected from the increase in wavelength of the $2\nu_3$ IR peak.

INTRODUCTION

The adsorption of water onto the surface of a hydroxylated a-silica surface causes changes in the vibrational modes producing the IR transmission spectrum of this surface. The production [1] of monolithic geometric samples of microporous silica gel has made the direct experimental investigation of these changes easier. A typical silica gel monolith is made by the acid catalysis of silicon tetramethoxide. It has a surface area of 750 m^2/g, a pore volume of 0.45 cc/g, an average pore radius of 12 Å and an average particle radius of 60 Å. This means that these fractal materials are dominated by their interfacial properties. Therefore, for a silica gel sample in the beam of an IR spectrometer, the properties of the material are dominated by the surface.

An isolated surface silanol ($SiOH_3$) group produces an IR transmission peak, ν_1, at 2.675 μm. ν_1 is due to the O-H stretching vibration of isolated SiO-H_3 groups [2]. A H_2O molecule H-bonded to $SiOH_3$ groups produces an IR peak (ν_3) at 2.82 μm. ν_3 is due to the O-H stretching vibration of $SiOH_3$ groups H-bonded to H_2O molecules [2]. In this investigation, the shift in the wavelength of the first vibrational overtone ($2\nu_3$ = 1.39 μm at W = 0.001 g/g) of ν_3 was measured as a function of the H_2O content W (g H_2O/g SiO_2).

The adsorption of H_2O into microporous silica gel monoliths has been shown experimentally to cause a small expansion of the gels [3-5]. It was proposed that the expansion was due to adsorption of H_2O molecules onto the hydroxylated surface of the silica gel [5]. West et al. [3] investigated this hypothesis using Intermediate Neglect of Differential Overlap (INDO) Molecular Orbital (MO) theory. They examined the adsorption of a H_2O molecule on a ring of four hydroxylated silica tetrahedra, i.e. a hydroxylated tetrasiloxane ring. The H_2O molecule was adsorbed via the formation of H-bonds with two hydroxyl groups [1]. The adsorbed H_2O molecule increased the average nearest neighbor Si---Si distance in the ring structure by 0.84%. The average Si---Si diagonal distance increased by 0.0873%. The silicate ring diameter decreased by 12.1% along the axis with the adsorbed H_2O molecule [3].

In this study, the same INDO MO structure was used to determine the cause of the increase in the wavelength of the $2\nu_3$ IR peak. The influence of the adsorbed H_2O molecule, H-bonded to the hydroxylated tetrasiloxane ring, on the structure of the hydroxylated ring and the H_2O molecule, was examined.

EXPERIMENTAL PROCEDURE

A metal alkoxide derived silica gel disc, sample number #114, was heat treated at 800°C for 4 hours. The gel disc had a thickness = 0.335 cm, bulk density = 1.55 g/cc, pore volume = 0.21 cc/g, surface area = 350 m^2/g and an average pore radius = 12 Å. A small amount of water was adsorbed into the micropores of the silica gel disc by condensation from the vapor phase. The disc was sealed in an airtight container and the water was allowed to equilibrate in the pores for 24 hours. The disc was then weighed and the transmission spectrum was measured using a Perkin-Elmer Lambda-9 UV-VIS-NIR Spectrophotometer. Another small amount of water was then adsorbed, allowed to equilibrate, weighed and the transmission spectrum measured again. This process was repeated until the pores were saturated with water.

RESULTS

Table I identifies the IR peaks and lists their wavelengths [2]. Figure 1 shows the IR transmission spectra of the silica gel disc #114 for various values of W. The peak at 1.365 μm, even though it is not exactly half the wavelength (2.675 μm) of the ν_1 peak, is the first vibrational overtone $2\nu_1$ [2]. $2\nu_1$ is due to isolated $SiOH_s$ groups and not due to H-bonded vicinal, or adjacent, $SiOH_s$ groups, because the gel has been heat treated to 800°C. Only one OH group per surface Si atom remains, and they are too far apart to form H-bonds. The $2\nu_1$ peak is also too sharp and symmetric to involve H-bonds, which would produce an asymmetric peak. The $2\nu_1$ peak can be seen to decrease in intensity as the $2\nu_3$ peak intensity increases concomitantly. The $2\nu_1$ peak disappears when the micropores are fully saturated, because all the $SiOH_s$ groups are H-bonded to H_2O molecules. The associated $2\nu_4$ peak (1.46 μm), due to the stretching vibration of O-H groups in H_2O molecules H-bonded to $SiOH_s$ groups, increases in intensity as the $2\nu_3$ peak increases. After the pores were full, #114 was heated at 180°C in vacuum to remove all the adsorbed H_2O and the

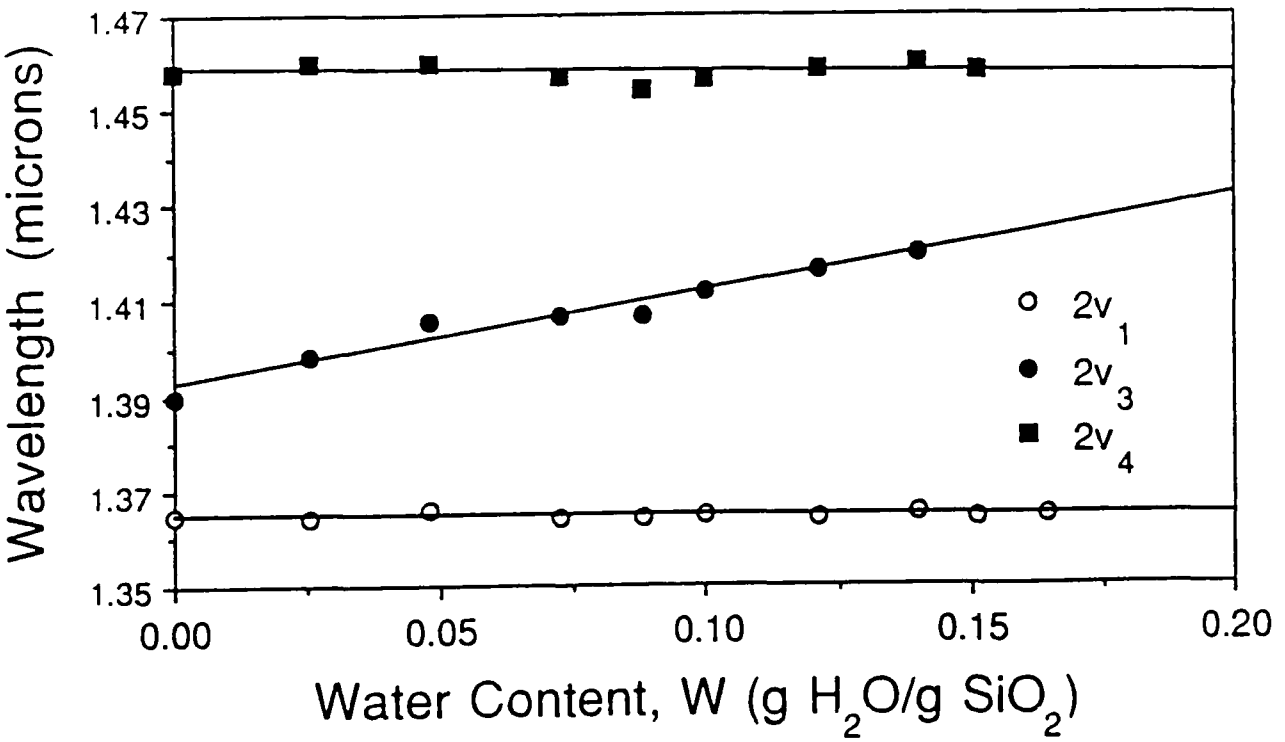

Figure 1. The near infrared (NIR) transmission spectra of the microporous silica gel disc #114 as a function of adsorbed water content W (g/g).

Table I. IR Transmission Peaks of H_2O Molecules H-bonded to Surface Silanols.

Wavelength (μm)	Identification	Peak Shape
2.208	$^{**}\nu_1 + {}^{*}\nu_{OH}$	a medium asymmetric peak
1.890	$^{***}\nu_3 + 2\nu_{OH}$	a large, broad asymmetric peak
1.460	$^{****}2\nu_4$	a small peak (compared to ν_4)
1.390	$2\nu_3$	a small peak (compared to ν_3)
1.365	$2\nu_1$	a very sharp symmetric peak

$^{*}\nu_{OH}$: on out-of-plane O-H bending vibration of surface $SiO-H_s$ groups.
$^{**}\nu_1$: O-H stretching vibration of isolated surface $SiO-H_s$ groups.
$^{***}\nu_3$: O-H stretching vibration of surface $SiO-H_s$ groups H-bonded to H_2O.
$^{****}\nu_4$: O-H stretching vibration of H_2O molecules H-bonded to $SiOH_s$ groups.

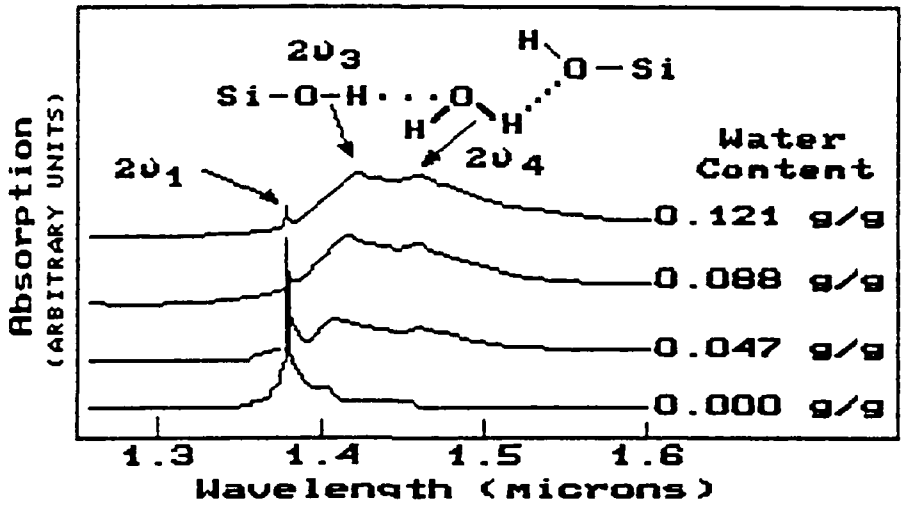

Figure 2. The dependency of the near infrared (NIR) peak positions on W (g/g).

IR spectrum was measured. It was very similar to the original spectrum at W = 0.00 g/g. Figure 2 shows the dependency of the $2\nu_1$, $2\nu_3$ and $2\nu_4$ peak wavelengths on W for #114. $2\nu_1$ and $2\nu_4$ are constant, while $2\nu_3$ increases as the H_2O content increases. The $2\nu_3$ peak initially appeared at 1.39 μm and shifted to 1.42 μm as W increased to 0.14 g/g. The same behavior was seen for other porous silica gel discs heat treated to different temperatures.

Figure 3. Schematic of the tetrasiloxane ring with no H_2O molecule adsorbed.

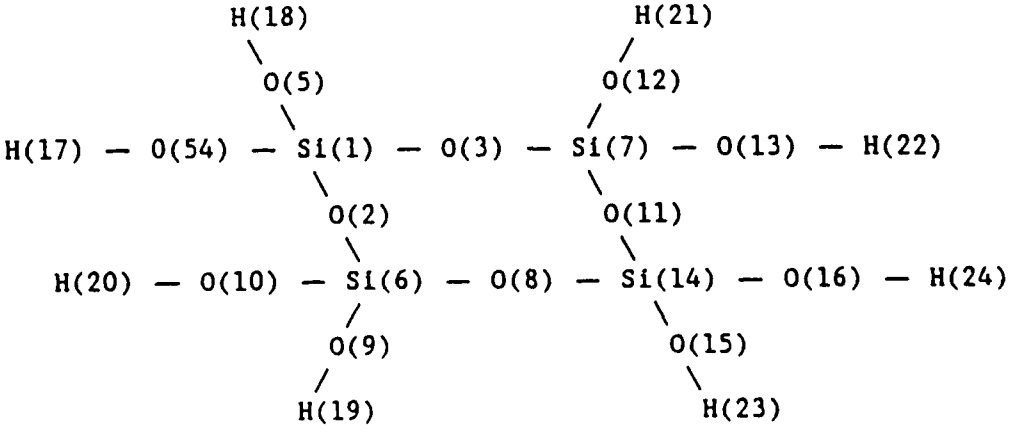

Figure 4. Schematic of the tetrasiloxane ring with a H_2O molecule adsorbed. (—) is a molecular bond. (..) is a hydrogen bond

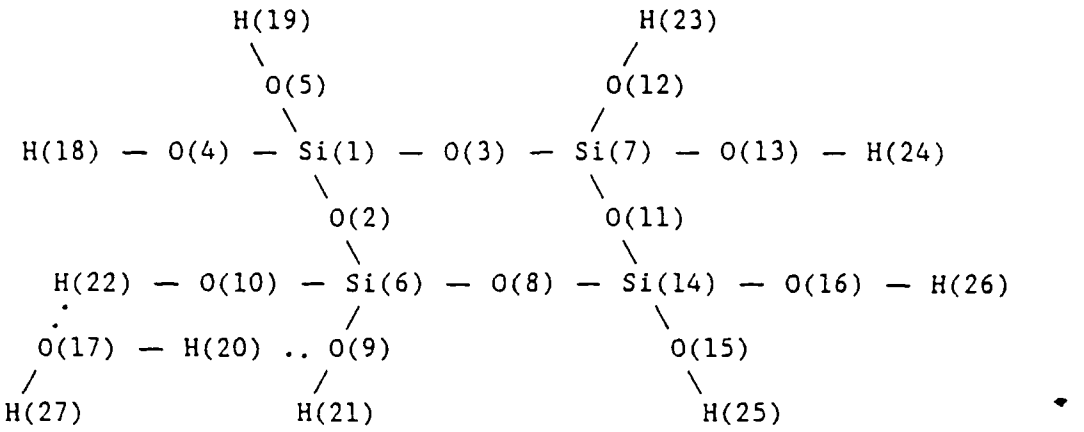

Figures 3 and 4 show the schematics of the hydroxylated tetrasiloxane rings, with atom number designations, without and with an adsorbed H_2O molecule respectively. These structures were both optimized geometrically using an INDO MO program from the Quantum Theory Project (QTP) at the University of Florida [6-7]. In each case the three dimensional optimized geometry was used to calculate the interatomic distances for the entire cluster. Table II lists various average and specific bond lengths, calculated from these interatomic distances, with and without an adsorbed H_2O molecule.

The INDO MO stabilized structure of a free H_2O molecule gives an average O-H bond length of 1.01913 Å, with an H-O-H angle = 102.35°.

DISCUSSION

The optimized structure produced by the INDO MO program showed that the H_2O molecule was adsorbed by H-bonding to two SiOH groups with a common Si(6) atom, as shown in Fig. 4. The adsorption of the H_2O molecule did not cause any statistically significant change in the average length of the Si-O and O-H bonds in the SiOH groups not H-bonded to the H_2O molecule, i.e, the standard deviation values σ of these average bond lengths, listed in Table II, are larger than the calculated bond length changes. The average length of the Si-O bonds in the bridging Si-O-Si bonds increased by 3.5%, supporting the proposal that H_2O adsorption causes porous silica gels to expand [3-5].

As the $2\nu_3$ peak wavelength increases when W increases, while the $2\nu_1$ and $2\nu_4$ peaks stay constant, the bond strength of the O-H group H-bonded to the H_2O molecule and associated with the $2\nu_3$ vibration must decrease. Therefore the O-H bond length must increase, so the INDO MO model O(10)-H(22) bond length should increase. The H_2O molecule formed one H-bond between its O(17) atom and the H(22) atom of the Si(6)O(10)H(22) group, and one H-bond between its H(20) atom and the O(9) atom of the Si(6)O(9)H(21) group (Fig. 4). These H-bonds have very similar lengths, = 1.34±0.004 Å. The O(10)-H(22) and H(20)-O(17) groups associated with the H atoms forming these H-bonds also have similar bond lengths = 1.062±0.002 Å. The O(10)-H(22) stretching vibration, in the Si(6)O(10)H(22) group, causes the $2\nu_3$ vibration, while the H(20)-O(17) stretching vibration, in the H_2O molecule, causes the $2\nu_4$ vibration. The average O-H bond length (1.062 Å) is 0.041 Å (= 4.0 %) longer than the average non H-bonded O-H group. The INDO MO model therefore agrees with the interpretation of the experimental data, as the O(10)-H(22) bond length increases in length (Fig. 4), as predicted.

The O(9)-H(21) and O(17)-H(27) bonds are shorter and are not directly involved in the H-bonds, so they do not contribute to the IR peaks. All the

Table II. Comparison of Some Average and Specific Bond Lengths and Interatomic Distances in a Tetrasiloxane Ring With and Without a H-bonded H_2O Molecule. (-) is a Molecular Bond. (..) is a H-bond. (---) is an Interatomic Distance.

Bond Type	Average Bond Length (Å)		Bond Length Change	
	Without H_2O (Å)	With H_2O (Å)	(Å)	(%)
Si-O (in the $SiOH_s$ groups not H-bonded to the H_2O molecule)	1.700729 (σ_8=0.00462)	1.704992 (σ_6=0.00544)	0.004263	0.25
O-H (in the $SiOH_s$ groups not H-bonded to the H_2O molecule)	1.021267 (σ_8=0.00369)	1.024074 (σ_6=0.00329)	0.002807	0.27
Si---H (in all the $SiOH_s$ groups)	2.259144 (σ_8=0.03661)	2.246547 (σ_8=0.09158)	-0.012597	-0.56
Si-O (in the Si-O-Si bridging bonds)	1.685868 (σ_8=0.002716)	1.744768 (σ_8=0.17996)	0.058900	3.50
Specific Bonds in the H_2O Molecule				
O(20)-H(17)	1.01913(i.e. free H_2O)	1.060329	0.041199	4.04
O(17)-H(27)	1.01913(i.e. free H_2O)	1.019337	0.000207	0.02
Specific Bonds in the ≡Si(6)O(10)-H(22)..(17)OH(20)H(27) Structure				
Si(6)-O(10)	1.700729	1.690545	-0.010184	0.60
O(10)-H(22)	1.021267	1.064406	0.043139	4.22
H(22)..O(17)	N/A	1.338446	-	-
Specific Bonds in the ≡Si(6)-[H(21)]O(9)..(20)HO(17)H(27) Structure				
Si(6)-O(9)	1.700729	1.737202	0.036473	2.14
O(9)-H(21)	1.021237	1.008782	-0.001246	-1.22
O(9)..H(20)	N/A	1.346744	-	-

bond length changes are due to charge redistribution caused by adsorption of the H_2O molecule. As the $2\nu_3$ wavelength increases as W increases, the length of the O(10)-H(22) bond should increase as the electron charge distribution is changed by adsorption of more H_2O molecules. As the $2\nu_1$ wavelength is constant as W increases, the length of the H-bonded O(17)-H(20) bond in the H_2O molecule should not be changed by the adsorption of more water molecules.

When the H-bonded groups are included, all the average bond lengths increase in length when a H_2O molecule is H-bonded to the silicate ring, but the Si---H distance decreases by 0.56%. This infers that, compared to the bare siloxane ring, the bond angles change to cause a distortion of the ring when a H_2O molecule is adsorbed. This affects both the IR spectra, as seen experimentally, and the thermal expansion behavior [3] due to adsorbed H_2O.

CONCLUSIONS

The adsorption of H_2O molecules onto the surface in the pores of a metal alkoxide derived silica gel monolith by H-bonding to surface $SiOH_s$ groups causes an increase in the wavelength of the associated IR peak, $2\nu_3$. This process can be modelled by INDO MO theory, showing the expected increase in bond length of the H-bonded O-H groups. The INDO MO model appears to reproduce the bulk properties of these silica gel monoliths. In typical MO theory the clusters do not in general predict bulk properties very well. One can therefore consider the possibility that the properties of these microporous gels are dominated by the surface chemistry and that the surface may be represented by this simple tetrasiloxane ring model.

ACKNOWLEDGEMENTS

The authors acknowledge support of AFOSR Contract #F49620-88-C-0073 and the SDI/AFOSR OGAMMS project and encouragement of D. R. Ulrich, L. Davis, and L. Burggraf. The INDO [7] program was made available by the Quantum Theory Project (QTP) at the University of Florida courtesy of Professors M. Zerner and R. Bartlett.

References

1. S.H. Wang, Ph.D Dissertation, University of Florida, 1988.

2. C.C. Perry and X. Li, N.I.R. Studies of Monolithic Silica Gels, to be published in J. Phys. Chem..

3. J.K. West, B.F. Zhu, Y.C. Cheng and L.L. Hench, "Quantum Chemistry of sol-Gel Silica Clusters," 5th International Workshop on Glasses and Glass Ceramics from Gels, Aug. 1989, Rio De Janeiro, Brazil.

4. L.L Hench and J.K. West, Chemical Reviews 90, 33-72 (1990).

5. B.F. Zhu, G.F. Wang and L.L. Hench, "Dilatometry of Gel-Silica," 4th International Conference on Ultrastructure Processing of Ceramics, Glasses and Composites, February 1989, Tucson, Arizona.

6. M.C. Zerner, G.H. Loew, R.F. Kirchner and U.T. Mueller-Westerhoff, J. Am. Chem. Soc. 102, 589 (1980).

7. M. Zerner et al., QTP, Univ. of Florida, Gainesville, Fl. Pgm No. 010183.

APPENDIX 10

Quantum Chemistry of Sol-Gel Silica Clusters

by

Jon K. West, Bing Fu Zhu, Yeu Chyi Cheng and Larry L. Hench
Advanced Materials Research Center
University of Florida
One Progress Blvd. No. 14
Alachua, Florida 32615

Abstract

Quantum calculations of rings and chains containing up to six hydrolyzed silica tetrahedra have been made using Intermediate Neglect of Differential Overlap (INDO) molecular orbital theory. Differences in the molecular energies between rings and chains appears to be responsible for limiting the growth of particles in the sol prior to gelation. Changes in the structure and molecular energies of a 4-membered silicon ring with adsorption and desorption of H_2O indicates a possible mechanism for the observed dilatometric behavior of porous Type VI sol-gel silica.

1. Introduction

Quantum mechanical calculations are becoming increasingly important in understand the processing and properties of sol-gel silica systems. For example, both hydrolysis and polycondensation of SiO_2 from an alkoxide precursor have been studied by Burggraf, Davis, and Gordon[1] using molecular orbital calculations. Their results indicate that a hypervalent silicon complex forms as an intermediate state in the polycondensation reaction. By studying the possible reaction paths for the removal of water, they show that pentacoordinated silicon has no activation energy for water removal. In contrast, the tetravalent silicon has a relatively large activation energy for

the removal of water. High pressure Raman spectroscopy studies by Zerda and Hoang[2] provide experimental evidence for existence of the pentacoordinated silicon. This confirmation of the intermediate state confirms how the polycondensation of sol-gel silica proceeds by elimination of a water molecule.

Recent developments in sol-gel silica optics have produced fully dense Type V amorphous silica monoliths with extremely wide optical transmission bands[3,4]. Semi-empirical quantum calculations using an Intermediate Neglect of Differential Overlap (INDO) molecular orbital program, made available by the Quantum Theory Project at the University of Florida,[5] were used to explain the improved UV cut-off of the gel-silica optics as OH^- ions are eliminated from the SiO_2 network[6]. The same INDO calculational method was used to interpret sol-gel Na_2O-SiO_2 UV cut-off wavelengths[6]. In both SiO_2-OH and SiO_2-Na_2O systems the energy gap between the Highest Occupied Molecular Orbital (HOMO) and Lowest Unoccupied Molecular Orbital (LUMO) was calculated for the single states[6].

In the same paper[6] Huckel Molecular Orbital (HMO) theory, as well as INDO, was used to calculate the energy difference between rings and chains of SiO_2 tetrahedra. Both HMO and INDO calculations showed that chain structures are more stable than rings for structures up to 3-4 silica tetrahedra (HMO) or 10-12 silica tetrahedra (INDO).

In the present work the effects of H_2O are included in INDO calculations of SiO_2 clusters. Two problems are addressed: 1) The structural energy differences between chains and rings; and 2) The change in structure and molecular energy when a stable ring composed of 4 silica tetrahedra is subjected to adsorption and desorption of an H_2O molecule. Results of the

INDO calculation are compared with dilatometry of gel-silica monoliths exposed to adsorption and desorption of H_2O.

2. Model Structures

The molecular structures evaluated contain from 1 to 6 silica tetrahedra. In each model two bridging oxygens and two non-bridging oxygens are bonded to each silicon. One hydrogen is bonded to each of the non-bridging oxygens to terminate the structure and balance the charge. Both ring and chain models of silica tetrahedra were evaluated and their energies compared (Figure 1).

The energy of free water was also determined using a geometrically optimized INDO structure. The INDO energy for this model of water is

$$E_{H2O} = -17.9733 \text{ a.u.} \qquad (1)$$

The bond length matrix was determined to be:

	(1)O	(2)H	(3)H
(1)	-0-		
(2)	1.019130 Å	-0-	
(3)	1.019130 Å	1.588026 Å	-0-

and the bond angle was

$$H\text{-}O\text{-}H = 102.35^\circ \qquad (2)$$

Figure 1 illustrates that an important difference in the number of atoms between chains and rings is the water content. A chain has one extra water molecule when it is compared to a ring. Thus, in order to compare more

accurately the energies of rings and chains than previously reported[6], the energy of free water must be included in the analysis:

$$E'_{CHAIN} = E_{CHAIN} \cdot E_{WATER} \qquad (3)$$

Consequently, when the energies of rings and chains are compared, the energy of one water molecule is subtracted from the chain energy.

Figure 1 shows the 2-D projection of a geometrically optimized INDO chain and ring structure for 4 silica tetrahedra. These projections are typical of the hydroxylated silica structures modelled in this study, which included 2, 3, 4, 5 and 6 tetrahedra per cluster.

The clusters were each optimized for minimum energy using a molecular mechanics (MM2)[9] routine. The molecular orbitals were then determined using geometrically optimized INDO calculations. The molecular energies were evaluated and compared to establish the relative stability of each structure.

Table 1 compares the cluster size and the INDO Energy per silica tetrahedron for rings and chains as a function of the number of tetrahedra with and without the correction for extra water in the chains. As expected, the chains are substantially larger axially than rings. Figure 2 compares the size and $\Delta E_{chain-ring}$ values for the clusters with the H_2O correction. Initially, the chain structures are more stable than the rings. This has been observed experimentally using NMR spectroscopy[10], where a linear, as opposed to a ring, growth model most consistently interprets the experimental structural evidence for early growth prior to gelation.

The relative stability of chains compared to rings decreases as the number of silica tetrahedra increases, as shown in Figure 2 by the decrease in the difference between their calculated water corrected, INDO energies. The

difference is shown to reach zero as the number of tetrahedra reaches 5 when the driving force for formation of rings becomes equally favorable to forming chains. This result is similar to the size range where primary particle growth stops in acidic silica sols for the larger or secondary type particles[9,10]. Acid catalysis ensures complete hydrolysis of the silica tetrahedra, as used in these calculations. The size of the INDO calculated rings or clusters for 5 tetrahedra appears to fall within the 10 to 20 Å range of the radius of gyration of the primary particles calculated from Small Angle X-ray Scattering analysis of acid catalyzed silica sols[9,10].

As gelation occurs, the cross-linking of the structure becomes more dominant. Statistical analysis indicates that chain growth is limited by this process and rings must be formed[11]. The energy differences between ring structures with 2 to 6 SiO_2 tetrahedra per ring are very small in the INDO model. This indicates that a broad distribution in the number of tetrahedra per ring is possible in a gel since there is very little difference in energy as the number of tetrahedra per ring increases.

The results shown in Figure 2 suggest that the most favored path for structural evolution is adding 4 to 5 membered rings (10 Å size) to each other by a condensation reaction.

These results are consistent with proposed models for the structure of acid catalyzed silica gels that contain two levels of structure formed before gelation[9,10]. These models suggest the formation of primary particles, of 10-20 Å diameter which agglomerate to form secondary particles of about 40-60 Å diameter. The secondary particles give rise to the pore structure after drying.

3. Dilation of Sol-Gel Silica Monoliths with Adsorbed Water

Understanding the interactions of water with gel-silica monoliths is vital both to controlling drying[12,13] and achieving stability of porous gel optical matrices[3]. A previous study of thermal behavior of porous gel-silica reported irreversible thermal hysterisis of the monoliths in a precision push-rod dilatometer[14]. When the sample is cooled to 23°C under an ambient, moisture-containing atmosphere the gel under goes considerable dilation, as illustrated in Figure 3(a). However, thermal cycling between 250°C and 400°C results in completely reversible thermal expansion and contraction. The expansion on cooling from 250° to 23°C was attributed to adsorption of water on the pores of the gel. TGA data[14] confirmed the adsorption of water during the cooling cycle. Figure 3(b) shows dilatometric evidence of continual expansion of a gel monolith exposed to ambient air for 23 hours at 23°C. Prior to exposure to the moist air the sample had been preheated to 600°C and dehydrated in vacuum at 180°C. Adsorption of water into the porous gel-silica structure appears to dilate the structure.

4. Quantum Calculations of Water Adsorption onto Sol-Gel Silica

There is roughly an equal distribution of 3-fold , 4-fold, 5-fold and 6-fold rings of silica tetrahedra in fused silica and equivalent structures are believed to be present in silica gels[15]. The 4-fold ring shown in Figure 4 shows the structure used in this investigation to study the theoretical effect of water on silica rings. The water was hydrogen bonded to the silica cluster as indicated by Takahashi[16]. Intermediate neglect of differential overlap (INDO) molecular orbital theory developed by Zerner, et al.[17] was used to optimize the structure in Figure 4. The 4-fold ring was geometrically

optimized with and without the adsorbed water molecule. Effects of other silica ring structures and location of the water molecule will be described elsewhere.

Table 2 shows the results of the calculations for the dilation of the 4-fold silica ring. The distances between the diagonal silicon atoms are shown. The ring without water is geometrically uniform. However, the ring with the water adsorbed is elongated along the axis with the adsorbed water molecule. Also, the average silicon-silicon distance for neighboring atoms increases.

In an amorphous structure there should be a random orientation of the elongation. Some of the expansion will occur in regions of the network where contraction of the ring will compensate. However, on the average there is predicted to be a small expansion when the water is bonded to the structure. This finding is consistent with the expansion data observed in Figure 3.

5. Summary

Quantum calculations for cluster of rings and chains of silica tetrahedra have been made using Intermediate Neglect of Differential Overlap (INDO) molecular orbital theory. Elimination of differences in the molecular energies between rings and chains appears to limit the growth of primary particles to rings of a ~5 tetrahedra per particle during the sol stage prior to the formation of the gel. The geometries of silica ring cluster were analyzed before and after bonding of water molecules. The changes in the structures predict an anisotropic expansion of the ring and indicate a possible mechanism for the observed dilatometric expansion of porous Type VI sol-gel silica caused by the absorption of water.

Acknowledgement

The authors are grateful to Air Force Office of Scientific Research for its financial support through contract #F49620-88-C0073.

References

1 L.W. Burggraf, L.P. Davis, and M.S. Gordon, "Neutral and Anionic Hypervalent Silicon Complexes in Silanol Polymerization," in proceedings of the 4th International Ultrastructure Conference, Tucson, AZ (1989).

2. T.W. Zerda and G. Hoang, "High Pressure Raman Study of Hydrolysis reaction in TMOS," to be published in J. Non-Cryst. Solids.

3. L.L. Hench, S.H. Wang and J.L. Noques, SPIE Vol. 878, Multifunctional Materials (1988) 76.

4. S.H. Wang, C. Campbell, and L.L. Hench in: Ultrastructure Processing of Advanced Ceramics, eds., J.D. Mackenzie and D.R. Ulrich (Wiley, New York, 1988) p. 145.

5. M. Zerner, et al., Quantum Theory Project, Gainesville, Florida, Program No. 010183.

6. J.K. West, S. Wallace, L.L. Hench and C.R. Lishawa, "Quantum Calculations on Sol-Gel Silica Structures," in Proceedings of 4th Ultrastructure Conference, Tucson, AZ (1989).

7. N.L. Allinger, et al., QCPE, Bloomington, Indiana, Program No. 318.

8. L.W. Kelts, N.J. Effinger and S.M. Melpolder, J. Non-Cryst. Solids 83 (1986) 353.

9. G. Orcel, L.L. Hench, I. Artaki, J. Jonas and T.W. Zerda, J. Non-Cryst. Solids 105 (1988) 223.

10. B. Himmel, Th. Gerber and H. Burger, J. Non-Cryst. Solids 91 (1987) 122.

11. J. Zarzycki, in: Science of Ceramic Chemical Processing, eds., L.L. Hench and D.R. Ulrich (Wiley, New York, 1986) p. 21.

12. G. W. Scherer, J. Non-Cryst. Solids 87 (1986) 199-225.

13. L.L. Hench, in: Proceedings of the 4th International Ultrastructure Conference, Tucson, AZ (1989).

14. B.F. Zhu, G.F. Wang and L.L. Hench, "Dilatometry of Gel-Silica," ibid.

15. W. G. Klemperer, V. V. Mainz, S. D. Ramanurthi, F. S. Rosenberg, in: Better Ceramics Through Chemistry III, eds., C. J. Brinker, D. E. Clark, and D. R. Ulrich, (Materials Research Society, Pittsburgh, PA, 1988) Vol. 121, p. 1, 15.

16. K. Takahaski, "Silanol and Water on Silica Studies by the CNDO MO Method," J. Am. Chem. Soc., Faraday Trans. I, Vol. 78, pp. 2059-2072 (1982).

17. M.C. Zerner, G.H. Loew, R.F. Kirchner and U.T. Mueller-Westerhoff, J. Am. Chem. Soc., Vol. 102, p. 589 (1980).

Figure Captions

Figure 1. Silica tetrahedra: (a) ring of 4 silica tetrahedra; and (b) chain of 4 silica tetrahedra.

Figure 2. Cluster size and $\Delta E_{chain-ring}$ for the clusters with H_2O correction.

Figure 3 (a) Thermal hysteresis of a titania-silica gel pre-heated to 400°C.

(b) Expansion at room temperature under ambient atmosphere for a silica gel pre-heated to 600°C.

Figure 4. Four-fold silica structure with one absorbed water molecule.

TABLE 1

Energy Difference between Chains and Rings
Corrected for Water

Number of Silica Tetrahedra	Cluster Size (Å)		INDO (a.u.) (Chain-Ring) (Ref. 6)	Water Corrected INDO (a.u.) (Chain-Ring)
	Rings	Chains		
2	6.5	9.1	8.9	0.09
3	7.1	12.6	5.9	0.11
4	9.3	16.2	4.4	0.04
5	11.3	19.8	3.6	0.01
6	11.8	23.4	2.8	0.24

TABLE 2

Silica Dilation

4 Fold Ring	INDO Energy (a.u.)	Diagonals Si-Si Distance (Å) (1)-(4)	(6)-(7)	Average Neighbor Si-Si Dist.	wt% Water Content	Average Expansion $\frac{\delta L}{L} \times 10^{-3}$
Without H_2O	-223.46242	4.659007	4.51665	3.24495	0%	0
With H_2O	-241.4056	5.15587	4.027797	3.27207	5.8%	836

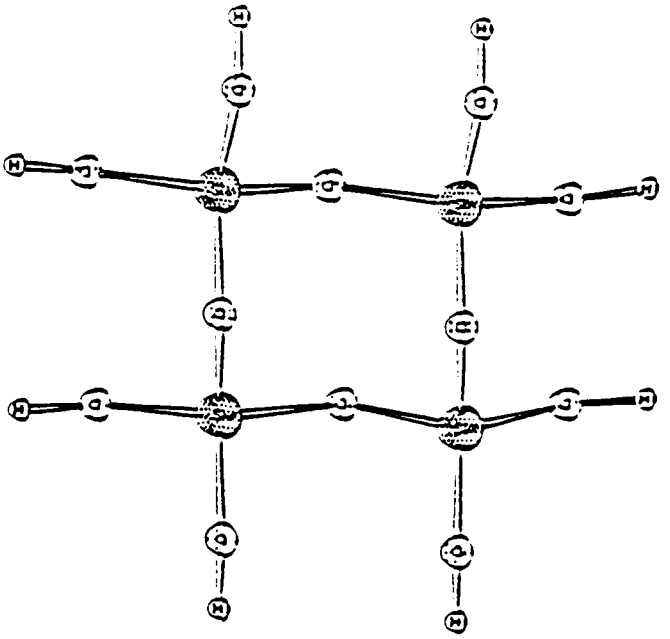

(a)

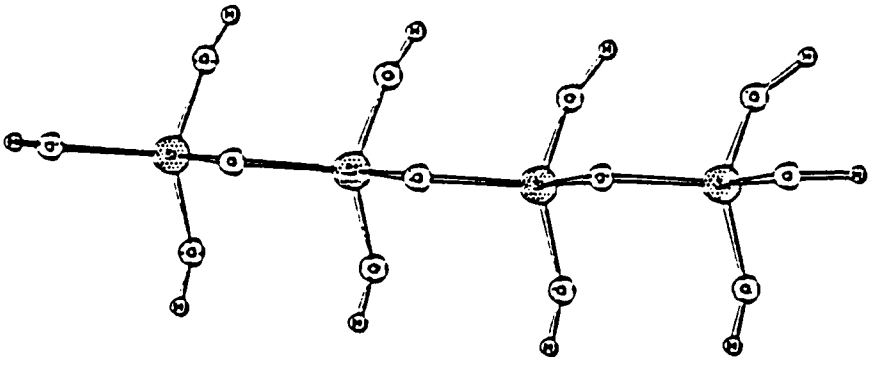

(b)

Figure 1

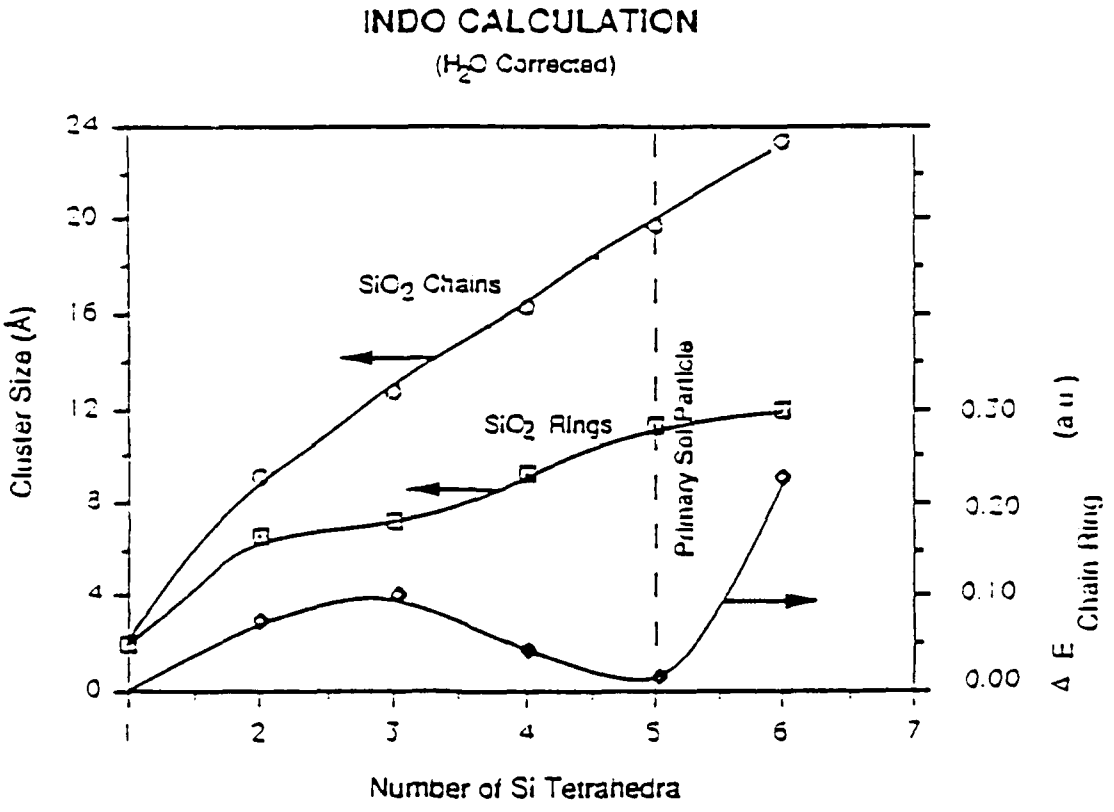
INDO CALCULATION
(H_2O Corrected)
Cluster Size (Å)
24
20
16
12
8
4
0
SiO_2 Chains
SiO_2 Rings
Primary Sol Particle
0.30
0.20
0.10
0.00
$\Delta E_{Chain\ Ring}$ (a.u.)
1
2
3
4
5
6
7
Number of Si Tetrahedra

Figure 2

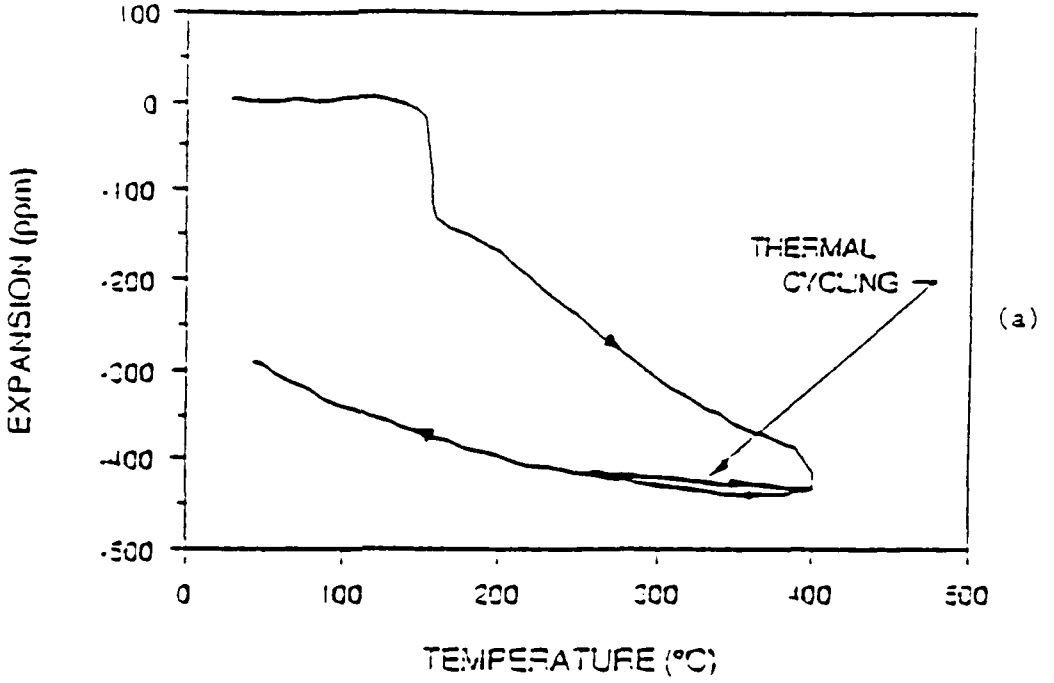
100
0
-100
-200
-300
-400
-500
EXPANSION (ppm)
THERMAL
CYCLING
0
100
200
300
400
500
TEMPERATURE (°C)

(a)

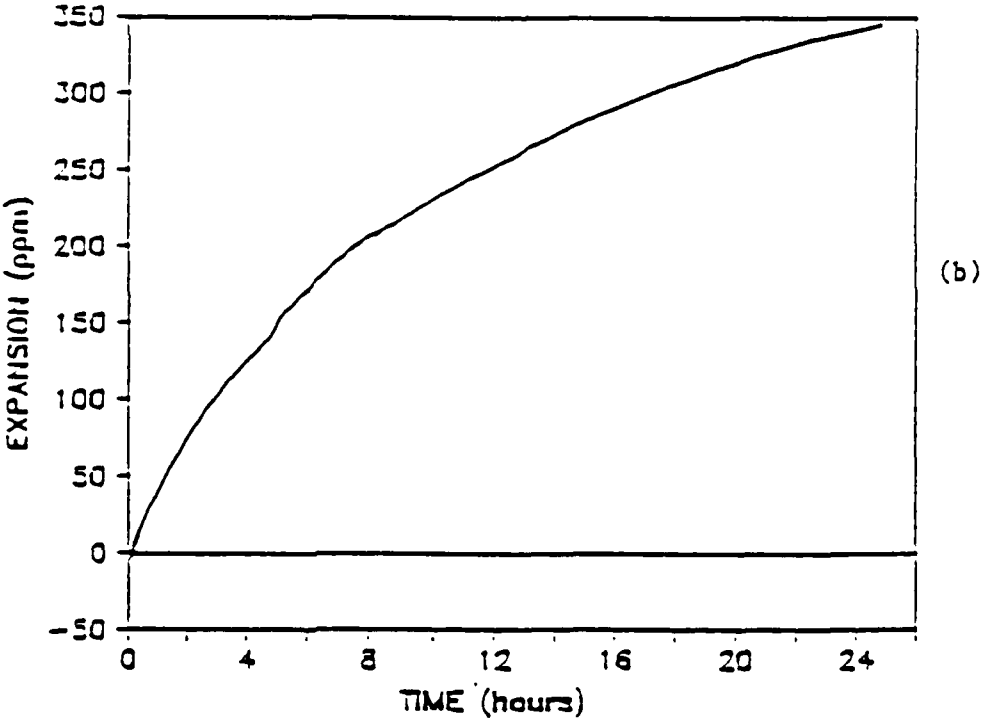
350
300
250
200
150
100
50
0
-50
EXPANSION (ppm)
0
4
8
12
16
20
24
TIME (hours)

(b)

Figure 3

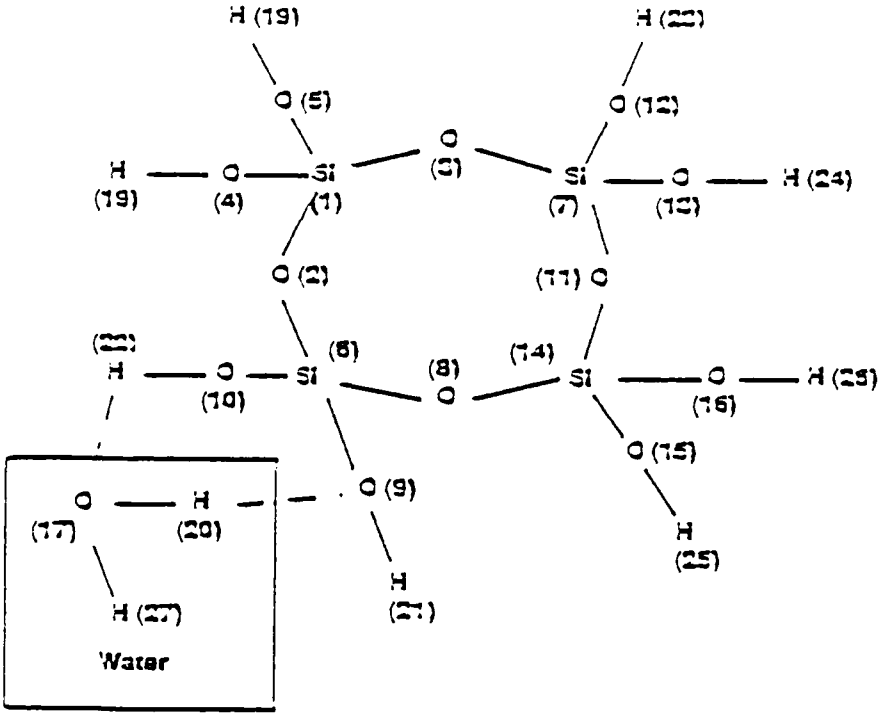
H (19)
H (22)
O (5)
O (12)
H (19)
O (4)
Si (1)
O (3)
Si (7)
O (12)
H (24)
O (2)
(11) O
(21)
H
(6)
(14)
H (23)
O (10)
O (8)
O (16)
O (15)
O (9)
O (17)
H (20)
H (18)
H (21)
H (25)
Water

Figure 4

APPENDIX 11

LIQUID CRYSTALS IN GEL-SILICA MATRICES.

H. J. Coles and H. F. Gleeson

Liquid Crystal Group,
The Physics Department,
The University,
Manchester, M13 9PL.
United Kingdom.

In collaboration with Prof. L. L. Hench, University of Florida.

Thanks to Prof G. Scherowsky and Dr. A. Schliwa, Technical University of Berlin.

AIMS:

To produce a new line of low cost liquid crystal devices and shutter arrays with

- broader operating temperatures
- large areas
- higher optical performance
- intrinsic processability.

APPROACH:

- Use of fast switching, bistable ferroelectric liquid crystals.
- New device configurations compatable with the porous Gel-Sil systems.
- Study of low molar mass and polymeric materials.
- Study of poled versus orientational order.

PROGRESS TO AUGUST 1988.

1. Incorporation of liquid crystals into Gel-Sil matrices.
2. Detailed examination of ferroelectric liquid crystal systems:
   - Single polariser dichroic guest-host device
   - Zero polariser black dye device
   - Fluorescent ferroelectric device
   - STRUCTURE PROPERTY CORRELATIONS IN GUEST-HOST SYSTEMS VERSUS HOST SYSTEMS ALONE.
3. Preliminary observation of orientation effects in liquid crystal-Gel-Sil systems.

1988 - 1989 OBJECTIVES.

- FERROELECTRIC POLYMER LIQUID CRYSTALS.
- New device configurations.
- Electroclinic materials.
- Dye structure effects.
- Optical effects in Gel-Sil matrices.
- Interaction of matrices with the liquid crystal.

SIDE CHAIN POLYMERS

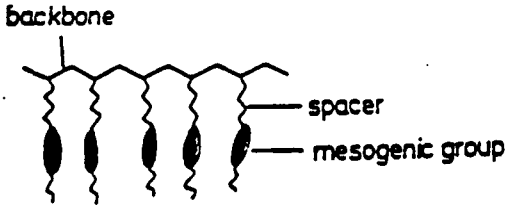

Backbones:- Acrylate, Methacrylate, Siloxane, Polyphosphazines.

Spacers:- $-(CH_2)_n-$, $-(CF_2)_n-$, $-(CH_2)_m(Si(CH_3)_2-O)_p(CH_2)_1-$

Mesogenic Groups:-(transverse or lateral substitution).

Nematic:- RO–⬡–CO_2–⬡–CN

Chiral Nematic:- (Cholesteric) RO–⬡–CO_2–(chiral)

Smectic:- RO–⬡–⬡–CN

Chiral Smectic:- RO–⬡–CO_2–⬡–⬡–O–$\overset{CH_3}{\underset{CH_3}{CH}}C_6H_{13}$

POLYACRYLATE STRUCTURE

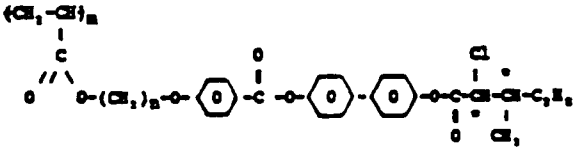

Transition Temperatures (for n = 10)

D.S.C. (°C) Tg —(-20)→ S_I —(60)→ S_C^* —(105)→ S_A —(164)→ I

Microscopy (°C) S_I —(65)→ S_C^* —(105)→ S_A —(135-164)→ I

The molecular weight of the polymer ferroelectric material was approx. 35,000. The important parameters to measure for any ferroelectric liquid crystal material are :

- STATIC PROPERTIES. Tilt angle, Spontaneous polarisation.
- DYNAMIC PROPERTIES. Response time.

These parameters were measured and are given on the following pages.

	S6 series			J1	Q41D
(temperature)	180	600	1000	180	600
Particle sizes (nm)	~2, 4-5	~2, 4-5	~2, 4-5	1-3	2-3
pores	4	smaller	virtually non existent	~1	~1
order (tramlines) 2nm	✓	< ✓	✗	~	~
block or chains of rings	✗	?	✓	✓	✓

Nitrogen Adsorption Data Table 2

	Q41D	Q41D (orange)	J1	
S_{BET}	390	380	120	m^2g^{-1}
pore volume	0.27	0.26	0.10	mlg^{-1}
micropore volume	~0.01	~0.003	~0.0	mlg^{-1}

Table 3 Observed IR, NIR Frequencies and Assignments of S6-series

Fundamental			Overtone			Combination		
Freq.		Assi.	Freq.		Assi.	Freq.		Assi.
cm-1	nm		cm-1	nm		cm-1	nm	
466	21459	ν_4 (SiO_2)	6873	1455	$2\nu_{OH}$ (H_2O,P)	4405	2270	ν_{OH}(SiOH,H) $+\nu_1$(SiO_2)
806	12407	ν_1 (SiO_2)	7143	1400	$2\nu_{OH}$ (H_2O,H) (SiOH,H)	4562	2192	ν_{OH}(SiOH,P) $+\nu_1$(SiO_2)
961	10406	ν_{Si-OH} ν_{Si-O^-}	7326	1365	$2\nu_{OH}$ (SiOH,P)	5128	1950	ν_{OH}(H_2O,P) + (H_2O,P)
1093	9143	ν_3 (SiO_2)	10438	958	$3\nu_{OH}$ (H_2O,P)	5285	1892	ν_{OH}(H_2O,H) + (H_2O,H)
1636	6112	(H_2O,P)	10753	930	$3\nu_{OH}$ (SiOH,P)	8130	1230	$2\nu_{OH}$(SiOH,P) $+\nu_1$(SiO_2)
3473	2879	ν_{OH} (H_2O,P)	10526	950	$3\nu_{OH}$ (H_2O,H) (SiOH,H)	8418	1188	$2\nu_{OH}$(H_2O,P) + (H_2O,P)
3680	2732	ν_{OH} (SiOH,H)				8757	1142	$2\nu_{OH}$(H_2O,H) + (H_2O,H)
3738	2675	ν_{OH} (SiOH,P)						

Table 4 The Spectroscopic Data and Magnetic Susceptibility Results

SAMPLES	TREATMENT	ABSORPTIONS (nm)	Xg ($x10^{-6}$ c.g.s)	% Co
Co-doped Q41-D (pink)	Dried in air	230 300 510 1250	0.754	0.65
Co-doped Q41-D (purple)	Dehydrated in vacuum	250sh 300 583 647 1670	0.931	
Co-doped Q41-D (orange)	Rehydrated in air	241 275sh 405 510	-0.126	
Co-doped Q41-D (red)	Re-dehydrated in vacuum (subsequent rehydration leads to orange)	280 522		
Co-doped J-1 (blue)	Dried in air	230 300 515 583 647 1265 1670	0.811	0.65
Co-doped J-1 (blue pink)	Dehydrated in vacuum	288 519 575 640	1.808	
Co-doped J-1 (blue)	Rehydrated in air	299 515 583 646	0.940	

[redacted]

[redacted]

1) [redacted]

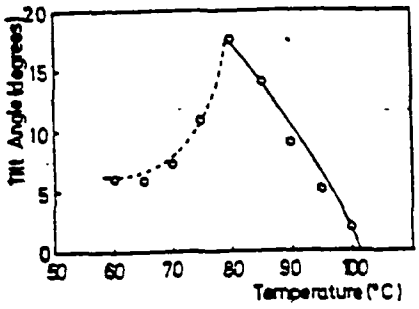

1. TILT ANGLE MEASUREMENTS.

- Lower than the ideal (approx. 22½°). More synthesis needs to be carried out for optimisation.
- Anomalous behaviour below 80°C. This is reflected by the dynamic measurements given later. The parameter should normally follow a Curie-Weiss behaviour.

[redacted]

3) [redacted]

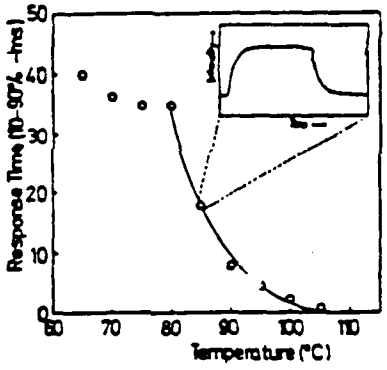

3. RESPONSE TIME.

- Most response measured. Until now the fastest response measured in a polymer liquid crystal system was approx 100ms (under equivalent field strength conditions). Although it was expected that the response of a ferroelectric polymer would be faster (cf low molar mass systems), these measurements confirm this.
- Relatively low electric fields were used (approx 14V/μm) gave fast switching.
- Electroclinic switching (tilt angle related to the field strength) was observed in the S_A phase.
- Anomalous response times were measured below 80°C (cf tilt angle measurements).

[redacted]

1. High apparent spontaneous polarisation.
2. Bistability in 2μm thick cells.
3. Sub-millisecond switching (10-90% response) for moderate fields (~ 10V/μm).
4. Polymer ferroelectric switching in the birefringence or guest-host modes.
5. Electroclinic effects observed above the $S_C^* \rightarrow S_A$ transition.

[redacted]

2) [redacted]

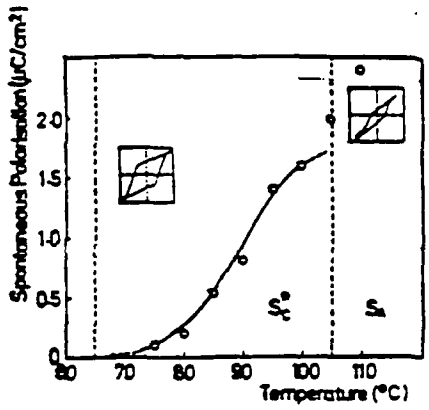

2. SPONTANEOUS POLARISATION.

- Much higher in liquid crystal polymers than in analogous low molar mass systems. Materials with a polysiloxane backbone show values approximately 4x greater than the low molar mass sidegroup alone. This is likely to be due to hindered rotation of the mesogenic groups in the polymers, as well as the intrinsically higher order parameter.
- Groups with larger dipoles can be supported by the polymer without loss of the ferroelectric phase. This allows an increase in obtainable P_s value.

[redacted]

1. [redacted]

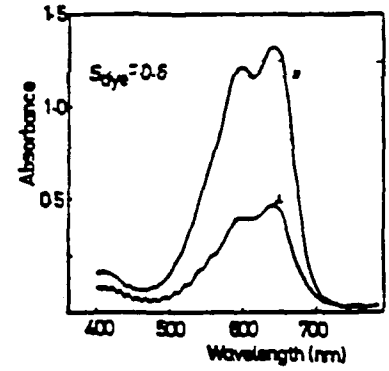

- Demonstrated for certain dichroic dyes in polymer hosts, as shown above. The maximal order parameter was measured for the dye.
- Optimisation of dye structure is currently in progress. Preliminary materials seemed to reduce tilt angle, but improved transition temps and response times. High dye solubility was achieved.
- The polymer dye guest-host systems maintain the advantages of the proven low molar mass devices (high contrast, single or zero polariser devices possible).

[redacted]

2) [redacted]

(i) $\tau_F \propto V^{-1}$ for T > 75°C.

complex for T < 75°C.

(ii) Tilt Angle independent of voltage.

THE NEXT STEPS:

There are clearly many directions which it is important to persue in this novel work. In particular, this project forms an interface between the Electro-active polymer programme and the Gel-Silica project supported by the USAF which come under Dr. Don Ulrich's direction. However, the following topics are of particular interest:

- Effects of polymer polydispersity. Specific fractions are currently being synthesised by colleagues in Berlin.

- Spontaneous polarisation studies in polymer/low molar mass mixtures. This will be relevant to POLED ORDER studies.

- Fluorescent and dichroic copolymer systems.

- Electroclinic effects in polymer and lmm materials. Do these provide model systems for Gel-Sil/ liquid crystal devices?

- Incorporation of these functional materials int Gel-Sil matrices.

- The influence of the sol-gel structures of liquid crystalline properties.

- Optical effects in Gel-Sil matrices as a function of pore size.

- Magneto- optic effects in Gel-Sil matrices.

APPENDIX 12

ORGANIC DYES IN SILICA GLASS

C Whitehurst, D Shaw and T A King

1. INTRODUCTION

Organic laser dyes provide a convenient, flexible and broadly tunable range of intense laser sources. Many of the dyes in the visible region of the spectrum possess high quantum yields of fluorescence, absorption and emission. However, the full potential of the lasing dye medium cannot be realised because the liquid host adversely affects many thermodynamic, spectroscopic and kinetic properties of the dye. These include non-radiative quenching of upper lasing levels, spectral shifts and thermal instability. Provision of a solid matrix would enhance the lasing properties of organic dyes to their full potential, reducing thermal restrictions, impurity and dye-dye quenching, and adverse migration of active molecules towards photodegrading impurities. In addition, hosting the dye in a solid matrix greatly increases the handling and convenience and reduces laser complexity, eg fewer pumps, pipes and reservoirs, and complexity in the construction of a laser system.

2. TWO METHODS FOR DYE DOPANT OF GEL-SIL

2.1 Sol-to-Gel Doping

Hydrolysis and condensation of $Si(OMe)_4$, incorporating an organic dye, leads to a gel that is dried at about 60°C for a few days to remove water and methanol. The incorporated dye is uniformly embedded in the resulting

inorganic host matrix. The fluorescence properties of sol-gel dyes have already been described by others[1-4].

Experimentally it was demonstrated that the photostability of the laser dye R6G increased by an order of magnitude when the liquid organic laser host was replaced by an inorganic glass[1]. R6G when introduced into a silica gel-glass showed an enhanced photostability. The amount of dimers which decrease the lasing ability of the dye in liquid media was negligible in gel glass as here the dye molecules were isolated in glass cages.

The advantages of this method of preparation are as follows:

Molecular Immobility: Reduction in intermolecular collisional deactivation by either other dye molecules, photodecomposition products or impurities. Migration of quenching molecules and products leading to repeated quenching and decomposition is prevented.

Molecular Isolation: Dye impurities are isolated within matrix cells and cannot quench upper laser levels. Active dye molecules are isolated from organic solvents and gases with low thermal and chemical stability. Higher quantum yields and other spectroscopic and kinetic properties of organic dyes are attainable in this state.

Greater Heat Dispertion: The higher thermal conductivity of glass over plastics or methanol leads to a more uniform temperature distribution throughout the active medium. This reduces the advent of refracting convection currents. Thus laser energy loss or a

reduction in beam quality due to thermal lensing can be reduced. Excess heat can be removed at a faster rate enabling laser outputs of higher powers to be achieved for the same cavity incorporating a traditional host.

Greater Dye Concentration: Relatively high dye concentrations are possible which enable more compact and efficient cavities to be constructed. These concentrations are possible without risking aggregation or dimerization, ie inducing unfavourable chemical reactions or collisional self-deactivation.

Disadvantages to this method of preparation:

Non Densification: Due to the low thermal stability of organic dyes, the temperature of the matrix must be kept low (< 100°C) and therefore the gel glass has to remain completely undensified. Further tests have shown this category of gel glass to be very susceptible to fracturing and cracking when exposed to fluids or small temperature cycles (over a few degrees).

Poor Optical Quality: Low temperature annealed glasses cannot be reliably polished (dry polishing only) as the samples frequently shatter.

Expensive: This method of preparation is expensive in both time and parts.

2.2 Adsorption Doping

Previously prepared undoped gel glass, at any densified states, is immersed in solvated R6G. The R6G fills the pores in a time dependent upon the viscosity of the solvent, and the sample left to dry. It has been shown that vapour pressures in excess of about 20 Torr can lead to catastrophic cracking of the sample and therefore drying must start at a reduced rate below 20 Torr, before a more serious attempt be made. Solvents whose vapour pressure is greater than 20 Torr at room temperature must be cooled to reduce their vapour pressure in the early stages of drying. It should also be noted that gel glass samples dried thoroughly have readsorbed water from the atmosphere reaching a stable equilibrium with their surroundings.

Advantages for this method of preparation:

Higher Densification: Addition of the dye after gelation means that the gel glass can be densified to any level almost to full densification, before the dye is added. This leads to a higher optical quality and more robust samples for polishing, drying and machining for laser cavity construction.

Availability: Undoped gel glass is obviously much more readily available than the predoped glass and leaves the user with the freedom to choose dye type and concentration to suit their own customised needs.

Disadvantages as follows:

Neo-Isolation: Although dye molecules are trapped in the nanometer scale pores of the glass matrix with bulk movement of residual solvents, impurities and decomposition

molecules eliminated, mobility will be possible within the pores. Thus interactions such as dye self-quenching, etc, may occur on a local scale although not to the same degree as for bulk solutions. Dimersation and aggregation are possible within the pores at high concentrations, although to what degree is not yet known.

Temporary Location: The dye and/or solvent molecules are adsorbed onto the surface of the pore walls and can be redissolved if the dried glass comes into contact with another solvent.

2.3 Both Doping Methods

Both doping methods compartmentise the bulk host matrix but to varying degrees. The sol-to-gel method on a molecular scale, the adsorption method on a molecular cluster scale. However, they both inhibit convection currents and migration of molecules throughout the bulk of the glass. The glass matrix provides a more thermally and chemically stable host, cf organic and liquid hosts, whose conductive properties allow for a more uniform temperature distribution throughout the bulk. This reduces refractive distortion of laser beams and a high capacity for forced cooling enabling higher input and output powers to be employed.

The two systems allows for unconventional dye concentrations (10^{-4} - 10^{-3}M ...) due to the lack (or reduced in the adsorbed case) of dimerisation and aggregation.

A desirable increase in the Stoke's shift is created, from 30 → 40nm for similar dye concentrations, thereby reducing the self-adsorption

cross-section, due to the reduced freedom of the excited dye molecules in reorientating themselves around the excited state, thus reducing the excited rotational energy level compared to the ground state.

The method described here is the doping of the gel glass using the adsorption technique.

3. DYE DISTRIBUTION

The sol-to-gel method incorporates the dye molecules within the bulk of the glass. They are held in isolation from gas, liquid and solid impurities in the host lattice. A direct result of this is attainment of relatively high concentrations.

Adsorption doping puts the dye molecules onto the exposed walls of the pores. In this situation dye molecules may well come into contact with solvent molecules and other dye molecules. Although excess solvents can be driven off with heat or partial vacuum, it appears that the water vapour is taken on until an equilibrium level has been attained by the gel glass. Hydrogen bonded solvents in contact with the pore surface can only be removed by higher temperatures (100°C) which cannot be used due to destruction of the dye molecules.

4. LASER CAVITY CONFIGURATION

Two cavity configuration have been designed employing transverse and longitudinal pumping techniques. The former enables high concentions of dye molecules to be doped within the gel glass whilst the latter requires a lower concentration.

The transverse arrangement users a cylindrical silica lens (f = 70mm) to focus 249nm, 5ns KrF excimer laser pulses to a thin strip of width 1mm

and length 27mm. Excimer lasers can produce short, very intense laser pulses useful for investigation of threshold levels for laser action in gel glass. If this strip is formed along a 25mm diameter of a gel glass disc then an excited region extending the full width of the disc can be created, with hopefully enough intensity to produce sufficient gain to overcome losses within the disc and produce laser emission. Such high concentrations, 10^{-4} - 10^{-3}M and high pump power densities, 10^{8}W/cm^{3}, can produce amplified spontaneous emission (ASE) without mirrors, ie amplified single pass emission, however multi-pass lasing requires the addition of two mirrors, a high reflector and an output coupler of 80% reflectance. Unfortunately, 249nm photons (5eV) can photodissociate the dye molecules and therefore only a few shots are possible before the dye ceases to perform. This problem can be overcome by rotating the disc to expose a fresh surface every few shots.

A further problem is the poor optical quality of the gel glass surface as polishing seems to be unsuccessful. This can be overcome by sandwiching the gel disc between two optical flats using index matching fluid. A frequency doubled Nd:YAG laser pulse injected at a shallow angle could then produce a gain region between the two flat surfaces.

Table 1 lists the spectroscopic and kinetic parameters used in the evaluation of threshold pump energy densities required for lasing action.

5. RESULTS

The spectrum of the side fluorescence for R6G in methanol when pumped by a KrF laser and pulsed extends from about 570nm to about 610nm with peak emission, in this case exhibiting slight ASE at 575nm.

THRESHOLD CONDITIONS

Population inversion density required for lasing threshold.

$$N_t = \frac{8\pi n^3 \tau \Delta\nu}{c t_c \lambda^2}$$

n = refractive index,

τ = spontaneous lifetime of upper laser level,

$\Delta\nu$ = transition linewidth,

t_c = cavity loss lifetime.

COMPARISON OF PARAMETERS FOR R6G IN MeOH AND GLASS HOSTS

	MeOH	gel glass
n	1.33	1.45
t_c	——— similar ———	
τ (ns)	~5	20
$\Delta\nu$ (nm)	~5	~1

Power density for R6G in methanol ~5.10^7 W/cm^3 for 5.10^{-4} M.

PULSE ENERGIES REQUIRED FOR THRESHOLD LASING

	Nd-YAG (532 nm)	EXCIMER (248 nm)
Pulsewidth (ns)	5	10
Geometry	longitudinal	transverse
Pump volume (cm^3)	0.01	0.04 - 0.1
Energy (mJ)	5	15-50

Table 1

This shows a similar spectrum for gel glass doped by the adsorption process with R6G. The fluorescence band is now shifted to a shorter wavelength, 530nm to 610nm, with peak emission at 560nm. This appears at odds with the results given by Avnir et al[1] who detected a shift to the red of about 5nm. This opposite shift can be explained if the average dye concentration is taken into account. The dye existed at 10^{-4}M in methanol, however because the fractional pore volume of the 700°C gel glass disc used was only 25% then even for a complete take-up of dye solution by the disc there would be a reduction in the average concentration for the disc bulk of one quarter. A reduction in dye concentration of this amount could certainly lead to a blue shift of at least 10nm and maybe more if total pore fill was not achieved. It must be remembered, however, that although the bulk dye concentration has dropped by at least one quarter, the cluster concentration within the pores should at least remain constant or even increase depending upon how much solvent in driven off at the drying stage. Further tests are required to determine whether emission shifts depend on the average bulk dye concentration, pore dye concentration or the existence of a solid lattice in close proximity to the dye molecules.

Showing the spectral emission and linewidth for a lasing sample of gel glass, alignment was achieved by superposition of internal He-Ne tracks within the sample. As can be seen, the laser emission has a linewidth of 3 to 4nm centred on the peak fluorescence emission at about 560nm.

For the pulse profiles of the KrF pump laser, R6G dye fluorescence, R6G + methanol and R6G + glass lasers, the multi-peak output profile of the two laser media arise from the oscillatory nature of the KrF pump laser, and the 15ns fluorescence lifetime of R6G. As can be seen the

R6G fluorescence lifetime in gel glass is about 10-15ns, which is about twice as long as in methanol. However, the stimulated lifetime for R6G in gel glass is less than 1ns (limit of detector) and as in the case of R6G in methanol the laser emission intensity closely follows that of the KrF pump laser.

6. CONCLUSION

We report the observation of lasing action for R6G in gel glass doped using the adsorption process. Laser linewidths and lifetimes are apparently similar to that of R6G in methanol although the lifetimes for R6G in both hosts would be much shorter than that measurable by our apparatus. Although the excimer laser was a good investigatory tool to study possible laser action and prototyping possible cavity configuration, the high energy ultra-violet photons are not conducive to a long-life, multi-shot capability and so future work will involve pump lasers with less energetic photons-double Nd:YAG (532nm) and Coumarin 504 dye laser (507nm). Recent work with a C504 pulsed dye laser (507nm, 4μs, 600mJ) shows great promise with no photodegredation of the dye-doped glass even after 100 high energy shots.

If lasing can be achieved using flashlamp pumped dye lasers then the possibility arises of using small cavities that currently house solid state rods, employing flashlamps and samarian down-conversion filters, to produce a low cost, compact laser along the lines of more conventional solid state lasers. This would require a different gel glass geometry either in slab form (20 - 30mm x 10mm x 2mm) or rod (30mm x 4mm diameter).

Current work is also studying longitudinal pumping as a means of producing a higher quality output beam using an optical flat sandwich, this

quality is currently denied the gel glass due to the lack of success in polishing it.

It was noted that in the glass, the bleaching process, brought about by intense pumping by high energy KrF photons, transformed R6G into colourless products[5]. Therefore, as one layer is bleached new deeper layers of undissociated R6G molecules are constantly exposed, and the pump energy of KrF laser is not blocked by the transparent photodecomposition products trapped in the pores of the dissociated/degraded layers.

An increase in the fluorescence lifetime of the upper laser level in the dye molecules has been confirmed. This increase is due to the presence of bonding between dye molecules and the glass matrix thus making the transition to lower states less allowed. This being the case, population inversion is easier to attain and threshold for gain is reduced.

Further studies have shown that solvents, eg methanol, still exist within the pores after drying, albeit to a lower degree than during immersion, and so dye molecules must exist in concentrated solutions as well as adsorbed onto pore wall surfaces both adjacent and remote to solvent molecules.

Future work will be involved in varying dye types (R6G, Kiton Red, Sulforhodamine 640, ...), dye concentrations, gel glasses within group II (500-1100°C), and solvents, the last to improve the robustness of the glass during drying or optical working. Different geometries need to be tried such as slabs and rods for ease of laser cavity fabrication and coupling of input energy.

Some form of hermetic sealing may have to be introduced to the glass as dried samples gain weight by taking on water from the atmosphere.

REFERENCES

1. D Avnir, D Levy and R Reisfeld, J Phys 88, 5956, 1984
2. D Avnir, U R Kaufman and R Reisfeld, J Non-Cryst Solids 74, 395, 1985
3. F Salin, G le Saux, P Georges, A Brun, C Bagnall and J Zorzyncki, Optics Lett 14, 785, 1989
4. Y Dulneva and S Koziov, Leningrad Inst of Fine Mechanics and Optics, USSR
5. I P Kaminov, L W Stulz, E A Chandross and C A Pryde, Appl Optics 7, 1563, 1972

APPENDIX 13

Inst. Phys. Conf. Ser. No 103: Part 1
Paper presented at Int. Conf. Materials for Non-linear and Electro-optics, Cambridge, 1989

Laser densification of sol-gel silica glass

D J Shaw, A J Berry and T A King

Physics Department, Schuster Laboratory. University of Manchester, Manchester M13 9PL.

ABSTRACT: Development of densification techniques for sol-gel matrices using laser radiation is presented. A carbon dioxide laser has been shown to be effective in producing full densification of thin surface layers of silica sol-gel. Microhardness as a characterisation method of the lower energy densification threshold and the upper (bloating) threshold and refractive index as a monitor of densification have been developed. Energies to effect full densification were measured as 6.3 ± 0.3 and 4.3 ± 0.2Jcm^{-2} of surface irradiated.

1. INTRODUCTION

The generally accepted structure for partially dense gel-silica is a microporous solid based on an SiO_2 skeleton (Klein 1988). Most of the pores are open and are, on average, 1.2nm diameter. Water molecules are hydrogen bonded to oxygen atoms on the pore surface as well as OH^- ions. Gallo et al (1984, 1987) describe the physical and chemical processes occurring during densification as

1. Physical desorption of hydrogen bonded water below 200°C
2. Decomposition of residual organic compounds over 300°C - 500°C
3. Pore collapse over 500°C - 1150°C.

OH^- ions are steadily eliminated by condensation polymerisation as below:

$$Si - OH + HO - Si \longrightarrow Si - O - Si + H_2O$$

This process increases the surface energy of the pores. OH^- ions are largely eliminated at temperatures >1100°C. The mechanism of pore collapse, known as viscous sintering, occurs because the gel-silica tends to a minimum energy state. In this instance a minimum energy state corresponds to minimum surface energy, hence the pores will tend to collapse. We find that a viscous relaxation of the pores takes place which is activated by heating the gel-silica.By about 1150°C densification is complete, giving a gel silica with a density equal to that of conventional vitreous silica, ie $2.21 gcm^{-3}$. The energy required to effect full densification may be estimated by determining the energy required to raise the temperature of a surface layer of gel silica to 1150°C. This energy H is

$$H = mc\Delta\theta \qquad (1)$$

where m is the mass of the surface layer, c is the specific heat, and $\Delta\theta$ is the temperature change.

It is convenient to work with the energy required per square centimetre of surface irradiated. Since the laser radiation is significantly absorbed by silica and is not absorbed in the pores we are justified to use the density of bulk silica, ie $2.21 gcm^{-3}$, in calculating the mass. Taking the $1/e^2$ penetration depth of 10.6μm radiation in gel-silica as 40μm every cm^2 of surface irradiated is equivalent to irradiating a volume of $1 \times 0.004 = 4 \times 10^{-3} cm^3$. Hence every cm^2 irradiated is equivalent to irradiating a mass $m = 2.21 \times 4 \times 10^{-3} = 8.84 \times 10^{-3} g$. For $\Delta\theta = 1150 - 20 = 1130$°C and c = 0.753 J/g°C the energy required is $7.4 Jcm^{-2}$.

This research investigates the feasibility of laser induced densification, the energies required and the properties of laser densified gel-silica. Techniques are being developed for the laser writing of refractive index profiles, in particular waveguides and densification of large surface areas.

2. EXPERIMENTAL PROCEDURE

Sol-gel prepared polymeric silica (Hench et al 1988) in the form of 1 inch diameter discs was supplied by GELTECH Inc. The samples had been pre-densified to 800°C by conventional thermal methods. This means that the samples provided have a density of $1.35 gcm^{-3}$ (with ~ 28% of the volume being pores), a microhardness of 190kg mm^{-2} and a refractive index of 1.42. Fully dense silica glass has a density of $2.21 gcm^{-3}$ a microhardness of 680kg mm^{-2} and a refractive index of 1.46. The laser written tracks were produced by mounting the gel-silica disc on a pendulum bob which is swung through the focused carbon dioxide laser beam once and then stopped. As the pendulum swings through the laser beam it interupts a second helium-neon laser beam incident normally on a photodiode which is connected to an oscilloscope, thus

the speed of the pendulum, and hence the incident energy can be calculated. The carbon-dioxide laser (Ferranti, model CM2000) produced up to 17 watts with a focused beam radius of up to 380μm. In general a densified/damaged track is written across the disc. Densified material was characterised by measuring the Vicker's microhardness with a Riechart 2683 model microhardness apparatus. Loads of 24g and in some cases 32g and 40g for harder material were used. None of these load values were found to be such as to exceed the stress factor when applied to appropriate regions. Refractive index methods based on a reflectivity technique to characterise laser written tracks are being developed.

3. RESULTS

Figure 1 shows some photographs of laser treated tracks taken with an Olympus AH2 photomicroscope. Figure 1a is a laser treated line with an energy of $2.34 Jcm^{-2}$, ie below threshold, here the beam has just 'cleaned up' the surface. Figures 1b and 1c show lines exposed to 6.67 and $5.98 Jcm^{-2}$. Both these photographs were taken under dark field photography; this method illuminates scattering centres brightly while smooth areas appear dark. Figure 1d shows a track produced by an energy density of $11.53 Jcm^{-2}$; the energy here is above the damage threshold, the gel-silica has been exposed to an energy above the damage level and bubbles of released gases have formed. The gel is said to bloat. Bloating occurs when gases and/or water vapour released during the densification process cannot escape because the pores have already collapsed. Thus in Figure 1b we see a bright bloated line whilst Figure 1c is mainly dark indicating a smooth and densified track. Thus we can deduce that the bloating, or upper densification threshold, is between 6.67 and $5.98 Jcm^{-2}$ giving a mean upper densification threshold of $6.32 \pm 0.34 Jcm^{-2}$. Figure 1e is a photograph of a densified track under interference photography.

Figures 2a and 2b are microhardness profiles of various laser treated tracks with different incident energies. The microhardness profiles are gaussian because the transverse profile of the CO_2 laser beam is gaussian. Fully dense silica has a microhardness of $680 kg\ mm^{-2}$. The three curves in figure 2a have peaks within errors of this value whereas the two curves of figure 2b are not within this value. We deduce that the lower densification threshold is between 4.45 and $4.06 Jcm^{-2}$, with a mean value for the lower densification threshold of $4.26 \pm 0.20 Jcm^{-2}$.

4. DISCUSSION AND CONCLUSIONS

The upper and lower densification thresholds have been measured as $6.32 \pm 0.34 Jcm^{-2}$ and $4.26 \pm 0.20\ Jcm^{-2}$ respectively. These energies using equation 1 correspond to raising the exposed gel-silica to temperatures of 950°C and 640°C. The values $6.32 Jcm^{-2}$ and $4.26 Jcm^{-2}$ are average beam intensities; since the laser beam has a gaussian profile the peak intensity is approximately twice (or exactly 2.066 x) the measured average intensity, thus the peak intensity thresholds are $13.06 Jcm^{-2}$ and $8.80 Jcm^{-2}$, which correspond to raising the temperature of the gel-silica to 1962°C and 1322°C. This lower threshold temperature is in reasonable agreement with the minimum temperature for densification of 1150°C. The lower energy threshold has been calculated as $7.42 Jcm^{-2}$ as an average value; the peak intensity for the measured lower densification is $8.80 Jcm^{-2}$, again this in good agreement with the calculated value.

Figure 1: Densified/Damaged Tracks

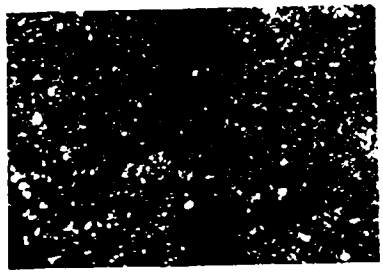

Figure 1a 200μm

Energy = 2.34Jcm^{-2}

1b 200μm

Energy = 6.67Jcm^{-2}

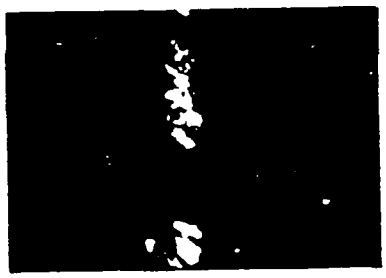

1c 200μm

Energy = 5.98Jcm^{-2}

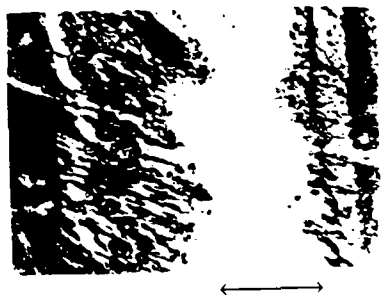

1d 200μm

Energy = 11.53Jcm^{-2}

1e 200μm

Energy = 4.72Jcm^{-2}

Figure 2: Microhardness profiles of laser written tracks with different incident energies

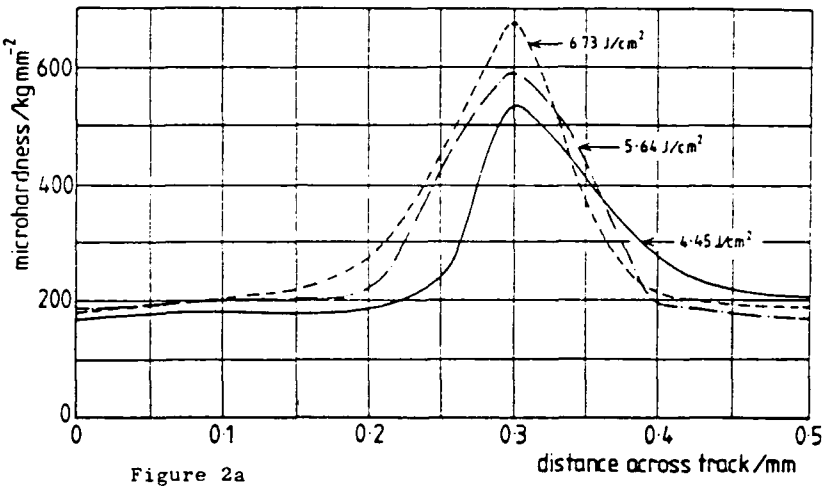

Figure 2a

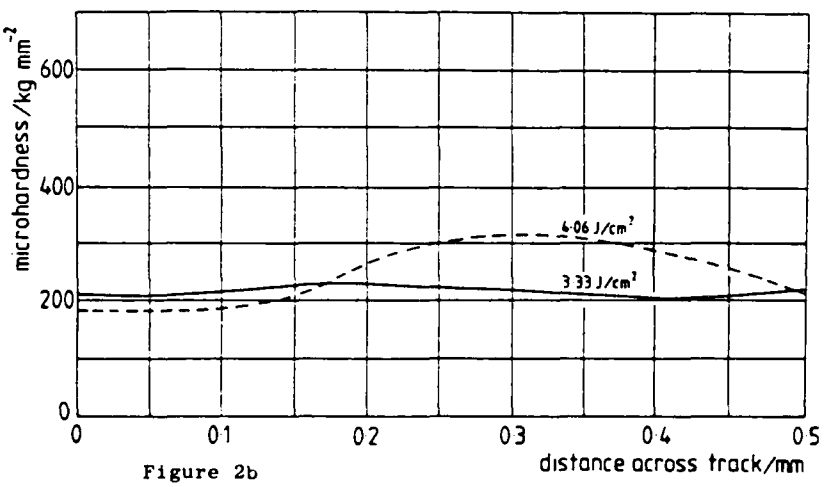

Figure 2b

REFERENCES

1. Gallo T A, Brinker C J, Klein L C, Scherer G W, 1984 "The Role of Water in Densification of Gels", "Better Ceramics Through Chemistry" Ed, C J Brinker, D E Clark and D R Ulrich, Amsterdam (North-Holland), pp85-90

2. Gallo T A, 1987 "Densification of Gel-Derived Silica", PhD Thesis, Rutgers State University of New Jersey, pp4-5

3. Hench L L, Wang S H and Nogues J L, 1988 Proc SPIE 878

4. Klein L C (Ed), 1988 "Sol-Gel Technology for Thin Fibres, Preforms, Electronics and Speciality Shapes", New Jersey (Noyes Publications)

ACKNOWLEDGEMENTS

This study forms part of a wider programme of research in collaboration with the Advanced Materials Research Center, University of Florida and GELTECH Inc. We have enjoyed extensive discussions with Professor Larry Hench of the ARMC and we thank Mr Bill Moreshead of GELTECH Inc for discussion and provision of samples. This research has been sponsored by the Air Force Office of Scientific Research (AFSC) under contract F49620-88-C-0010. The United States Government is authorized to reproduce and distribute reprints for governmental purposes notwithstanding any copyright notation hereon.

APPENDIX 14

LASER DENSIFICATION MODELLING

TAIPAU CHIA*, L. L. HENCH*, CHAOBIN QIN** AND C. K. HSIEH**
*Advanced Materials Research Center, University of Florida, One Progress Blvd., #14, Alachua, FL 32615.
**Department of Mechanical Engineering, University of Florida, Gainesville, FL 32611.

ABSTRACT

A three-dimensional transient model for heat conduction in a silica glass is developed. The model simulates the three-dimensional temperature distribution in the silica glass irradiated by a moving CO_2 laser. Both the reflectivity of the glass surface and the strong attenuation of the laser energy in the glass medium are accounted for by a detailed radiation analysis. The energy absorbed by the glass is found to be confined in a 10 μm thickness; the laser irradiation is thus treated as a boundary condition. The heat diffusion equation is solved by an alternating-direction-implicit method. Parameters tested in the study encompass the laser power and moving speed, the heat transfer coefficient and the thermal diffusivity of the glass medium.

This study provides the analytical basis for the thermal effect of laser densification on a gel-derived silica glass. The properties of the gel glass are known to be strongly related to its processing temperature and the resulting ultrastructure. The results presented in this paper permit a prediction of the change of the glass properties with temperature.

INTRODUCTION

Many models have been developed for predicting the temperature distribution inside materials treated with laser heating [1-3]. Phase transformations are involved during laser heating. In this paper the temperature rise by applying a moving CO_2 laser on a porous gel silica glass monolith is analyzed. Previous papers report the processing and properties of the alkoxide derived gel silica investigated in this paper [4-6].

The laser energy is assumed to be absorbed and totally transformed into heat. As the absorption coefficient [7] of the glass is very large, the laser energy is absorbed primarily within a very thin layer at the irradiated side of the glass surface. The Gaussian distribution of the laser energy can be integrated within the absorption layer, and the absorbed energy can be treated as a boundary condition in the analysis.

The model developed in this paper simulates the three dimensional heat transfer in the silica glass irradiated by a moving CO_2 laser. Relative temperature distributions at various laser power settings and travelling velocities are evaluated numerically. Parametric studies for the effects of the heat transfer coefficient on the glass surface and the thermophysical properties of the glass medium are also investigated. It is well known that the properties of the gel silica glass is strongly related to its processing temperature. The results presented in this paper can thus be used to determine the processing parameters vital to the changes of the density and refractive-index gradients in glass treated with laser heating. Furthermore, with the knowledge of the mechanisms of the glass densification, the temperature distribution in glass is also useful in predicting the ultrastructural changes within the gel network. These structural changes play an important role in changing the overall glass properties.

FORMULATION OF THE PHYSICAL MODEL

The physical system under investigation is shown in Figure 1. A focused CO_2 laser beam is travelling in the x direction. The thickness of the glass slab is in the z direction, and because of the motion of the beam, the temperature distribution in glass is symmetrical with respect to the x-z plane; only one half of the medium is thus needed for analysis.

The thermal conductivity of the glass is small; the heat affected zone is highly localized and represented by the dashed line in the figure. The irradiated energy is transformed into heat and diffused into the glass medium by conduction, while the surface of the glass dissipates heat by convection and radiation to the surroundings. Radiation is lumped into convection by defining a overall heat transfer coefficient following a linearization process [8].

The thermal effect of the laser irradiation can be evaluated by a detailed radiation analysis. Accounting for both the reflectivity of the glass surface and the absorption of the glass medium, the heat generated by the laser beam can be evaluated as

$$Q = \int_0^w I_o(1-R) \exp(2r^2/w^2) [1-\exp(-\alpha\Delta z)] 2\pi r dr \qquad (1)$$

Here all notations have been defined in Table I. For the CO_2 laser (10.6 μm) used in this work, the laser generated heat is confined to a glass thickness of 10 μm, at which depth the laser energy is attenuated to 0.15% of its surface value. This depth is small enough to permit the laser heating to be treated as a boundary condition. As for the condition on the other side, an adiabatic condition is imposed there because of the small thermal conductivity of glass. The problem can then be formulated mathematically as follows:

Governing Equation:

$$\rho c \partial T/\partial t = \nabla \cdot (k\nabla T),\ T(x,y,z,t)\ \begin{matrix} 0<x<a \\ -b<y<b \\ 0<z<d \end{matrix},\ t>0 \qquad (2)$$

Initial Condition:

$$T(x,y,z,0) = T_\infty \qquad (3)$$

Boundary Conditions:

$$k\partial T(0,y,z,t)/\partial x = h[T(0,y,z,t)-T_\infty] \qquad (4)$$

$$T(a,y,z,t) = T_\infty \qquad (5)$$

$$T(x,\pm b,z,t) = T_\infty \qquad (6)$$

$$q(Vt,y,0,t)+k[\partial T(Vt,y,0,t)/\partial z]-h[T(Vt,y,0,t)-T_\infty] = 0 \qquad (7)$$

$$\partial T(x,y,d,t)/\partial z = 0 \qquad (8)$$

The problem as given can only be solved exactly for a special case in which the laser beam has travelled a long distance to the extent a quasi-steady state is reached. At that time the glass temperature is invariant with time in a coordinate system that is travelling along with the beam. For the general case of small time or sample size in a fixed coordinate system, the temperature is time dependent, and the problem must be solved numerically.

For the present work, a finite-difference, alternating-direction-implicit (ADI) method is used to solve the problem. The intense heat from the laser beam requires the use of a very thin surface layer together with small time

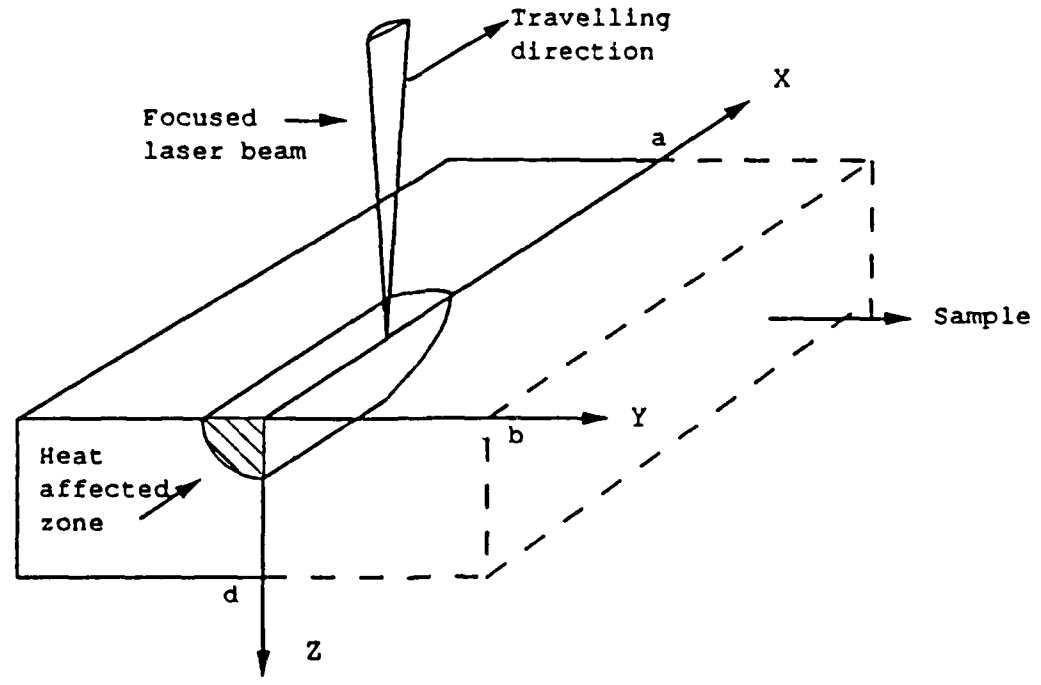

Figure 1 . Physical system under investigation

Table I. Calculational Variables and Values

	Nomenclature	Values
a	Sample length	0.4 cm
b	Sample width	0.2 cm
c	Specific heat [9]	10.5 J/g°C
d	Sample thickness	0.3 cm
D	Heat diffusivity	6.5×10^{-4} $(-k/\rho c) \cdot cm^2/sec$
h	Heat transfer coefficient	7.1×10^{-3} $w/cm^2 °C$
I_o	Laser intensity	3.3×10^4 w/cm^2
k	Thermal conductivity [10]	1.5×10^{-2} w/cm°C
q	Heat flux	
Q	Absorbed laser power density	10^7 $(-q/\Delta z)$ w/cm^3
Q	Absorbed laser power	
R	Reflectivity	0.17
t	Time	
Δt	Time step	
T	Temperature	
T_∞	Room temperature	24°C
V	Travelling velocity	0.04 cm/sec
W	Half width of laser beam	0.01 cm
ΔZ	Depth	
α	Absorption coefficient	6.5×10^{-1} μm^{-1}
ρ	Density	2.2 g/cm^3

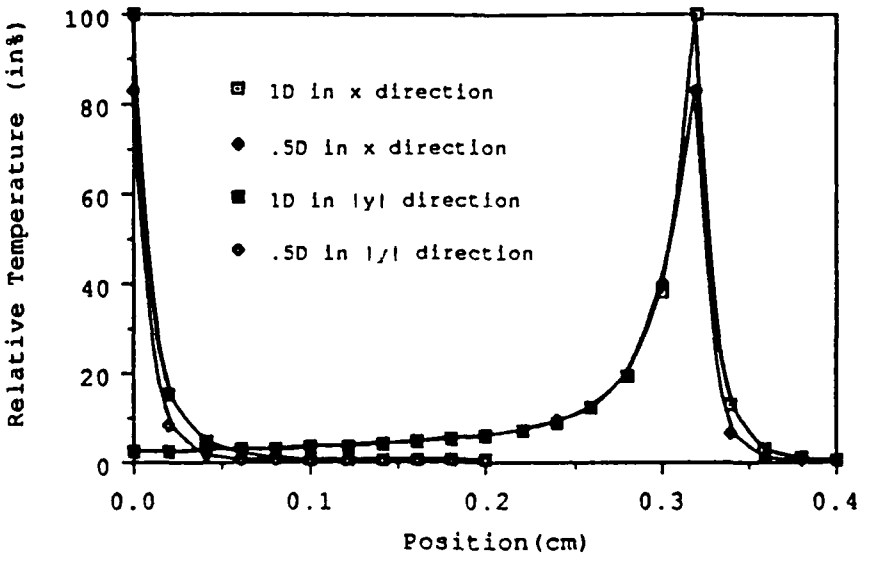

Figure 2. Relative temperature profiles with different heat diffusivity

step in order to assure a convergent solution. The criteria for stable solution is that $D\Delta t/(\Delta z)^2<0.5$, which governs the selection of time steps and spatial increments in the numerical solution. Computation was effected by using an IBM Converted Monitor System (CMS) system available on the University of Florida Campus.

RESULTS AND DISCUSSION

Values of the parameters used in the computation are summarized in Table I. Of those listed in the table, the values of D, h, Q, and V are also changed in order to examine their effects on the temperature changes. For graphical presentation of results, composite diagrams (see Figures 2 through 5) are constructed so that the temperature profiles in both x and |y| directions can be viewed simultaneously. All temperatures are plotted for the distributions at the surface (z=0), and they are normalized by using the peak values evaluated at the beam center; in all instances those evaluated with the tabulated parameters are used for control. It is noted that in each of these plots, the laser beam has moved to x equal to 0.32 cm, and the temperature profiles in the y direction are those of T evaluated at this x position.

As shown in Figure 2, a reduction of the thermal diffusivity by one half has a small effect of lowering the peak temperatures. For the temperature distributions in the x direction, the temperature gradients at the leading sides (x>0.32 cm) are always greater than the temperature gradients at the trailing sides (x<0.32 cm), a typical phenomenon for the problem investigated. In fact, the trailing side temperatures are practically unchanged with the diffusivity changes. Physically the temperature drops at small thermal diffusivities can be attributed to the large heat capacitance, which permits more heat to be stored in the glass medium.

An increase of the heat transfer coefficient by 100% has a negligible effect in changing the surface temperatures; see Figure 3. The h value quoted in the table accounts for both free convection and radiation. It is noted that, while the peak surface temperature at the beam cneter is high, the area over which this temperature is found is small. As a result, the heat transfer coefficient has negligible effect on the surface temperatures.

It is expected that a reduction of laser power setting and an increase of the laser travelling velocity have an effect of lowering the peak temperatures found on the surfaces; see Figures 4 and 5. The major difference, however, is

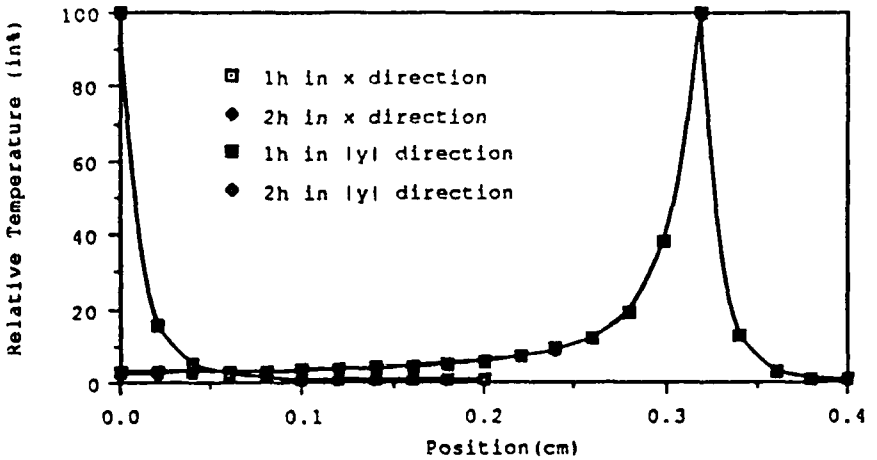

Figure 3. Relative temperature profiles with different heat transfer coefficient

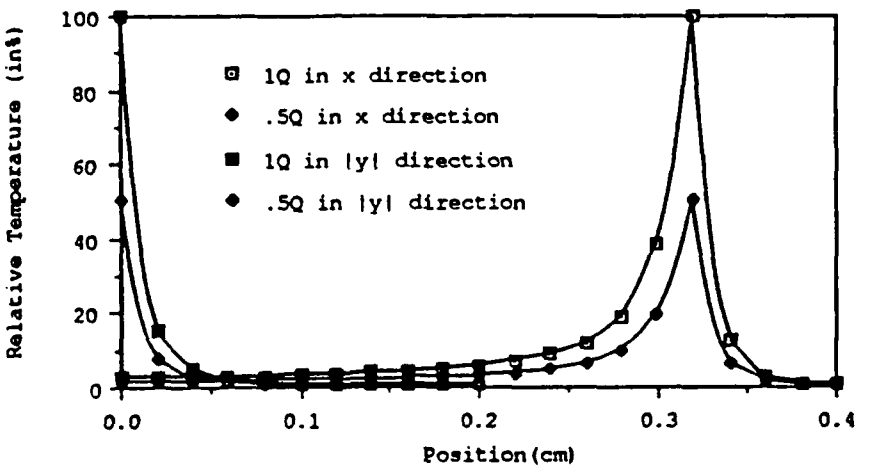

Figure 4. Relative temperature profiles under different power settings

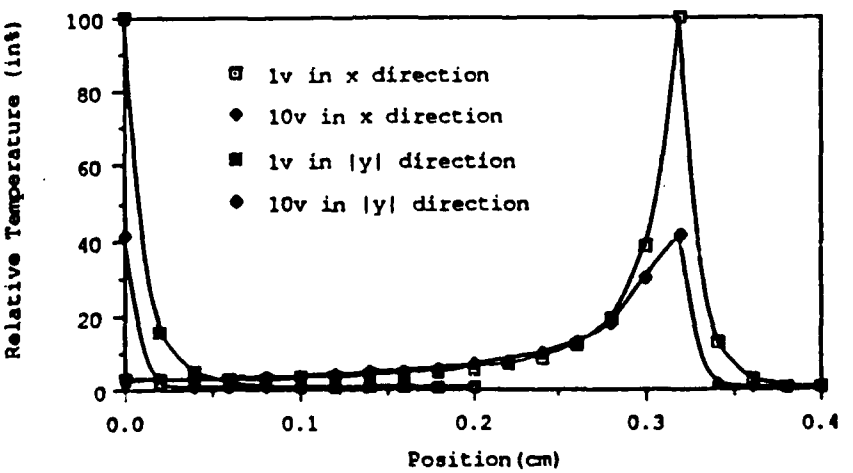

Figure 5. Relative temperature profiles with different travelling velocity

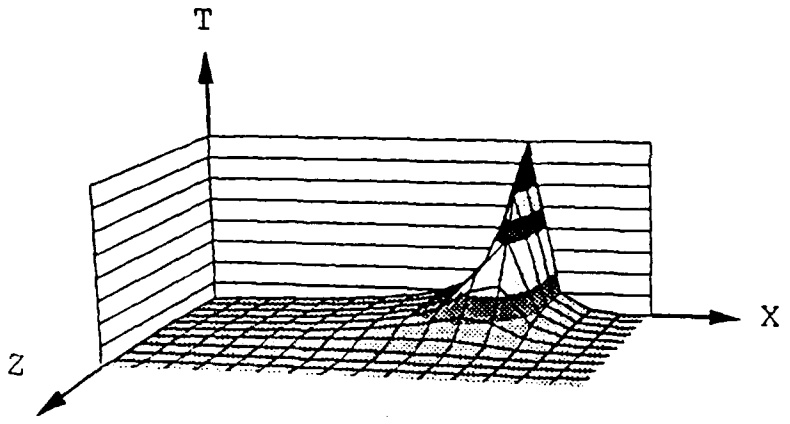

Figure 6. Three-dimensional temperature distribution on X-Z plane

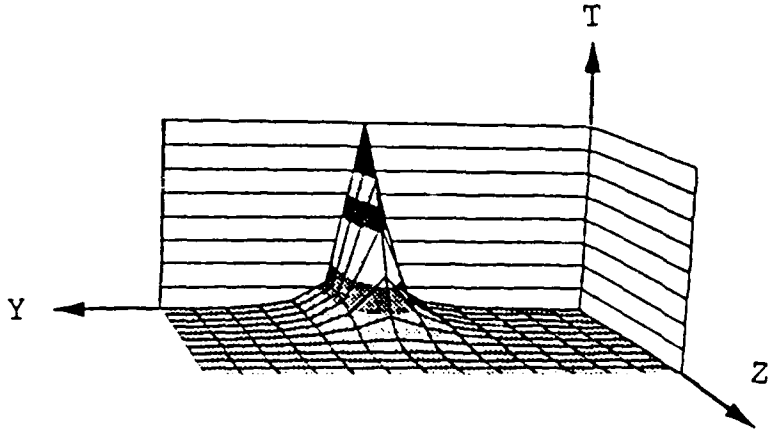

Figure 7. Three-dimension temperature distribution on Y-Z plane

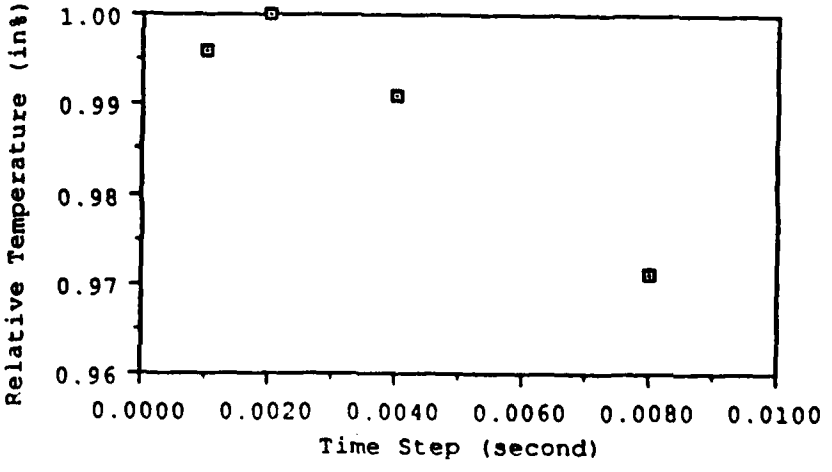

Figure 8. Convergence of the Solution

in the trailing sides. A reduction of the power setting is shown to have a dominant effect in lowering the trailing side temperatures.

To show the temperature attenuation in the z direction, three dimensional plots are provided as shown in Figures 6 and 7. In these figures, the values of the parameters are taken to be those listed in Table I. Those peak temperatures at z=0 correspond to peak curves presented earlier in the composite plots in Figures 2 through 5.

To complete this study, a numerical experiment is performed to test the convergence of the numerical solution. The time steps are successively reduced by half and the peak temperatures are compared for convergence. As shown in Figure 8, the temperatures have converged to within 0.4% for time steps changing from 0.002 to 0.001 second. The results presented in this paper were obtained by using a time step of 0.002 second, a compromise between accuracy and economy.

ACKNOWLEDGEMENTS

The authors are grateful for the financial support of the Air Force Office of Scientific Research under contract #F49620-88-C-0073, and the encouragement of Dr. Donald R. Ulrich.

REFERENCES

1. M. Rappaz, B. Carrupt, M. Zimmermann and W. Kurz, Helvetica Physica Acta 60, 924-936 (1987).

2. C. Y. Chang, Y. K. Fang, B. S. Wu, and R. M. Chen, Mat. Res. Soc. Symp. Proc. 23, 497 (1984).

3. I. D. Calder and R. Sue, J. Appl. Phys. 53 (11), 7545 (1982).

4. L. L. Hench, S. H. Wang, and J. L. Nogues, SPIE 878, 76 (1988).

5. L. L. Hench, in Science of Ceramic Chemical Processing, edited by L. L. Hench and D. R. Ulrich (Wiley-Interscience, 1986), pp. 52-64.

6. S. C. Park and L. L. Hench, in Science of Ceramic Chemical Processing, edited by L. L. Hench and D. R. Ulrich (Wiley-Interscience, 1986), pp. 168-172.

7. C. K. Hsieh and K. C. Su, The Journal of Solar Energy Science and Technology 22, 37 (1979).

8. J. H. Batteh, J. Appl. Phys. 53 (11), 7537 (1982).

9. Y. S. Touloukian and C. H. Buyco, in Thermophysical Properties of Matter, The TPRC Data Series, Vol. 2, 1970, p. 202.

10. Y. S. Touloukian, R. W. Powell, C. Y. Ho, and P. G. Klemens, in Thermophysical Properties of Matter, The TPRC Data Series, Vol. 2, 1970, p. 922.

APPENDIX 15

MULTIFUNCTIONAL SILICA OPTICS

L. L. HENCH AND A. FOSMOE
Advanced Materials Research Center, University of Florida, One Progress Blvd., #14, Alachua, FL 32615

ABSTRACT

The sol-gel chemical processing method of producing fully dense silica optics provides an intermediate product termed Type VI silica ideally suited for use in engineering multifunctional silica optics. This paper reviews the sol-gel process, the Type V dense gel-silica produced by this process and the Type VI ultraporous gel-silica intermediate product. Included is a comparison of two different porous ultrastructures with 1.2 nm and 8.0 nm average pore radii. Two uses of the porous gel-silica components as multifunctional optics are described. The first is for use in transpiration cooled windows in high-speed rocket guidance systems. Flow rates of He and N_2 through the 1.2 nm and 8.0 nm ultrastructures are as high as 0.9 m/min at 0.75 MPa. High temperature UV transmission in contact with an impinging oxy-acetylene flame is demonstrated. Use of Type VI gel-silica as a host matrix for fast radiation-hard scintillating detectors is also reviewed.

INTRODUCTION

Precision optics have been made by basically the same process since the time of Galileo; i.e., silica sand has been melted with various fluxes, homogenized at very high temperatures above the liquidus and cast into glass ingots. Sections of the ingots with minimum bubbles, seeds, striae or other defects have been selected by hand for grinding by skilled opticians into the shape of lenses, prisms, windows, or mirrors, followed by successive polishing steps, again performed by highly trained optical technicians. The quality of each optical component is therefore dependent on the summation of the quality of each step of processing, which in turn is a function of the skill, training, and time devoted by technicians. The performance of an optical system is an aggregate of the quality of the individual components and therefore is highly dependent on the availability and skill of technical manpower.

Until recently, optical components have for the most part also served only a single function in an optical system; i.e., lenses refract, mirrors reflect, windows transmit, filters absorb and lasers amplify. As optical systems requirements become ever more demanding there is a great incentive for components to serve more than one function. This need is very difficult to satisfy with traditional methods of making precision optics. The fundamental characteristics of glass as an isotropic, homogeneous solid generally restrict its use to a single optical function.

Sol-gel chemical processing of silica provides a new approach to each of the historical restrictions of silica optical components summarized above; i.e., 1) elimination of hand operations in manufacturing by net shape casting, and 2) development of multifunctional optics by producing ultraporous silica matrices that are optically transparent.

SOL-GEL PROCESSING

Recent publications have presented in detail the important features of sol-gel technology [1-3]. The use of sol-gel processing for producing monolithic silica optical components has also been previously described [1,2]. In summary, there are three approaches to making sol-gel monoliths:

Method 1 -	Gelation of colloidal powders.
Method 2 -	Hydrolysis and polycondensation of alkoxide precursors, followed by hypercritical drying to form aerogels.
Method 3 -	Hydrolysis and polycondensation of alkoxide precursors followed by aging and drying under ambient atmospheres to form xerogels.

Method 1 has been used by Shoup to make silica for reflective optics. Method 2 has been used by Kistler [4], Fricke [5], Zarzycki [6], and others to make aerogels, which can be used as very low density optical components with an index of refraction close to 1.00 [7], or densified to form silica glass [8].

In order to make net shape multifunctional optics we use Method 3 with an emphasis on controlling at a molecular level each of the seven steps of processing listed in Figure 1.

In our process the alkoxide is tetramethylorthosilicate (TMOS) and the catalyst is either nitric acid or hydrofluoric acid, depending upon the average pore size desired after drying. Full density net shape precision optics termed Type V gel-silica, require all seven steps listed in Figure 1. Partially dense, controlled porosity Type VI gel-silica optics require the first six steps listed in Figure 1.

TYPE V, DENSE GEL-SILICA

The average pore size of the dried monoliths used in making Type V dense gel-silica is very small, in the range of 1.2 nm, with a very narrow size distribution, see Figure 2. Densification occurs at a low temperature, 1150°C, in a dry atmosphere due to the very small pore radii and very large, >700 m^2/g, surface area. There is almost no change in pore radii as densification occurs, see Figure 3. As shown by Vasconcelos [9], nearly all the change in texture during the densification is due to a decrease in connectivity of the pore network which decreases the surface area and volume fraction of the pores per unit volume, Figure 3. At 1150°C all the pores are eliminated and the bulk density of the glass is 2.2 g/cc, equivalent to that of vitreous silica, Types I-IV, made by other processes [1].

The shape of the optical component is determined by the shape of the mold used for gelation, Step 2. Nogues et al. [10] report that it is possible to achieve as-cast tolerances for the diameter, thickness, and radius of curvature of silica lenses made by sol-gel processing which are within, or supass, tolerances achieved by precision grinding and polishing.

The optical properties of Type V gel-silica are also superior than most of the commercial grades of optical silica, as discussed previously [1,11,12]. Figure 4 compares transmission from the vacuum ultraviolet to the visible for

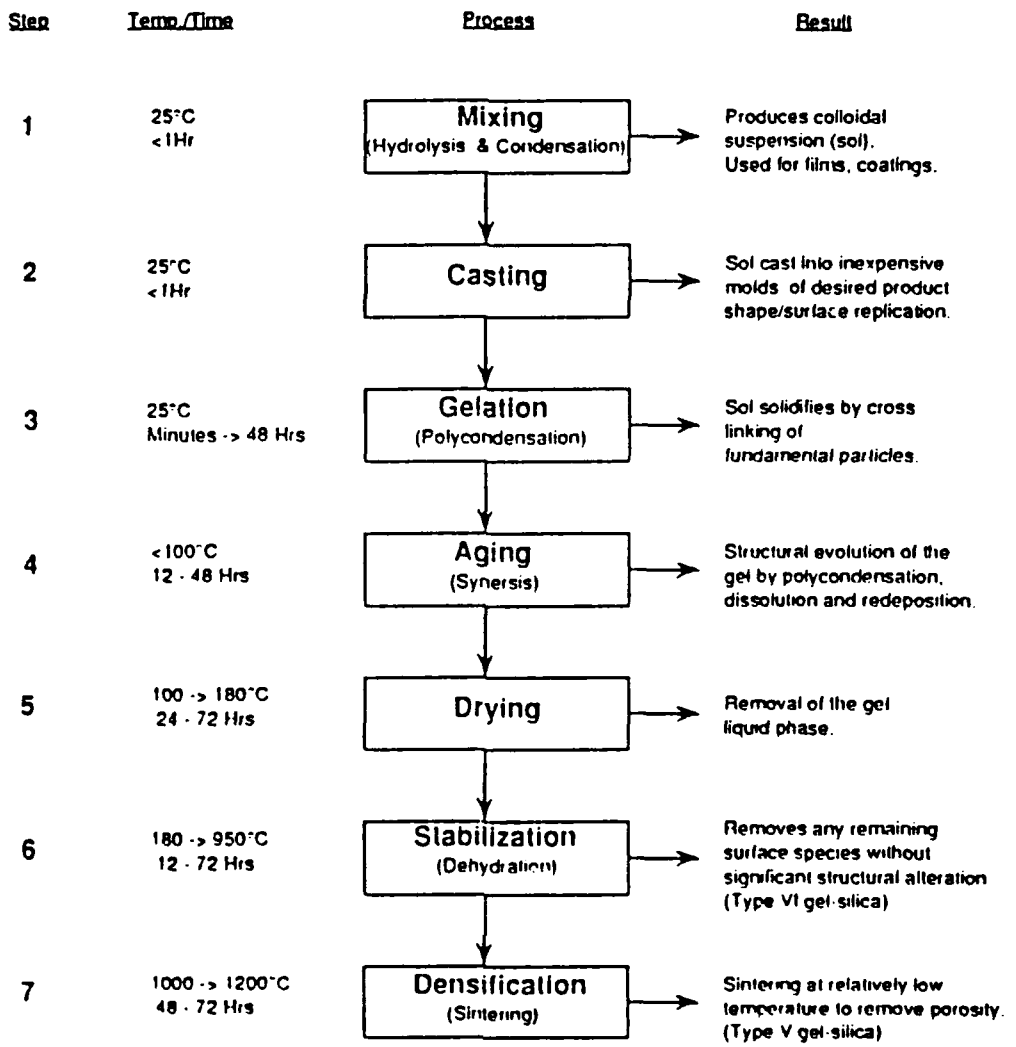

Figure 1. Sol-gel processing sequence for multifunctional optics.

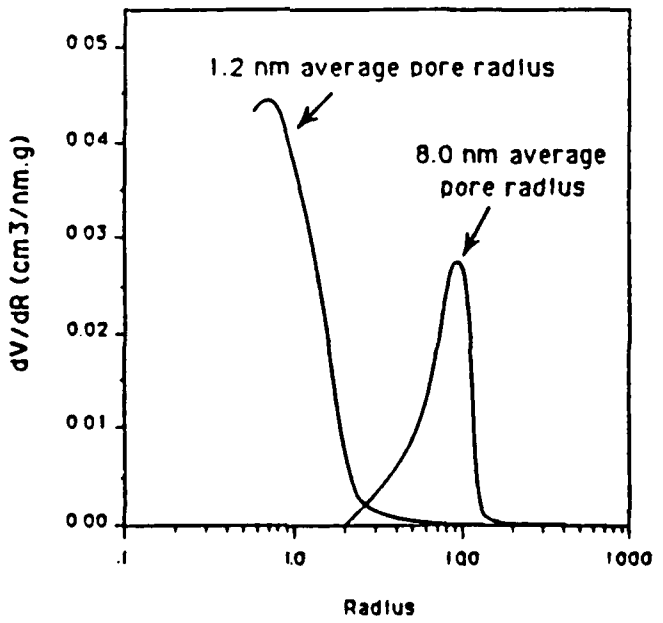

Figure 2. Pore size distribution for dried silica gel monoliths with 1.2 nm and 8.0 nm average pore radii.

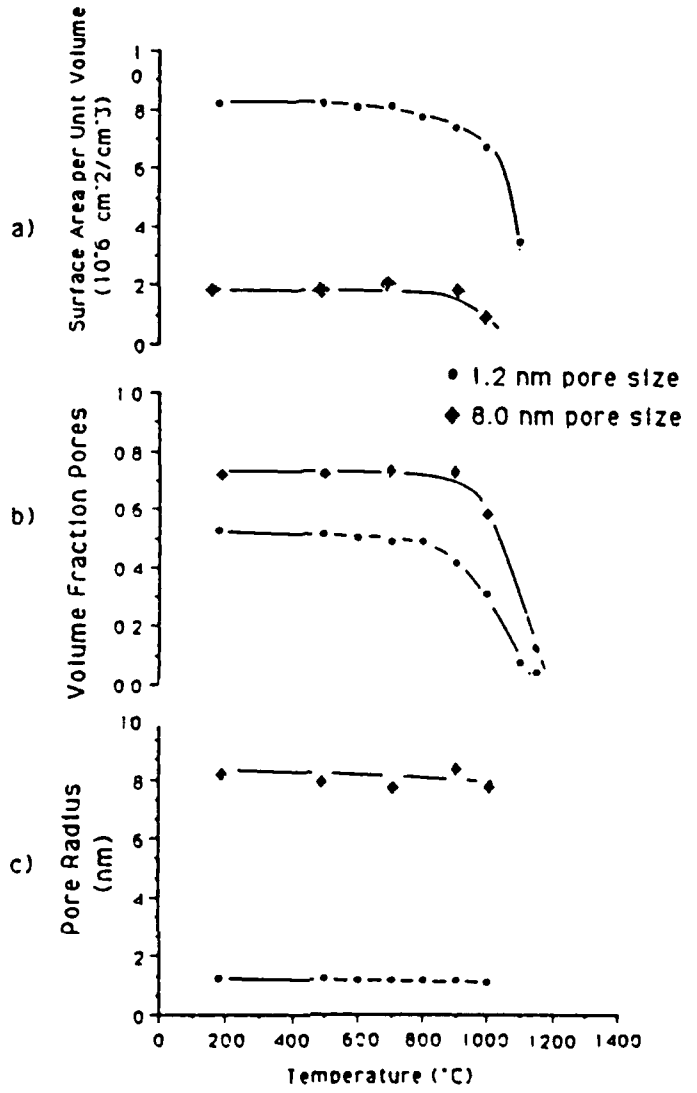

Figure 3. Variation of: a) surface area per unit volume (Sv), b) volume fraction of pores (Vv), and c) pore radius (R), all as a function of temperature.

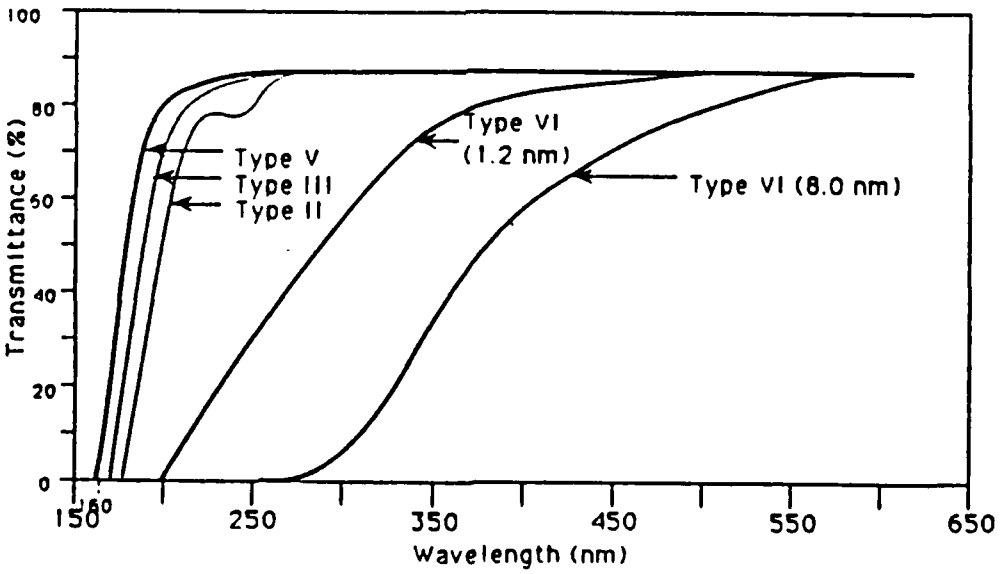

Figure 4. UV cut-offs of Types I, II, III, V, and VI silica.

Type V gel-silica with typical curves for Types II and III optical silicas. Type V gel-silica has a lower wavelength UV cut-off than even Type III silica, made by flame hydrolysis of $SiCl_4$, which is sold for UV applications. Removal of cation and hydroxyl impurities in sol-gel silica processing is responsible for the improvement in optical transmission.

Transmission in the near IR of Type V gel-silica is also excellent, as illustrated in Figure 5. There are no absorption peaks due to hydroxyl impurities, see Table I, unlike Type III optical silicas.

TYPE VI, ULTRAPOROUS GEL-SILICA

Figure 3 shows that gel-silica monoliths heated up to 800°C to 900°C still retain a large volume fraction of porosity. Vasconcelos' studies of the topological characteristics of these gels show that this porosity is completely interconnected [9]. Because of the very small size of the pores, Figure 2, the material is optically transparent, Figure 6. By heating to 800-900°C stabilization, Step 7 in Figure 1, the concentration of silanols on the surface of the pore network can be controlled, as illustrated in Figures 5 and 7 thereby making the material chemically stable when exposed to an aqueous environment.

The ultraporous, optically transparent gel-silica, termed Type VI gel-silica [1], is uniquely suited for many multifunctional optical applications, as discussed by Hench et al. [1,12] and Nogues et al. [13].

It is possible to vary the pore size and volume fraction of porosity of the Type VI gel-silica by using HF as a catalyst in Step 1, as discussed by Parsell [14], Vasconcelos [9], and Elias [15]. Figure 2 compares the pore distribution curves for monoliths with 1.2, and 8.0 nm average pore sizes. Details of textural characteristics and the thermal behavior of these, and monoliths with other pore sizes, are presented elsewhere by Vasconcelos [9] and Elias [15]. Increasing the pore size of the network is important for a number of multifunctional optical applications, as shown below. However, the larger pores do degrade the UV cut-off to some extent, from 160nm to 235nm as shown in Figure 4, probably due to Rayleigh scattering, as calculated by West and Elias [15]. The porous Type VI optics also have residual hydroxyls retained on the pore network, Figure 5, with the concentration dependent on the maximum stabilization temperature. Since the larger pore network is more thermally stable,[9,15] the larger pore optics can be heated to higher stabilization temperatures to decrease the OH content and still retain a very large volume fraction of porosity (Figure 3). This increase in volume fraction of porosity and greater thermal stability of the 8.0 nm Type VI gel-silica offers a major advantage for the multifunctional optical applications discussed below.

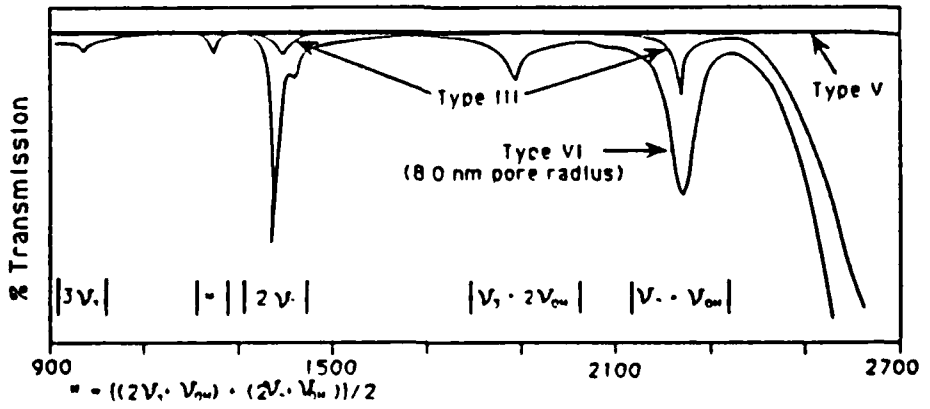

Figure 5. NIR transmission curves for Types III, V and VI silica.

Table I. Si-O-H Fundamental Vibrational Assignments

ν_{OH}	Si-O-H Out of Plane Bending
ν_1	Si-O-H (Isolated) Stretch
ν_2	Si-O-H (Adjacent) Stretch
ν_3	Si-O-H (Hydrogen Bonded to Water) Stretch

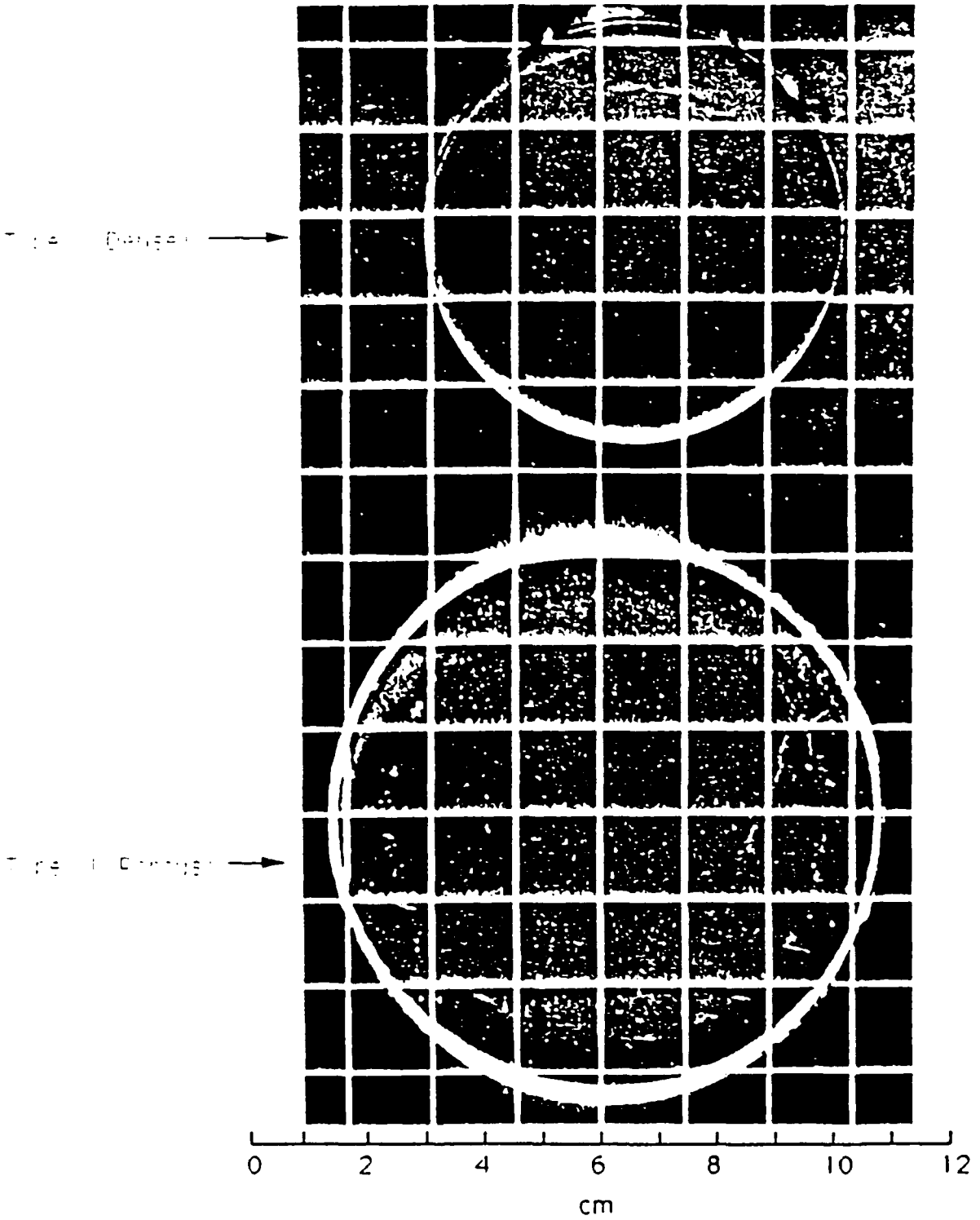

Figure 6. Optical transparency of Type V (dense) and Type VI (porous) gel-silica.

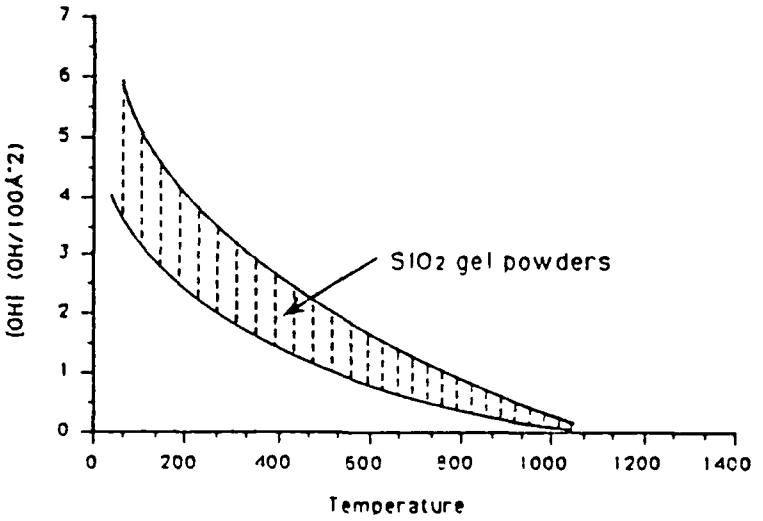

Figure 7. Hydroxyl concentration of silica gel powders as a function of processing temperature (from Davydov, et al. [16]).

TRANSPIRATION COOLED UV WINDOWS

Multifunctionality is highly desireable for optically transmitting windows in high speed rocket guidance systems due to severe operating conditions. The windows need to transmit light over a broad range of wavelengths, including the ultraviolet. Most importantly, the optical transmission must not be affected by very high ambient temperatures and impingement of very energetic gases. Reasonably good structural strength, thermal stability, and thermal shock resistance is also required for rocket windows.

A unique approach to achieving thermally resistant properties is to cool the window by passing gases <u>through</u> the window. Such a concept is possible with the ultraporous Type VI gel-silica monoliths.

The objective of the multifunctional optical component is to cool the window via transpiration of gases through the interconnecting pore structure while optical transmission is maintained.

The first step in evaluation of the concept of a transpiration cooled window is to determine whether transpiration of gases is possible through a porous Type VI gel-silica medium. The second step, if transpiration is possible, is to characterize the transpiration rate as a function of pressure, pore radius, sample thickness, and type of gas. The third step is to determine whether UV transmission occurs through the Type VI porous gel-silica window at elevated temperatures and with gases impinging on it. Fourth, thermal shock characterization of the window is also needed.

A preliminary report of these multifunctional performance characteristics follows. A low pressure (<700 psi) test chamber was designed and built to quantify the rate of gas transpiration through the porous optical windows. The results are shown in Figure 8 with the flow rates of helium through samples with pore radii of 1.2nm and 8.0nm (processed to 180°C and 500°C stabilization temperatures) measured as a function of pressure. Figure 9 shows the difference in flow between helium and nitrogen through the sample with 1.2nm pores stabilized to 180°C. The flow rate of the He is considerably

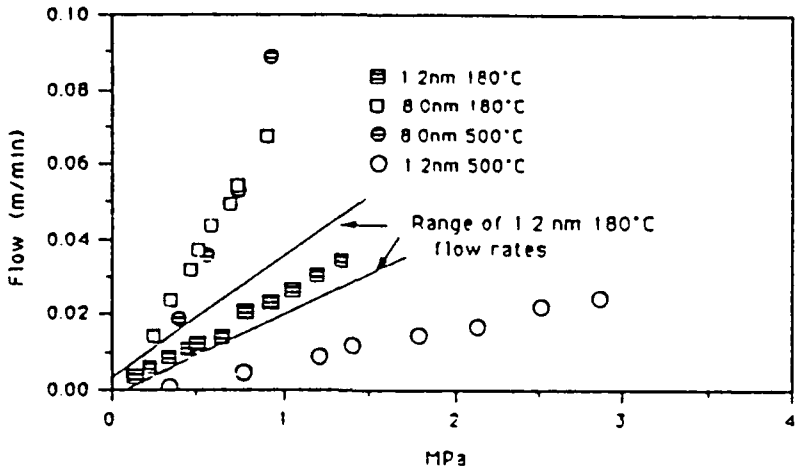

Figure 8. Helium transpiration through 1.2 nm and 8.0 nm porous gel-silica windows.

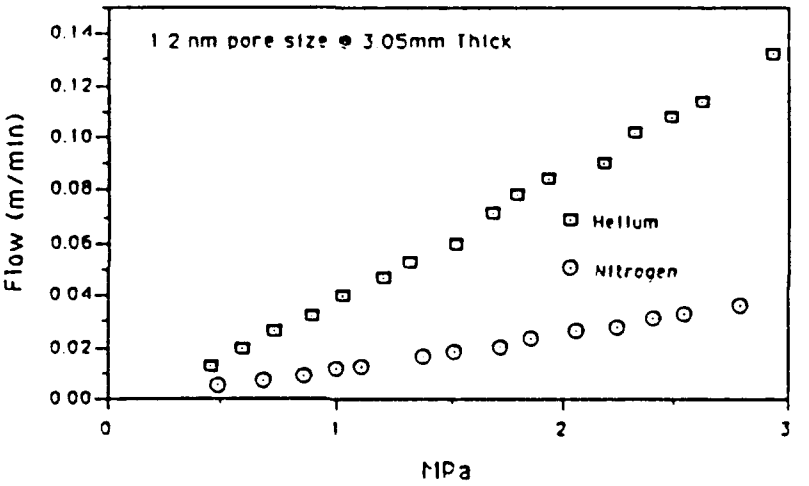

Figure 9. Helium versus nitrogen transpiration flow in a 1.2 nm pore size gel-silica window.

faster than nitrogen due to the difference in size* and the diatomic nature of nitrogen; i.e., He = 0.36 nm, N_2 = 0.42 nm.

To determine the effect of elevated temperature upon the UV transmission of gel-silica, a high temperature test apparatus was constructed, Figure 10. This apparatus includes a UV light source, sample holder with thermocouple, an oxygen-acetelyene torch heat source, and a multifunctional gel-silica optical component as a UV detector. This detector component is described in the next section. Fluorescent activity was observed in the detector at T > 1000°C due to the UV transmission of the window, absorption in the detector and emission at ~600nm by the wavelength shifter. The upper limit of temperature performance of the gel-silica UV window under transpiration cooling is presently unknown but is probably much higher than can be measured in this experimental set-up. Tests are underway and results will be presented at the Spring 1990 MRS meeting.

---

*Sizes (diameters) are approximated using twice the van der Waals radii and adding the N ≡ N bond length for N_2 (values taken from Huheey [17].

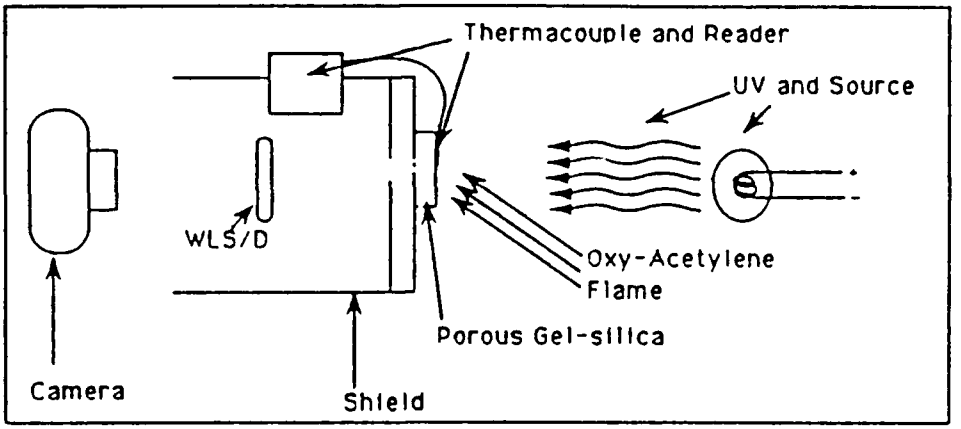

Figure 10. Experimental setup for UV detection at elevated temperature.

FAST, RADIATION-HARD SCINTILLATING DETECTOR

The physical features of Type VIA porous gel-silica described above are attractive to use as matrices for doping or impregnation with fluors, non-linear optical polymers or compounds, wavelength shifters, or lasing dyes. The result is a hybrid multifunctional optical component.

Table II lists examples of some organic and inorganic compounds that have been successfully impregnated into several Type VI gel-silica samples [1].

The results described above show that it is possible to select various combinations of second phase loading which are a function of pore size and total pore volume of the porous optical matrix. Previous studies [9] have shown that physical properties such as flexural strength, compressive strength, elastic modulus, coefficient of thermal expansion, density, and microhardness are also a function of pore size and volume fraction of porosity. For example, an 800°C heat treatment of a 1" diameter x 1/4" thick plano-plano Type VI gel-silica blank with 1.2 nm pores produces an optically transparent component that weighs 4.02 g, has a 117 HV microhardness, and has nearly 2500 m^2 surface area with pores ~1.2 nm radius. This component can accept 1.6 cc of a dopant second phase using various impregnation techniques. Thus, 40-50 volume percent of the component can be filled with a second phase.

Table II. Compounds Impregnated into Type VI Porous Gel-Silicas.

Non-Linear Optical Polymers	Transition Metals
-PBT [Phenylenebenzobisthiazole]	- Cu
-MNA [2-Methyl-4-Nitroaniline]	- Ni
	- Cr
Organic Flours	- Ce
-B-PBD[2-4'-t-Butylphenyl)	- Ag
5-(4"-Biphenylyl)-1,3,4-Oxadiazole]	- Fe
-P-TP [p-Terphenyl]	- Co
-P-QP [P-Quarterphenyl]	
Wavelength Shifter	**Rare-Earths (Lanthanides)**
-3-HF [Hydroxyflavone]	- Nd
	- Er
Laser Dye	
-Rhodamine 6G	

If a harder and stronger component is desired, a 900°C heat treatment can be used although the amount of dopant phase is reduced to 1.31 cc.

The Type VI gel-silicas with larger pore sizes described above make it possible to impregnate the component with higher molecular weight polymers. The same 800°C treatment of a 1" diameter x 1/4" thick sample with 8.0nm pores produces an optical component that weighs 1.98 g, has a 18 HV microhardness, and has nearly 583 m^2 surface area with pores ~ 8.0 nm radius. This component can accept 2.36 cc of a dopant second phase in its 70-75 volume percent porosity. Differences between a gel-silica matrix with 1.2 nm pores versus matrix with 8.0 nm are tabulated in Table III. These differences are large and provide a wide range of textural features for use in tailoring multifunctional optics.

For example, consider the fast radiation hard scintillator developed by Nogues, et al.[13]. They utilized a Type VI gel-silica matrix with a 1.2nm average pore radius and 0.35 volume fraction porosity as a host matrix for organic fluors to produce a fast, radiation hard scintillaton detector. The silica matrix provides high radiation resistance compared to the organic plastic scintillators [13] and the organic fluor provides fast scintillation response. Both properties are advantageous for high-speed counting necessary in high-energy physics applications. The primary fluors used by Nogues, B-PBD, P-TP & P-QP (Table II) have good radiation resistance and short decay times of a few nanoseconds, but the fluorescence spectra typically peaks at wavelengths below 400 nm, making it difficult to measure. To overcome this problem Nogues, et al. [13] used another fluor termed a wavelength shifter (WLF) (WLS) 3-HF (Table II) which absorbs the < 400 nm radiation of the primary fluor and re-emits in wavelengths of ≈ 500-600 nm. These wavelengths are advantageous as they are less absorbing in glass than the shorter wavelengths and also result in higher quantum efficiency for silicon photodiodes. When analyzed for scintillation efficiency with α-, β-, and γ-ray sources, the light output was reported to be only 6-7 times lower than the much more highly developed plastic scintillator [13]. The γ-radiation resistance of the silica matrix was many times greater than the organics. These are very encouraging results for the first generation of multifunctional optical components.

This same type detector with the 3-HF fluor dopant was supplied by Nogues for use as the WLS/detector shown in Figure 10 and was used for the high-temperature UV transmission test in the above mentioned transpiration study. A source emitting 365 nm radiation passes through the heated porous window being tested for transmission and is absorbed and re-emitted by the detector as visible green → yellow-green light from the WLS/detector. Thus, a qualitative and visual method for testing high temperature UV transmission through a porous silica matrix was achieved.

Table III. Property Comparisons Between 800°C Heat Tested Samples of 1.2 nm and 8.0 nm Average Pore Radius.

Property	1.2 nm	8.0 nm
Bulk Density (g/cc)	1.25	0.62
Surface Area per Unit Volume (cm^{-1})	7.63×10^6	1.81×10^6
Volume fraction Porosity	0.[illegible]	0.73
Vickers Hardness Number	117.3	16.8

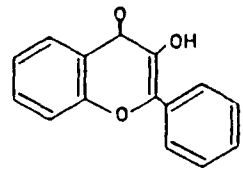

3-HYDROXYFLAVONE

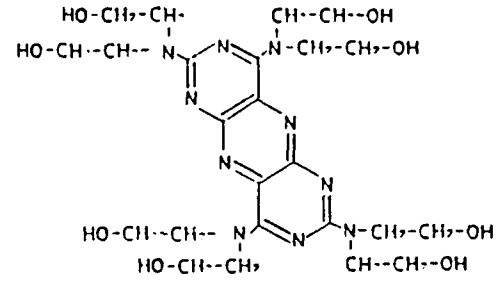

2,2',2'',2''',2'''',2''''',2''''''',2'''''''-[(PYRIMIDI
[4,5-g]-PTERIDINE-2,4,7,9-TETRAYL)TETRA-
NITRILO]OCTAETHANOL

Figure 11. Fluors of different size requiring different pore size matrices.

Organic fluors and dopants come in various sizes, many much larger than the 3-HF fluor used by Nogues (Figure 11). The octaethanol fluor exhibits strong excitation (absorption) bands peaking at 315 and 520 nm while its emission peak is shifted to 590 nm (up 85 nm from 3-HF which is 535 nm max). The strong 315 nm excitation and 590 nm emission band make it better suited for a high temperature UV transmission detector, provided one adds an optical filter to eliminate the oxy-acetylene flame effect on this fluor. With the larger (i.e., 8.0 nm) Type VI matrix it is feasible to use this larger organic molecule which do not fit in the 1.2 nm pore size matrix, or to have a much larger volume fraction of dopant (Table III).

ACKNOWLEDGMENTS

The authors are grateful for the financial support of the Air Force Office of Scientific Research under contract #F49620-88-C-0073 and the encouragement of D. R. Ulrich throughout this research. A special thanks is extended to J. L. Nogues for the use of the wavelength shifter/detector.

REFERENCES

1. L. L. Hench, S. H. Wang, and J. L. Nogues, in Multifunctional Materials, edited by Robert L. Gunshor, (SPIE: Bellingham, Washington, 1988) Vol. 878, p 76.

2. L. L. Hench and J. K. West, in Chemical Reviews, Main Group Chemistry Thematic Issue, edited by J. Michl, (American Chemical Society, New York, 1990).

3. J. D. Mackenzie and D. R. Ulrich, eds., Ultrastructure Processing of Advanced Ceramics, (J. Wiley and Sons, New York, 1988).

4. M. Prassas, J. Phalippou, and J. Zarzycki, presented at the XIII Int. Conf. on Glasses, Hamburg, Germany, 1985.

5. B. E. Yoldas, Bull. Am. Ceram. Soc. 54, 286 (1975).

6. J. Zarzycki, editor, J. Non-cryst. Solids. 1-3, 1-436 (1986)

7. J. Fricke and R. Caps, in Ultrastructure Processing of Advanced Ceramics edited by J. J. Mackenzie and D. R. Ulrich, (J. Wiley and Sons, New York, 1988) pp. 613-622.

8. J. Zarzycki, M. Prassas and J. Phallipou, J. Mater. Sci. 17, 3371-3379 (1982).

9. W. Vasconcelos, Ph.D. Thesis, University of Florida, 1989.

10. J. L. Nogues, C. Balaban, W. V. Moreshead and R. S. Sheu, Advanced Ceramics, edited by W.P.E. Longo, S. N. Monteiro and J. D. Filho (Florida-Brazil Institute, Rio de Janeiro, 1989) pp. 51-60.

11. L. L. Hench, M.J.R. Wilson, C. Balaban, and J. L. Nogues, presented at the 4th International Conference on Ultrastructure Processing of Ceramics, Glasses and Composites, Tucson, Arizona, 1989.

12. S. H. Wang, C. Campbell, and L. L. Hench, in Ultrastructure Processing of Advanced Ceramics, edited by J. D. Mackenzie and D. R. Ulrich, (J. Wiley and Sons, New York, 1988) pp. 145-160.

13. J. L. Nogues, S. Majewski, J. K. Waler, M. Bowen, R. Wojcik, and W. V. Moreshead, J. Am. Ceram. Soc. 71 (12), 1159-1163 (1988).

14. L. L. Hench and D. Parsell (personal communication).

15. E. Elias, Masters Thesis, University of Florida, December 1989.

16. V. Ya. Davydov, A. V. Kiselev, and L. T. Zhuravlev, Trans. Faraday Soc. 60, 2254 (1964).

17. James E. Huheey, in Inorganic Chemistry, 3rd ed. (Harper & Row, New York, 1983), p. 258.

APPENDIX 16

Characterisation of doped sol–gel derived silica hosts for use in tunable glass lasers

A J Berry and T A King

Physics Department, Schuster Laboratory, Manchester University, Manchester M13 9PL, UK

Received 10 April 1989

Abstract. Measurements of laser-relevant properties of neodymium doped sol–gel derived silica hosts are described. Samples with Nd as the only dopant reveal anomalously short fluorescence lifetimes characteristic of concentration quenching, TEM measurements revealing clumping of the neodymium. Co-doping with aluminium allows better dispersion of the neodymium throughout the gel–silica matrix, but fluorescence lifetimes and efficiencies are still lower than expected. Phonon quenching by residual OH^- ions is suspected, absorption, FTIR and Raman spectroscopy being used to support this theory.

1. Introduction

The ability to dope sol–gel derived silica hosts with controlled amounts of a lasing species affords the possibility of developing a new generation of advanced tunable solid state lasers. Such lasers, as well as possessing the limited tunability common to all glass lasers, can also take advantage of the superior physical properties of sol–gel derived silica. These properties include: low non-linear refractive index coefficient; low strain birefringence; coefficient of thermal expansion close to zero; low temperature dependence of expansion coefficient and low impurity levels.

As a first step towards the construction of a working laser it is necessary to investigate the laser-relevant properties of the doped sol–gel derived silica hosts of interest. These properties are indicated by the equation for the population inversion density required for lasing threshold (Yariv 1976)

$$N_2 - N_1 = N_t = \frac{8\pi n^3 \tau \Delta\nu}{c t_c \lambda^2}$$

where τ is the spontaneous lifetime of the upper lasing level, $\Delta\nu$ is the linewidth of the transition and t_c is the loss-dependent cavity lifetime. To reach threshold easily, therefore, one requires low losses, narrow linewidth and short lifetimes. For tunability, however, the linewidth needs to be large. Thus, one needs low losses and short lifetimes. It is crucially important, however, that the effective lifetime is the spontaneous lifetime and not a much shorter lifetime resulting from non-radiative quenching processes which drastically reduce the fluorescence efficiency and thereby increase the pump energies needed. Initial experiments in this study have therefore concentrated on measuring the fluorescence lifetimes, linewidths and efficiencies of variously doped gel–silica samples.

The samples themselves were manufactured by Geltech Inc., Florida, USA and generally took the form of small discs or cylindrical rods. Neodymium was the obvious lasing element to investigate first, the preponderance of Nd–glass laser systems testifying to its superior lasing qualities. The well known $^4F_{3/2} \rightarrow {}^4I_{11/2}$ transition at about 1.06 μm has the highest gain and typically has a bandwidth of $\approx$30 nm in a silicate-based glass (Levine 1968). It therefore represents the best chance of obtaining tunable operation of this new class of solid state glass lasers. Dopants of possible future interest will include other rare earths, such as erbium and holmium, and various transition metals, particularly chromium.

2. Experimental method

A standard pulsed excitation and wavelength-selective temporal observation technique was employed consisting of a flashlamp-pumped dye laser (FPDL), sample, monochromator, filter, PMT and storage oscilloscope. Neodymium has a convenient absorption at 585 nm, a wavelength easily accessed by a FPDL operating on the dye Rh6G. 200 mJ pulses could be obtained with durations of $\sim$2 μs FWHM, much shorter than the expected fluorescence lifetimes. A PMT with an S1 photocathode was used to detect fluorescence at about 1.06 μm, as well as fluorescence at about 900 nm from the

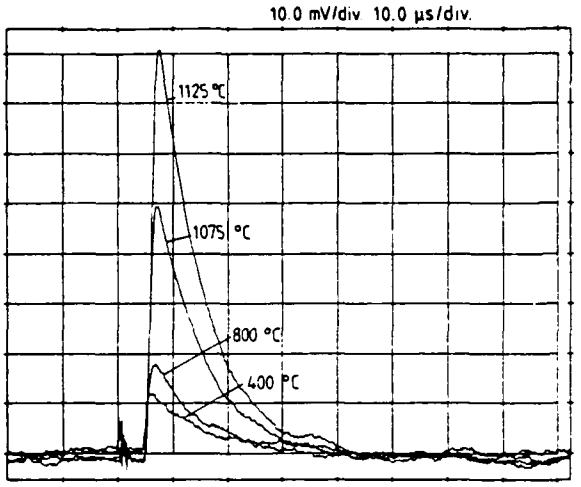

Figure 1. Temporal profiles of the 1.06 μm fluorescence from 5 wt% Nd_2O_3 doped gel–silica samples densified to different temperatures.

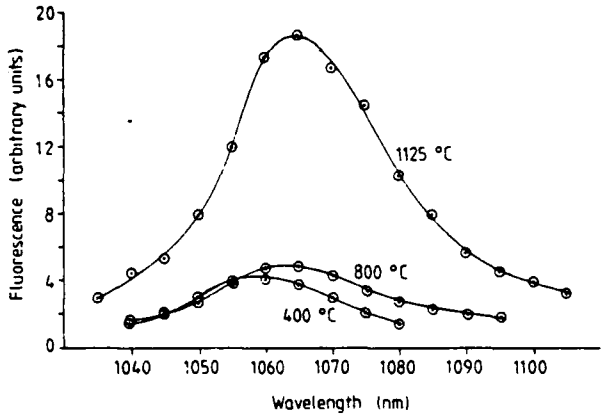

Figure 2. Fluorescence intensity against wavelength for 5 wt% Nd_2O_3 doped gel–silica samples densified to different temperatures.

$^4F_{3/2} \rightarrow {}^4I_{9/2}$ transition. Standard laboratory spectrometers were used for absorption and FTIR measurements. Raman spectra were taken using an argon ion laser, double monochromator, cooled PMT and dedicated computer set-up.

3. Results and discussion

Initial results on samples doped only with various concentrations of neodymium gave surprisingly short lifetimes and low (qualitatively estimated) fluorescence efficiencies. Figure 1 shows the results for a batch of 5 wt% Nd_2O_3 doped samples densified to various temperatures. (Fully densified, non-porous gel–silica is obtained at a densification temperature of ~1200 °C.) Note that all the lifetimes are less than 10 μs, in stark contrast to expected values of 200–800 μs (Yariv 1976). Figure 2, however, shows that the linewidths are comparable to those for conventional laser glasses. Fuller densification appears to favour the fluorescence

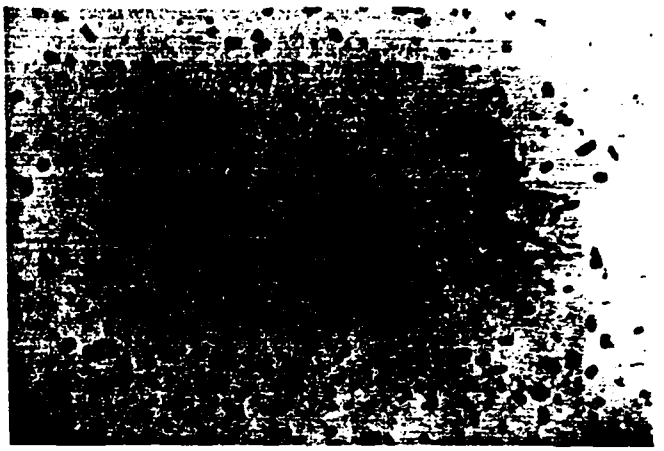

Figure 3. Transmission micrograph of a 5 wt% Nd_2O_3 doped gel–silica sample.

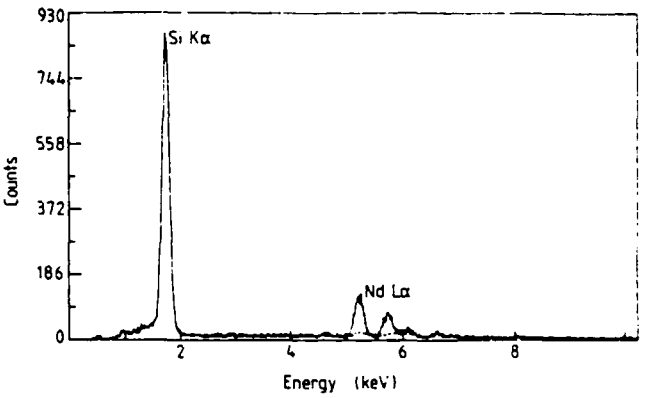

Figure 4. SEM–EDAX analysis of a 5 wt% Nd_2O_3 doped gel–silica sample from a region containing a clump (full curve) and a region not containing any clumps (broken curve).

efficiency and increase the tuning range, also shifting the peak to longer wavelengths. Similar results are obtained for the fluorescence band around 900 nm, which, since it emanates from the same $^4F_{3/2}$ lasing level, lends weight to the theory that this level is being seriously quenched. Concentration quenching is known to be a problem with Nd doping (Peterson and Bridenbaugh 1964) and clumping or clustering is known to be a problem with rare earth doping of pure silica (Arai *et al* 1986). The two effects combined could explain the short lifetimes in gel–silica samples even though their overall doping levels are below those where the effect should be observable.

Figure 3 shows a transmission micrograph of a 5 wt% Nd_2O_3 doped sample. Clumps with dimensions of the order of 100 nm are clearly visible. A greater magnification still shows structure within a single clump and electron diffraction traces show rings, again indicative of structure within the clumps. That all the neodymium is contained within the clumps is confirmed by SEM–EDAX measurements performed on a region of the sample containing a clump and one without. The results are shown in figure 4 and reveal an Nd signal from the clump-containing region only.

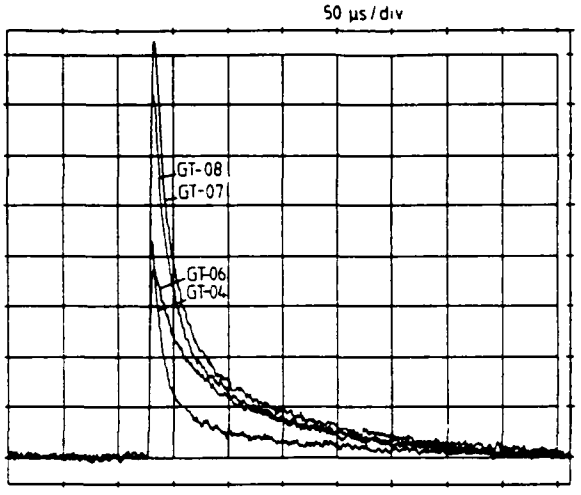

Figure 5. Temporal profiles of the 1.06 μm fluorescence from various gel–silica samples co-doped with Nd and Al.

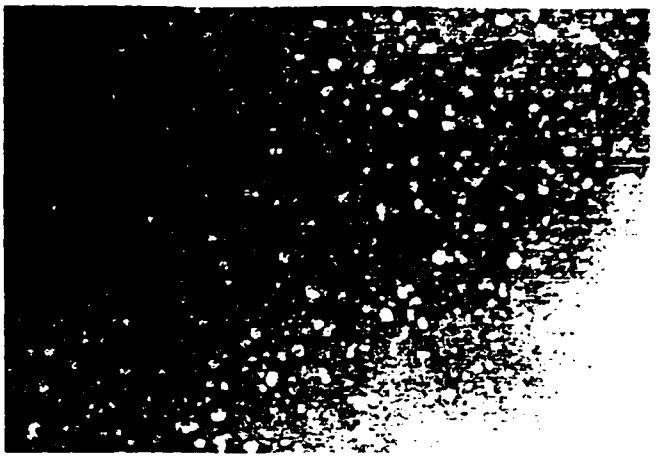

Figure 6. Transmission micrograph of the co-doped sample GT-06.

Clearly the Nd ions are not being dispersed adequately throughout the gel–silica matrix. With conventional silica the solution was to co-dope with a glass modifier such as aluminium or phosphorus. Aluminium lends itself well to the sol–gel process and so the same lifetime, linewidth and fluorescence efficiency studies were performed on a new batch of samples which were co-doped with Nd and Al, the concentrations being determined by SEM–EDAX measurements.

Figure 5 shows the lifetime results for fluorescence at around 1.06 μm. The concentrations of dopants were (wt% of oxides); GT-04 (3.5% Nd:5.0% Al), GT-06 (1.5% Nd:7.0% Al), GT-07 (3.5% Nd:7.4% Al) and GT-08 (4.6% Nd:7.1% Al). The lifetimes are now much longer, although the temporal profiles appear to consist of the same initial rapid decay seen in the samples doped only with Nd followed by a more long-lived decay. This is except for sample GT-06 which does not appear to have the initial decay, and has, in fact, got a longer final decay than the other samples (>100 μs). Note also that this sample has the highest Al/Nd dopant ratio of those shown, these results and others indicating that a dopant ratio Al/Nd ≥ 5 is required. A similar result was obtained by Arai *et al* (1986) for the co-doping of conventional silica. It appears, therefore, that co-doping with a glass modifier can overcome the clumping and consequent concentration quenching problem in sol–gel derived silica. This result is verified by the fact that fluorescence efficiencies are greatly improved. Conclusive proof is given, however, by the transmission micrographs of sample GT-06 shown in figure 6. The clumps (dark patches in figure 3) have clearly disappeared, being replaced, in this case, by white patches. These patches represent holes in the matrix caused by bloating in the as yet unperfected densification process for co-doped samples. SEM–EDAX measurements performed anywhere on the sample give the same Nd signal, a result again indicative of good dispersion throughout the matrix.

Although much improved, however, the linewidths are still not as long as expected and the fluorescence efficiencies are still not as high as those for samples of conventional silicate laser glasses. (The linewidths are, however, comparable.) An additional quenching process is suspected, the nature of the sol–gel process leading credence to the theory that phonon quenching due to residual OH^- ion content is a likely candidate. This has been identified as a problem in other laser glasses by, for example, Bondarenko *et al* (1976), where the effect can be quite large. As an example, Bondarenko *et al* derive an equation for a phosphate glass

$$1/\tau = 3.3 \times 10^3 + 2.2 \times 10^2\sigma$$

where τ is the upper lasing level lifetime and σ (cm^{-1}) is the absorption coefficient at 2.85 μm (i.e. the fundamental absorption band of OH). If our sol–gel derived silicate glasses are anything like this example then the lifetime is being reduced if the transmission through a typical 5 mm thick sample falls below ~50% at 2.85 μm. Incomplete densification and an unperfected dehydration technique for co-doped samples results in a large residual OH^- ion content, as the absorption profiles of figure 7 reveal for the GT series of co-doped samples. None of these samples reveal any transmission at all at 2.85 μm, and so some quenching effect is not unexpected. Complete removal of OH^- ions would mean, for example, that the trace for GT-04 would be level right out to 3300 nm, showing no troughs at the OH absorptions of about 2700, 2200, 1900 and 1380 nm. This has been achieved for undoped sol–gel derived silicas, but the presence of dopants makes the process more difficult. Another manifestation of this difficulty is the falling off in the transmission of some of the samples in figure 7 as one goes to shorter wavelengths. This is caused by scattering from the small voids in the matrix caused by bloating during the densification process, an effect which also gives the samples a slight milky appearance.

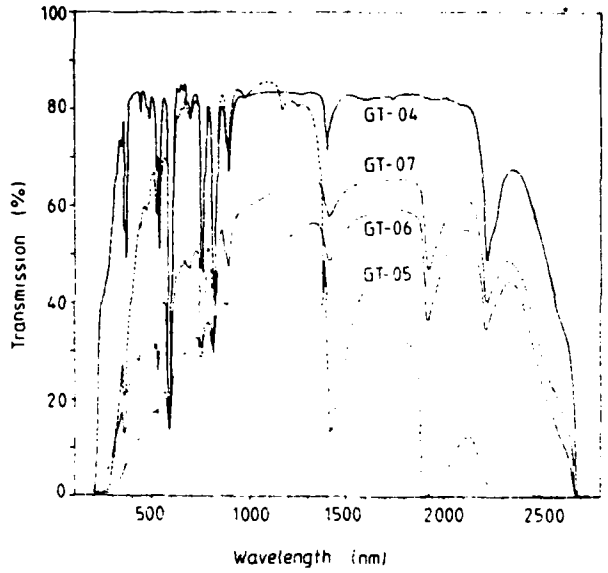

Figure 7. Absorption spectrometry traces of various gel–silica samples co-doped with Nd and Al.

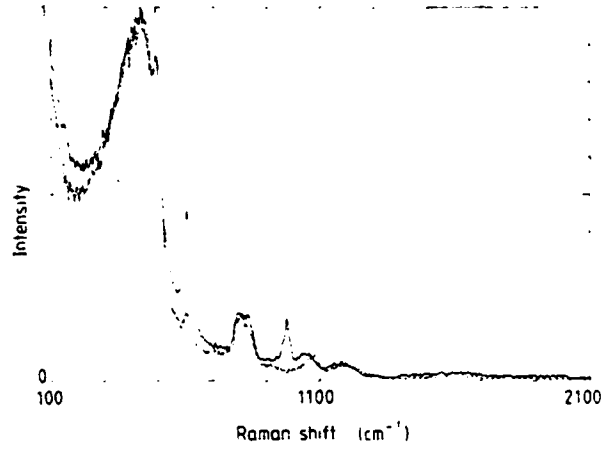

Figure 8. Raman spectra of partially densified undoped gel–silica (full curve) and fully densified and dehydrolysed undoped gel–silica (broken curve).

FTIR spectroscopy, scanning the wavelength range 2.5–25 μm, also reveals the 'wetness' of all the doped samples tested to date, as does Raman spectroscopy. Using the experimental arrangement already described, Raman spectra such as those shown in figure 8 are obtained for an undoped, partially densified sample and an undoped, fully densified and dehydrated sample. These spectra are essentially the same as those obtained by Stolen and Walrafen (1976) for conventionally produced silica. Particular points to note are the peak at about 970 cm^{-1} in the partially densified sample—a peak which Stolen and Walrafen attribute to the Si-(OH) vibration—and the relatively larger sizes of the defect peaks at about 490 and 604 cm^{-1}, again in the partially densified sample. Raman spectra from all the co-doped samples show various levels of fluorescence signal which either totally or partially obscure the Raman signal, the effect appearing to be in proportion to the visual milkiness of the sample. The samples that gave traces most like those of figure 7 were two with Al/Nd $\geq$ 5, the defect peaks not being present and fluorescence only starting at shifts greater than about 1100 cm^{-1}. Although little understood as yet, it is clear that Raman spectroscopy is a powerful tool in the investigation of the microstructure of doped sol–gel derived silica matrices.

4. Conclusions

Initial measurements of the fluorescence lifetime of the $^4F_{3/2} \rightarrow {}^4I_{11/2}$ transition of Nd doped into sol–gel derived silica found it to be too short and the fluorescence efficiency much too low. Both these effects suggested concentration quenching. TEM measurements revealed the expected clumping of the Nd_2O_3 and we have shown that co-doping with a glass modifier such as Al prevents this effect provided the dopant ratio Al Nd $\geq$ 5. We show, however, that the samples available to date are still too 'wet', residual OH^- ions probably being responsible for the still lower than expected lifetimes and fluorescence efficiencies that we are observing. OH^- can be successfully removed in undoped samples, however, and Geltech Inc. are confident that the same will also apply to co-doped samples. When this has been achieved, and high-optical-quality rod-shaped samples have been manufactured, it will only be a matter of time before successful lasing action, with limited tunability, can be reported for the first time in a rare-earth doped sol–gel derived silica host.

Acknowledgments

This study forms part of a wider programme of research in collaboration with the Advanced Materials Research Center, University of Florida and Geltech Inc. We have enjoyed extensive discussions with Professor Larry Hench of the AMRC and we thank Mr Bill Moreshead of Geltech Inc. for discussion and provision of samples. This research has been sponsored by the Air Force Office of Scientific Research (AFSC) under contract F49620-88-C-0010.

References

Arai K, Namikawa H, Kumata K, Honda T, Ishii Y and Handa T 1986 *J. Appl. Phys.* **59** 3430

Bondarenko E G, Galant E I, Lunter S G, Przhevaskii A K and Tolstoi M N 1976 *Sov. J. Opt. Technol.* **42** 333

Levine A K 1968 in *Lasers* vol 2 (London: Edward Arnold)

Peterson G F and Bridenbaugh P M 1964 *J. Opt. Soc. Am.* **54** 644

Stolen R H and Walrafen G E 1976 *J. Chem. Phys.* **64** 2623

Yariv A 1976 *Introduction to Optical Electronics* 2nd edn (New York: Holt, Rinehart and Winston)

APPENDIX 17

Progress in the study of gel-silica optics for intra-cavity laser use.

A presentation to the second O.G.A.M.M.S. review meeting Ilkley August 1989.

Nicholas J. Phillips
Spencer P. Modica
Loughborough University of Technology
Department of Physics

August 1989

Summary

This report deals with advances both at a theoretical and experimental level in the study of intra-cavity etalons using sol-gel materials. In past work, the etalon has been seen as a device associated with a one way pass role for light with special reference to interferometers. The problem of what an etalon does when inserted into the optical cavity of a laser has not been thoroughly addressed. This report reveals new work which begins to tackle the problem of 'an etalon within an etalon' i.e. the etalon within the laser cavity. From these theoretical ideas we are building up a series of experimental measurement techniques and first results are reported.

1. Introduction

In this work programme, we see the intra-cavity etalon as a vital piece of diagnostic apparatus. The reason is quite simple. In an intra-cavity situation, the multipass behaviour of the light provides an extremely sensitive diagnostic of absorption losses and refractive index performance.

To our knowledge, this problem has not been tackled before in a rigorous fashion; the main reason being that it is theoretically messy. It seems that previous workers have assumed that an estimate of performance obtained by measurements of transmittance outside the laser cavity is of sufficient merit. We feel that this cannot be the case because of the profound feedback that occurs when the element is placed within the cavity of the laser. It was felt wise to attempt some sort of theoretical discussion based upon a real situation of the etalon sitting within the cavity of the laser. We saw this problem from a start point of a lossless resonator within a lossless resonator. The mathematics has turned out to be messy but closable and may now reveal important new performance

criteria. Thus it is our aim to specify new theoretical criteria which are a sort of hierarchical form of reflectance, finesse and free spectral range.

At the practical end, we have now established an experimental system for measurement of the etalon's parameters. This includes an accurate oven control system to permit a sweeping of the oven temperatures and hence a control of the etalon's thickness. We have also installed a spectrum analyser to examine the mode structure of the laser output. At present, this analyser will not allow us to study the profile of an individual laser mode but we shall add a new piece of equipment at the next round of funding that will make such a measurement feasible. This extra equipment, a further swept spectrum analyser, will be able to resolve the mode profile of a single cavity mode.

2. Theoretical Developments

We have examined a model of the etalon within the laser cavity as shown below:

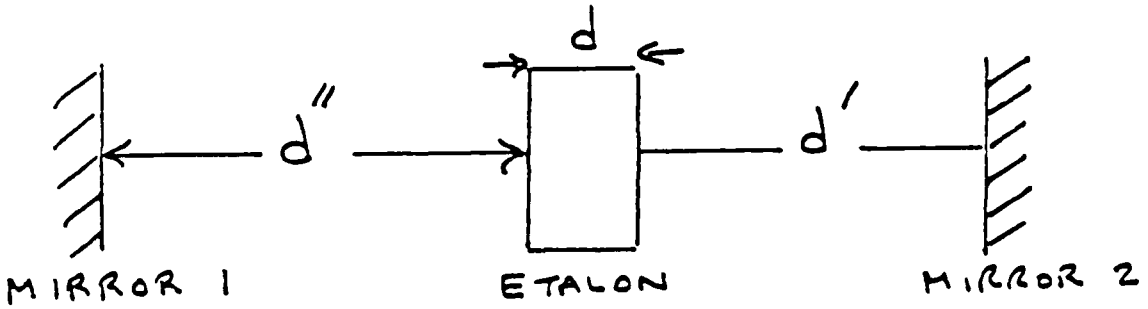

Figure 1. Showing the basic resonator model.

The model is simplified by making both mirrors perfectly reflecting and considering a self consistent phase shift for the round trip excursion of the light.

The characterisation of the etalon is now achieved by conventional wisdom as follows:

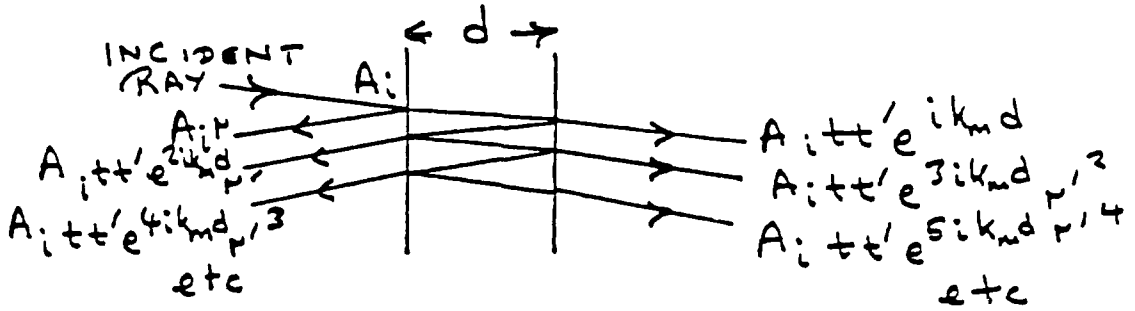

Amplitude reflectance at the surfaces, r from without and r' from within.

Figure 2. Model for multiple internal reflection in etalon.

We can thus evaluate the performance to give a net amplitude reflectance.

$$\rho = \frac{r\,[\,1 - \exp(2ik_m d)\,]}{1 - r'^2 \exp(2ik_m d)} \qquad (2.1)$$

where $k_m = \frac{2\pi n}{\lambda_a}$ and λ_a is the wavelength in air.

The net amplitude transmittance is

$$\tau = \frac{tt'\exp(ik_m d)}{1 - r'^2 \exp(2ik_m d)} \qquad (2.2)$$

where t, t' are the amplitude transmittances at the individual surfaces seen from without and within.

We note that if A_i is the amplitude of an incident beam, A_{TT} is the total transmitted amplitude and A_{RT} is the total reflected amplitude then by energy conservation we must have

$$|A_i|^2 = |A_{TT}|^2 + |A_{RT}|^2 \qquad (2.3)$$

But since $A_{TT} = \tau A_i$; and $A_{RT} = \rho A_i$ then we need

$$1 = |\tau|^2 + |\rho|^2 \qquad (2.4)$$

which follows easily from our earlier definitions of ρ and τ.

The parameters ρ and τ are of course well understood and the conservation of energy reflected in equation (2.4) is an essential ingredient of physical correctness.

To take the next step towards understanding the problem of the etalon within the resonator, we take a new look at the overall optical problem. If a single ray of light is incident on the etalon from the left as below:

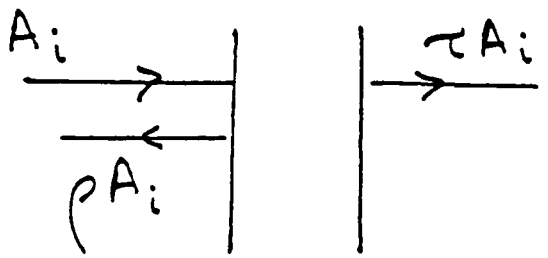

Figure 3. Simplified model of etalon. The amplitude values are assigned at the etalon surface.

we can assign to this etalon the complex reflectance and transmittance ρ and τ. Such a ray will in part reflect off the etalon and in part transmit through it. Thus the physical model can be reduced to a pair of oppositely travelling wavefronts in the three spaces, mirror 1 → etalon, within the etalon and etalon → mirror 2. For physical correctness, we must expect the behaviour in the two cavities external to the etalon to be similar. This symmetry condition must emerge from the theory.

Now let us consider the problem below:

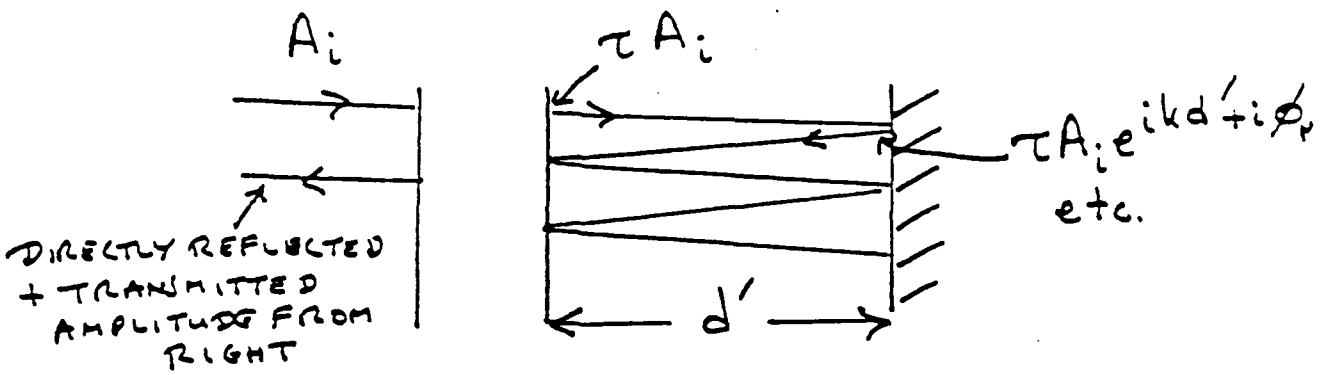

Figure 4. Transmitted amplitude allowing for multiple internal reflection **outside** etalon.

We sum the total amplitude of light incident on the right hand face of the etalon after reflection off the mirror. Then allowing for a phase shift φ_r on reflection at the mirror and allowing for the distance factor d', we have a set of right to left travelling components at the right hand face of the etalon as follows:

$$A_i \tau \exp(i\varphi_r) \exp(2ikd') + A_i \tau\rho \exp(2i\varphi_r) \exp(4ikd') + A_i \tau\rho^2 \exp(3i\varphi_r) \exp(6ikd') + \text{etc.}$$

This gives the total right to left amplitude of the right hand face of the etalon in the form

$$\frac{A_i \tau \exp(2ikd' + i\varphi_r)}{1 - \rho \exp(2ikd' + i\varphi_r)}$$

which then yields a **transmitted** amplitude at the left of the etalon in the form

$$\frac{A_i \tau^2 \exp(2ikd' + i\varphi_r)}{1 - \rho \exp(2ikd' + i\varphi_r)}$$

For this to travel on and match the input amplitude (left to right) at the etalon, we then need a further reflectance phase shift and distance phase shift i.e. we must have

$$A_i = \frac{A_i \tau^2 \exp(2ikd' + i\varphi_r) \exp(2ikd'' + i\varphi_r)}{1 - \rho \exp(2ikd' + i\varphi_r)} \qquad (2.5)$$

where we assume that each mirror generates the same phase shift φ_r. Equation (2.5) is the controlling equation for the problem and it should state conservation of phase in simplistic cases. Let us now set the etalon thickness so that $\rho = 0$ and $\tau = 1$ and equation (2.5) yields the condition

$$\exp(2ikd' + 2i\varphi_r + 2ikd'') = 1 \qquad (2.6)$$

We recognise this as the round trip phase condition for a resonator. Evidently, the effect of the etalon is not seen in this condition.

The complexity of (2.5) is an obvious result of the fact that the influence of the etalon when placed within the cavity formed by the two mirrors is dependent on the mirror separation and is linked with the etalon's thickness d by the conservation condition.

$$d' + d'' + d = \text{const.} = d_0 \qquad (2.7)$$

where d_0 is the effective resonator length.

Thus before we analyse the situation in terms of behaviour with d variable, we need to specify how the etalon behaves in a very tight way.

The framework of the theoretical problem is now well defined but there are further subtleties of these experiments which are not normally encountered.

We can effectively write the refractive index n in the form

$$n = f(\sum_i N_i \alpha_i) \qquad (2.8)$$

where f is some function of the sum of species of molecules each with a number density N_i and polarizability α_i. For example in the formula of Lorenz and Lorentz, we write

$$n^2 = \frac{1 + \frac{8\pi}{3}\sum_i N_i\alpha_i}{1 - \frac{4\pi}{3}\sum_i N_i\alpha_i} \qquad (2.9)$$

which is clearly highly non-linear. For the purposes of our work, we see that the phase shift $k_m d$ is in fact $2\pi n\, d/\lambda_a$ where λ_a is the wavelength in air. The question to be answered in how does nd vary as d varies? We note that strictly, if d changes and matter is conserved then to a first approximation, we shall have

$$d\sum_i N_i = \text{Const.} \qquad (2.10)$$

This can be simplified for a single species to state that

$$\rho d = \text{Const.} \qquad (2.11)$$

where ρ is the material density.

We normally tacitly assume that n and ρ are linearly related. Certainly if a relationship of the Lorentz Lorenz form applies then this is patently not true. Our task must be to consider carefully the rôle of the expansion process in terms of whether nd remains constant. For example if we could write

$$n = 1 + g(\sum_i N_i\alpha_i)$$

where g is an appropriate function, then since matter is conserved, it looks as though nd = d + constant. Thus the expansion of the etalon mirrors affects the result by the movement of its boundaries as if it contains air. These effects which clearly stem from the Clausius Mosotti relationship of solid-state physics are as yet not understood in terms of experimental

reality. The etalon and its diagnostic ability probably provides some of the most sensitive methods of fully understanding the minutiae of solid state behaviour of the amorphous gel-silica products.

To round off our discussion of theoretical matters, we return to equation (2.5) which we have demonstrated as an equation illustrating a round trip phase condition when the etalon is so matched that its presence is lossless.

We have to ask what happens when the condition $\rho = 0, \tau = 1$ is **not** satisfied. Under such conditions, the mismatched resonator problem causes the level of energy **inside** the etalon to rise above that **outside**. The ratio of amplitudes within and without the etalon has been calculated and this leads to a new cautionary tale vis à vis the simplistic understanding of intra-cavity etalon performance.

As the etalon is tuned off the optimum transmission condition ($\tau = 1$) the amplitude within the etalon rises with respect to that outside the etalon. Further theoretical work has established that for an etalon of 20% intensity reflectance at each face a ratio of intensities of some 8 x can be obtained. This leads to a new consideration of thermal stability of the etalon performance.

Consider the model below:

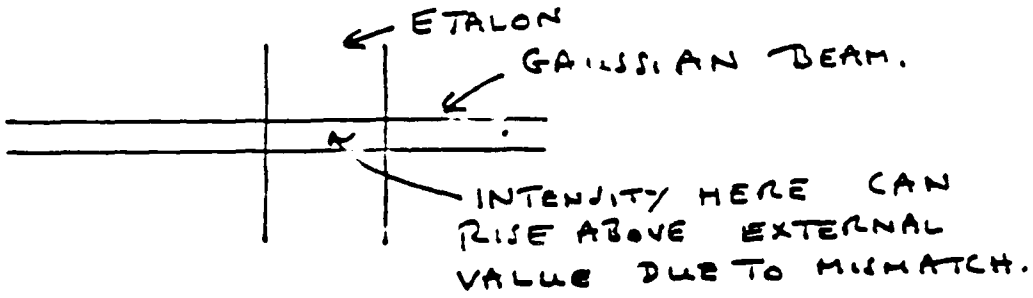

Figure 5. Localisation of intense intra-cavity light can cause local changes of etalon thickness.

In an **extra**-cavity situation the etalon experiences a beam power limited by that of the laser output (e.g. 1 Watt total beam power) but because of the mismatch situation with respect to the surrounding free space a trapped resonator pattern is created within the etalon, thus pushing up the local power density.

In an intra-cavity situation the beam power may be some 100 x the emergent power and furthermore, the trapped resonator effect provides close to a further order of intensity magnitude. If we assign a notional $1/e^2$ beam diameter of say 0.8 mm (a common value) then we have an approximate power density approaching 200,000 Watts/cm^2.

It is our impression that local heating effects can occur thus altering the effective path length of the sample in the z direction.

Even very small levels of absorptance may be a problem because of the low level of thermal conductivity of the silica matrix. New modelling is now taking place to assess the importance of the phenomenon but undoubtedly we need to be extremely careful about any form of absorptance from whatever origin.

3. Experimental Progress

Experimental work has been divided into two areas; out-of-cavity measurements of the physical properties of the etalon material and an examination of the performance of etalons of various types in a laser cavity.

Let us firstly consider the out of cavity measurement of etalon performance. We have undertaken two types of measurement as follows:

(a) The measurement of optical path changes in an etalon under conditions of thermal expansion.

In this case the light from the laser is incident on the etalon plate which itself is housed in an oven. The oven is controlled by a 12 bit digital controller with an accurate platinum resistance sensor. The accuracy of control and readout is better than 0.1° C.

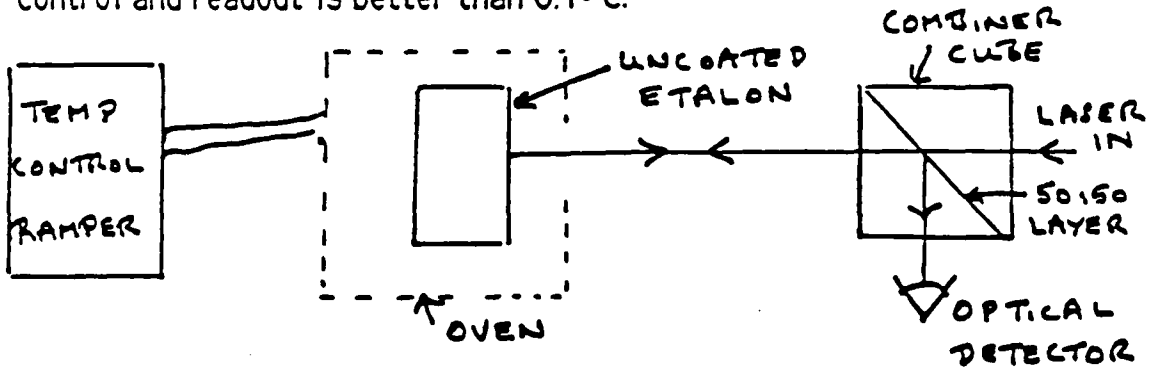

Figure 6. Schematic of thermal ramp experiment.

For an uncoated dielectric block of thickness d and refractive index n, the reflectance is given by the ratio of reflected to incident intensity.

$$\frac{I_R}{I_i} = \frac{F \sin^2\left(\frac{\phi}{2}\right)}{1 + F \sin^2\left(\frac{\phi}{2}\right)} \qquad (3.1)$$

where for a head on beam

$$\phi = \frac{4\pi n d}{\lambda_a}$$

where λ_a is the wavelength in air and ϕ is the double pass phase shift factor and

$$F = \frac{4R}{(1 - R)^2} \qquad (3.2)$$

where R is the intensity reflectance at each etalon face. For an uncoated dielectric sample, $R = [(n - 1)/(n + 1)]^2$.

If n is changed then the most sensitive effect is on the phase factor ϕ due to the presence of the large numerical contribution from $1/\lambda_a$. Likewise changes of d affect the phase factor with high sensitivity.

We note that as we change the temperature then d and hence n change. However, the reflectance of the etalon peaks where $\phi/2 = \pi/2, 3\pi/2, 5\pi/2$ etc.

We may write

$$\phi = \frac{4\pi n d}{\lambda_a} \qquad (3.3)$$

and hence

$$\Delta\phi = \frac{4\pi}{\lambda_a}\left(n\Delta d + d\Delta n\right) \tag{3.4}$$

where Δ stands for an increment. Hence as the temperature of the etalon changes, we shall observe that

$$\frac{\Delta\phi}{\Delta t} = \frac{4\pi}{\lambda_a}\left(n\frac{\Delta d}{\Delta t} + d\frac{\Delta n}{\Delta t}\right) \tag{3.5}$$

where Δt is the temperature increment.

We may write this in the form

$$\frac{\Delta\phi}{\Delta t} = \frac{4\pi nd}{\lambda_a}\left(\frac{1}{d}\frac{\Delta d}{\Delta t} + \frac{1}{n}\frac{\Delta n}{\Delta t}\right) \tag{3.6}$$

and we note that

$$\frac{1}{d}\frac{\Delta d}{\Delta t} = \alpha \tag{3.7}$$

where α is the thermal expansion coefficient.

Experimentally, we observe the values of t at which the reflectance maximises and note the temperature increment between these conditions. A typical graphical output of the experiment is shown in Figure 7. The linear temperature ramp is plotted simultaneously with the reflected intensity from the surface of the etalon.

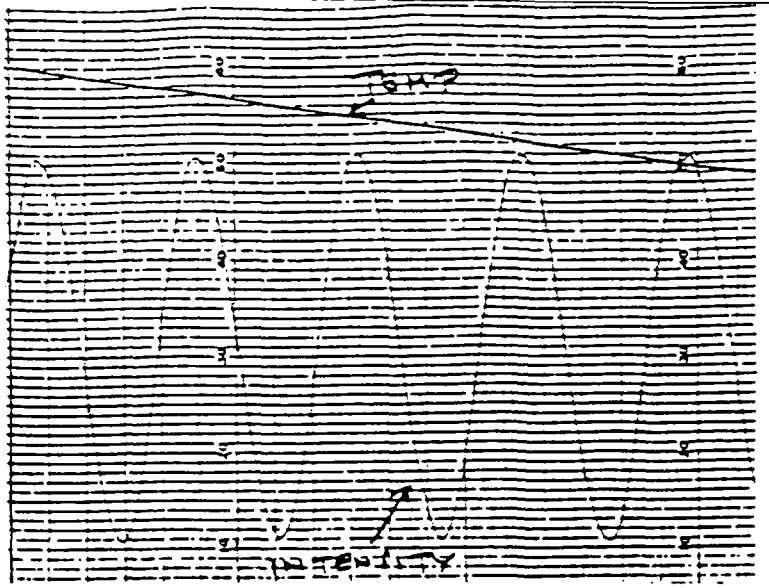

Figure 7. Typical plot of reflected intensity against temperature.

A careful study of the linearity of the system and repeatability on reversal of the temperature cycle gives a confident feeling for the accuracy of the measured results. For example for an etalon with the following characteristics

$d = 10.18$ mm
$\alpha = 5.5 \times 10^{-6}/^{o}C$
$n = 1.46$

We observe a value of $\Delta t = 2.5^{o}C$ for a phase increment $\Delta\phi$ of 2π. This gives a clear indication of the dominance of the factor $\Delta n/n\Delta t$ in the phase increment equation.

If we define the quantity

$$\beta = \frac{1}{n}\frac{\Delta n}{\Delta t} \qquad (3.8)$$

we call β the **thermal dispersion**; it is the fractional rate of change of refractive index with temperature. We expect this fractional change to be caused by the expansion effect but the true interaction of expansion and change of refractive index is complex.

Let us take the example of a Lorentz-Lorenz model for the refractive index e.g.

$$n^2 = \frac{1 + \frac{8\pi}{3} N\alpha}{1 - \frac{4\pi}{3}\alpha} \qquad (3.9)$$

where N is the concentration of the molecular space whose polarizability is α. Let us furthermore suppose that

$$A\,Nd = \text{constant} \qquad A = \text{cross section} \qquad (3.10)$$

i.e. assume that matter is simply conserved. To avoid tedious repetition of constants, let us define

$$x = \frac{4\pi}{3} N\alpha \qquad (3.11)$$

Now let us consider relevant increments as follows:

$$2n\Delta n = \Delta\left[\frac{1 + 2x}{1 - x}\right] = \frac{2\Delta x}{1 - x} - \frac{(1 + 2x)(-\Delta x)}{(1 - x)^2} = \frac{3\Delta x}{(1 - x)^2} \qquad (3.12)$$

Now since

$$x = \frac{n^2 - 1}{n^2 + 2} \qquad (3.13)$$

we have

$$2n\Delta n = \frac{3x}{(1 - x)^2}\frac{\Delta N}{N} = \frac{(n^2 - 1)(n^2 + 2)}{3}\frac{\Delta N}{N} \qquad (3.14)$$

or

$$\frac{1}{n}\Delta n = \frac{(n^2 - 1)(n^2 + 2)}{6n^2}\frac{\Delta N}{N} \qquad (3.15)$$

Evidently, from (3 10) we also have

$$\frac{\Delta N}{N} = -\frac{3\Delta d}{d} \qquad (3.16)$$

so that a Lorentz-Lorenz model coupled with conservation of matter implies that

$$\beta = \frac{1}{n}\frac{\Delta n}{\Delta t} = -\frac{(n^2-1)(n^2+2)}{6n^2}\frac{\Delta d}{d\,\Delta t} \qquad (3.17)$$

$$= -1{\cdot}11\,\alpha \qquad (3.18)$$

for a refractive index $n = 1.46$.

Such a model indicates that the thermal dispersion should be similar to the thermal expansion effect in its influence on nd. **In practice, the converse is true and it is felt that the relationship between α and β should give a powerful insight into the structure of the optical material of the etalon.**

The second class of experiments which we have attempted in the area of phase shift measurement consists of an attempt to measure the thermal expansion directly using an interferometer thus

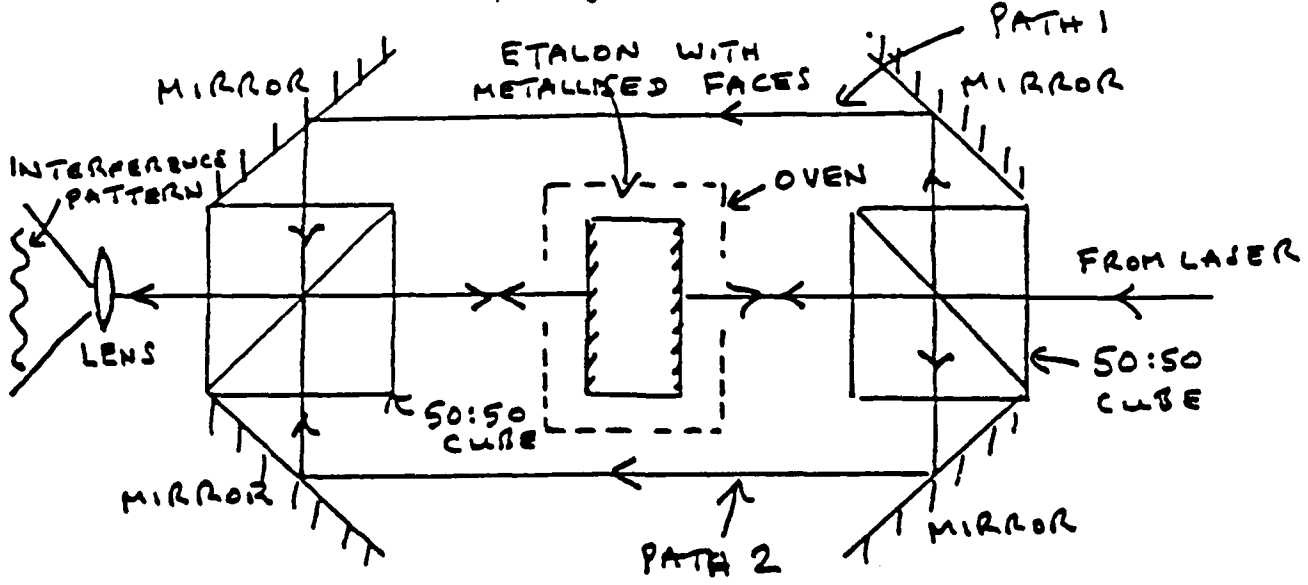

Figure 8. Interferometer for expansion measurement.

A sample etalon, measured as in the previous geometry is first metallised on both faces and then inserted into the interferometer above.

The role of the interferometer is to cause the incoming beam to divide into two paths 1 and 2. The light travelling along path 1 travels straight to the diverging lens L whereas the light in path 2 interrogates **both** faces of the etalon before travelling to the lens. This experiment is designed to avoid anomalous fringe movement due to translation of the etalon along the optical axis. The system is only sensitive to **relative** movement of the two faces of the etalon. Thus it yields a true measure of the expansion of the etalon material.

The fringe pattern is interrogated by a final photodiode detector and a change Δd of the etalon thickness causes a phase change $\Delta\phi$ of magnitude $2k\Delta d$ where $k = 2\pi/\lambda_a$. When this phase change is equal to 2π the detector sees the replacement of a bright by a bright or a black by a black. Thus the temperature increment Δt created by the oven can be read off and the equation

$$2k\Delta d = 2\pi \qquad (3.19)$$

used to determine Δd for the given value of Δt. Evidently we have

$$\frac{1}{d}\frac{\Delta d}{\Delta t} = \frac{1}{d}\frac{\lambda_a}{2}\cdot\frac{1}{\Delta t} \qquad (3.20)$$

which gives a value for the thermal expansion coefficient.

Unlike the measurement of intensity reflectance this second experiment being **externally** interferometric is sensitive to path changes **outside** the etalon. This leads to a need for extreme rigour in the performance of the surrounding optical apparatus.

We have found that the heating of the etalon leads to air path changes outside the etalon that cannot be ignored. To see this, we note that the refractive index of air is given by the expression

$$n - 1 = \frac{(n_s - 1)\,p\,[1 + p(61.3 - t)\,.\,10^{-10}]}{96095.4\,[1 + 0.003661t]} \qquad (3.21)$$

where n_s is a standard value observed at t = 15°C and p = 101325 P_a. Here p is the pressure which we shall assume **constant** at a typical laboratory value of 10^5 P_a and t is the temperature in degrees Centigrade.

We can then calculate incremental changes thus: using (3.21) with p = 10^5 P_a and t = 20°C, we have the result

$$\Delta n = -9.246 \cdot 10^{-7} \Delta t \qquad (3.22)$$

Now consider an experiment in which a region near the heated etalon changes its temperature by an increment of say 2.5°C (characteristic increment between reflection peaks off the etalon). Consider also a path of say 4 cms (there and back). The net optical phase change is then

$$|\Delta\phi| = \frac{2\pi}{\lambda_a} \cdot 4 \cdot (9.246 \cdot 10^{-7}) 2.5 \qquad (3.23)$$

or

$$\frac{|\Delta\phi|}{2\pi} = \frac{4(9.246 \cdot 10^{-7}) 2.5}{5.145 \cdot 10^{-5}} \qquad (3.24)$$

$$\approx 0.18 \qquad (3.25)$$

By comparison, suppose that a 1 cm thick etalon expands by an amount Δd under the same temperature increment (2.5°C). We then have

$$\Delta d = 2.5\alpha \qquad (3.26)$$

where α is the thermal expansion coefficient. Taking a value for α of say $0.4 \cdot 10^{-6}$ °C we have

$$\Delta d = 10^{-6} \text{ cms} \qquad (3.27)$$

This then yields a reflective phase shift of

$$\Delta\phi = 2 \cdot \frac{2\pi}{\lambda_a} \cdot \Delta d = \frac{2 \cdot 2\pi \cdot 10^{-6}}{5.145 \cdot 10^{-5}}$$

or

$$\frac{\Delta\phi}{2\pi} = 0.039 \qquad (3.28)$$

This shows that changes of air path in fact dominate the measurements. For this reason, a new vacuum enclosed interferometer is being constructed.

(b) In-laser measurements of etalon performance

We have acquired a scanning interferometer system that provides an analysis of the modal pattern of light emitted by the laser.

A piezo driven Fabry-Perot interferometer scans the profile of the emitted light from the laser. This reveals whether or not the output is in single or multiple mode but does not resolve the profile of an individual mode.

A typical line width for the strong lines of an Argon laser is of the order of 10 GHz so the chosen Fabry-Perot head scans over this range. A typical single mode of the laser covers a spectral range of about 5 MHz so the transition from single line to single mode output is a striking observation.

The thickness of the etalon determines the free spectral range. (The range of wavelengths or frequencies between two adjacent transmission maxima of the etalon). We note that the transmittance of the etalon is given by

$$\frac{I_t}{I_i} = \frac{1}{1 + F \sin^2\left(\frac{\phi}{2}\right)} \qquad (3.29)$$

where I_t is the transmitted intensity and I_i the incident intensity.

Here $\phi = 4\pi nd/\lambda_0$ as before. A phase change of 2π (corresponds to a change of frequency given by $\Delta f = c/2dn$ where c is the speed of light in vacuo. This is normally chosen to correspond to the line width of the laser output. This choice of free spectral range permits the etalon to be maximally transmissive for a given laser mode but not to encourage more than one mode to exist.

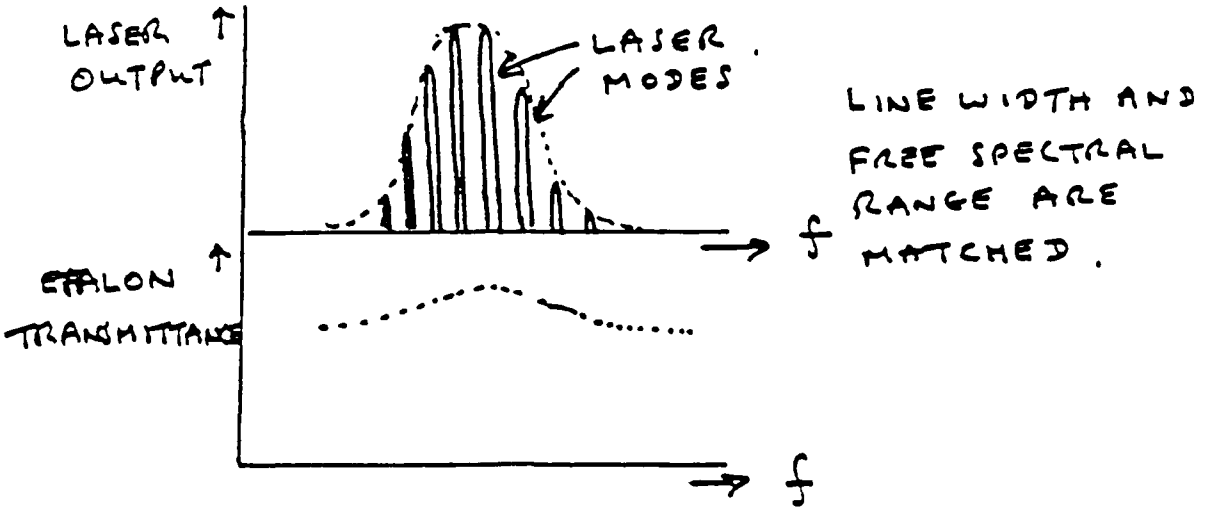

Figure 9. Shows the line width and free spectral range relationship.

To date, we have examined a small number of GEL SIL samples with a thickness range of some 3 - 5 mm. Note that a free spectral range of 10 GHz corresponds to an etalon thickness d of the order of 1.5 cms. Practical values are usually at a level of $d \approx 1$ cm.

The use of reduced levels of etalon thickness results in the transmittance of the etalon rising again before the edge of the line profile is reached thus risking the simultaneous emission of more than one laser mode.

Results showing 1, 2, 3 and multi mode operation are shown on the accompanying view graphs. When the free spectral range of the etalon is too small then the usual result is that at high laser gain levels, i.e. at high tube currents in an ion laser, a transition from single to multi mode lasing occurs as the current is advanced.

Of great interest is the 'conversion efficiency' (the ratio of output intensity in single mode to that in single line). Conventional results usually indicate a performance in the range 50 - 60%.

4. Requirements of Etalon Flatness

A key aspect of etalon characteristic is the parallelism and flatness of the sample. Any lack of parallelism of the faces tends to cause a prismatic deflection of the transmitted beam. Even if the individual faces are flat to say $\lambda/20$, transmitted beam deviation can walk off the intra-cavity beam when the etalon is installed in a laser and destabilise the cavity. A simple reflectance interferometer test as below:

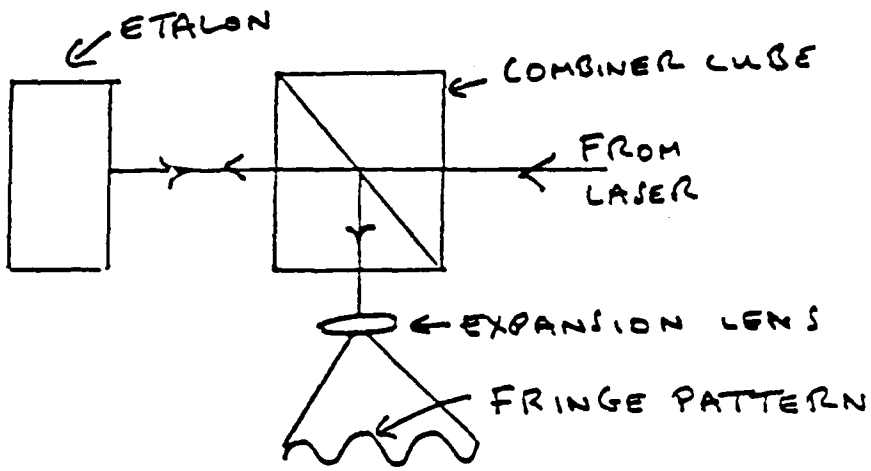

Figure 10. Simple interferometer test for etalon flatness and parallelism of faces.

serves to show whether faces 1 and 2 of the etalon are adequately parallel. Essentially a lack of parallelism leading to of the order of one fringe deviation within the working beam diameter is just about acceptable. We have now located a polishing shop that can provide a very quick and accurate service to the required standard.

5. Summary

Experimental procedures and results are reported leading to a detailed study of etalon performance. New thick samples of GEL SIL are now being made available and results will be reported in the near future.

We have shown that etalon reflectance is relatively easy to measure but that the interferometric measurement of thermal expansion must be performed under vacuum to avoid air path contributions to beam phase shift.

Of great interest is the conversion efficiency of different types of etalon. The conventional figures of 50 - 60% are likely to be exceeded by GEL SIL samples simply because of the intrinsically low loss of the material. Results are to be referred to a synthetic material Dynasil as a standard.

The optics industry admits that colour centre formation in conventional silica optics prevents a satisfactory performance of ion lasers in the near ultra violet. The extraordinary transmittance of ultra-pure GEL SIL is likely to lead to greatly improved confidence in the use of u.v. generating lasers for lithographic applications.

The future of our programme of work is to be directed as follows

(i) The evaluation of standards of performance of uncoated and if necessary coated etalons in the intra-cavity situation. This work to include an evaluation in the far blue (457.9 nm) and in the near u.v. (363.8 nm).

(ii) The testing of fitted GEL SIL Brewster windows on ion laser tubes in the same part of the spectrum. This work will require sophisticated polishing methods for thin window samples.

(iii) The fabrication and testing of dispersing prisms made of GEL SIL.

(iv) The testing of etalons in the red spectrum particularly at the 647 nm of the Krypton laser.

(v) The establishment of the working model of the interferometer for expansion coefficient testing.

(vi) The installation of storage oscilloscope and plotter facility for printout of modal diagrams from the swept Fabry-Perot spectrum analyzer.

(vii) A study of the modal profile of the individual laser modes in an attempt to detect structural differences in the trapped interference pattern in GEL SIL etalons and other types fabricated material.

(viii) The fabrication and testing of curved etalons (concentric) on the lines of discussion of GEL Tech Report No.1. **These might be the most attractive way to introduce GEL SIL to the laser consumer market.**

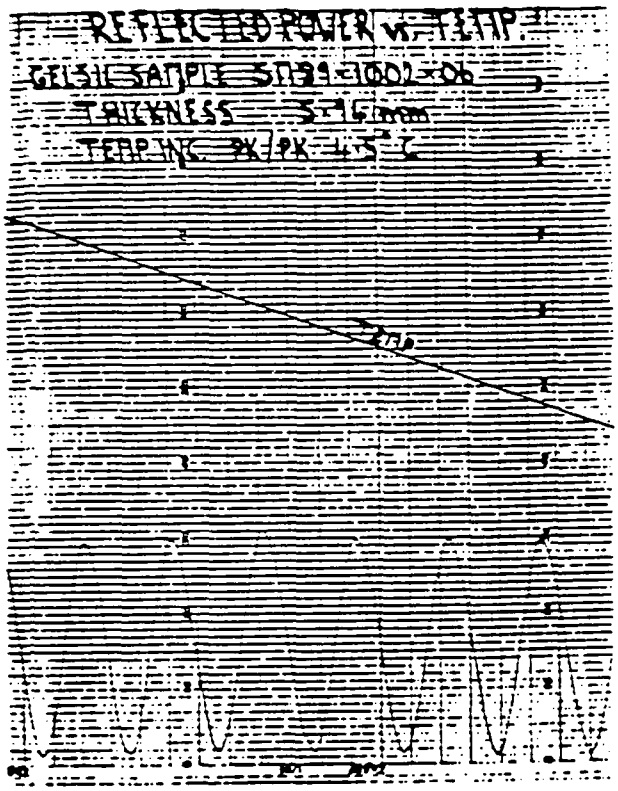
REFLECTED POWER vs. TEMP
GELSIL SAMPLE SIG99-1002-06
THICKNESS 5.16 mm
TEMP INC. PK/PK 4.5° C

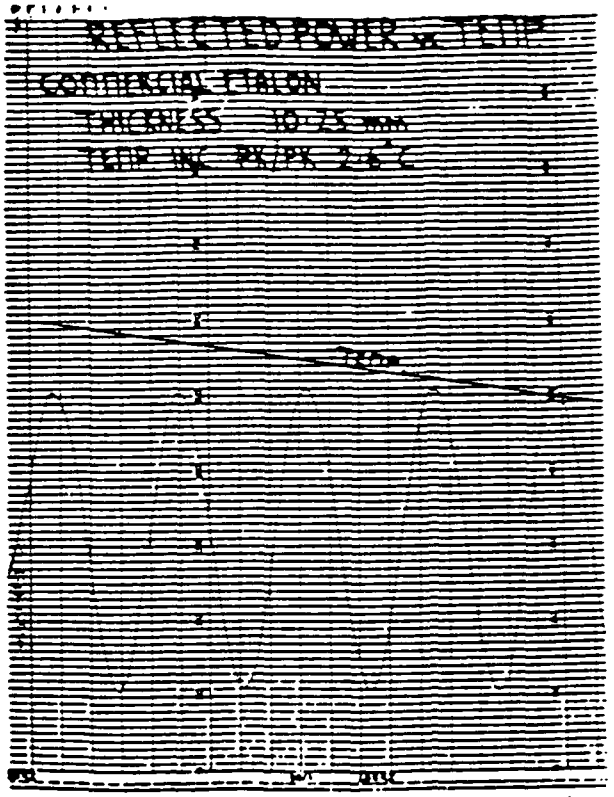
REFLECTED POWER vs. TEMP
COMMERCIAL SILICON
THICKNESS 10.25 mm
TEMP INC. PK/PK 2.6° C

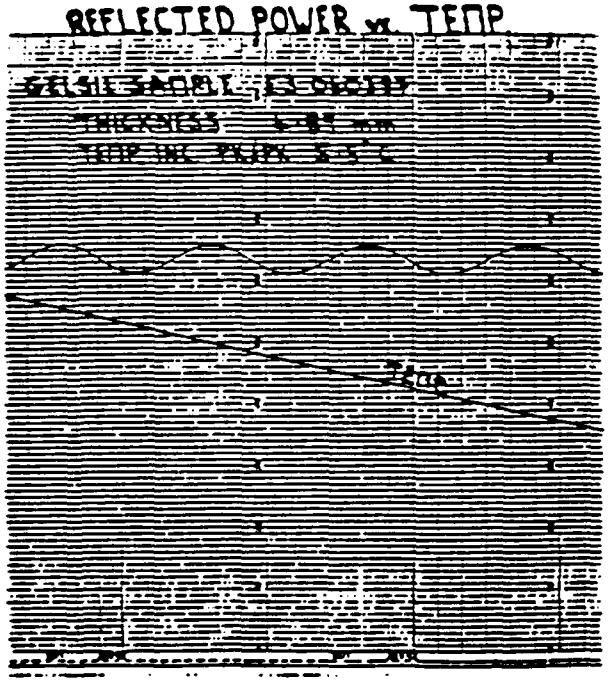
REFLECTED POWER vs. TEMP

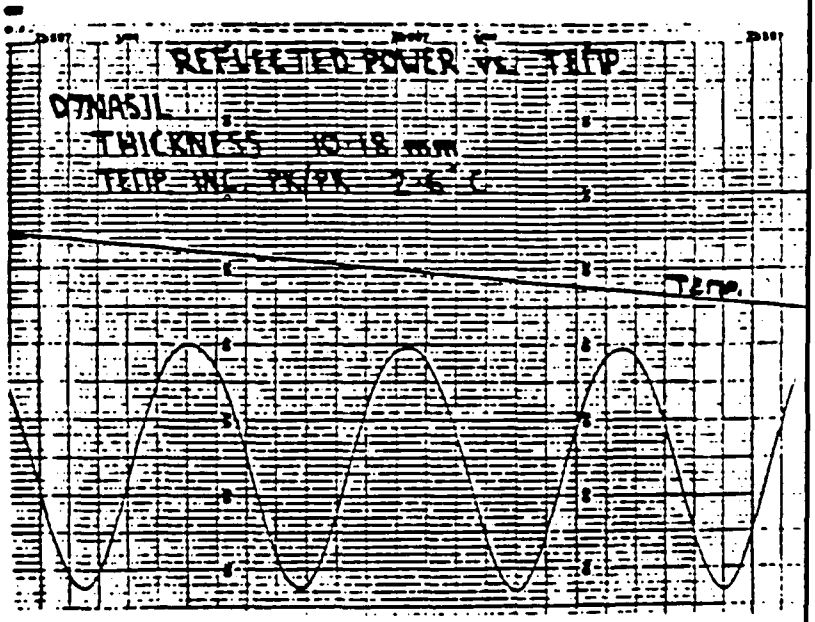
REFLECTED POWER vs. TEMP
THICKNESS 10.18 mm
TEMP INC. PK/PK 2.6° C
Temp.